Dyregulation of microRNA-124 and microRNA-383 in Medulloblastoma

LI, Ka Wai Kay

A Thesis Submitted in Partial Fulfillment of

the Requirements for the Degree of

Doctor of Philosophy

in

Anatomical and Cellular Pathology

The Chinese University of Hong Kong

July 2011

AUTHORIZATION

I hereby declare that I am the sole author of the thesis

I authorize The Chinese University of Hong Kong to lead this thesis to other institutions or individuals for the purpose of scholarly research.

I further authorize The Chinese University of Hong Kong to reproduce the thesis by photocopying or by other means, in total or in part, at the request of other institutions or individuals for the purpose of scholarly research.

ACKNOWLEDGEMENTS

With the completion of my PhD study, I would like to take this opportunity to express my sincere gratitude to my supervisor Professor Ho-keung Ng. He gave me the opportunity to persuade my education and handle this research project. I have to thank Professor Ng for his invaluable effort to smoothen my study, and his support, advice and guidance throughout my study.

My grateful thanks also go to my co-supervisor, Mr. Jesse Chung-sean Pang, for his advices on project design and technical problem solving during my study, especially when I encountered difficulties in my research progression. Special thanks for his patience in research project discussion and guidance.

I would also like to express my thanks to all past and present members of the Brain Disease Laboratory in Department of Anatomical and Cellular Pathology. They are Dr. Aden Ka Yin Chan, Ms. Belle Wing Sze Cheung, Ms Nellie Yuk-Fei Chung, Dr. Hui Ming Li, Mr. Yeung Lam Ng and Ms Ling Yang. They have kindly provided technical support and cooperation in my study.

Last but not least, I would like to thank all the colleagues on 5th floor of Cancer Centre, for their assistance in different areas.

In the end, I would like to especially thank to my parents who have given me never-ending support and provided the strength in my life. Without them, my study would not complete.

ABSTRACT

Medulloblastoma (MB) is an invasive embryonal tumor of the cerebellum, accounting for ~ 20% of all primary pediatric brain tumors. The overall survival rate is 60–70% in standard-risk MB patients, but merely ~30% in high-risk group. Patients who survive often suffer from long-term neurologic and cognitive deficits. New therapy is needed to reduce the mortality rate and to improve the quality of life of survivors. Understanding the molecular pathogenesis of MB is critical to the development of efficacious therapeutic treatment.

MicroRNAs (miRNAs) are short non-protein-coding RNAs that function in diverse biological processes through negative regulation on gene expression at the post-transcriptional level. Accumulative evidence indicates that miRNAs play an important role in the development of human cancers, with their deregulation resulting in altered activity of downstream tumor suppressors, oncogenes and other signaling molecules.

The aim of my project is to identify and characterize deregulated miRNAs located on chromosome 8p in MB. Our group has previously identified a minimally deleted region on 8p22-23.1 and partial or interstitial deletions at 8p22-23.2 in MBs. Despite extensive investigation, no promising candidate genes were identified in these. I questioned if miRNAs (miR-124, miR-383 and miR-320) were the targets on chromosome 8p. Quantitative expression analysis of 29 MBs revealed that miR-124 and miR-383 were downregulated in 72% and 79% of tumors, respectively, compared to normal cerebella. In contrast miR-320 expression was variable. Ectopic expression of miR-124 and miR-383 in MB cell lines (DAOY and ONS-76) showed significant growth inhibition. Cell cycle

profiling revealed miR-124 and miR-383 inhibited cell cycle progression and induced apoptosis. These results suggest that miR-124 and miR-383 are potential growth suppressors.

To identify gene targets of miR-124, computational analysis was carried out. Twelve candidate genes predicted as miR124 target were selected for analysis. One candidate gene, *SLC16A1*, showed downregulation at transcript and protein levels after miR-124 transfection. Luciferase reporter assay demonstrated that miR-124 interacted at the 3' untranslated region of SLC16A1. These results suggest that miR-124 negatively regulates *SLC16A1*. Expression analysis further revealed that overexpression of *SLC16A1* was common in MBs.

To identify miR-383 targets, global gene expression analysis and computational approach were applied. Two genes (*PRDX3* and *RBMS1*) showed downregulation upon miR-383 transfection. Reporter assay confirmed that miR-383 interacted at 3' untranslated regions of these genes, suggesting that *PRDX3* and *RBMS1* are targets of miR-383.

In conclusion, downregulation of miR-124 and miR-383 is a frequent event in MB. Restoration of miR-124 and miR-383 inhibited cell growth and cell cycle progression in MB, suggesting these miRNAs harbor growth suppressor function. In addition, this study demonstrates *SLC16A1* and *PRDX3* are the direct targets of miR-124 and miR-383, respectively. Together, these data shed new light on miR-124 and miR-383 in MB pathogenesis, and suggest that miR-124/SLC16A1 and miR-383/PRDX3 pathways are potential therapeutic targets for treatment of MB.

摘要

髓母細胞瘤是一種侵襲性的小腦胚胎性腫瘤，占兒童腦腫瘤大約 20%。其平均生存率在標準危險群是 60-70% ，但在高危險群大約是 30%。 病人經過治療後常伴有長期的神經和認知的障礙。新的治療目標是減少死亡率，改善生存品質。闡明髓母細胞瘤的分子病理機制是開發有效治療方法的關鍵。

微小 RNA 是 RNA 中非編碼蛋白的短小片段，但在轉錄後水平通過抑制調節基因表達來實現對多種生物功能的調控。大量的證據已經證明微小 RNA 在人類腫瘤的發展中起重要的作用，他們抑制調節改變了下游腫瘤抑制基因，腫瘤基因和其它的信號分子的活性。

本研究的目的是鑒定位於 8 號染色體短臂的微小 RNA 的抑制調節對髓母細胞瘤的作用。 本研究組以前已經鑒定了髓母細胞瘤 8 號染色體短臂 8p22-23.2 的最小丟失片段和多間斷的丟失片段。儘管已經有廣泛的研究，但是在這個區域還沒有候選基因的表達異常被發現。爲了探討微小 RNA (miR-124, miR-383 and miR-320) 靶點是否在 8 號染色體，本研究對 29 例髓母細胞瘤進行了定量表達的分析。結果顯示，與正常小腦相比，miR-124 和 miR-383 在髓母細胞瘤表達下調比例分別 72%和 79%。微小 RNA miR-124 和 miR-383 在髓母細胞瘤細胞株(DAOY and ONS-76) 異位表達異常顯著抑制了細胞生長。這些結果提示 miR-124 和 miR-383 是潛在的生長抑制因子。

爲了尋找和鑒定 miR-124 的靶點，本研究挑選了 12 個候選基因進行了電腦分析。當 miR-124 被轉染到細胞內之後，其中一個候選基因 *SLC16A1* 顯示了 RNA 轉錄和蛋白表達水平的下調。螢光素報告基因檢測證實了 miR-124 作用在 *SLC16A1* 的

非編碼區（3’ untranslated region）。 這些結果提示 miR-124 是 *SLC16A1* 基因的抑制調節因子。蛋白表達分析進一步證實了 *SLC16A1* 在髓母細胞瘤是過度表達的。

本研究也使用電腦分析技術鑒定了 miR-383 的靶點。當 miR-383 被轉染到細胞內之後，*PRDX3* 和 *RBMS1* 這兩個基因表達受到了抑制。螢光素報告基因檢測證實了 miR-383 作用在這兩個基因的非編碼區，提示 *PRDX3* 和 *RBMS1* 是 miR-383 的靶點。

綜上所述，miR-124 和 miR-383 在髓母細胞瘤的表達下調是常見的。恢復 miR-124 和 miR-383 表達可以抑制髓母細胞瘤的細胞生長和細胞循環，提示這些微小 RNA 有生長抑制的功能。本研究也證實了 miR-124 和 miR-383 的直接靶點分別是 *SLC16A1* 和 *PRDX3* 基因。這些結果揭示了 miR-124 和 miR-383 在髓母細胞瘤的病理機制，提示 miR-124/SLC16A1 和 miR-383/PRDX3 是未來靶向治療的通路，給髓母細胞瘤治療帶來了曙光。

LIST OF PUBLICATIONS

Publication directly related to this thesis

1. Li KK, Pang JC, Ching AK, Wong CK, Kong X, Wang Y, Zhou L, Chen Z, Ng HK. miR-124 is frequently down-regulated in medulloblastoma and is a negative regulator of SLC16A1. Hum Pathol 2009; 40(9): 1234-43.

Publications indirectly related to this thesis

1. Lau KM, Chan QK, Pang JC, Li KK, Yeung WW, Chung NY, Lui PC, Tam YS, Li HM, Zhou L, Wang Y, Mao Y, Ng HK. Minichromosome maintenance proteins 2, 3 and 7 in medulloblastoma: overexpression and involvement in regulation of cell migration and invasion. Oncogene 2010; 29(40), 5475-89.

2. Pang JC, Li KK, Lau KM, Ng YL, Wong J, Chung NY, Li HM, Chui YL, Lui VW, Chen ZP, Chan DT, Poon WS, Wang Y, Mao Y, Zhou L, Ng HK. KIAA0495/PDAM is frequently downregulated in oligodendroglial tumors and its knockdown by siRNA induces cisplatin resistance in glioma cells. Brain Pathol 2010; 20(6), 1021-32.

3. Li KK, Pang JC, Chung NY, Ng YL, Chan NH, Zhou L, Poon WS, Ng HK. EMP3 overexpression is associated with oligodendroglial tumors retaining chromosome arms 1p and 19q. Int J Cancer 2007; 120(4), 947-50.

4. Chang Q, Pang JC, Li KK, Poon WS, Zhou L, Ng HK. Promoter hypermethylation profile of RASSF1A, FHIT, and sFRP1 in intracranial primitive neuroectodermal tumors. Hum Pathol 2005; 36(12), 1265-72.

Presentations related to this thesis

1. Pang JC, Li KKW, Wang Y, Ellison D, Ng H. Identification of candidate tumor suppressor genes on chromosome 8p in medulloblastomas by expression profiling. EANO Congress 2007.

2. Li K, Pang J, Kong X, and Ng HK. miR-124a and miR-383 on chromosome 8p are candidate tumor suppressors in medulloblastoma. 98th AACR Annual Meeting 2007.

3. Li KKW, Pang JCS, Chung NYF, Poon WS, and Ng HK. miR-124a and miR-383 on chromosome 8p are candidate tumor suppressors in medulloblastoma. Cancer 2007.

TABLE OF CONTENT

LIST OF TABLES

LIST OF FIGURES

CHAPTER 1

INTRODUCTION AND LITERATURE REVIEW OF MY STUDY

1.1 Introduction to medulloblastoma (MB)

1.1.1 Overview of MB

MB is an invasive embryonal tumor arising in the cerebellum. It is the most common malignant brain tumor in children and accounts for about 20% of all central nervous system (CNS) tumors in children (Dhall 2009; Jozwiak et al. 2007; Rickert and Paulus 2001). MB was first described by neurosurgeon Harvey Cushing and his associate Percival Bailey. They named the tumor after the putative medulloblast, which was never found in reality (Kershman 1938).

1.1.2 Incidence

In United States, the annual incidence rates of MB in childhood up to 19 years is 0.48 in girls and 0.75 in boys per 100,000 persons, 0.17 per 100,000 persons in young adulthood (age of 20-34 years), and 0.06 per 100,000 persons in the elderly (age of 55-64 years) (Crawford et al. 2007).

1.1.3 Age and sex distribution

The peak incidence of MB is in the seventh year and most MB present in the first two decade of age (Gurney and Kadan-Lottick 2001; Pfister et al. 2010; Roberts et al. 1991). About 70% of MBs occur before the age of 16. In adults, 80% of MBs occur at the age 21-40, but rarely beyond the fifth decade of life. There is a slight male predominance over female with a ratio of 1.4:1 (Crawford et al. 2007; Curran et al. 2009; Das et al. 2009). Recent studies have demonstrated both sex ratio and age distribution vary among molecular subgroups (Cho et al. 2010; Kool et al. 2008; Northcott et al. 2010; Pfister et al. 2010). Detailed information on these issues is described in Chapter 1.5.

1.1.4 Classification

The current World Health organization (WHO) classification of MB, which was updated in 2007, recognizes five variants: classic MB, desmoplastic/nodular MB, MB with extensive nodularity (MBEN), large cell MB, and anaplastic MB. All variants are classified as grade IV (Giangaspero et al. 2007). Moreover, two tissue differentiate patterns are identified, namely MB with myogenic differentiation (medullomyoblastoma) and MB with melanotic differentiation (melanocytic medulloblastoma). Recent studies of genetic aberration and expression profiling have indicated that specific histopathological subtypes are associated with molecular

subgroups (Cho et al. 2010; Kool et al. 2008; Northcott et al. 2010; Pfister et al. 2010). Furthermore, histopathological subtypes exhibit age group specific patterns (Northcott et al. 2010; Pfister et al. 2010).

Classic MB accounts for 70% of MBs (Min et al. 2005; Northcott et al. 2009). It is composed of small round or ellipsoid cells with round-to-oval or carrot-shaped nuclei with abundant chromatin and scanty cytoplasm. However, cells with round nuclei in which the chromatin is not highly condensed are frequently intermingled with the hyperchromatic cells and occasionally form the dominant population. Homer-Wright rosettes or pseudorosettes, which consist of tumor cell nuclei arranged in a circular fashion around fine tangled cytoplasmic processes, are found in less than 40% of classic MBs (Gilbertson and Ellison 2008). Classic MB predominantly arises in the vermis of the cerebellum and has the tendency to spread through the cerebrospinal fluid to the spinal canal (Haas et al. 2006). Classic MB can be found in all molecular subgroups, including wingless (WNT), sonic hedgehog (SHH), and non-WNT/SHH (Kool et al. 2008; Northcott et al. 2010; Thompson et al. 2006). In addition, 75-84% of MBs in adults show classic histologic features (Kool et al. 2008; Korshunov et al. 2010; Northcott et al. 2010).

Desmoplastic/nodular MB accounts for 15% of MBs (Ellison 2002). It is characterized by reticulin-free nodular areas, or "pale islands", surrounded by densely

packed cells along with an intercellular network of reticulin fibers. In contrast to classic variant, desmoplastic MB often arises in the hemispheres (Haas et al. 2006). The desmoplastic histology has been reported to be an independent and significant prognostic factor for favorable outcome in young children compared to classic variant (Rutkowski et al. 2005). Desmoplastic MB is predominantly found in infants (Ellison 2010). McManamy et al. reported that with up to 57% of cases in patients of ages <3 years exhibited desmoplastic histology (McManamy et al. 2007). Two recent studies have demonstrated that the majority of desmoplastic variant is found in infants or children under the age of 16 (Kool et al. 2008; Northcott et al. 2010). Furthermore, infants presented with desmoplastic histology have a significant better clinical outcome than those with classic or large cell/anaplastic histology (Rutkowsi et al. 2005; Rutkowsi et al. 2009).

MBEN represents less than 5% of MBs (Jozwiak et al. 2007). It is marked by an expanded lobular architecture caused by unusually elongated reticulin-free zones that are rich in neuropil-like tissue. Such zones contain a population of small cells with round nuclei (Gulino et al. 2008). This histology is primarily found in infants with favorable prognosis (Eberhart et al. 2011).

Large cell MB accounts for 2-5% of MBs (Crawford et al. 2007; Giangaspero et al. 1992; McManamy et al. 2003). This type of variant is featured by large, round or

pleomorphic, molded nuclei with prominent nucleoli and abundant cytoplasm. Cell-cell wrapping, large area of necrosis, high mitotic activity and high apoptotic rate are commonly found (Verma et al. 2008). Often, metastatic disease is recognized with this histological type (Ellison 2010). The tumor is considered highly malignant and appears to be associated with shorter survival and poor clinical outcome (Giangaspero et al. 1992; Brown et al. 2000; Verma et al. 2008).

Anaplastic MB constitutes 10-22% of MBs (Ellison 2002; McManamy et al. 2003). It is marked by large tumor cells, prominent nucleoli, abundant mitotic figures, and numerous apoptotic bodies (Brown et al. 2000; Giangaspero et al. 1992). The nuclei are pleomorphic and crowded, and show molding frequently (Eberhart and Burger 2003). Some of the cytological features are overlapped between large cell MB and anaplastic variant, and these two subtypes appear to form a continuum. Some large cell MBs containing anaplastic regions are frequently found, and a combined large cell/anaplastic (LC/A) category has been proposed (Brown et al. 2000; Min et al. 2006; von Hoff et al. 2010). Both large cell and anaplastic tumors are observed solely in infants or children (Northcott et al. 2010; von Hoff et al. 2010).

1.1.5 Risk stratification

At present, the risk stratification in MB is partly based on the Chang's clinical

staging systems, which separates MB into high-risk and average-risk groups according to age, metastatic stage at diagnosis and extent of surgical resection (Ellison et al. 2003). The average-risk patients are those diagnosed at the age greater than three years, have non-metastases at presentation, and have manageable residual tumor (≤ 1.5 cm^2) post-operation. High-risk patients are those which do not fulfill these criteria. Recent advances in multimodality therapy have improved the 5-year survival rate to 75-85% in average-risk patients (Gajjar et al. 2006; Gottardo and Gajjar 2006; Packer et al. 2006). However, the 5-year survival rate for high-risk patients is lower at a frequency of about 40-70% due to recurrence or dissemination within the CNS (de Haas et al. 2008; Gajjar et al. 2006; Gajjar and Pizer 2010; Khalil 2008).

1.1.6 Current treatment after risk stratification

Management of MB includes complete or near complete surgical resection, craniospinal radiotherapy, and chemotherapy. In average-risk patients, current therapy consists of surgical excision followed by radiotherapy and maintenance with chemotherapy (Pizer and Clifford 2009). Chemotherapy is used to reduce radiation dose for most patients or to work synergistically to improve outcome (Packer et al. 2006). Common chemotherapeutic agents for MB treatments include cisplatin, vincristine, lomustine, prednisone, and cyclophosphamide (Evans et al. 1990; Zeltzer et al. 1999).

Patients presenting with metastatic disease would be treated with a higher dose craniospinal radiation (36.0-39.6 Gray) (Gajjar et al. 2006). In patients younger than three years, chemotherapy-based treatment is usually used to delay irradiation because craniospinal radiation causes significant long-term brain damage in the very young children (Geyer et al. 2005; Rutkowski et al. 2005).

1.1.7 Side effects

The majority of survivors exhibit long-term neurocognitive and neuroendocrine sequelae post therapy (Mulhern et al. 2005; Ribi et al. 2005). It is believed that radiotherapy is the major cause of cognitive deficit; however, surgery and chemotherapy may also exert adverse effect on cognitive function (Saury and Emanuelson 2011). The adverse effects include learning difficulties, attention difficulties, short-term memory deficits, social adjustment problems, hearing, speech and language problems, and impaired physical growth. The side effects are especially problematic in young patients who experience long-term side effects mainly due to radiation therapy to the developing brain. Thus, multiple approaches have been undertaken to reduce long-term toxicity induced by therapy. These include the reduction of total dose of craniospinal radiation reduction in the volume of local boost radiotherapy, and use of less neurotoxic chemotherapeutic agents (Kieffer-Renaux et al. 2000).

1.18 Prognostic factors

Clinical feature are the major prognostic factors for MB. For instance, average-risk patients have better prognosis than high-risk patients. Moreover, the presence of residual tumor after operation is a negative prognostic factor in MB (Rutkowski et al. 2010). In addition, certain histological subtypes have been associated with different prognosis. Desmoplastic and MBEN variants exhibit the most favorable survival rate, followed by classic MB, with LC/A variant shows the poorest survival (Pfister et al. 2009; Rutkowski et al. 2010).

Molecular features, such as chromosomal aberration, gene expression, gene mutation, and molecular subtyping have been implicated in prognosis. For examples, isochromosome 17q, 17q gain, amplification of *MYC* and *MYCN* have been associated with poor clinical outcome (Ellison et al. 2010; Pan et al. 2005; Pfister et al. 2009, Korshunov et al. 2010, Aldosari et al. 2002). Recent study has demonstrated that even low level copy number increase in *MYCN* gene is correlated with poor survival (Zitterbart et al. 2010). In contrast, loss of chromosome 6q or monosomy 6 is associated with favorable clinical outcome (Clifford et al. 2006; Ellison et al. 2010; Pfister et. al 2009).

In addition, several genes are proposed as markers in prediction of outcome. These include high expression of cyclin-dependent kinase 6 (CDK6), survivin and *MYC*

as unfavorable prognostic markers (Mendrzyk et al. 2005; Haberler et al. 2006; Herms et al. 2000; Grotzer et al. 2001; Eberhart et al. 2004), and low expression of *TRKC*, a receptor of neurotrophins, as a predictor of long survival (Grotzer et al. 2000; Rutkowski et al. 2007; Segal et al. 1994).

Integrated genomic analysis has revealed that MB can be classified into four to six molecular subgroups (Cho et al. 2010; Kool et al. 2008; Northcott et al. 2010), which have prognostic implication. For instance, activation of WNT pathway is associated with favorable prognosis (Clifford et al. 2006). The presence of *β-catenin (CTNNB1)* gene mutation, nuclear staining of CTNNB1 protein, and monosomy 6 are good indicators of WNT activation (Clifford et al. 2006; Kool et al. 2008; Northcott et al. 2010; Pfaff et al. 2010). In contrast, tumors belonged to non-WNT/SHH subgroups, which shows high frequency of recurrence, metastasis, *MYC* amplification and isochromosome (i17q), are associated with adverse outcome (Northcott et al. 2006; Kool et al. 2008).

Mutation of *TP53* is a hallmark in cancers. *TP53* mutation is found in approximately 7-16 % of MB (Lindsey et al. 2011; Pfaff et al. 2010; Tabori et al. 2010). Immunostaining of TP53 protein is a useful surrogate marker for *TP53* mutation (Pfaff et al. 2010). Recently, Tabori et al. has shown *TP53* mutation is associated with adverse outcome in MB (Tabori et al. 2010). However, such association was not seen in the

study conducted by Pfaff et al. (Pfaff et al. 2010). The discrepancy of these findings might have been due to the low proportion of WNT subgroup in Tabori et al's study (Tabori et al. 2010) and the overrepresented *TP53* mutation rate in the WNT subgroup in Pfaff et al's investigation (Pfaff et al. 2010).

1.2 Genetic aberrations

1.2.1 Chromosomal aberrations

Comparative genomic hybridization (CGH) studies have revealed multiple chromosomal aberrations in MB. These include gains of chromosomes 1q, 2p, 7, 8q, 17q and 18 and losses of chromosomes 6, 8p, 9q, 10q 11, 16q and 17p (Avet-Loiseau et al. 1999; Bayani et al. 2000; Gilhuis et al. 2000; Nicholson et al. 1999; Nishizaki et al. 1999; Readon et al. 1997; Russo et al. 1999; Schutz et al. 1996; Shlomit et al. 2000).

1.2.2 Chromosome 17 abnormality

Isochromsome 17q (i17q), that is the presence of two long arms due to duplication and a loss of the short arm, is the most common chromosomal aberration in MB. Originally, it was identified in 30-60% MBs by conventional karyotyping (Giordana et al. 1998). Other molecular techniques, CGH and fluorescence in situ hybridization (FISH) analyses have revealed the presence of i17q in 14% and 15-30%

MBs, respectively (Pan et al. 2005; Thompson et al. 2006; Vagner-Capodano 1994). Analysis of DNA copy number variants by array CGH and single nucleotide polymorphism (SNP) array have shown the presence of i17q in 22-48% MBs (Cho et al. 2010; Northcott et al. 2010; Pfister et al. 2009). Loss of 17p without gain of chromosomal 17q or gain of 17q without loss of 17p is also identified in 9-20% and 9-18% of MBs, respectively (Avet-Loiseau et al. 1999; Clifford et al. 2006; Gilbertson et al. 2001; Gilhuis et al. 2000; Pfister et al. 2009; Pan et al. 2005). The common chromosomal breakpoint at 17p11 and 17p11.2 and the common deletion region at17p13.1-17p13.3 have been identified, and several genes within these loci have been suggested to be involved in MB pathogenesis (Aldosari et al. 2000; Batra et al. 1995; McCabe et al. 2006; McCabe et al. 2009; Mendrzyk et al. 2006; Rossi et al. 2006). Recently, using array CGH, McCabe et al. has identified three discrete breakpoints on chromosome 17, namely 17p11.2, 17p11.2-17q11.2, and 17q21.31 (McCabe et al. 2010). The breakpoints on 17p11.2 and 17p11.2-17q11.2 are the most common aberrations (McCabe et al. 2010).

TP53 is one of the candidate tumor suppressor genes (TSGs) located at the common deletion region. Mutation analysis has revealed that 5-10% of MBs harbored *TP53* mutation (Orellana et al. 1998; Raffel et al. 1993). The importance of *TP53* in MB pathogenesis has been emphasized by mouse models (Wetmore et al. 2001). Loss of one

allele for *Ptch* in mice resulted in a 14% incidence of MB, but the incidence of MB increased to >95% when the mice were heterozygous for *Ptch* and lacked *TP53* (Wetmore et al. 2001).

Another candidate gene on chromosome 17p is hypermethylated in cancer gene 1 (*HIC-1*), which is a zinc-finger transcriptional factor ubiquitously expressed in normal cerebellum (Waha et al. 2003). Aberrant hypermethylation of *HIC-1* was demonstrated in 85% MBs and the methylation status was correlated with *HIC-1* downregulation, suggesting that epigenetic silencing of *HIC-1* may contribute to MB pathogenesis (Waha et al. 2003).

REN(KCTD11) is mapped to 17p13.1 and is implicated in cell proliferation and differentiation of neural progenitor cell (Gallo et al. 2002). Allelic loss of *REN(KCTD11)* was observed in 39% of MBs and downregulation *REN(KCTD11)* was found in 70% of MB (Marcotullio et al. 2004; Zawlik et al. 2006). Ectopic expression of *REN(KCTD11)* suppressed MB cell growth and inhibited tumorigenicity in MB (Marcotullio et al. 2004). *REN(KCTD11)* was implicated in the proliferation of granule cell progenitors (Argenti et al. 2005) through negative regulation on GLI1, an effector of the SHH pathway (Canettieri et al. 2010). Dysregulation of SHH signaling in granule cell progenitors is thought to contribute to MB tumorigenesis.

1.2.3 Loss of chromosome 10q

Loss of 10q was detected in 16-67% of MBs (Avet-Loiseau et al. 1999; Blaeker et al. 1996; Clifford et al. 2009; Gilhuis et al. 2000; Lo et al. 2007b; Pan et al. 2005; Reardon et al. 1997; Scott et al. 2006; Yin et al. 2001). Two TSGs, *Phosphatase and tensin homolog (PTEN) and deleted in malignant brain tumors 1 (DMBT1)*, mapped to chromosome 10q were examined for potential involvement in MB. PTEN is a protein tyrosine phosphatase that functions as an inhibitors of the PI-3 kinase pathway through dephosphorylation of phosphatidylinositol-3,4,5-triphosphate (PIP_3) (Castellino et al. 2010). Downstream effectors of PIP_3 include v-akt murine thymoma viral oncogene homolog 1 (*AKT*). Microsatellite analysis showed loss of heterogyzsity (LOH) of *PTEN* in 24% of MBs (Yin et al. 2001), whereas FISH analysis demonstrated homozygous deletion of *PTEN* in 32% of MBs (Inda et al. 2004). Furthermore, MB tumors exhibited reduced mRNA and protein levels of *PTEN* compared to normal cerebellum and loss of *PTEN* expression was correlated with poor survival (Castellino et al. 2010; Hartmann et al. 2006). Promoter hypermethylation of *PTEN* was reported in 50% of MBs (Hartmann et al. 2006). *PTEN* gene mutation was found in a small population of MBs (Hartmann et al. 2006; Rasheed et al. 1997). The animal study demonstrated that activated Smoothened *SmoA1(+/+)* and *Pten(+/−)* mice had decreased survival compared to *SmoA1(+/+);Pten(+/+)* mice. These mice exhibited increased signaling in the PI-3K

pathway and showed an increase in angiogenesis (Castellino et al. 2010). Taken together, the data reveal a critical role of *PTEN* in MB pathogenesis.

Allelic loss of *DMBT1* was observed in 33-47% MBs (Inda et al. 2004; Yin et al. 2001). However, genomic sequencing failed to identify any somatic mutations of *DMBT1* in MB (Pang et al. 2003). Recently, a detailed deletion study identified a minimal deletion region of 21.7 Mb at 10q23.3-10q25.3 in MB (Scott et al. 2006). Three genes, *beta-transducin repeat containing (BTRC), MAX interactor 1 (MXI1),* and *suppressor of fused* (*SUFU)* are located within this deletion region. These genes function in signaling pathway critical for MB oncogenesis. MXI1 regulates the activity of MYC oncogene (Foley and Eisenman 1999). SUFU is a negative regulator of SHH pathway, and BTRC negatively regulates the WNT pathway (Taipale and Beachy 2001). None of these genes were hypermethylated and no somatic mutations of *MXI1* were detected in MB (Scott et al. 2006). Nevertheless, *SUFU* mutation was identified in a subset of MB leading to activation of SHH signaling, suggesting that *SUFU* mutation predisposes to MB (Taylor et al. 2002).

1.2.4 Loss of chromosome 8p

Loss of chromosome 8p is a recurrent structural abnormalities described in MB. Loss of 8p was identified in 6-40% by comparative genomic hybridization (CGH)

(Avet-Loiseau et al. 1999; Gilluis et al. 2000; Nishizak et al. 1999; Readon et al. 1997; Schutz et al. 1996) and 15-48% by array CGH (Coco et al. 2011; Lo et al. 2007b; Rossi et al. 2006). My research colleagues had identified interstitial deletions on chromosome 8p22-23.2 and a homozygously deleted region on 8p22-23.1 (Yin et al. 2002). The results suggest that the presence of TSGs on chromosome 8p that are critical for MB tumorigenesis. Several genes have been suggested as the TSGs on 8p. One candidate TSG, *deleted in liver cancer 1* (*DLC-1*), located on 8p22, was found to have loss of expression in 1 of 9 tumors examined (Pang et al. 2005). However, the result indicated that loss of expression was detected in 1 out of 9 MBs (Pang et al. 2005). Another candidate TSG is *PIN2/TERF1 interacting, telomerase inhibitor 1 (PINX1)*. Depletion of this gene increase tumorigenicity in nude mice (Zhou and Lu 2001). Loss of *PINX1* was associated with short survival in ovarian cancer (Cai et al. 2010). However, the study carried by my research colleagues did not detect the downregulation of *PINX1* in MBs and the result of the study did not suggest *PINX1* as the TSG in MB (Chang et al. 2004). Thus, further investigation is needed to elucidate the TSG on 8p in MB.

1.2.5 Gain of chromosome 2p

Chromosomal 2p gain was detected in 6-50% of MBs (Avet-Loiseau et al. 1999; Nishizaki et al. 1999; Shlomit et al. 2000). The proto-oncogene *MYCN*, located at

2p24.1, was found amplified in 4-15% of MBs (Aldosari et al. 2002; Eberhart et al. 2002; Korshunor et al. 2008; Larront et al. 2004; Massimiliano De Bortoli et al. 2006; Pfister et al. 2009). Recent study using genetically engineered mouse model demonstrated that *MYCN* contributed to the initiation, progression, and maintenance of MB, and downregulation of *MYCN* led to apoptosis and senescence. These findings suggest that dysregulation of *MYCN* may contribute to MB pathogenesis (Swartling et al. 2010). *MYCN* amplification was found in classic, desmoplastic and LC/A variants (Northcott et al. 2010; Pfaff et al. 2010) and was not associated with clinical outcome (Ellison et al. 2010). A recent study demonstrated that *TP53* mutation was associated with *MYCN* amplification (Pfaff et al. 2010).

1.2.6 Gain of chromosome 8q

Gain of 8q was observed in 6-38% of MBs (Avet-Loiseau et al. 1999; Nishizaki et al. 1999; Shlomit et al. 2000). The proto-oncogene *MYC*, located on 8q24.41, is implicated in MB oncogenesis. *MYC* is a key regulator of cell proliferation, differentiation and apoptosis (Amati et al. 1998; Henriksson and Luscher 1996; Packham and Cleveland 1995). It forms heterodimer complex with MAX to bind DNA in a sequence specific manner, leading to cell cycle progression and triggering transcriptional activations of its downstream genes such as *FBJ murine osteosarcoma*

viral oncogene homolog (C-FOS) and B-cell CLL/lymphoma 2 (BCL2) (Miyazaki et al. 1995; Smith et al. 2004). *MYC* amplification was reported in about 5% of MBs with mixed histology (Eberhart et al. 2002; Ellison et al. 2010; Gilberton et al. 2001; Korshunov et al. 2008; Larront et al. 2004). However, up to 36% of the LC/A tumors exhibited *MYC* amplification (Brown et al. 2000). High-level of *MYC* amplification (>10 copy number gain) was detectable in LC/A MB, whereas copy number gain <10 was observed in other histology variants (Takei et al. 2009). A correlation existed between LC/A histology and *MYC* amplification (Eberhart et al. 2002; Leonard et al. 2001). Moreover, among the patients with LC/A histology, *MYC* amplification was associated with metastases and younger age (Takei et al. 2009). Molecular subtyping of MB revealed that *MYC* amplification was exclusively found in the non-WNT/SHH subgroups (Cho et al. 2010; Northcott et al. 2010).

1.2.7 Gain of chromosome 1q

Gain of 1q was reported in 10-30% of MBs (Avet-Loiseau et al. 1999; Gilhuis et al. 2000; Readon et al. 1997). The study conducted by Lo et al. indicated a correlation between 1q gain and poor survival (Lo et al. 2007a), but such association was not found in an independent study (Clifford et al. 2009). The significance of 1q gain in survival prediction remains unclear. Gain of 1q gain was predominantly found in the

non-WNT/SHH subgroups, but absent in the WNT subgroup (Northcott et al. 2010).

1.2.8 Gain of chromosome 7

CGH and array CGH studies have revealed gain of chromosome 7 in 20%-50% of MBs (Nishizaki et al. 1999; Reardon et al. 1997; Tong et al. 2004, Clifford et al. 2006; Lo et al. 2007a; Mendrzyk et al. 2005). Chromosome 7 gain was predominantly observed in pediatric MB (Korshunov et al. 2010). A novel DNA amplicon was identified at 7q21.2, where *cyclin-dependent kinase 6* (*CDK6*) is mapped. This gene plays an important role in proliferation and differentiation by phosphorylation of *retinoblastoma 1* (RB1). Overexpression of CDK6 was common in MB and was associated poor survival (Mendrzyk et al. 2005).

1.2.9 Loss of chromosome 6

By CGH and array CGH analysis, loss of chromosome 6 was described in 6-18% of MBs (Nicholson et al. 1999; Reardon et al. 1997; Korshunov et al. 2010; Lo et al. 2007a) and was associated with the WNT subgroup (Kool et al. 2008; Northcott et al. 2010; Thompson et al. 2006). Despite similarity in incidence rate among adult and pediatric MB, the pattern of chromosome 6 loss was different between these age groups (Korshunov et al. 2010). Pediatric MBs showed complete loss of chromosome 6,

whereas most adult MBs exhibited partial chromosome 6. In addition, chromosome 6 loss was frequently detected in concomitant with chromosome 17 abnormality in adult MBs. In contrast, none of the pediatric MBs showed concurrent chromosome 6 and chromosome 17 aberrations (Korshunov et al. 2010). More importantly, monosomy 6 has been associated with favorable survival (Clifford et al. 2006).

1.2.10 Other chromosome abnormalities

Other recurrent abnormality in MB included losses of 16q which were seen in 4%-37% of MBs, respectively (Avet-Loiseau et al. 1999; Eberhart et al. 2002; Nicholson et al. 1999; Reardon et al. 1997). The minimal deletion region for loss of chromosome 16q was marked at 16q22.2-qter (Lo et al. 2007a). Chromosomal 16q aberration was predominantly found in the non-WNT/SHH subgroups and absent in the WNT subgroup (Northcott et al. 2010). Study involving a large cohort of MBs indicated that 16q loss was over-represented in pediatric MBs (Korshunov et al. 2010).

1.3 Essential signaling pathways altered in MB

1.3.1 Sonic hedgehog (SHH) pathway

SHH is a major developmental pathway in many organisms (Lee et al. 2010). It plays a pivotal role in patterning, proliferation, and differentiation in a variety of

tissues. In addition, it is proposed that SHH participates in the establishment and maintenance of adult neurogenic niches and regulates the proliferation of neuronal or glial precursors in several brain areas (Traiffort et al. 2010).

PATCHED 1 (*PTCH1*) is a major player in the SHH pathway, which regulates the expansion and proliferation of cerebellar granule neuron precursor cells (GNPs) in the external granular layer (EGL) of the cerebellum during postnatal development (Wechsler-Reya and Scott 2001). During postnatal development, GNPs receive mitogenic SHH signals from Purkinje cells and become proliferating and expanding cells. Ultimately, they migrate from the EGL, pass the Purkinje cell layer, and arrive at the final destination in the internal germinal layer where they exit the cell cycle and differentiate into mature granule cells and become the most abundant neuronal cells in the cerebellum (Wechsler-Reya and Scott 2001).

Gorlin's syndrome, or nevoid basal cell carcinoma (NBCCS), is an autosomal dominant disease characterized by multiple developmental defects such as skeletal anomalies, jaw cysts, and macrocephaly. Affected individuals are also predisposed to develop multiple tumors, especially basal cell carcinoma, rhabdomyosarcoma and MB (Cowan et al. 1997; de Bont et al. 2008; Evan et al. 1991; Gorlin 1987). About 3-5% of patients with Gorlin's syndrome develop MBs (Cowan et al. 1997; Evan et al. 1991; Dhall 2009).

It was identified that NBCCS patients harbor *PTCH* mutations (Hahn et al. 1996). PTCH is a transmembrane receptor with 12 membrane-spanning domains and two extracellular loops (Hahn et al. 1996; Hooper and Scott 1989; Nakano et al. 1989). In the absence of ligand, PTCH represses the SHH pathway by repressing the activity of SMO, a seven transmembrane G coupled protein (Carpenter et al. 1998). Upon activation, PTCH relieves the inhibition of SMO receptor on the membrane. SMO is then translocated into the cytoplasm where transcription factor GLI family zinc finger 1 (GLI1) activity is repressed by the antagonist *suppressor of fused (SUFU)* through an unidentified mechanism (Gilbertson and Ellison 2008). In return, GLI1 is modified and translocated from cytoplasm to nucleus (Stecca et al. 2002). The presence of GLI1 in nucleus would activate transcription of SHH targets, including *MYCN* and *cyclin D1 (CCND1),* and *cyclin D2 (CCND2)* (Epstein et al. 1996; Kenney and Rowitch 2000; Kenney et al.2003), and drives GNP proliferation in cerebellum. Dysregulation of SHH pathway has been implicated in MB.

Activation of the SHH pathway is found in about 25% of MBs (Zurawel et al. 2000) and can occur through inactivation of *PTCH, SMO* or *SUFU.* Inactivation of *PTCH* by deletion or mutation has been found in about 10% of MBs (Raffel 2004). Mutations of *SMO* and *SUFU* have been described in less than 5% and about 10% of MBs, respectively (Reifenberger et al. 1998; Taylor et al. 2002). No mutations were

detected in other genes involved in SHH pathways, including *engrailed homeobox 1 (EN-1), engrailed homeobox 2 (EN-2), SMAD family members 1-7 (SMAD1-7), cAMP-dependent protein kinase (PKA) subunits RIα, RIβ, RIIβ, Cα*, and *Cβ* (Zurawel et al. 2000). The importance of *PTCH* in MB development is supported by animal studies. Although mice homozygous for *Ptch*$^{(-/-)}$ died at embryonic stage, hemizygous mice survived (Goodrich et al. 1997). About 19% of these hemizygous mice developed tumors closely resembled human MB within the first 25 weeks after birth (Goodrich et al. 1997). Further analysis showed that tumor cells expressed *Ptch* from the remaining wild-type allele, suggesting haploinsufficiency of *Ptch* would lead to MB in the mouse cerebellum (Zurawel et al. 2000). In fact, haploinsufficiency of *PTCH* may occur in human MB. Mutation of *PTCH* has been reported in tumors that do not harbor LOH of *PTCH* loci (Pietsch et al. 1997; Vorechovsky et al. 1997; Zurawel et al. 1999). Similarly, LOH of the 9q22 loci has been reported in tumors without harboring *PTCH* mutation in the remaining allele (Xie et al., 1997; Raffel et al., 1997; Zurawel et al. 2000). The important role of SHH signaling pathway in cerebellar tumor development was further emphasized by the observation that 58% of *Sufu(+/-)* and *p53(-/-)* mice developed MB (Lee et al. 2007).

1.3.2 Wingless (WNT) signaling pathway

WNT signaling is essential for development processes such as cell fate specification, cell proliferation, cell polarity, cell migration and organogenesis (Boras-Granic and Wysolmerski 2008; Itoh et al. 1998; Lee et al. 1999; Miller et al. 1999; Tsuda et al. 1999; Widelitz 2008). This pathway is activated when the ligand Wingless (WNT) binds to a receptor complex composed of a seven transmembrane Frizzled (FZ), serpentine receptor and low density lipoprotein receptor-related protein (LRP). This leads to phosphorylation of dishevelled (DVL), association with the AXIN, and prevention of *CTNNB1* phosphorylation by glycogen synthase kinase-3β (GSK-3β) (Jozwiak et al. 2007). The stabilized CTNNB1 is then translocated to the nucleus where it interacts with transcription factors T-cell factor (TCF) and lymphoid enhancer factor (LEF) (Behrens et al. 1996; Molenaar et al. 1996), and triggers transcription of genes such as *MYC, JUN, FRA and CCND1* (Gordon and Nusse 2006; He et al. 1998; Tetsu and McCormick 1999).

The role of WNT signaling in CNS development has been investigated by mouse model. Knockout of *Wnt-1* in mice led to failure in midbrain and cerebellum development (McMahon and Bradley 1990; Thomas and Capecchi 1990). In addition, mice lacking the *Fz* receptor showed loss of cerebellar granule and Purkinje cells in cerebellum (Wang et al. 2001). *Wnt-3* is expressed in cerebellum from embryonic to adult stages, (Salinas and Nusse 1992; Salinas et al. 1994). In adult, *Wnt-3* is found in

Purkinje cells and white matter of cerebellum (Salinas et al. 1994). These data suggest that the WNT signaling pathway is required for development and maintenance of cerebellum.

The other familial tumor syndrome associated with MB is the Turcot syndrome. It is characterized by the increased risk of colon cancer, glioblastoma and MB (de Bont et al. 2008). Patients with Turcot syndrome have a 92-fold higher relative risk of developing MB than the general population (Hamilton et al. 1995). Turcot syndrome patients carry germ-line mutations of the adenomatous polyposis coli (APC) gene in the WNT pathway (Hamilton et al. 1995).

APC acts as a negative regulator in the WNT pathway. It forms a multiprotein complex with other proteins, such as glycogen synthase kinase 3 (GSK-3β), axin 1 (AXIN), β-catenin (CTNNB1), casein kinase I (CKI), and protein phosphatase 2A (PP2A) in the cytoplasm. Phosphorylation of CTNNB1 by GSK-3β leads to inactivation of CTNNB1 through ubiquitin-mediated degradation (Orford et al. 1997).

In MB, activation of the WNT pathway was observed in 20-25% of cases (Clifford et al. 2006; Jozwiak et al. 2007). Aberrations in this pathway occur mainly through mutations of the *APC, CTNNB1, AXIN* and *GSK-3β* genes. Mutation of *CTNNB1* was observed in 2%-9% of MBs (Eberhart et al. 2000; Eberhart et al. 2004; Huang et al. 2000; Koch et al. 2001), and occurred at the GSK-3β phosphorylation sites

in exon 3 (Zurawel et al. 1998). This exon contains four potential GSK-3β phosphorylation sites. The affected GSK-3β phosphorylation sites reduce ubiquitin-mediated degradation resulting in nuclear CTNNB1 protein accumulation (Huang et al. 2000; Clifford et al. 2006; Koch et al. 2001 Zurawel et al. 1998). The *APC* mutations detected in MBs occurred in domains that interact with CTNNB1 or AXIN (Huang et al. 2000). These mutations may impair the APC protein to bind CTNNB1 or AXIN (Huang et al. 2000). Further investigation revealed that *APC* and *CTNNB1* mutations are mutually exclusive in MB, indicating that one of these aberrations is enough to activate the WNT pathway (Huang et al. 2000). Mutation analysis of *GSK-3β* gene has been investigated in a panel of 32 sporadic MBs. However, mutation was not detected in any of the cases, suggesting that *GSK-3β* gene mutation is not the major mechanism for WNT activation in MB (Zurawel et al. 1998). Mutation of *AXIN*, another negative regulator of the WNT signaling pathway, has been detected in 5% MBs (Baeza et al. 2003). The mutations were located at the amino acid responsible for binding to APC. This may decrease the ability of AXIN to bind APC and alter the downregulation of CTNNB1 (Baeza et al. 2003; Dahmen et al. 2001).

1.3.3 The Notch pathway

The Notch signaling pathway is important in determination of cell fate, cell

differentiation, cell proliferation and cell survival (Ehebauer et al. 2006). The Notch family consists of four receptors (NOTCH-1, -2, -3, and -4). Each of them is a single-pass transmembrane protein with an epidermal growth factor-like repeats within the extracellular domain and an intracellular domain containing RAM23 domain, ankyrin repeats, and PEST sequences (Guessous et al. 2008). The ligands known to bind Notch receptors include Delta-like proteins 1, 3 and 4 (DLL-1, -3, and -4) and Jagged proteins 1 and 2 (JAG-1 and -2) (Guessous et al. 2008). Upon the binding of ligands to Notch receptors, the alpha-secretases (ADAM-10 and ADAM-17) and gamma-secretase/presenilin complex cleave the extracellular domain and intracellular domain, respectively. The cleaved intracellular domain of NOTCH then translocates to nucleus, where it displaces the transcription repressor CBF-1 and recruit a coactivator complex, including histone acetyl-transferase p300 (p300), mastermind-like protein (MAML1-3) and other chromatin-modifying enzymes (Guessous et al. 2008; Pannuti et al. 2010). This in return activates the transcription of target genes included *hairy and enhancer of split 1 (HES1), hairy/enhancer-of-split related with YRPW motif 1 (HEY1), MYC,* and *cyclin-dependent kinase inhibitor 1A (p21).*

Accumulative data have indicated the importance of Notch signaling in MB. First, increase in copy number of *NOTCH2* gene was detected in 15% of MBs (Fan et al. 2004). Upregulation of Notch components, such as *NOTCH2* and *HES5*, was reported

in MB (Hallahan et al. 2004). Furthermore, the expression of *HES1*, a target gene of Notch signaling, was associated with shorter survival rate in MB (Fan et al. 2004). In addition, γ-secretase inhibitors (GSIs), which inhibit Notch signaling by preventing transmembrane NOTCH proteins from cleavage, decrease viable cell number in MB cells (Hallahan et al. 2004). More recently, it is of interest to reveal that blockage of Notch pathway caused viable populations of rapidly growing cells to continue to grow but these cells were unable to form soft-agar colonies or tumor xenografts efficiently (Fan et al. 2006). Further analysis of the stem cell marker CD133 in this population revealed that cell population for CD133 positive was reduced upon the inhibition of Notch pathway. These data suggest that the decrease in tumor-forming capacity could be due to the depletion of stem-like cells and maintenance of MB stem cells might require Notch signaling pathway (Fan et al. 2006).

1.4 Cancer stem cells in MB

With accumulative data showing that a subset of cancer cells may be responsible for tumor growth and resistance to therapy (Jorden et al. 2006), the hypothesis of cancer stem cells (CSCs) has been proposed. CSCs are a subset of cells within a tumor that exhibit significant proliferation capacity and the power to generate new tumor (Hadipansyis and Van Meir 2009). These CSCs are believed to arise from

transformation of proliferating neural stem cells (NSCs), which are found in different areas of the brain, including subventricular zone, dentate gyrus, hippocampus, and subcortical white matter. Similar to NSCs, CSCs are mulitpotent and have self-renewal and tumor-initiating capacity (Lapidot et al. 1994; Ignatova et al. 2002; Singh et al. 2004). Currently, CSCs have been successfully isolated from various brain tumors, including glioblastoma (GBM), MB and ependymoma (Galli et al. 2004; Hemmati et al. 2003; Singh et al. 2004; Taylor et al. 2005).

CSCs originally from MB specimens were isolated by culture conditions that favor the growth of stem cells (Singh et al. 2003). The conditions allowed the development of tumor sphere, which was characterized by clusters of neurosphere-like cells. Specifically, the conditions included the use of serum-free neural stem cell medium to maintain cells in undifferentiated state and the use of basic fibroblast growth factor (bFGF) and epidermal growth factor (EGF) to induce proliferation of multipotent, self-renewing stem cells. Frequency of stem cell isolated from MB primary tumors was ranged from 13.8-25.1% (Singh et al. 2003). These CSCs showed positive for CD133 (cluster of differentiation 133) marker (Singh et al. 2003). CD133 or Prominin-1, is a cell surface transmembrane glycoprotein with a molecular weight of 120 kilodalton (kDa). CD133-positive MB cells exhibited increased proliferation capacity and grew as nonadherent tumor sphere. In contrast, the CD133-negative cells neither showed

proliferation nor form tumor sphere (Singh et al. 2003).

Subsequent study demonstrated that CD133-positive cells had acquired the capability for tumor initiation. CD133-positive cell was contributed 6-21% of MB population (Singh et al. 2004). Injection of as few as 1000 CD133-positive cells could form MB tumors in severe combined immunodeficiency mice, whereas 10-fold excess CD133-negative cells did not form tumors (Calabrese et al. 2007; Singh et al. 2004). The results provide an insight that by modulating the fraction of CSCs in MB, the clinical outcome could be improved.

1.5 Molecular subtyping of MB

Integrative genomic studies using gene expression profiling, aCGH, miRNA microarray and SNP microarrays have identified several molecular subgroups (Kool et al. 2008; Northcott et al. 2010; Thompson et al. 2006; Cho et al. 2010). This finding highlights the heterogeneous property of MB. Using unsupervised hierarchical clustering methods, Kool et al. and Thompson et al. suggested the presence of five subgroups in MB, whereas Northcott et al. argued for the presence of four subgroups. The discrepancy among these studies can be explained by difference in the microarray platforms and the number of genes used for clustering. Nevertheless, all of these studies have identified the subgroups as WNT, SHH, and the non-WNT/SHH. The WNT and

SHH subgroups account for 15% and 25% of MBs, respectively, whereas the non-WNT/SHH subgroups constitute 60% of MBs (Ellison 2010). In addition, each of these subgroups exhibits distinct expression signature, specific genetic defects, and some of these subgroups exhibit activation of distinct pathways. The clinical, histological characteristic and outcomes are also different among these subgroups. Table 1 summarizes the clinicopathological features and genetic aberration associated with these molecular subgroups in MB.

1.5.1 MB with activated SHH signaling

A subgroup of MB is marked by the activation of SHH signaling. The genes involved in this signaling pathway such as *PTCH, secreted frizzled-related protein 1 (SFRP1), GLI1 and GLI family zinc finger 2 (GLI2)* were overexpressed. Mutations of *PTCH* and *SUFU* were found in this subgroup, confirming the activation of SHH pathway. Loss of chromosomal 9q is a frequent event in this subgroup. SHH subgroup tumors are common in infants with age under three years old and adulthood with age over 16 years old (Kool et al. 2008; Northcott et al. 2010). Both Kool et al. and Northcott et al. studies demonstrated that 40-60% and 20-30% of SHH subgroup were infants and adult, respectively. In addition, most of the tumors present with classic or desmoplastic histology (Kool et al. 2008; Northcott et al. 2010). Occassionally, LC/A

Table 1. Clinicopathological and genetic features of molecular subtypes in MB

Subtypes	WNT	SHH	non-WNT/SHH
Expression characteristic	WNT/TGF signaling NOTCH/PDGF signaling	SHH signaling NOTCH/PDGF signaling	Neuronal and/ or photoreceptor markers
Chromosomal characteristic	monosomy 6 *CTNNB1* mutation	loss of 9q *PTCH/SMO/SUFU* mutation	i17q loss of X gain of 18
Pathological variants	classic	desmoplastic/ classic	classic/ LC/A
Metastasis at presentation	rarely metastatic	rarely metastatic	frequently metastatic
Age groups	older children	mainly infants and adults	mainly children
Prognosis	good	infant good other intermediate	poor

References: Cho et al. 2010; Kool et al. 2008; Northcott et al. 2010; Thompson et al. 2006

tumors were seen (Ellison 2010).

1.5.2 MBs with activated WNT signaling

One of the major molecular subgroups is the WNT subgroup which shows activation of WNT signaling. Overexpression of genes that are involved in this pathway includes *lymphoid enhancer-binding factor 1 (LEF1), WNT inhibitory factor 1 (WIF1), dickkopf homolog 1 (DKK1), dickkopf homolog 2 (DKK2), and dickkopf homolog 4 (DKK4)* (Kool et al. 2008; Northcott et al. 2010; Thompson et al. 2006). In agreement with the involvement of *CTNNB1* in WNT signaling, only this subgroup showed *CTNNB1* mutation as revealed by direct sequencing (Kool et al. 2008; Thompson et al. 2006). Monosomy of chromosome 6 was a distinctive feature in this subgroup. Loss of 9q, i17q and *MYCN/MYC* amplification were absent in WNT subgroup (Kool et al. 2008). Moreover, classic histology and distributed age presentation ranging from infancy to adult were prevalent (Cho et al. 2010; Kool et al. 2008; Northcott et al. 2010). The prognosis of this subgroup was good if high-risk features were not presented.

1.5.3 Non-WNT/SHH subgroups

Kool et al. and Northcott et al. showed that about 85% of cases in non-WNT/SHH subgroups were children greater than three years old (Kool et al. 2008;

Northcott et al. 2010). These subgroups were characterized by the activation of phototransduction pathway (Pfister et al. 2010). Furthermore, these subgroups displayed similar chromosomal defects. For examples, i17q was strongly associated with these subgroups (Kool et al. 2008; Northcott et al. 2010; Thompson et al. 2006). Moreover, about one-third of tumors in these subgroups displayed loss of chromosome 18, which was not found in any of the tumors in WNT and SHH subtypes. This indicates that loss of chromosome 18 is a common event in non-WNT/SHH subtypes (Kool et al. 2008). Other overlapped chromosomal abnormalities in these subtypes include loss of chromosome 8 and gain of chromosome 17q (Kool et al. 2008 and Northcott et al. 2010). Similar to the WNT subtype, most of the tumors showed classic histology. However, tumors in this subtype showed poor clinical outcome. This may be attributed to a high prevalence of metastatic tumors in these subtypes.

CHAPTER 2

INTRODUCTION TO MICRORNAS (miRNAs)

2.1 Properties of miRNAs

MiRNAs are a group of small noncoding RNAs of 22-25 nucleotides (nts) that function to regulate gene expression at the post-transcriptional level. They have been implicated in diverse biological functions including development (Moss et al. 1997), differentiation (Chen et al. 2004), cell fate determination (Tiscornia and Izpisúa Belmonte 2010), cell patterning (Sehm et al. 2009), cell morphogenesis (Giraldez et al. 2005), and fat metabolism (Xu et al. 2003). MiRNAs are found in the exonic and intronic regions of protein-coding and noncoding genes of all chromosomes except the Y chromosome in human.

2.2 Discovery of miRNAs

In 1993, Lee and his coworkers discovered the first miRNA, lin-4, through genetic screen for mutant phenotype of timing development in *Caenorhabditis elegans* (Lee et al. 1993; Wightman et al. 1993). It was not until seven years later that the second miRNA, let-7, was identified (Reinhart et al. 2000). Both lin-4 and let-7 were evolutionarily conserved from flies to humans, implicating a universal role for these genes across species (Lagos-Quintana et al., 2002; Pasquinelli et al., 2000).

2.3 miRNA registry

The human genome is predicted to encode as many as 1000 miRNAs, which account for 1-4 % of expressed genes (Bentwich et al. 2005; Griffiths-Jones et al. 2004). Currently, the miRBase registry (http://www.mirbase.org/; version 16, September 2010) contains 14,940 miRNAs from 122 species, in which 1,048 of them are of human.

Computational algorithm predicts that a miRNA can modulate about 200 transcripts and each gene can be regulated by many miRNAs (Krek et al. 2005). It is estimated that miRNAs potentially regulate between 10-30% of the human genes (John et al. 2004; Lewis et al. 2003).

2.4 Nomenclature of miRNAs

MicroRNAs are named with the "miR" prefix followed by a number (Ambros et al. 2003). Mature miRNAs of nearly identical sequences, usually differ by 1-3 nts, are designated with a letter. Examples are let-7b and let-7c. MiRNAs that are located on different chromosomes but have identical mature sequences are designated with a number. Examples are let-7a-1 and let-7a-2.

2.5 Approaches for miRNA identification

The major approaches for miRNA identification include forward genetics,

directional cloning and *in silico* predictions. For example, *bantam,* which is involved in growth control during development of *Drosophila melanogaster*, was identified by forward genetics. Directional cloning of miRNAs involves size-fractionation of RNAs in a denaturing polyacrylamide gel, cloning them into vectors, and sequencing the RNA library (Lagos-Quintana et al. 2001; Lagos-Quintana et al. 2002). Another method for miRNA identification is computational prediction. Most algorithms rely on the distinctive properties of miRNAs, including hairpin folding, thermodynamic stability of the hairpins, and phylogenetic conservation.

2.6 Biogenesis of miRNAs

The biogenesis of miRNAs is tightly regulated. Most miRNA genes are transcribed by RNA polymerase II into primary miRNAs (pri-miRNAs) of hundreds bases to kilobases in length (Cai et al. 2004; Lee et al. 2004). The pri-miRNAs, resembling protein-coding transcripts, contain 7-methylguanosine cap and poly-A tail (Cai et al. 2004; Lee et al. 2004). The pri-miRNAs are cleaved by type III ribonuclease DROSHA to generate precursor miRNAs (pre-miRNAs) of about 70 nts in the nucleus (Lee et al. 2003; Zeng et al. 2006). The pre-miRNAs are characterized by a hairpin structure with a 2-nt overhang at the 3' ends (Lee et al. 2003). The pre-miRNAs are transported to the cytoplasm by exportin-5 through GTP hydrolysis (Bohnsack et al.

2004; Yi et al. 2005). In the cytoplasm, a type III ribonuclease, DICER, cleaves pre-miRNA near the terminal loop to generate the ~22-nt miRNA duplexes (Bernstein et al. 2001; Grishok et al. 2001; Hutvágner et al. 2001; Ketting et al. 2001). The miRNA duplex is then loaded onto the RNA-induced silencing (RISC) complex (Gregory et al. 2005). This process requires ATP hydrolysis (Kwak et al. 2010). After loading onto RISC, the two strands of the duplex are unwound (Kwak et al. 2010; Salzman et al. 2007). Usually, one strand becomes the mature miRNA, whereas the other strand is subjected to degradation. The relative thermodynamic stability of two strands determines which strand remains the RISC. This miRNA containing complex functions to modulate the expression of target genes by translational repression and/or mRNA degradation of target mRNA.

2.7 Mechanisms of miRNA-mediated gene expression

2.7.1 Interactions between miRNA and target gene

MiRNAs negatively regulate gene expression by complementary base-pairing interactions between the miRNAs and usually the 3' UTRs of their target mRNAs (Bartel 2009; Lai 2002). The 5' regions of miRNAs (nts 2-8) are thought to be a major determinant for miRNA targeting (Lewis et al. 2005). This region is referred to the 'seed region' (Brennecke et al. 2005). As few as 4 continuous base-pairings in nts 2–5 at

the 5'end can confer efficient target recognition (Brennecke et al. 2005). However, other features on the 3'UTR are important for target recognition (Lewis et al. 2005; Grimson et al. 2007). These include the presence of A (first nt) prior to the seed region on the target, base-pairing to miRNA nts 13-16, the target position within the 3'UTR at least 15 nts from the stop codon and away from the centre of long UTRs, and target position near both ends of the 3'UTR (Lewis et al. 2005; Grimson et al. 2007). The mechanisms by which miRNAs regulate gene expression include mRNA cleavage and translational repression, depending on the extent of base pairing between miRNAs and target mRNAs (Ambro 2004; Cullen 2004).

2.7.2 miRNA-mediated translational repression

Accumulative evidence shows that miRNAs can downregulate protein expression without altering mRNA abundance. For example, miR-155 regulates angiotensin II type 1 receptor (AT1R) at the protein level (Card et al. 2008; Martin et al. 2006).

The mechanism of translational repression is largely unknown. MiRNA-mediated translational repression may occur at the initiation phase of protein synthesis and at the stage of post-initiation elongation (Baek et al. 2008; Bhattacharyya et al. 2006; Humphreys et al. 2005, Mathonnet et al. 2007; Nottrott et al. 2006; Olsen et

al. 1999; Petersen et al. 2006; Pillai et al. 2005; Wakiyama et al. 2007; Wang et al. 2006). Several lines of evidence support translational repression at the translational initiation phase. First, miRNA-repressed mRNAs are sedimented in the subpolysomal fractions suggesting they are translationally inactive (Bhattacharyya et al. 2006; Pillai et al. 2005). Second, a sequence similar to eukaryotic initiation factor 4E (EIF4E) was identified within the human Argonaute2 (AGO2) and it was proposed that AGO2 competes with eIF4E for the 7-methyl guanosine (m7G) cap of mRNA through the EIF4E-like motif and thus represses the formation of the translation initiation complex (Kiriakidou et al. 2007). Moreover, miRNAs have been shown to inhibit translation initiation by suppression of ribosome assembly (Chendrimada et al. 2007).

Moreover, evidence also points to miRNA-silenced gene expression through blockage of protein synthesis after the initiation of translation. First, the amount of *lin-14* mRNA in polyribosomes remains unaltered in the presence of lin-4 RNA binding, suggesting that post-translational inhibition occurs at a point downstream of translation initiation (Olsen and Ambros 1999). Moreover, two independent studies have demonstrated that miRNA-repressed mRNAs remain associated with actively translating polyribosomes, leading to the hypothesis that miRNAs may cause elongation retardation leading to premature translation termination or induction of degradation of nascent polypeptides during the translational process (Nottrott et al. 2006; Petersen et al.

2006).

2.7.3 miRNA-mediated mRNA cleavage

Studies have indicated that miRNAs could reduce the levels of their target transcripts by mRNA degradation. Perfect matching of the seed region was thought to be necessary for mRNA cleavage, but subsequent studies revealed that imperfect base-pairing could also induce transcript degradation (Goswami et al. 2010).

It has been suggested that deadenylation and the removal of the 3' poly(A) tail initiate mRNA degradation (Wu et al. 2006). The processing bodies (P-bodies) are believed to be the final site for mRNA turnover (Sen and Blau 2005). They are discrete cytoplasmic domains where untranslated mRNA is stored and contain the enzymes needed for mRNA degradation (Dijk et al. 2002).

2.8 Identification of miRNA targets

2.8.1 Computational prediction

Comparative phylogenetic studies reveal conserved miRNA-binding sequences in more then one-third of all genes. However, only a small number of predicted targets have actually been validated (Lewis et al. 2003). In the absence of high-throughput experimental techniques to identify miRNA targets, several computational algorithms

have been developed to predict miRNA targets. These algorithms aim to predict targets with high degree of specificity (few false-positive) and sensitivity (few false negative). To my knowledge, a total of 11 algorithms are available for miRNA target prediction. Here, four of them are described, namely, miRanda (http://www.microrna.org) (Enright et al. 2003), TargetScan (http://www.targetscan.org/archives.html) (Lewis et al. 2003), TargetScanS (http://www.targetscan.org/) (Lewis et al. 2005), and PicTar (http://www.pictar.bio.nyu.edu) (Krek et al. 2005). In each of these programs, a scoring system is established based on various degrees of consideration in the following issues: the degree of complementary between target and miRNA pairing, thermodynamic stability analysis and the conservation of the target sequence across species.

miRanda is a position-weighted scoring system that has been established based on emphasizing the degree of complementary in the seed region (Enright et al. 2003; Stark et al. 2003). The complementary base-pairing at the 5' end of the miRNA is rewarded more than that that the 3' end. The complementary base-pairing at 3' end is considered less important (Brennecke et al. 2005; Kiriakidou et al. 2004; Stark et al. 2003). Nevertheless, strong binding at the 3' end may compensate for the weak binding in the 5' end (Brennecke et al. 2005; Doench and Sharp 2004). Hence, potential targets without perfect matching at the seed region can still be predicted. The binding sites are then evaluated thermodynamically using the Vienna RNA folding package (Wuchty et

al. 1999) which estimates free energy and secondary structure of the miRNA-target interaction. Cross-species conservation of the binding sites is also considered. This algorithm has correctly identified 9 out of 10 validated miRNA targets and has an estimated 24%-39% false positive rate (Enright et al. 2003). A new version of miRanda has tightened the binding requirement to almost-perfect complementarily in the seed region and allows only a single wobble pairing (John et al. 2004). The G:U wobble base pairing is considered weak base pairing that could reduce silencing efficiency (Doench and Sharp 2004).

TargetScan and TargetScanS algorithms were developed by Lewis and colleagues to identify potential miRNA targets in mammals. In contrast to other prediction alogorithms including miRanda, and PicTar, TargetScan requires 7-nt perfect Watson-Crick matching in the seed region starting from the second nucleotide to the 5' end of miRNAs (Lewis et al. 2003). In addition, the program accounts complementarily outside the region, extending until encountered a mistmatch with allowance for G:U pairs. This aims to filter as many false positive as possible from the beginning of prediction. The predicted binding sites are then tested for thermodynamic free energy (ΔG) using the Vienna RNA folding package and for conservation across mouse, rat and pufferfish genomes. This ranking system has an estimated false-positive rate of 31% for mammalian miRNA targets. TargetScanS is a modified version algorithm that requires a

6-nt match in the seed region preceded by an adenosine (Lewis et al. 2005). Calculation of the free energy is no longer required, but it requires target-site conservation across all five genomes (human, mouse, rat, dog, and chicken). The definition of conservation in TargetScanS is that the seed region required at the same corresponding positions in multiple species UTR alignment. These changes reduce the estimated false-positive rate to 22% in mammals (Lewis et al. 2005).

PicTar was developed by Krek and co-workers (Krek et al. 2005). It relies fully on comparative data from several species to identify common targets of miRNAs. Its input is a group of miRNAs and a group of orthologous 3'UTRs from multiple species (human, chimpanzee, mouse, rat, dog, chicken, pufferfish and zebrafish). The algorithm then scans for alignments of 3'UTRs for those miRNAs have base pairing in the seed region. In contrast to TargetScanS, PicTar only requires the complementary found in overlapping positions in the 3'UTRs of multiple species. In addition, perfect complementary is not definitely required in the seed region given that it is thermodynamic stable. The scoring system also considers the co-expression of miRNAs and their targets in spatially and temporally manners. PicTar has been tested on 13 predicted targets of two miRNAs using western blotting analysis or luciferase reporter assay. Validation was shown in seven out of these 13 predicted miRNA targets (Krek et al. 2005).

One of the pitfalls of these algorithms is that they only predict potential targets that are conserved across species. Nonconserved miRNA-target interactions may not be predicted by these programs. MirTarget2 (http://mirdb.org) is an algorithm allowed for prediction of non-conserved miRNA-target interactions in five species (Wang and El Naqa 2008). In addition, the miRNA database TarBase (http://microrna.gr/tarbase) collects experimentally validated miRNA-target pairs, of which some are nonconserved miRNA-target interactions. Examples are miR-124/RELA and miR-375/C1QBP.

2.8.2 Experimental strategies

Besides bioinformatic analysis to identify miRNA targets, several experimental methods have been applied to search for miRNA target genes. One approach is to use microarray to profile the global expression changes upon overexpression or knockdown of miRNAs (Nicolas et al. 2008; Ziegelbauer et al. 2009). This method is based on the observation that miRNAs would downregulate mRNA levels of their target genes. The reduced mRNAs are then searched for base-pairing in the seed region of miRNAs to filter out downregulated genes without miRNA-mRNA interaction. Potential miRNA targets can be further confirmed by luciferase reporter assay, in which the 3'UTRs of target genes are cloned into luciferase reporter plasmids (Lim et al. 2005) or by western blotting analysis to examine the change in protein level (Pais et al. 2010). Another

experimental method is the application of co-immunoprecipitation assay to isolate miRNA targets (Beitzinger et al. 2007; Easow et al. 2007). This method is based on the observation that AGO proteins or RISC bind to both miRNAs and mRNAs. Using antibodies against AGO proteins, the AGO-bound mRNA can be isolated. A cDNA library is then generated. Validation of miRNA–mRNA interaction can be carried by luciferase reporter assay. This method has an advantage to isolate tissue specific miRNA-mRNA interaction. Recently, a new strategy to identify the target genes of miRNAs has been established. It is based on the incorporation of an isotope-labeled amino acid in cell culture followed by quantitative-mass-spectrometry-based study to examine the effect of miRNAs in the abundance of many proteins (Baek et al. 2008; Selbach et al. 2008). In conclusion, multiple approaches have been developed for accurate identification of miRNA targets. Combination of these strategies may enhance the efficiency and increase sensitivity and specificity of target identification.

2.9 Expression pattern of miRNAs in normal tissues

Systematic analysis of the spatial expression of miRNAs indicates that many miRNAs are expressed in a tissue-specific manner (Lagos-Quintana et al. 2002; Wienholds et al. 2005). The term tissue specific has been defined recently as a mature miRNA that is expressed at >20-fold higher level in a specific tissue as compared to the

mean expression in all other tissues (Lee et al. 2008). For examples, expression of mature miR-1 is reported to be expressed only in the human heart but not in the brain, kidney, liver, lung, and HeLa cells (Lee et al. 2001; Lagos-Quintana et al. 2001; Lim et al. 2005; Chen et al 2006), whereas the miR-18/19a, miR-122 and miR-9/miR-124 are specifically found in lung, liver, and brain respectively (Sempere et al. 2004). Evidence has been provided to demonstrate that the processing of precursor to mature miRNAs is not in a stoichiometric manner (Jiang et al. 2005). Moreover, many miRNAs display dynamic temporal expression patterns. For instance, miR-124 shows increasing expression during the embryonic development in forebrain and its expression remains stable postnatal. MiR-19b exhibits strong expression in prenatal forebrain and is undetectable at adult stage (Krichevsky et al. 2003). These findings suggest that miRNAs possess unique functions in the establishment and maintenance of tissues types. More important, inappropriate regulation in miRNA expression either in a spatial or temporal manner may be responsible for disease pathogenesis.

2.10 MiRNAs in cancers

2.10.1 Deregulation of miRNAs in cancers

The first evidence for miRNA involvement in tumorigenesis was the identification of loss of miR-15a and miR-16a, residing on a commonly deleted interval

on chromosome 13q14, in chronic lymphocytic leukaemia (CLL). Expression analysis demonstrated that deregulation of these miRNAs occurred in approximately 70% of CLL (Calin et al. 2002). Downregulation of miR-15a and miR-16a was also found in pituitary adenomas and prostate cancer, in which loss of chromosomal 13q14 is a common event (Bonci et al. 2008; Bottoni et al. 2005; Fan et al. 2001). Moreover, about half of the miRNAs are located within the cancer-associated genomic regions or fragile sites, including regions of allelic loss, amplification and common breakpoint regions (Calin et al. 2004).

Aberrant expressions of miRNAs are common in human cancers. MiR-143/145 cluster and miR-7 were downregulated in pancreatic tumors and schwannoma, respectively (Kent et al. 2010; Saydam et al. 2010). MiR-92a and miR-183 were overexpressed in esophageal squamous cell carcinoma and colon cancer, respectively (Chen et al. 2010; Sarver et al. 2010).

2.10.2 MiRNAs with oncogene- or tumor suppressor gene-like functions

Tumor formation is the result of abnormalities in the control of cell growth or in the loss of apoptosis. MiRNAs involved in cell growth, apoptosis or differentiation can be deregulated in tumors and may function as oncogenes or tumor suppressors.

MiRNAs that promote tumor development are called "oncomirs", whose

expressions are increased in tumors. Oncomirs can repress TSGs or genes involved in apoptosis. For example, the first validated oncomir was the miR-17-92 cluster, which targets TSGs *PTEN* and *retinoblastoma-like 2 (RB2)* (He et al., 2005; Hammond, 2006; Voorhoeve et al. 2006).

The tumor suppressor-like miRNAs prevent tumor formation by inhibiting oncogenes or genes controlling apoptosis. Their expressions are reduced in tumors. For example, lung tumors showed downregulation of let-7 and overexpression of RAS protein. It was demonstrated that let-60/RAS was the target of let-7 in lung tumors (Johnson et al., 2005).

2.10.3 Mechanisms of miRNA deregulation

Several mechanisms have been identified for miRNA deregulation in tumors. The most common one is alteration of genomic copy number, including deletion and amplification. An example of miRNA inactivation through genomic deletion is miR-15a and miR-16-a in CLL mentioned above. The miR-17-92 cluster is an example of upregulated miRNA in B-cell lymphoma through copy number gain at 13q31.3 where the cluster is resided (He et al. 2005; Tagawa et al. 2005).

Other mechanisms for the abnormally expressed miRNAs in tumors are mutation, SNP, disruption of miRNA processing machinery players, CpG island

hypermethylation and activation of transcription factors. For example, substitution mutation in the pri-miR-16-1 sequence was identified in CLL patient, leading to reduced expression in vivo (Calin et al. 2005). Mutation is not limited to pri-miRNA; recently, mutation in the mature miRNAs (miR-125a) has been found in 8.3% of breast cancer (Li et al. 2009).

In addition, a SNP in the pre-miR-146a sequence was identified in papillary thyroid carcinoma, and this common polymorphism decreased the amount of mature miRNA, and was a predisposing factor for papillary thyroid carcinoma (Jazdzewski et al. 2008). Aberration of miRNA processing machinery players, such as *DICER1* and *DROSHA* has been identified in multiple cancers (Merritt et al. 2008; Pampalakis et al. 2010; Sand et al. 2010). The expression level of *DICER1* was significantly associated with clinical parameters, such as tumor stage in ovarian cancer and poor prognosis in lung cancer (Karube et al. 2005; Merritt et al. 2008). Functional analysis of *DICER1* indicated that monoallelic loss of *DICER1* promoted tumorigenesis in vivo (Lambertz et al. 2010).

The fact that most miRNAs are transcribed by the same RNA polymerase II as protein-coding genes, it is likely that the epigenetic mechanisms which modulate the expression of protein-coding genes also apply to miRNAs. Such epigenetic mechanisms commonly refer to the methylation of cytosines in the CpG islands located in miRNA

promoters and this alteration results in a suppression of gene expression (Taby and Issa 2010). Saito et al. demonstrated the expression miR-127 was under the control of promoter methylation and its expression was decreased in bladder and prostate cancers. Expression of miR-127 could be restored by the demethylating agent 5-aza-2'-deoxycytidine (5-aza-dC) and the histone deacetylase inhibitor phenylbutyrate (Saito et al. 2006). A number of other studies have also reported DNA hypermethylation of miR-34b, -137, -148a, -181c, -193a, and -203 in multiple cancers (Hashimoto et al. 2010; Kozaki et al. 2008; Lujambio et al. 2008; Toyota et al. 2008).

Recent DNA structure analysis has revealed features in protein-coding gene promoters can be found in miRNA promoters (Corcoran et al. 2009). This suggests the mechanisms such as transcription factors that govern the expression of protein coding genes can be exerted on miRNAs. An example is the well characterized helix-loop-helix leucine zipper transcription factor, *MYC*. This gene not only regulates ~10 to 15% of human gene expression (Eilers and Eisenman 2008), but also positively and negatively modulates miRNA expression. It promotes the expression of miRNAs in miR-17-92 cluster through interaction with the promoter (O'Donnell et al. 2005; Chang et al. 2008).

2.10.4 Clinical significance of miRNAs

MiRNAs have been implicated in multiple clinical applications. MiRNA profile

has been shown to be more accurate than transcript pattern in classifying some tumor types (Lu et al. 2005). MiRNA signatures were possibly more effective diagnostic biomarkers for tracing back the origin of cancers with unknown primary origin (Rosenfeld et al. 2008). Moreover, miRNAs could be a potential marker for disease progression. miR-196a showed increasing expression from low grade lesion to esophageal adenocarcinoma (Maru et al. 2009). Besides serving as diagnostic and disease progression markers, miRNA expression would be a potential biomarker for treatment response. For instance, miR-34a was associated with impaired DNA damage response, apoptosis resistance in response to γ-irradiation and chemotherapy resistance (Zenz et al. 2009). High expression of miR-21 was associated with poor fluorouracil based treatment in colon adenocarcinoma (Schetter et al. 2008). Lastly, miRNAs have been suggested as a potential survival marker. High expression of miR-21, miR-155, and miR-196a-2 was associated with poor survival in colon, lung and pancreatic cancers respectively (Bloomston et al. 2007; Schetter et al. 2008; Yanaihara et al. 2006). Combination of low let-7d and miR-205 expression was associated with poor survival in head and neck squamous cell cancer (Childs et al. 2009). Taken together, miRNA expression may serve as potential markers for diagnosis, disease progression, treatment prediction and prognosis.

2.11 MiRNAs in brain tumors

Accumulative evidence indicates that miRNAs are aberrantly expressed in CNS tumors. For instance, in gliomas, upregulation of miR-10b, miR-21, and miR-221 and downregulation of miR-128, miR-124, miR-137, miR-139, miR-218 and miR-323 have been identified using global expression profiling and quantitative RT-PCR (Chan et al. 2005; Ciafrè et al. 2005; Silber et al. 2008). Table 2 summarizes the aberrantly expressed miRNAs observed in gliomas.

Increased miR-21 expression was observed in high-grade gliomas (Chan et al. 2005; Ciafrè et al. 2005; Silber et al. 2008). *In vitro,* inhibition of miR-21 reduced cell proliferation by inducing apoptosis (Chan et al. 2005). Suppression of miR-21 also reduced tumor migration, invasion, and tumorigenicity through regulation of reversion-inducing-cysteine-rich protein with kazal motifs (RECK) and metalloproteinase inhibitor 3 (TIMP3), which are inhibitors of matrix metalloproteinases essential for invasiveness and metastasis of various cancers (Correa et al. 2006; Gabriely et al. 2008; Oh et al. 2001). Other targets of miR-21 are heterogeneous nuclear ribonucleoprotein K (HNRPK), tumor protein p63 (TP73L) and programmed cell death 4 (PDCD4), all of which have been implicated in tumorigenesis (Papagiannakopoulos et al. 2008). Together, these data suggest an oncogenic role of miR-21.

Table 2. Dysregulated miRNAs found in gliomas

Overexpressed miRNAs	References	Underexpressed miRNAs	References
miR-9-2	81	miR-7	449
miR-10b	81, 167, 449	miR-29b	449
miR-16	153	miR-31	449
miR-21	449	miR-101	449
miR-25	81	miR-107	449
miR-26a	167	miR-124	167, 449
miR-107	153	miR-124-2	449
miR-123	81	miR-128-1	81, 167, 449
miR-125b-1	81	miR-128-2	167
miR-125b-2	81	miR-129	449
miR-130	81	miR-132	449
miR-155	449	miR-133a	449
miR-185	153	miR-133b	449
miR-210	449	miR-137	167, 449
miR-221	81	miR-138	449
miR-383	167	miR-139	449
miR-425	153	miR-149	449
miR-451	153, 167	miR-153	449
miR-486	153, 167	miR-154	449
miR-516-3p	167	miR-181a	81
miR-519d	167	miR-181b	81
		miR-181c	81
		miR-185	449
		miR-187	449
		miR-190	167
		miR-203	449
		miR-218	167, 449
		miR-299	167
		miR-323	167, 449
		miR-328	449
		miR-330	449
		miR-483	167
		miR-511-1	167

Overexpression of miR-17-92 cluster has been reported in glioblastoma multiforme (GBM) (Ernst et al. 2010). Copy number gain was one of the mechanisms for miR-17-92 upregulation (Ernst et al. 2010). Knockdown of the miR-17-92 cluster led to inhibited cell proliferation and induced apoptosis (Ernst et al. 2010). These data suggest a role of miR-17-92 cluster in GBM oncogenesis.

Downregulation of miR-128 has been reported in gliomas (Ciafrè et al. 2005; Godlewski et al. 2008; Gaur et al. 2007). MiR-128 inhibited cell proliferation through targeting E2F transcription factor 3 (E2F3) (Zhang et al. 2009). It also downregulated BMI1 polycomb ring finger oncogene (BMI-1), a member of polycomb group complex 1 that is involved in stem cell renewal (Godlewski et al. 2008). Forced expression of miR-128 inhibited glioma cell growth *in vitro* and glioma xenograft growth *in vivo*, indicating the involvement of miR-128 in oncogenesis (Godlewski et al. 2008).

miR-124 and miR-137 were found to have reduced expression in high-grade gliomas including GBM and anaplastic astrocytoma (Siber et al. 2008). In GBM cells lines, treatment with a combination of 5-aza-dC and histone deacetylase inhibitor, trichostatin A (TSA) enhanced 2-fold and 8-fold expression in miR-124 and miR-137, respectively. This result suggests epigenetic modification may contribute to underexpression of miR-124 and miR-137 in GBM. Furthermore, overexpression of miR-124 and miR-137 induced G0/G1 arrest, reduced both CDK6 expression and

phosphorylated retinoblastoma (RB) expression. Thus, aberrant expression of miR-124 and miR-137 may contribute to gliomagenesis through modulating cell cycle progression by targeting important cell cycle regulator.

Aside from gliomas, miRNAs are associated with a number of other CNS tumors. For example, dysregulation of miR-200a was found in meningioma (Saydam et al. 2009). MiR-200a conferred a growth inhibition effect in meningioma, through targeting CTNNB1 and inhibiting WNT signaling pathway. Moreover, miR-222 and miR-222 were upregulated in atypical teratoid/rhabdoid tumors and these miRNAs modulated the expression cell cycle inhibitor p27 (KIP1) (Sredni et al. 2009).

Other studies have been taken to investigate the relationship between miRNAs expression and clinicpathological features or clinical outcome. MiR-21 expression was correlated with glioma grade, and its expression increased during progression from low to high grade (Gabriely et al. 2008). Members of the miR-17-92 cluster showed increased expression during tumor progression in glioma (Ernst et al. 2010). These results are in line with the data shown by Malzkorn et al (Malzkorn et al. 2010).

The value of miRNA in predicting treatment outcome has been recently determined by Slaby and his colleagues. They demonstrated that miR-181b and miR-181c expression were significantly downregulated in GBM patients who responded to concomitant chemoradiotherapy with temozolomide (Slaby et al. 2010).

Together, these studies provide implication that miRNAs expression may have diagnostic, predictive and prognostic values.

2.12 MiRNAs in MB

Accumulative data have indicated that miRNAs are involved in MB tumorigenesis. The first miRNA study in MB was reported by Pierson and his colleagues who demonstrated that miR-124 expression was reduced in all primary MB and cell lines, and this miRNA modulated the expression of CDK6, a critical cell cycle regulator (Pierson et al. 2006). Tumors with low miR-124 showed an increased CDK6 expression. Furthermore, ectopic expression of miR-124 inhibited cell growth in MB. Recently, miR-129 was shown to downregulate CDK6, and its expression was reduced in MB (Wu et al. 2010). Taken together, these results provide the first link between miRNAs and MB tumorigenesis.

Ferretti and his colleagues identified specific miRNAs that were involved in a subset of MBs with activated SHH pathway (Ferretti et al. 2008). They compared the miRNA profiles of 250 miRNAs between two groups of MBs with either high or low level of *GLI1*, an effector of SHH pathway, and identified 30 differential expressed miRNAs, with downregulation of miR-125b, miR-326, and miR-324-5p detected in *GLI1*-high expressed cases. These miRNAs were able to suppress the activator *SMO*

through direct binding to the 3'UTR of *SMO*. Overexpression of these miRNAs reduced expressions of *SMO, GLI1* and *PTCH*. In addition, re-expression of these miRNAs inhibited cell proliferation and reduced the number and size of colony formation *in vitro*, whereas depletion of these miRNAs enhanced cell proliferation. These results suggest that deregulation of miRNAs involved in SHH pathway plays a role in MB formation.

Besides, miR-125b, miR-326, and miR-324-5p were upregulated during differentiation of granule progenitor cells (GPCs) when growth rate was reduced (Ferretti et al. 2008). When these miRNAs were repressed during the course of GPC differentiation, cell proliferation increased (Ferretti et al. 2008). Transfection of these miRNAs suppressed GPC proliferation induced by SHH. Together, these results demonstrated that dysregulation of miRNAs in MB would lead to activation of SHH signaling, disruption in GCP differentiation and promotion of MB development.

To elucidate the role of miRNAs in MB development, Uziel and his colleagues applied comparative expression analysis and identified upregulation of miR-92, miR-19a, and miR-20, all of which resided in the miR-17/92 cluster, in mouse and human MB with constitutively active SHH pathway (Uziel et al. 2009). Enforced expression of these miRNAs in proliferating GNPs derived from *Ink4c-/-;Ptch+/-* mice caused MB formation with complete penetrance. In contrast, enforced expression of these miRNAs in GNPs in *Ink4c(-/-);Tp53(+/-)* mice never gave rise to MB. These

results underline a collaboration between miR-17/92 cluster and the SHH pathway in MB pathogenesis.

In line with upregulation of miR-17/92 cluster in MB, Northcott et al. identified a recurrent focal amplification of chromosome 13q31.3 in MB, where the miR-17/92 cluster is mapped (Northcott et al. 2009). Upregulation of miR-17/92 cluster was found in MB with activated SHH signaling and those with high *MYC* and *MYCN* expression. The results further illustrate the aberrant expression of miR-17/92 cluster in a subset of MB, and a link between miR-17/92 and SHH signaling pathway that may contribute to the MB pathogenesis.

Ferretti and his colleagues have applied global expression analysis to identify differentially expressed miRNAs in MBs (Ferretti et al. 2009). They examined the expression pattern of 248 miRNAs in 14 primary MBs and 7 normal adult and fetal normal cerebella. The results showed that 78 miRNAs were differentially expressed between tumors and either adult or fetal controls. Repressed miRNAs were more common than overexpressed miRNAs in MBs. In summary, through global miRNA profiling, a series of altered expressed miRNAs in MB has been identified. This approach may help to identify upregulated miRNAs having oncogenic function and those repressed miRNAs having tumor suppressor function in MB development. Table 3 summarizes the differentially expressed miRNAs in MB.

Table 3. Dysregulated miRNAs found in MB

References	Ferretti et al. 2009		Uziel et al. 2009	
Overexpressed miRNAs	miR-17-5p		miR-9*	miR-106b
	miR-148a		miR-17	miR-130a
	miR-199b		miR-17*	miR-130b
			miR-18	miR-191
			miR-19a	miR-216a
			miR-19b	miR-216b
			miR-20a	miR-217
			miR-20a*	miR-217*
			miR-25	miR-335
			miR-32	miR-423
			miR-34c	miR-449
			miR-92	miR-503
			miR-93	miR-672
Downregulated miRNAs	let-7a	miR-149	miR-29a	
	let-7b	mir-150	miR-29b	
	let-7d	miR-153	miR-124	
	let-7e	miR-154	miR-125a	
	let-7f	miR-181b	miR-127	
	let-7g	miR-181c	miR-127*	
	let-7i	miR-190	miR-128-1	
	miR-22	miR-191	miR-128-2	
	miR-26a	miR-192	miR-129	
	miR-26b	miR-194	miR-136	
	miR-29c	miR-212	miR-138	
	miR-30b	miR-219	miR-143	
	miR-30c	miR-320	miR-150	
	miR-31	miR-323	miR-204	
	miR-98	miR-324-3p	miR-206	
	miR-103	miR-324-5p	miR-218	
	miR-107	miR-326	miR-300	
	miR-124	miR-328	miR-338	
	miR-125a	miR-330	miR-378	
	miR-127	miR-331	miR-381	
	miR-128-1	miR-346	miR-382	
	miR-128-2	miR-370	miR-433	
	miR-129	miR-381	miR-434	
	miR-132	miR-382	miR-487b	
	miR-133b	miR-383		
	miR-134	miR-425		
	miR-138			
	miR-143			
	miR-145			

modified from Pang et al. 2009

Recently, the functional role of miR-128a in MB tumorigenesis has been delineated (Venkataraman et al. 2010). Expression of miR-128 was reduced in MB compared to either adult or pediatric normal cerebella. Restoration of miR-128a inhibited cell proliferation, cell viability and colony formation in MB cells. Further analysis demonstrated that miR-128a exhibited tumor suppressor function by suppressing oncogene BMI-1 at protein level. By targeting BMI-1, miR-128 prevented the repression of CDK4, a cell cycle inhibitor. Thus, miR-128a decreased MB cell growth through mechanisms involving cell cycle regulator.

CHAPTER 3

OBJECTIVES OF STUDY

At present, the primary treatment therapy for MB includes surgical resection, chemotherapy and radiotherapy. However, the survival rate of MB, especially of high-risk patients, remains unsatisfactory. Patients with recurrent disease after primary treatment do poorly, with 2-year survival rate of about 9% (Zeltzer et al. 1999). In addition, survivors commonly suffer from significant adverse therapeutic effects including neurocognitive impairment and neuroendocrine problems. Thus, development of novel therapy is urgently needed. Understanding MB pathogenesis would be the first step to achieve this goal.

The ultimate aim of my study is to provide hints on the development of new treatment strategy for MB. Understanding the molecular abnormalities in MB may enable the development of novel pathway specific drugs that can effectively cure the disease with reduced side effects. Furthermore, determination of particular signaling pathways affected by the molecular abnormalities may have implication on risk stratification. This in return allows tailored design treatment strategy for individual patients. Those less aggressive diseases could be prescribed with reduced dose treatment to reduce side effects and those aggressive diseases could be treated with multiple modalities to improve clinical outcome. Lastly, the identified molecular

abnormalities may either help in classification of current molecular subtypes or in finding a previously unrecognized molecular subgroup.

Our research group had previously examined chromosomal abnormalities in MB using CGH and microstatellite analyses. The results showed that losses of chromosomes 8p, 16q and 17p, and gains of chromosomes 7q and 17q were frequent genetic changes. Finer deletion mapping on chromosome 8p led to delineation of multiple partial or interstitial deleted intervals on 8p22-23.2 and a homozygously deleted region of 1.8 cM on 8p22-23.1. These results suggested that candidate TSG(s) critical for MB development might be located within the deletion regions on 8p. Thus, the objectives of my study were:

1. To conduct a systematic analysis to identify the candidate TGS(s) on chromosome 8p,
2. To determine the expression patterns of miRNAs located on chromosome 8p and evaluate their candidacy as tumor suppressor-like genes,
3. To evaluate the functional significance of aberrantly expressed miRNAs in relation to tumorigenesis of MB,
4. To identify and characterize the target genes of deregulated miRNAs, and
5. To evaluate the clinical significance of deregulated miRNAs.

CHAPTER 4

MATERIALS AND METHODS

4.1 Tumor specimens

A cohort of 29 MBs, collected from Prince of Wales Hospital, Hong Kong and Huashan Hospital, Shanghai were examined in this study. All tumors were classified according to current WHO criteria (Giangaspero et al. 2007). Part of tumor tissues resected at the time of surgery were immersed immediately in the RNALater solution (Ambion, Inc., Austin, TX, USA) and stored at -80°C until use. Histologic examination revealed that these RNALater-preserved samples had tumor cell content greater than 80%. There were 22 pediatric and 7 adult patients and the respective median age for each group was 10 years (range 5-17 years) and 32 years (range 20-40 years). The male/female ratio was 1.6:1. There were 24 classic, 2 anaplastic and 3 desmoplastic variants. A total of 3 normal cerebella were purchased from Ambion, Clontech Laboratories Inc. (Palo Alto, CA, USA), and Biochain Institute, Inc. (Hayward, CA, USA). Clinicopathological information of the patients is summarized in Table 4.

4.2 Cell lines

Seven MB cell lines DAOY, D283, D341, D384, D425, D458 and ONS-76 were included in this study. DAOY, D283 and D341 were obtained from American Type

Table 4. Clinicopathological features and gene/miRNA expression profiles of 29 MBs studied

	Case No.*	Age (year)	Sex	Normalized expression relative to normal cerebella +								
				miR-124	miR-383	miR-320	LZTS1	TUSC3	EFHA2	DKFZp761PO423	SLC16A1	PTBP1
Classic MB												
	26 (HS498)	4	M	0.00	0.01	0.17	ND	ND	ND	ND	55.82	5.93
	4 (HS499)	5	M	0.94	0.33	3.45	ND	ND	ND	ND	1.98	7.56
	14 (HS403)	7	M	0.22	0.64	1.02	8.08	2.60	0.47	0.70	2.67	0.96
	9 (HS412)	8	F	0.40	0.46	1.02	0.89	2.40	0.13	0.30	4.93	2.33
	15 (HS501)	9	M	0.20	1.00	2.26	ND	ND	ND	ND	11.13	1.36
	16 (HS411)	10	M	0.20	0.04	1.81	4.29	0.06	0.02	0.03	6.05	4.06
	19 (HS493)	10	F	0.10	0.02	0.75	ND	ND	ND	ND	9.76	2.74
	22 (HS413)	10	M	0.03	0.02	0.20	11.85	0.34	0.20	0.57	3.32	3.89
	23 (HS355)	10	M	0.03	UD	0.21	6.90	0.88	0.18	0.32	8.08	1.14
	17 (HS491)	11	M	0.14	0.01	1.90	1.48	2.78	0.26	0.17	14.24	1.93
	12 (HS414)	12	M	0.27	UD	1.04	1.55	2.52	0.12	0.29	5.04	4.02
	20 (HS409)	12	M	0.10	0.13	0.78	2.93	0.79	0.08	0.26	3.25	3.16
	11 (HS353)	13	M	0.35	0.42	1.88	9.05	2.07	0.30	1.08	5.60	1.41
	7 (HS406)	14	F	0.63	0.43	1.22	6.14	1.08	2.15	3.70	3.04	6.33
	8 (HS486)	14	F	0.62	0.23	0.91	19.42	1.48	0.15	0.39	11.89	4.75
	27 (HS489)	14	F	0.00	0.00	0.67	1.83	0.87	0.08	0.09	1.55	1.08
	18 (HS495)	16	M	0.11	0.64	0.11	ND	ND	ND	ND	1.34	0.73
	5 (HS497)	17	M	0.73	0.11	0.49	ND	ND	ND	ND	8.29	1.58
	3 (HS405)	20	F	0.95	0.13	3.40	1.70	1.34	2.85	2.79	24.19	5.39
	24 (HS352)	22	M	0.03	0.07	0.80	3.43	1.28	0.03	0.27	5.49	2.34
	29 (HS500)	24	M	0.00	0.01	3.47	ND	ND	ND	ND	3.12	3.45
	25 (HS487)	32	F	0.01	0.00	0.19	1.06	0.77	0.08	0.06	3.32	1.52
	10 (HS496)	36	F	0.36	0.72	1.21	ND	ND	ND	ND	9.02	3.63
	6 (HS408)	40	M	0.66	0.66	1.07	2.93	0.69	0.13	0.06	1.64	2.95
Desmoplastic MB												
	13 (HS407)	9	M	0.24	0.18	1.64	7.76	2.47	1.17	21.27	16.17	10.94
	21 (HS490)	10	F	0.07	0.01	0.25	9.38	0.58	0.02	0.16	6.91	1.71
	28 (HS410)	16	F	0.00	UD	0.23	0.40	3.09	0.20	0.02	8.44	3.60
Anaplastic MB												
	2 (HS494)	5	F	1.06	0.40	2.22	ND	ND	ND	ND	4.57	0.70
	1 (HS416)	37	M	1.60	0.56	3.11	4.35	1.45	UD	0.15	9.67	3.15

*Parenthesis indicates laboratory number. M represents male; F represents female. ND, not determined; UD, undetectable.

+Expression of miRNAs and genes was normalized to GAPDH in all samples examined. Expression of normal cerebella was defined as 1.

Culture Collection (Manassas, VA, USA) and cultured in Minimum Essential Medium Alpha Medium (Invitrogen, Carlsbad, CA, USA) supplemented with 10% fetal bovine serum (FBS). D384, D425 and D458 were generous gifts from Dr. Darrell Bigner (Department of Neuro-oncology, University of Durham, North Carolina, USA) and were grown in Improved MEM Zinc Option Medium (Invitrogen, Carlsbad, CA, USA) supplemented with 10% FBS. ONS-76 was purchased from Japanese Cancer Research Resources Bank and cultured in RPMI-1640 medium (Sigma-Aldrich Corporation, St. Louis, MO, USA) supplemented with 10% FBS. All MB lines grew in suspension except DAOY and ONS-76 which grew as a monolayer attached to the substratum. P19 mouse embryonal carcinoma cells was purchased from American Type Culture Collection and cultured in Dulbecco's Modified Eagle's Medium (Invitrogen) supplemented with 10% FBS. All cell lines were maintained in a humidified atmosphere containing 5% CO_2 at 37°C. Adherent cells were passaged at 80% confluence by trypsinization, and suspension cells were split every 4 days. Cell culture was ensured devoid of mycoplasma contamination by DNA specific Hoechst staining of cell culture regularly.

4.3 DNA extraction

Genomic DNA was extracted from tumor samples by conventional proteinase K

digestion and phenol:chloroform DNA extraction method. Briefly, approximately 10 mg of tumor was minced into small pieces and incubated in 2 ml of lysis buffer [50 mM Tris-HCl (pH 7.6), 200 mM $NaCl_2$, 1 mM ethylenediaminetetraacetic acid (EDTA), 0.5% sodium dodecyl sulfate (SDS) and 0.5 mg/ml Proteinase K] overnight at 55°C to lyse cells and digest proteins. To remove proteins from DNA, an equal volume of phenol:chloroform:isoamyl alcohol solution (25:24:1, v/v/v, pH 8.0; Amresco, Solon, OH, USA) was added to the lysate, which was mixed gently for 5 minutes and subjected to centrifugation at 13,000 g for 15 minutes at room temperature. Centrifugation separated the mixture into an upper aqueous phase and a lower organic phase. The upper aqueous layer containing DNA was carefully removed and to which was added 1/10 volume of 3M sodium acetate (pH 5.2) and 2.5 volumes of absolute alcohol. This DNA mixture was left at -80°C for 2 hours prior to centrifugation at 13,000 g for 10 minutes. The DNA pellet was washed with 70% ethanol to remove the salt, air-dried completely, and dissolved in 1X TE buffer [10 mM Tris-HCl (pH 8.0) and 1 mM EDTA]. DNA quantification was determined by spectrophotometry and was calculated based on an absorbance reading of 1.0 at 260 nm equivalent to a DNA concentration of 50 μg/ml. DNA with an absorbance ratio of 260 nm to 280 nm of 1.8-2.0 was considered of good quality.

4.4 RNA extraction

Total RNA was extracted using Trizol reagent according to manufacturer's recommendation (Invitrogen). Briefly, about 50 mg of tissue was cut into small pieces of about 0.25 cm^3 and subjected to homogenization by a homogenizer in the presence of 1 ml Trizol on ice. Chloroform (0.2 ml) was added to lysates and the mixture was shaken vigorously, sat for 2 minutes at room temperature, and centrifuged at 12,000 g for 15 minutes at 4°C. The upper aqueous phase containing RNA was transferred to a fresh tube, and 0.5 ml isopropanol was added to the solution to precipitate RNA. The mixture was incubated for 10 minutes at room temperature before it was centrifuged at 12000 g for 10 minutes at 4°C. The pellet was washed with 70% ethanol, air-dried completely, and dissolved in 0.1% (w/v) diethylpyrocarbonate-treated water. To examine the integrity of RNA, total RNA samples were subjected to agarose gel electrophoresis. The 28S and 18S ribosomal RNA bands were visualized after ethidium bromide staining. RNA with the fluorescence intensity ratio of 28S to 18S close to 2 and with no smearing was considered of good quality. RNA concentration was determined by spectrophotometry and was calculated based on an absorbance reading of 1.0 at 260 nm equivalent to a concentration of 40 μg/ml.

Total RNA of cell lines were isolated using the same procedures as mentioned above with the exception that cells, after washing three times with chilled

phosphate-buffered saline (PBS), were directly lysed by addition of 1-2 ml of Trizol.

4.5 Quantitative reverse transcription-polymerase chain reaction (qRT-PCR)

4.5.1 Reverse transcription

RNA was reverse transcribed into complementary DNA (cDNA) prior to PCR. The reverse transcription reaction in a final volume of 20 μl contained 1 μg RNA, 1X reverse transcription buffer, 2.5 μM random hexamers, 2 mM deoxyribonucleoside triphosphates (dNTPs), 50 units of MultiScribe™ reverse transcriptase (Applied Biosystems, Foster City, CA, USA), and 4 units of RNase inhibitor. The reaction was incubated at 25°C for 10 minutes, 48 °C for 30 minutes and terminated at 95 °C for 5 minutes.

4.5.2 TaqMan®-based real-time PCR

TaqMan®-based real-time PCR was conducted to evaluate the expression of *LZTS1, PTBP1, PRDX3, SLC16A1, TUSC3*, and *GAPDH*. Probes and primers were purchased from Applied Biosystems: *LZTS1* (Hs00232762_m1), *PTBP1* (Hs00738538_g1), *PRDX3* (Hs00428953_g1), *SLC16A1* (Hs01560299_m1), *TUSC3* (Hs00185147_m1), and *GAPDH* (Hs99999905_m1). The PCR reaction was prepared in a final volume of 20 μl containing 30 ng cDNA, 1X TaqMan Universal PCR master mix

(Applied Biosystems), and 1X of probes and primers. Amplification was conducted under the conditions of 95°C for 10 minutes, followed by 40 cycles of 95°C for 15 seconds and 60°C for 1 minute in the iCycler real-time PCR detection system (Bio-Rad Laboratories, Hercules, CA, USA). To determine gene copy number, PCR product of each gene was cloned into the pCR2.1 vector. A serial dilution of the resultant plasmid was prepared and included in each PCR run. A graph of copy number versus threshold cycle (Ct) was generated and a standard curve was plotted. The gene copy number in a given sample was extrapolated from the standard curve using the Ct value obtained. The relative gene expression in each sample was determined as a ratio of copy number of target gene to copy number of internal control gene (*GAPDH*), and compared between tumors and 3 normal cerebella. A normalized expression value of 2-fold lower or higher that the mean expression level of 3 normal cerebella was considered downregulation or upregulation, respectively. All PCR reactions were carried out in triplicates.

4.5.3 SYBR® Green-based real-time PCR

SYBR® Green-based real-time PCR was performed for the following purposes: 1) validation of expression profiling data, and 2) expression analysis of putative miRNA targets and *Sgcz*. Each PCR reaction in a final volume of 20 μl contained 30 ng cDNA,

1×Power SYBR® Green PCR master mix (Applied Biosystems) and 0.125 μM of each forward and reverse primer (Table 5). PCR amplification was performed under the conditions of 95°C for 10 minutes, followed by 40 cycles of 95°C for 15 seconds, 60°C for 20 seconds and 72°C for 20 seconds. Standard curves were generated by the procedure described in section 4.5.2. The relative gene expression in each sample was determined as a ratio of copy number of target gene to copy number of internal control gene (*GAPDH*), and compared between tumors and normal cerebella. The average of 3 normal cerebella was normalized to 1.0 and the relative gene expression level in tumors was calculated with respect to the average normal cerebella. A normalized expression value of 2-fold lower or higher that the mean expression level of 3 normal cerebella was considered downregulation or upregulation, respectively. PCR was carried out in triplicate and the data represented the results of 3 independent experiments.

4.5.4 TaqMan® miRNA assay

The expression of mature miR-124 and miR-383 was determined using TaqMan miRNA assay (Applied Biosystems). Briefly, the reverse transcription reaction was prepared in a final volume of 15 μl containing 10 ng of total RNA, 50 nM miR-124- or miR-383-specific reverse transcription primer, 1× reverse transcription buffer, 1 mM dNTPs, 50 units of MultiScribe™ reverse transcriptase and 3.8 units of RNase inhibitor.

Table 5. Primers used in SYBR® Green-based qRT-PCR analysis

Genes	Primer sequence	Expected size (bp)
AKAP12	F: 5' CCCAAGCACAGGAGGAGTTA R: 5' GTGCCTGCTCTCCAATTCTC	199
CD164	F: 5' CAGCCCTCCCCTTCTACAAC R: 5' CCCAAGACCAGGACAATTCC	110
CDK6	F: 5' CATTCAAAATCTGCCCAACC R: 5' GGTCCTGGAAGTATGGGTGA	107
CNIH	F: 5' ATTGTCAGAAGGAAGGATGGTG R: 5' GCATGCACTTAACTGGACCAA	133
CTDSP2	F: 5' AACACGGCTCCATCATCAC R: 5' CCACGAGGCTTCTTAGGAGA	97
CTNNAL1	F: 5' CCACTGAAAACTTCCCAGGATTT R: 5' AGCTTTAAACCCTCTGCAGCAA	65
DKFZp761P0423	F: 5' TTGTAACAAGCCCTGCTGTG R: 5' GAGACTGTTTTGGGCTCAGG	120
EFHA2	F: 5' CCATAGAGGATTCCGGGGTTA R: 5' CAGGCAGGATTTGAAAGTGG	62
EZH2	F: 5' CCTGTGCACATCCTGACTTC R: 5' CTGCTGTAGGGGAGACCAAG	156

GAPDH	F: 5' AGCCGAGCCACATCGCTCA R: 5' TGGCAACAATATCCACTTTACCAGAGTT	123
IQGAP1	F: 5' GGAGATGGATGAAAGGAGACG R: 5' CCTCCTCCAGTTCTGTGGTG	125
LAMC1	F: 5' TCCTGACCGACTACAACAACC R: 5' GGAACTTGAGACGCACATAGG	144
LASS2	F: 5' CTGGTCATCCTGCCCTTCT R: 5' CGGTCACTGCGTTCATCTT	205
MAL2	F: 5' CAGCCACTCCTGAGTGATAACC R: 5' CCCAAACTGCAACCATAACAAG	92
MAPK14	F: 5' CGAGCGTTACCAGAACCTGT R: 5' CGTAACCCCGTTTTTGTGTC	84
MAPKAP1	F: 5' CAATGACCGTGGTGACAATG R: 5' GCAATATGCAGGCAGTAGGC	130
MCM7	F: 5' CCCACTTTCATGCCTCTGAT R: 5' CCACAGGCACCTGATCACTA	148
NCKAP1	F: 5' GAAAATTGGCCAGGAGACAGAT R: 5' AGCATGGTATGCATTTCTCAGC	154
NHLH1	F: 5' CCCACAATGTGTACCCCTCT R: 5' AGTCTCCTCTGGGTGCTCAA	125

PGRMC2	F: 5' ATGGGAAAGTCTTCGACGTG R: 5' CAAAATGTGGCCAGTCCTCT	107
PKIB	F: 5' AATGCCTTACCAGACATCCA R: 5' GAGGTTTTCCAATTGGTCT	134
PRDX3	F: 5' TGAACATCGCACTCTTGTCAGA R: 5' GACGCTCAAATGCTTGATGACT	134
PREI3	F: 5' ACTTGATGGTGCTGCATGTCTT R: 5' CGGCATACTGATCCTAGTTTCG	99
PTBP1	F: 5' AAGGACTACGGCAACTCACC R: 5' GCTGGAAAACAGGACCTTGA	147
PTPN12	F: 5' GCCATGAAGAGTCCTGACCA R: 5' TTTTTCTCCAGTGGCTGTGG	120
PTTG1IP	F: 5' GCAGAGATGAAGACAAGACATGA R: 5' GCTGGAGCGCTTTAGTTGTT	101
RBMS1	F: 5' GTGGCTGTCGAGACGTCTAATG R: 5' GTTCAGCCTTCACACCCTTCTT	111
SCD	F: 5' CACCTCTTCGGATATCGTCCTT R: 5' GGGAAAGGAGTGGTGGTAGTTG	111
SLC16A1	F: 5' ATGCTGTCCTGTCCTCCTG R: 5' CTGCTCGTTTGCTTTCTGTTC	178

SLC35A3	F: 5' TGCAGCTACTTATCAGGTCACG R: 5' GCCACTGGTATACACCCAATTT	98
SOX5	F: 5' CCAGCAGCGTTAGCTAGTCC R: 5' ATTCACAACAGCCACCTTCC	156
STRN3	F: 5' TCATCCCACACTTCCTGTTACAA R: 5' CAGCATCCAAGTGAGCTACCA	112
WFDC1	F: 5' TACGCCTGCCTAGAAGCTGT R: 5' ACGCCTCTGCTTGTAACACC	132
mmu-SGCZ	F: 5' TTTATGGATGGCGAAAGAGG R: 5' TTCCCCATACCATCCACAGT	127
mmu-GAPDH	F: 5' GTCCCGTAGACAAAATGGTGAA R: 5' GTTGATGGCAACAATCTCCACT	110

The reaction mix was incubated at 16°C for 30 minutes, 42°C for 30 minutes, and 85°C for 5 minutes. Quantitative PCR was performed in a 20-μl volume containing one tenth of the reversed transcribed product, 1× TaqMan Universal PCR master mix, and 1× TaqMan miRNA assay reagent. Amplification was conducted under the conditions of 95°C for 10 minutes, followed by 40 cycles of 95°C for 15 seconds, and 60°C for 1 minute. Similar to other qRT-PCR assays, standard curves for miRNAs and internal control gene (*GAPDH*) were generated for copy number assessment. The relative expression of miRNA in each sample was calculated as a ratio of copy number of miRNA to copy number of GAPDH, and compared between tumors and 3 normal cerebella. A normalized expression value of 2-fold lower or higher that the mean expression level of 3 normal cerebella was considered downregulation or upregulation, respectively. All PCR reactions were performed in triplicates.

4.6 Comprehensive gene expression profiling

Seven MBs (cases 16, 17, 21, 23, 24, 25 and 28) and 2 normal cerebella were subjected to gene expression profiling using Affymetrix Human Genome U133 Plus 2.0 Array (Affymetrix, Santa Clara, CA, USA). The microarray experiment was performed by Shanghai Institutes of Biological Science (Second Medical University, Shanghai) according to manufacturer's recommendation. Global mean normalization was

performed to normalize gene expression of array (Quackenbush 2002). A logarithmic transformation based 2 was then applied for subsequent gene expression comparison between tumor samples and normal cerebella.

Expression profiling was also performed to identify candidate genes modulated by miR-383 in MB cells. The 4x44K Whole Human Genome Oligo Microarray (Agilent, Diegem, Belgium) was used to assess gene expression. The microarray experiment was conducted by Dr. Richard K.W. Choy (Department of Obstetrics and Gynecology, The Chinese University of Hong Kong) according to manufacturer's recommendation. The spot intensity was normalized using global mean normalization, and log ratios compared to negative control transfected cells were determined using linear-fit modeling.

4.7 DNA methylation analysis

4.7.1 Sodium bisulfite modification of genomic DNA

To detect DNA methylation, genomic DNA was subjected to sodium bisulfite modification prior to PCR with methylation specific primers or PCR followed by DNA sequencing. In DNA modification, all unmethylated cytosines are converted to uracil while 5'-methylcytosines resistant to modification remain unchanged. Thus methylated and unmethylated DNA, after modification, can be discriminated using bisulfite

sequencing analysis or methylation specific primers. For each sample, 2 μg of genomic DNA was subjected to bisulfite modification using Methylamp DNA Modification Kit (Epigentek, Brooklyn, NY, USA) according to manufacturer's recommendations.

4.7.2 Bisulfite sequencing analysis

The methylation status of *TUSC3* in MB case 22 was assessed by bisulfite sequencing. Modified genomic DNA was amplified by PCR in a 20-μl reaction containing 1X PCR buffer II, 0.25 mM $MgCl_2$, 0.25 μM of primer pair (Table 6), 0.2 μM dNTPs, and 0.5 unit of AmpliTaq Gold® DNA polymerase (Applied Biosystems) under the conditions of 95°C for 10 minutes, 35 cycles at 95°C for 15 seconds, 62°C for 15 seconds, and 72°C for 20 seconds, with a final extension reaction at 72°C for 10 minutes. The MethPrimer program (http://www.urogene.org/methprimer/index1.html) was applied to design optimal primers for methylation studies. The PCR product of 176 bp was cloned into pCR2.1 using TOPO-TA cloning kit according to manufacturer's recommendation. The pCR2.1 vector carries a reporter gene β-galactosidase spanning the polylinker site. The β-galactosidase can cleave 5-bromo-4-chloro-3-indolyl-β-galactopyranoside (X-gal) to produce a blue product, resulting in bacterial colonies that stained blue. However, β-galactosidase activity is destroyed when a DNA fragment is inserted at the polylinker site. Thus, recombinant

clones containing inserts can be distinguished by blue/white colony selection. Ten white bacterial colonies were picked for miniprep DNA preparation. DNA sequencing was performed using BigDye Terminator kit v3.1 (Applied Biosystems), and analyzed by ABI 3130 Genetic Analyzer (Applied Biosystems).

4.7.3 Methylation-specific PCR (MSP) analysis of *EFHA2*

The methylation status of *EFHA2* was determined by MSP. Two genomic regions covering the putative promoter and exon 1 of EFHA2 were interrogated for aberrant methylation. Modified DNA was subjected to independent PCR containing either methylation- or unmethylation-specific primers. The PCR reaction in a final volume of 20 μl contained 2 μl of modified DNA, 1X PCR buffer II, 0.25 mM $MgCl_2$, 0.2 μM dNTPs, 0.25 μM of methylation-specific or unmethylation-specific primer pairs (Table 6), and 0.5 units of AmpliTaq Gold® DNA polymerase (Applied Biosystems). The PCR conditions were 95°C for 10 minutes, 35 cycles at 95°C for 15 seconds, 62°C for 15 seconds, and 72°C for 20 seconds, with a final extension at 72°C for 10 minutes. The products were resolved by 2.0% (w/v) agarose gel electrophoresis, stained with eithidium bromide and visualized under ultraviolet light. The detection of PCR bands using methylation-specific primers was considered positive for methylation. The DNA methylase SssI-treated DNA was served as a positive control. DNA was treated with

Table 6. Primers used in methylation analyses

Genes	Primer sequence	Expected size (bp)
Bisulfite sequencing		
BS-TUSC3	F: 5' GGATGTTTTGTTAGTTTTTTTT R: 5' ACAAAACAATATCTCCTCCAC	176
MSP		
M1-EFHA2	F: 5' GAATGTGAGTGTTTTAGACGGGCGT R: 5' CATAAAAAAAACGACGAATCCCGAC	243
U1-EFHA2	F: 5' GAATGTGAGTGTTTTAGATGGGTGT R: 5' CATAAAAAAAACAACAAATCCCAAC	243
M2-EFHA2	F: 5' TCGGTTTGGTATGTTATTAGTTGTACG R: 5' AACGAATCCTCGAACTCCGT	100
U2-EFHA2	F: 5' TTGGTTTGGTATGTTATTAGTTGTATG R: 5' AACAAATCCTCAAACTCCAT	100

SssI methylase (New England Biolabs, Ipswich, MA, USA) at 37°C for 1 hour. Normal cerebellum was served as a negative control in PCR.

4.8 Transfection of miRNAs

Two types of miRNA mimics were employed in functional studies. The miRIDIAN miRNA mimics from Dharmacon (Lafayette, CO, USA) were used in the miR-124 study, and the Pre-miR™ miRNAs from Ambion were used in the miR-383 study. The Pre-miR™ miRNAs were efficacious and used at low concentration in transfection.

Transfection conditions were optimized using fluorescent RNA duplex siGLO or FAM™ dye-labeled Pre-miR™ negative control mixed with Lipofectamine™ 2000 (Invitrogen) in different ratios (w/v) according to manufacturer's recommendation. Cells which had taken up the labeled RNA molecules appeared fluorescent when observed under a fluorescent microscope.

The adherent MB cells (0.8-1.2 X 10^4 cells/well) were seeded onto 24-well plates. After incubation for 24 hours, 16.7 nM of miRIDIAN miRNA or 6.25 nM of Pre-miR miRNA was mixed with Lipofectamine™ 2000 at pre-determined ratio and added to each well. The cells were then incubated for 24 hours followed by replacement

with fresh media. For suspension cells, 2.5 X 10^4 cells were seeded in 24-well plate. As control, the respective miRIDIAN miRNA negative control #1 (Dharmacon) or Pre-miR miRNA negative control (Ambion) was included in each transfection experiment. The controls had no significant sequence similarity to miRNAs in human.

4.9 Gene knockdown by RNA interference

Knockdown of *SLC16A1* was carried out using two Stealth RNAi™ siRNAs (Invitrogen): siSLC16A1-1 and siSLC16A1-2 which specifically target exons 4 and 5 of *SLC16A1*, respectively. Each siRNA duplex was composed of two chemically modified oligonucleotides annealed to each other (Table 7). Cells (4-6 X 10^4 cells/well) were seeded onto 6-well plate. After 24 hours when cell confluence reached about 20%, 16.7 nM siRNA was mixed with Lipofectamine™ 2000 and the mixture was added to cells. Cells were incubated for 24 hours followed by replacement with fresh media. The Stealth RNAi™ siRNA negative control with low GC content (36% GC) was used as a negative control.

Knockdown of *PRDX3* was performed using two Silencer® Select Validated siRNAs (Ambion): siPRDX3-1 and siRPDX3-2 which specifically target exons 4 and 5 of *PRDX3*, respectively (Table 7). The transfection protocol was similar to that of SLC16A1 knockdown except that the concentration of siRNA used was adjusted to 12.5

Table 7. siRNAs used in gene silencing studies

siRNA names	Duplex sequence	Targeted region (exon)
SLC16A1		
siSLC16A1-1	5′-AUAGGUAGUGGAUAAAGGUGCUAGC 5′-GCUAGCACCUUUAUCCACUACCUAU	4
siSLC16A1-2	5′-AAAUAAUUAGGACGACGCCACAUGC 5′-GCAUGUGGCGUCGUCCUAAUUAUUU	5
PRDX3		
siPRDX3-1	5′-GUGACAAAGCUAACGAAUU 5′-AAUUCGUUAGCUUUGUCAC	4
siPRDX3-3	5′-GUGACAAAGCUAACGAAUU 5′-UUAAGUCUGACAAGAGUGC	5

nM. The Silencer® Select siRNA negative control (Ambion), which showed minimal sequence identical to human gene sequence, was used as a control.

4.10 Determination of cell growth by cell count assay

Cells transfected with miRNA mimic were harvested by trypsinization every day for 4 successive days, stained with 0.4% (w/v) trypan blue, and counted with a hemocytometer. Dead cells with damaged membrane were stained up by trypan, while viable cells excluded the dye. Three independent experiments were performed.

4.11 Determination of cell growth by MTT assay

This assay measures the reduction of yellow 3-(4,5-dimethylthiazol-2-yl)-2,5-diphenyl tetrazolium bromide (MTT) to purple formazan crystals by the mitochrondrial enzyme, succinate dehydrogenase. The amount of insoluble purple formazan produced, after dissolution, can be quantified by spectrophotometry. Since succinate dehydrogenase is active in living cells, the level of enzymatic activity on MTT reduction is a measure of cell viability.

Cells (1.6-5.0 X10^3 cells/wells) seeded onto 96-well plate were transfected with miRNA mimic or siRNA. At various time after transfection, MTT (5 mg/ml in PBS;

USB Chemicals, Cleveland, OH, USA) was added to cells to a final concentration of 0.5 mg/ml, followed by incubation at 37°C for 2-4 hours. The medium was removed and the purple precipitate was dissolved in 100 μl of dimethyl sulfoxide. The absorbance of the colored solution was measured at a wavelength of 570 nm with background subtraction at 630 nm by spectrophotometric mean using VICTOR3 plate reader (Perkin-Elmer, Waltham, MA, USA). Each experimental condition was done in triplicate wells and at least 3 times.

4.12 Cell cycle profiling by flow cytometry

Cells were plated at a density of 2.4 to 3.6×10^5 on 100-mm dishes a day before transfection. At designated time after miRNA transfection, both floating and attached cells were collected in centrifuge tubes, washed with PBS, fixed in cold 70% ethanol at -20°C overnight, and treated with PBS containing 20 μg/ml propidium iodide (Sigma-Aldrich) and 200 μg/ml DNase-free RNase A (Sigma-Aldrich) in the dark for 30 minutes. After passing through the 40 μm strainer, cells were subjected to cell cycle profiling using FACSCalibur (Becton Dickinson, San Jose, CA, USA). The percentage of cells in different phases of cell cycle was determined by Cell Quest version 3.2 software (Verity 214 Software House, Topsham, ME, USA).

4.13 Evaluation of miRNA-target gene interaction by luciferase reporter assay

The dual-luciferase reporter system is a useful tool to study the regulation of gene expression. The potential miRNA binding site is first inserted downstream of a firefly luciferase gene. The construct is then co-transfected with miRNA and a renilla encoded vector serving as an internal control to which the firefly luciferase reporter is normalized. The relative change in the expression of firefly luciferase activity is correlated to changes in the transcriptional activity of the gene. In return, this reflects the regulation of miRNA on the gene expression.

4.13.1 Construction of reporter plasmids

To construct the luciferase reporter plasmid, a partial 3′ UTR fragment of *SLC16A1* (212 bp), containing the putative miR-124 miRNA recognition element (MRE) corresponding to +1966 to +2177 of human mRNA sequence (NM_003051.3), was amplified with primers containing an XbaI linker (Table 8), and cloned into the pCR2.1-TOPO vector. The *SLC16A1* fragment was released from the recombinant plasmid with XbaI restriction enzyme and subcloned into the unique XbaI site downstream of luciferase gene in the pGL3-control vector (Promega Corporation, Madison, WI, USA). The resultant plasmid was termed pGL3-WT-SLC16A1. A control plasmid (pGL3-MUT-SLC16A1) carrying a 9-bp substitution mutation at the seed

Table 8. Primers used in preparation of luciferase reporter constructs

	Primer sequences	Expected size (bp)
SLC16A1		
pGL3-SLC16A1-F:	5'-ATTCTAGACATTTGTGTGGAAATCA	212
pGL3-SLC16A1-R:	5'-TCTCTAGAGTTCTAAAGACTAAAAC	
PRDX3		
pGL3-PRDX3-F:	5'-GATCTAGAGCCTTACTTGAATCTTGCC	326
pGL3-PRDX3-R:	5'-TCTAGAAATATACATAGACAAAGT	
RBMS1		
pGL3-RBMS1-F:	5'-GGTCTAGATGTACAGAAAGGTGTTCTTAC	732
pGL3-RBMS1-R:	5'-AATCTAGACTACCTTTTAAAAGCCCTATG	

Underline represents the XbaI cloning site.

region of the miR-124 MRE of *SLC16A1* 3'UTR was created using the Gene-Tailor site-directed mutagenesis system (Invitrogen) with primers 5′-TCATAAAGATTATAATATACAAAGCTTGTTTTAGTCTTTAGAACTC-3′ and 5′-ATATTATAATCTTTATGACACTATTAAAAGCTAAGATT-3′. All constructs were sequenced to ensure authenticity.

To prepare reporter plasmids for *PRDX3* and *RBMS1*, a partial 3′ UTR fragment of *PRDX3* (326 bp), corresponding to +1123 to +1448 of human mRNA sequence (NM_006793.2) and a partial 3'UTR fragment of *RBMS1*, corresponding to +1672 to +2403 of human mRNA sequence (NM_016836.3) were amplified with primers containing an XbaI linker. The respective 326-bp and 732-bp products of *PRDX3* and *RBMS1* were cloned into the pCR2.1-TOPO vector. The 3'UTR fragment were released from the plasmids and subcloned into the unique XbaI site downstream of the firefly luciferase gene in pGL3-control. The resultant plasmids were termed pGL3-WT-PRDX3 and pGL3-WT-RBMS1, respectively. The reverse sequence of the seed region (nt 2-8) was served as control plasmids, named pGL3-reverse-PRDX3 and pGL3-reverse-RBMS1.

4.13.2 Luciferase reporter assay

Cells ($7\text{-}9\times10^4$ cells/well) were seeded on 24-well plates a day before

transfection. The next day, cells were cotransfected with 1 μg of pGL3 plasmid containing the wild-type or mutant 3'UTR fragment of tested gene, 20 pmol of either miRNA mimic or miRNA negative control, and 200 ng of pRL-TK (Renilla) using Lipofectamine™ 2000. After incubation for 24 hours, cells were washed with PBS and lysed in 100 μl Passive Lysis Buffer (Dual Luciferase Reporter Assay System, Promega, Madison, WI, USA). A 20-μl aliquot was then transferred to 96-well black microtiter plates (Thermo Scientific, San Jose, CA, USA). Luciferase Assay Reagent II (100 μl) was added to generate signal for firefly activity measurement and an equal volume of Stop & Glo® Reagent was then added sequentially to generate signal for renilla activity measurement. Both firefly and renilla luminescent intensities were measured by IVIS 100 imaging system (Xenogen Corporation, Hopkinto, MA, USA). Transfection efficiency was corrected by normalizing the firefly luciferase activity to that of Renilla. Data were then normalized to the pGL3-control/miRNA negative control cotransfection. Each experiment was performed in triplicate and repeated 3 times.

4.14 Cell death assay

The presence of apoptotic cells was evaluated by the Cell Death Detection ELISA^{PLUS} assay (Roche Diagnostics) according to manufacturer's instructions. This is an enzyme immunoassay (ELISA) for quantitatively measurement of histone-associated

DNA fragments (mono- and oligonucleosomes) in the cytoplasmic fraction of cells. The detection of mono- and oligonucleosomes is an indication of DNA degradation, resulting from an activation of endonuclease in the apoptotic cells.

Cells were washed with PBS, and incubated with Lysis Buffer for 30 minutes at room temperature. The lysates were then centrifuged at 1500 rpm for 10 minutes. The supernatant together with the antibodies-contained Immunoreagent were incubated into microplate for 2 hours. The reaction was stopped by adding Stop Solution. The absorbance was measured at 405 nm with background substraction at 490 nm by VICTOR3 plate reader. All samples were normalized to untreated cells. The enrichment factor for cell death was calculated as ratio of absorbance of sample cells to absorbance of siRNA negative control cells. The data were derived from 3 experiments performed in triplicate.

4.15 Western blot analysis

Cells were lysed in RIPA buffer containing 50 mM Tris-HCl pH 7.4, 150 mM NaCl, 1% Triton X-100, 1% sodium deoxycholate, 0.1% SDS and 1X protease inhibitor mix (GE Healthcare Corporation, Piscataway, New Jersey) and incubated on ice for 15 minutes. Insoluble material was removed by centrifugation. Protein concentration was determined by the Protein Assay (Bio-Rad). Soluble proteins were resolved by

SDS-polyacrylamide gel electrophoresis with 8 to 15% gels depending on the size of protein under investigation. Resolved proteins were transferred from gel to polyvinylidene difluoride membrane by wet transfer technique with Trans-Blot® Electrophoretic Transfer Cell (Bio-Rad). Transfer was conducted in Transfer buffer (25 mM Tris-HCl and 192 mM Glycine) at 100 V for 1 hour or 20 V for 10 hours. The blot was incubated in 5% non-fat milk for 1 hour to block non-specific protein binding sites, washed 3 times with TBST buffer (20 mM Tris-HCl pH7.6, 15 mM NaCl, and 0.1% Tween 20), and probed with rabbit anti-human SLC16A1 polyclonal antibody (Abcam Incorporation, Cambridge, MA, USA) at a concentration of 0.4μg/ml, rabbit anti-human PRDX3 polyclonal antibody 4G10 (Abcam) at a concentration of 0.5 μg/ml, rabbit anti-human RBMS1 polyclonal antibody (Abcam) at a concentration of 1 μg/ml, mouse GALC monoclonal antibody clone mGalC (Millipore, Temecula, CA, USA) at a concentration of 1 μg/ml, mouse β-tubulin III (TUBB3) monoclonal antibody TU-20 (Exbio, Praha, Vestec, Czech Republic) at a concentration of 0.5 μg/ml, or mouse anti-human GAPDH monoclonal antibody (Abcam) at a concentration of 0.2 μg/ml. The blot was washed 3 times with TBST buffer and incubated with appropriate horseradish peroxidase-conjugated secondary antibody for 1 hour at room temperature. Protein expression was assessed by ECL Plus western blotting reagent (GE Healthcare), or Immobilon™ Western Chemiluminescent HRP substrate western blotting reagent

(Millipore) according to manufacturer's recommendation. Signals were detected by exposing the treated blot to Hyperfilm ECL (GE Healthcare) for 45-60 seconds.

4.16 Determination of allelic status by FISH analysis

The dual-color FISH analysis was employed to evaluate the allelic status of chromosome 8p in MBs using an established in-house protocol (Dong et al. 2004).

4.16.1 Preparation of DNA probes

Nick translation was employed to label DNA isolated from BAC clones. The target probe, prepared from BAC clone RP11-403C10 (8p23.1), was labeled with Spectrum-Orange-dUTP (Vysis, Downers Grove, Ilinois, U.S.A.), whereas the reference probe, prepared from BAC clone RP11-67O16 (8q12.3), was labeled with Spectrum-Green-dUTP. The nick translation reaction of 50 μl contained 5 μg of BAC DNA, 100 mM Tris-HCl (pH 7.5), 10mM $MgCl_2$, 0.01% bovine serum albumin, 0.4 mM dNTPs, 0.1 nM β-mercaptoethanol, 0.03 unit of DNase I, 20 units of DNA polymerase I, and 0.85 nM of Spectrum-Orange-dUTP (for target probe) (Enzo Inc. Plymouth Meeting, PA, USA) or 1.9 nM of Digoxigenin-11-dUTP (for reference probe) (Roche Diagnostics, Mannheim, Germany). The reaction mix was incubated at 15°C for 90-120 minutes to achieve labeled DNA fragments with size between 300-1000 bp, and

terminated by addition of 1 μl of 0.5M EDTA and 0.5 μl of SDS and incubation at 65°C for 10 minutes. To prepare the hybridization mixture, both the target probe and reference probe were mixed in 1:1 ratio and diluted in Hybrisol containing 50% formamide, 2X SSC, pH 7.0 (Oncor Gaithersburg, MD, USA).

4.16.2 Preparation of slide for hybridization

The formalin-fixed paraffin-embedded section of 5-μm thickness was dewaxed with xylene and rehydrated with serial graded ethanol rinses. To overcome the protein-DNA crosslinkage and enhance probe penetration, the section was pretreated with 1M sodium thiocyanate in distilled water at 80°C for 10 minutes, digested with pepsin (2-8 mg/ml in 0.2 N HCl) for 30 minutes. The reaction was stopped by washing with PBS. The sections were then heated in microwave (600W) in the presence of citrate buffer (pH 6.0) for 10 minutes followed by incubation at 80°C for 30 minutes.

4.16.3 Hybridization and signal detection

The labeled probes were hybridized to the sections at 37°C overnight. After hybridization, sections were washed with 1.5 M urea/1X SSC (150 mM NaCl and 15 μM sodium citrate (pH 7.0)) at 45°C for 30 minutes, and 2X SSC at 45°C for 15 minutes to eliminate non-specific binding. The anti-digoxigenin antibody conjugated

with fluorescein (Roche Diagnostics; 2μg/ml) was added to the section and incubated at 37°C for 1.5 hour. Slides were then washed in PBS, dehydrated in ethanol series, air dried, and counterstained with anti-faded 4'6-diamidino-2-phenylindole (DAPI). The fluorescent signals were viewed under the fluorescence microscope (Zeiss, Axioplan 2, Carl Zeiss Inc., Thornwood, NY, USA) equipped with three single band-pass filters at the excited wavelength of 350 nm, 490 nm and 559 nm to detect DAPI, fluorescein isothiocyanate (FITC), and Spectrum Orange, respectively. A total of 200 non-overlapping nuclei were scored on each section.

4.17 Induced neuronal differentiation of P19 cells

Single P19 cells were cloned by limiting dilution in 96-well plates. The clones were passage at about 60% confluence to prevent differentiation. Two criteria were used for selection of clones for investigation: the morphologic resemblance of subclones to parental cells and the ability to undergo induced neuronal differentiation with expression of TUBB3 and morphological changes with long processes extending out from cells, as described by Jones-Villeneuve (Jones-Villeneuve et al. 1983).

Exponential growing P19 cells plated at 10^5 cells/ml in petri dish were treated with 0.5 μM of all-trans-retinoic acid (RA; prepared at 0.1 M in dimethyl sulfoxide) (Sigma-Aldrich). Cells were stimulated to form embryonic bodies (EBs) and grown as

aggregates. Fresh RA-containing medium was replaced at 48-hour interval. After incubation for 4 days, cells were trypsinized and re-plated in medium without RA on poly-L-lysine-coated plate to allow for differentiation. The next day, cytosine β-D-arabinofuranoside (Ara-C) (Sigma-Aldrich) was added to cells at a final concentration of 5 μg/ml to inhibit cell division. Growth medium was replaced every 48 hours. Cells were examined for morphological change and harvested for miRNA and protein expressions at designated time points. The appearance of polygonal epithelial cell-like morphology in RA treated P19 cells after replating was suggestive for neuronal differentiation. Subsequently, the cytoplasmic volume of these RA treated cells decreased. Long neurite-like processes were appeared and they formed network.

CHAPTER 5

RESULTS

5.1 Identification of TSGs on chromosome 8p

5.1.1 Previous data on chromosome 8p

Using comparative genomic hybridization (CGH), several groups including ours have demonstrated that loss of chromosome 8p is a recurrent genetic abnormality in 12%-50% of MB (Avet-Loiseau et al. 1999; Bayani et al. 2000; Eberhart et al. 2002; Gilhuis et al. 2000; Nishizaki et al. 1999). Our group had also performed a detailed microsatellite analysis on chromosome 8p and identified multiple partial or interstitial deletions on 8p22-23.2 and a homozygously deleted interval of 1.8 cM on 8p22-23.1 (Yin et al. 2002). Frequent loss of heterozygosity involving a discrete chromosomal region is generally considered an indication of the presence of TSGs and whose loss or inactivation may contribute to the development of tumor (Murthy et al. 2002). Taken together, the results suggest that the deleted regions on chromosome 8p may harbor TSG critical for MB development.

To identify the TSG on chromosome 8p22-23.1 in MB, our group had employed the candidate gene approach. One of the candidate TSGs examined was *DLC-1* located on 8p22. Previous studies demonstrated lost or reduced expression of *DLC-1* in liver, breast and lung cancers (Ng et al. 2000; Plaumann et al. 2003; Wong et al. 2003; Yuan

et al. 2004). Restoration of *DLC-1* suppressed cell growth, inhibited colony formation and induced apoptosis (Ng et al. 2000; Yuan et al. 2004). When *DLC-1* was examined in MB, loss of expression was detected in 1 of 9 tumors examined (Pang et al. 2005). Neither somatic mutations nor promoter hypermethylation was detected in MB including the sample that showed absent *DLC-1* expression. These data suggested *DLC-1* did not play a major role in MB oncogenesis.

Within the homozygously deleted region on 8p22-23.1 laid a potential TSG, *PINX1*. Functional study indicated that *PINX1* encodes for a potent inhibitor of telomerase and its depletion increased tumorigenicity in nude mice (Zhou and Lu 2001). These findings suggest that *PINX1* may act as a TSG. However, results from our group indicated that *PINX1* transcript level was not deregulated and no somatic mutation was detected in a series of 52 MB examined (Chang et al. 2004). The results were not supportive of *PINX1* as TSG in MB.

5.1.2 Search for TSG on chromosome 8p

To continue the search for candidate TSG on chromosome 8p in MB, I had employed multiple approaches. The first approach was to review the available literature and selected the most probable TSG candidates located within the deletion regions for molecular analysis. The two genes that have been suggested to act like TSG in previous

studies were selected to analyze. Two genes were worthy of examination, namely leucine zipper, putative tumor suppressor 1 (*LZTS1*) on chromosome 8p21.3 and tumor suppressor candidate 3 (*TUSC3*) on chromosome 8p22.

5.1.3 Expression analysis of *LZTS1* in MB

Previous studies have demonstrated that *LZTS1* was markedly underexpressed in gastric, bladder, kidney and lung tumors (Nonaka et al. 2005; Vecchione et al. 2001; Vecchione et al. 2002). Introduction of *LZTS1* inhibited tumor cell growth and suppressed tumorigenicity in nude mice (Ishii et al. 2001; Vecchione et al. 2001). These data prompted an evaluation of *LZTS1* for its potential involvement in MB.

With reduced expression in tumors as one of the features of TSGs quantitative RT-PCR was taken to examine the transcript levels of *LZTS1* and *TUSC3* in MB. The series contained 20 primary MBs, of which 15 cases were of childhood and 5 were of adults, and 3 normal cerebella. Using a value 2-fold lower than the mean expression level of 3 normal cerebella as a cutoff for reduced expression, only one (5%) MB showed decreased *LZTS1* level (Figure 1). The result revealed that downregulation of *LZTS1* occurred in a small subset of MB.

5.1.4 Transcript expression and epigenetic study of *TUSC3* in MB

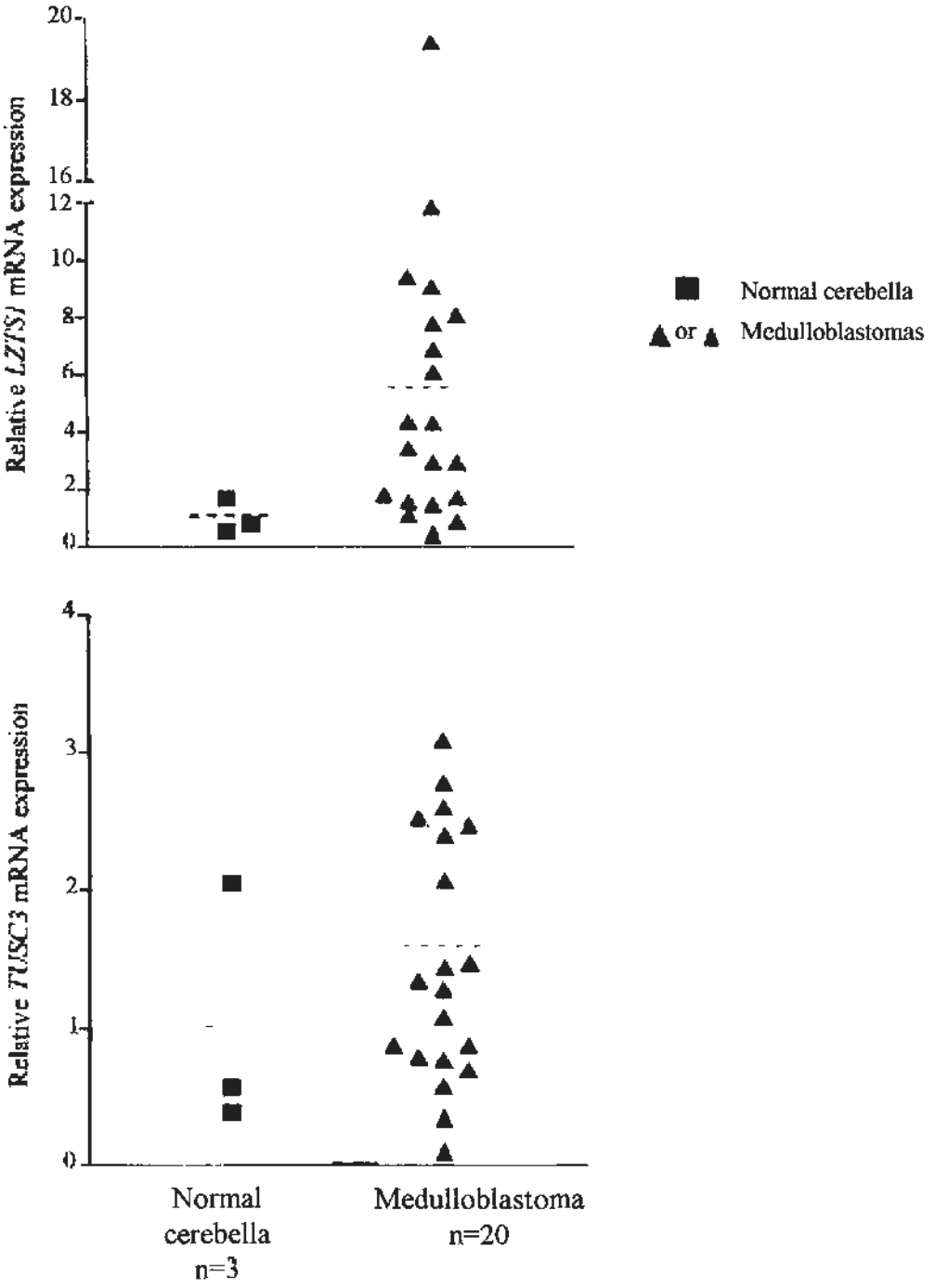

Figure 1 Relative expressions of *LZTS1* and *TUSC3* in MB by qRT-PCR The expression of these genes was normalized to *GAPDH* A minor fraction of MBs show reduced *LZTS1* (top) and *TUSC3* (bottom) transcript expression compared to normal cerebella The dashed lines indicate the mean expression level of normal cerebella and MB The red triangle represents tumors with reduced expression

Loss or reduced expression of *TUSC3* was reported in carcinomas of ovary, larynx and pharynx (Guervós et al. 2007; Pils et al. 2005). Decreased *TUSC3* expression was correlated with advanced stage and poor survival of larynx and pharynx carcinomas and with advanced stage of ovarian tumor (Guervós et al. 2007; Pils et al. 2005). These findings prompted an investigation on *TUSC3* status in MB.

Quantitative RT-PCR analysis revealed that 2 of 20 MBs examined showed reduced *TUSC3* level (Figure 1), with case 16 exhibiting a 16-fold reduced level and case 22 displaying a 3-fold decreased level relative to the mean expression of 3 normal cerebella. The allelic status at chromosome 8p23.1 was determined by FISH. Case 16 harbored a homozygous deletion whereas case 22 carried allelic gain of 3-4 copies at 8p23.1. In cases exhibited no reduced *TUSC3* expression, seven of them displayed allelic gain at 8p23.1, three of them showed 8p loss, and the remaining eight cases demonstrated 8p retention. For case 16, although the extent of the homozygously deleted interval in this tumor was unclear, the extremely low transcript level of *TUSC3* was consistent with chromosomal loss. Alternatively, *TUSC3* might have been a bystander co-deleted with the target gene in the homozygously deleted region.

To delineate the mechanism of reduced *TUSC3* expression in case 22, the involvement of epigenetic change was evaluated. The MethPrimer algorithm indicated that the promoter region and exon 1 *TUSC3* contained a high G/C content. A single CpG

island with a size of 651 bp comprising a total of 67 CpG sites was predicted at the promoter region and exon 1 of *TUSC3* (NM_006765 and NM_178234; Figure 2) by MethyPrimer. Bisulfite sequencing analysis was employed to determine the methylation status of *TUSC3* in case 22. A set of primers was designed to amplify an interval that covered 20 CpG sites of *TUSC3*. The PCR product was subcloned into pCR2.1 and ten randomly picked clones were selected for direct DNA sequencing. Figure 2 summarizes the results of bisulfite sequencing. Of 10 clones sequenced, three clones exhibited low methylation. Clone #8 showed DNA methylation in 2 of 20 CpG sites examined and clones #7 and #9 displayed DNA methylation at the last CpG site examined, with the rest of the CpG sites showing unmethylation. No hypermethylation was detected in the remaining clones. The infrequent hypermethylation indicated epigenetic mechanism was unlikely to explain downregulation of *TUSC3* transcript. Other unidentified mechanisms might be responsible for regulating *TUSC3* expression.

Collectively, the results indicated that downregulation of *TUSC3* expression occurred in a small fraction (10%) of MBs, but further study is needed to clarify the involvement of *TUSC3* in MB oncogenesis. This candidate gene approach was time-consuming to elucidate TSG in MB. Thus, the next approach was taken.

5.1.5 Global expression profiling to identify candidate TSG on chromosome 8p

A

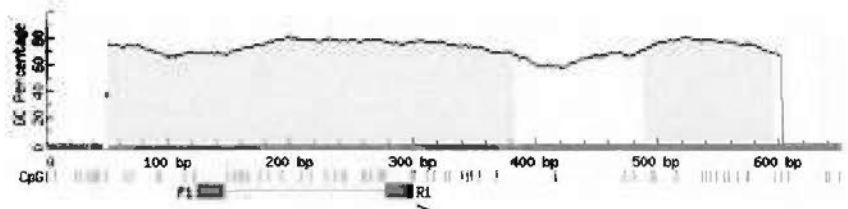

B

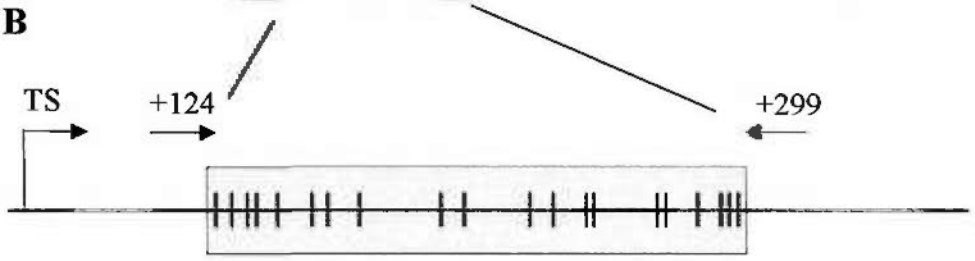

C

CpG site

Clone	1	2	3	4	5	6	7	8	9	10	11	12	13	14	15	16	17	18	19	20
1	U	U	U	U	U	U	U	U	U	U	U	U	U	U	U	U	U	U	U	U
2	U	U	U	U	U	U	U	U	U	U	U	U	U	U	U	U	U	U	U	U
3	U	U	U	U	U	U	U	U	U	U	U	U	U	U	U	U	U	U	U	U
4	U	U	U	U	U	U	U	U	U	U	U	U	U	U	U	U	U	U	U	U
5	U	U	U	U	U	U	U	U	U	U	U	U	U	U	U	U	U	U	U	U
6	U	U	U	U	U	U	U	U	U	U	U	U	U	U	U	U	U	U	U	U
7	U	U	U	U	U	U	U	U	U	U	U	U	U	U	U	U	U	U	U	M
8	U	U	U	U	U	U	U	U	U	U	M	M	U	U	U	U	U	U	U	U
9	U	U	U	U	U	U	U	U	U	U	U	U	U	U	U	U	U	U	U	M
10	U	U	U	U	U	U	U	U	U	U	U	U	U	U	U	U	U	U	U	U

Figure 2: Bisulfite sequencing analysis of *TUSC3* in case 22. (A) CpG island identification by MethPrimer software. The blue area indicates the CpG island identified. A CpG island is a genomic region with a GC percentage that is > 50% and with an observed/expected CpG ratio >60%. The F1 and R1 represent the location of forward and reverse primers for bisulfite sequencing, respectively. (B) A schematic diagram showing 20 CpG sites on exon 1 (grey box) of *TUSC3*. Each vertical line represents a CpG dinucleotide. The arrow indicates the PCR primer orientation and the number above represents primer location relative to the transcriptional start (TS) site set as +1. (C) Result of bisulfite sequencing. PCR products were cloned and subjected to sequencing. Each row represents the methylation status of 20 CpG sites for each sequenced clone. Clones 7, 8 and 9 show methylation at 1 or 2 CpG sites. Hypermethylation is an infrequent event in this MB case. M, methylation; U, unmethylation.

A genome-wide profiling approach was undertaken to identify candidate TSG on chromosome 8p. Expression microarray was performed on seven MBs (cases 16, 17, 21, 23, 24, 25 and 28) and 2 normal cerebella, using the Affymetrix Human Genome U133 Plus 2.0 Array. Each microarray contained 56,000 probes representing 47,000 transcripts. There was a total of 664 probes on chromosome 8p, and 211 probes of them represented 78 transcripts (55 known and 23 unknown genes) in the homozygously deleted region on 8p22-23.1.

5.1.6 Validation of global expression profiling

To validate the microaray data, qRT-PCR was performed on six differentially expressed genes, which showed increase or decrease expression by 2-fold in all the seven MBs compared to the normal cerebella. These included three upregulated genes *EZH2* (7q35-q36), *MCM7* (7q21.3-q22.1), *NHLH1* (1q22), and three downregulated genes *AKAP12* (6q24-q25), *PK1B* (6q22.31), and *WFDC1* (16q24.3). The microarray and qRT-PCR data are shown in Figure 3. Consistent with the microarray result, an upregulation of *EZH2, MCM7,* and *NHLH1* and downregulation of *AKAP12, PK1B*, and *WFDC1* in all seven tumors examined as compared to normal cerebella was observed by qRT-PCR. Notably, significant correlation between qRT-PCR and microarray data was evidenced in all tested genes ($p<0.04$). The gene expressions from both methods

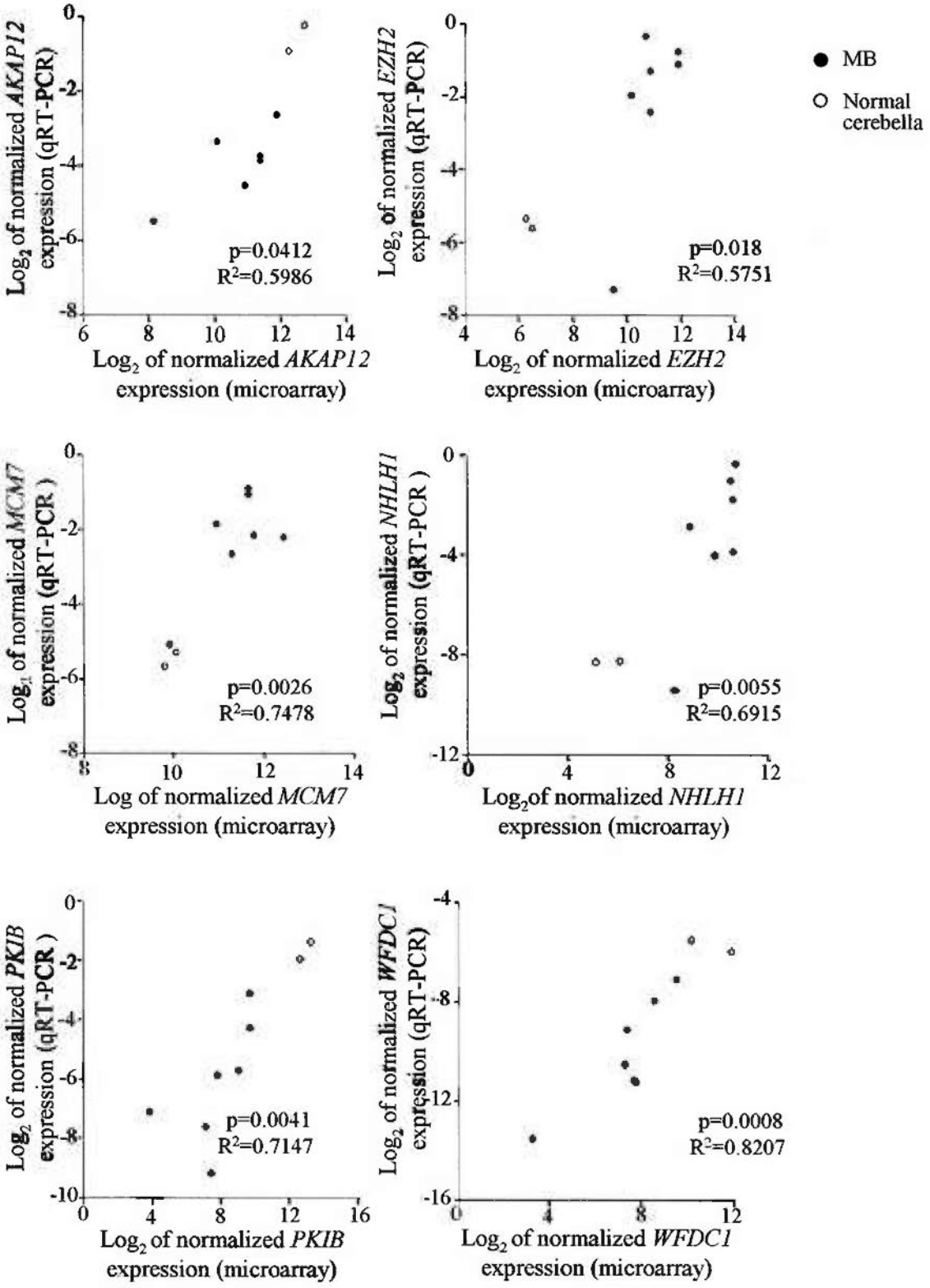

Figure 3. Validation of microarray results by qRT-PCR. A significant correlation is observed between expression determined by microarray and qRT-PCR for each gene ($p<0.05$). The x-axis represents $\log_2$ of the array-based raw data after global median normalization (Quackenbush 2002). The y-axis represents $\log_2$ of gene expression after normalized with *GAPDH*.

were in excellent agreement with each other, indicating the microarray data were reliable and accurate.

5.1.7 Identification of potential TSGs

To identify the potential TSG on chromosome 8p, I evaluated gene expression using student's t-test. On chromosome 8p, a total of 132 probes representing 49 transcripts exhibited significant differential expression ($p<0.05$), with 13 of them being unknown genes. Within the homozygously deleted region, 18 genes showed differential expression. *TUSC3* which were previously studied was found to be differentially expressed in one case (14%). The fraction of MBs demonstrated reduced expression was in consistent with the qRT-PCR. To narrow down the number of candidate TSGs, genes on the homozygously deleted interval were subjected to further statistical evaluation. To this end, the data of seven MBs and two normal cerebella on gene expression within this region was first taken. And, a comparison between gene expression of each tumor and each normal cerebellum was then made. In return, a sum of 7 comparisons was obtained by comparing the expression of 7 MBs to a normal cerebellum, and a total of 14 comparisons was found for the two normal cerebella. The genes were then ranked according to the extent of underexpression. Six genes exhibited reduced expressions in all 14 comparisons, including *DKFZp761P0423,*

dihydropyrimidinase-like 2 (DPYSL2), EF-hand domain family, member A2 (EFHA2), chromosome 8 open reading frame 79 (C8orf79), lipoprotein lipase (LPL) and methionine sulfoxide reductase A (*MSRA).* Two novel genes *DKFZp761P0423* and *EFHA2* showed the lowest expression level compared to normal cerebella. An average of 12-fold and 5.5-fold underexpression of *DKFZp761P0423* and *EFHA2* was observed, respectively. These two genes were further investigated by qRT-PCR in a series of 20 MBs (including the seven cases that were examined by microarray).

5.1.8 Expression analysis of *EFHA2*

As depicted in Figure 4, 17 of 20 (85%) MBs examined showed downregulation of *EFHA2* transcript. Case 1 showed no detectable *EFHA2* transcript, while cases 16 and 21 exhibited 52- and 61-fold decreased expression compared to normal cerebella, respectively. The remaining 14 cases demonstrated a 2- to 29-fold reduced expression compared to normal cerebella. FISH analysis showed that case 16 harbored homozygous deletion at chromosome 8p23.1 and case 21 carried an allelic loss at 8p22. This suggested the chromosome loss attributed in part to *EFHA2* downregulation. Case 1 showed retention for 8p. There was no significant association between reduced *EFHA2* expression and allelic loss. Nevertheless, the three cases without downregulation of *EFHA2* displayed 8p gain.

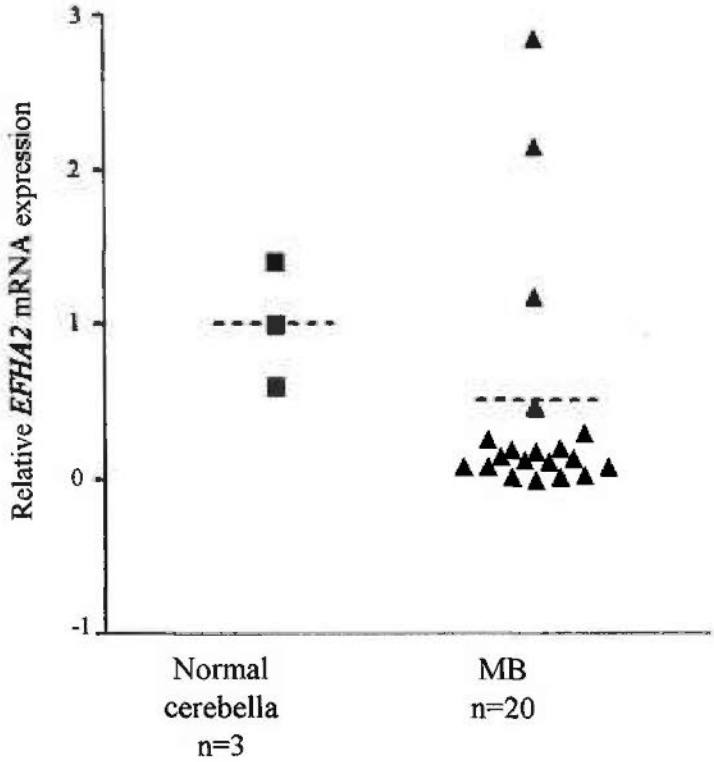

Figure 4. Relative expression of *EFHA2* transcript in MB as determined by qRT-PCR. Using 2-fold as a cutoff, seventeen of 20 (85%) MBs exhibit reduced *EFHA2* mRNA level compared to normal cerebella. *EFHA2* expression was normalized to *GAPDH*. The expression of *EFHA2* in average normal cerebella was set to 1, and *EFHA2* expression in MB represents the relative expression compared to the average normal cerebella. Dashed line represents the mean expression level.

The presence of CpG islands at the promoter and exon 1 of *EFHA2* prompted for investigation whether DNA methylation was a mechanism for transcriptional silencing. Two sets of MSP primers were designed to interrogate the methylation status of *EFHA2* in MB. Primer set 1 (M1) covers about 240 bp in the promoter region and set 2 spans 100 bp within exon 1 (M2) (Figure 5). The results showed that hypermethylation within exon 1 (M2) was detected in eight cases, namely case 6, 7, 8, 9, 20, 25, 27 and 28 (Figure 5 and Table 9), while no aberrant methylation was found at the promoter region (M1), suggesting region-specific DNA methylation. None of the three normal cerebella displayed any methylation in both CpG regions examined. Of the eight cases that showed DNA methylation at exon 1, seven of them had >2-fold reduced *EFHA2* expression. There were 10 cases with reduced expression displaying unmethylated alleles. The findings indicate that exon 1 of *EFHA2* gene is methylated in a fraction of MBs.

In conclusion, reduced *EFHA2* expression occurred in 85% of MB (Table 9). Two cases (10%) demonstrated loss of 8p and DNA methylation. Two cases (10%) exhibited 8p loss without hypermethylation and five cases showed DNA methylation without 8p loss. Loss of chromosome 8p and epigenetic silencing may be the possible mechanisms for downregulation of *EFHA2* in 10 MB cases. However, other mechanisms that have yet to be determined may account for the reduced expression in

A

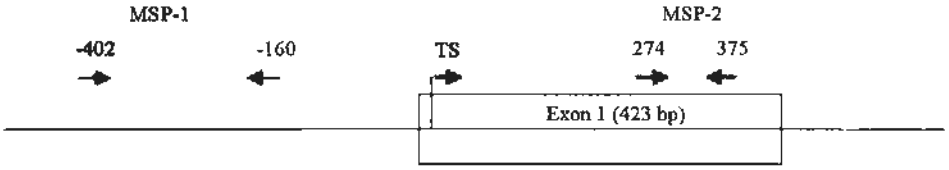

B

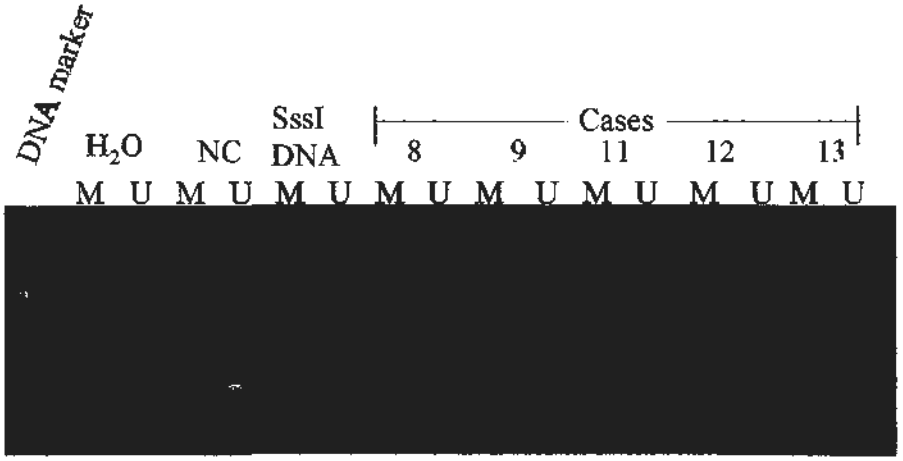

Figure 5. Determination of methylation status of *EFHA2* by MSP analysis. (A) A schematic representation of the two regions of *EFHA2* gene subjected to MSP analysis. The arrow indicates primer orientation and the number above represents primer location relative to the transcriptional start site (TS) set at +1. (B) Representative results of MSP within exon 1 of *EFHA2*. Modified genomic DNA was subjected to PCR with methylation (M)- and unmethylation (U)-specific primers. Aberrant methylation is observed in cases 8 and 9 but not in cases 11, 12 and 13. The SssI methylase-treated placental DNA (SssI DNA) and normal cerebellum (NC) are used as methylation and unmethylation controls, respectively. The sample containing no DNA template (H_2O) serves as a PCR control.

Table 9. Summary of *EFHA2* transcript expression, chromosome 8p status and DNA methylation status of 20 MBs

Case no. [a]	*EFHA* expression [b]	Chromosome 8p status	DNA methylation status [c]
1 (HS416)	UD	Retention	-
16 (HS411)	0.02	Homozygous deletion	-
21 (HS490)	0.02	Loss	-
24 (HS352)	0.03	Retention	-
20 (HS409)	0.08	Monosomy	+
27 (HS489)	0.08	Monosomy	+
25 (HS487)	0.08	Gain	+
12 (HS414)	0.12	Gain	-
9 (HS412)	0.13	Retention	+
6 (HS408)	0.13	Retention	+
8 (HS486)	0.15	Retention	+
23 (HS355)	0.18	Retention	-
22 (HS413)	0.20	Gain	-
28 (HS410)	0.20	Retention	+
17 (HS491)	0.26	Gain	-
11 (HS353)	0.30	Gain	-
14 (HS403)	0.47	Retention	-
13 (HS407)	1.17	Gain	-
7 (HS406)	2.15	Gain	+
3 (HS405)	2.85	Gain	-

a. Parenthesis indicates laboratory number.
b. Relative *EFHA* transcript expression was normalized to *GAPDH*. The expression of *EFHA* transcript expression in normal cerebella was set to 1. The data represent the relative *EFHA* expression compared to normal cerebella. UD represents undetectable expression.
c. DNA methylation at exon 1 of *EFHA* gene was examined by MSP.

the remaining 8 cases. Further investigation is needed to elicit *EFHA2* in MB development.

5.1.9 Expression analysis of *DKFZp761P0423*

To investigate the role of *DKFZp761P0423* in MB, qRT-PCR was performed. As shown in Figure 6, expression of *DKFZp761P0423* was reduced by more than 2-fold in 14 of 20 (70%) MBs examined. Five cases (cases 6, 16, 25, 27, and 28) showed >10-fold decreased *DKFZp761P0423* relative to normal cerebella. Case 27 showed monosomy of 8p and case 16 exhibited homozygous deletion at 8p (Table 10). Two cases (case 6 and 28) showed 8p retention and the remaining case exhibited a gain of chromosome 8p. In contrast, none of the 6 cases displayed no *DKFZp761P0423* downregulation displayed a loss of 8p. Gain of chromosome 8p was observed in five of these cases and the remaining one displayed a retained for 8p. The loss or retained chromosome 8p was significant correlated with reduced *DKFZp761P0423* expression (Fisher's exact test; p=0.049). This data suggested loss of 8p might be a mechanism for reduced expression of *DKFZp761P0423* gene. Other mechanisms, such as DNA methylation, leading to downregulation of *DKFZp761P0423* are yet to be identified. In this study, *DKFZp761P0423* gene methylation was not analyzed. Further analysis needed to be performed to elucidate DNA methylation of *DKFZp761P0423*.

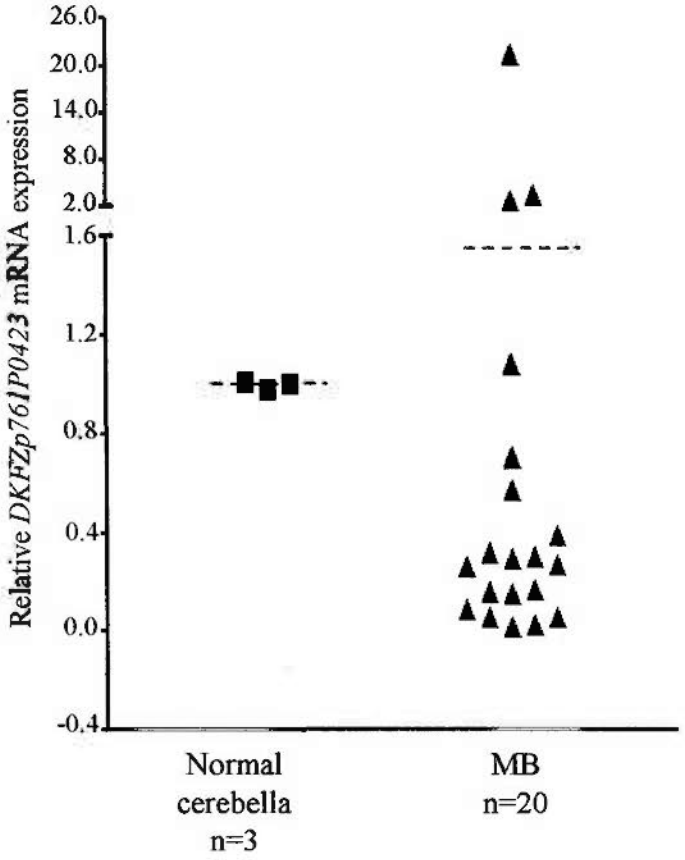

Figure 6. Relative expression of *DKFZp761P0423* in MB as determined by qRT-PCR. Fourteen of 20 (70%) MBs examined demonstrate reduced *DKFZp761P0423* transcript level compared to normal cerebella. *DKFZp761P0423* expression was normalized to *GAPDH*. The expression of *DKFZp761P0423* in average normal cerebella was set to 1, and *DKFZp761P0423* expression in MB represents the relative expression compared to the average normal cerebella. Dashed line represents the mean expression level.

Table 10. Summary of *DKFZp761PO423* transcript expression and chromosome 8p status of 20 MBs

Case no. [a]	*DKFZP761PO423* expression [b]	Chromosome 8p status
28 (HS410)	0.02	Retention
16 (HS411)	0.03	Homozygous deletion
25 (HS487)	0.06	Gain
6 (HS408)	0.06	Retention
27 (HS489)	0.09	Monosomy
1 (HS416)	0.15	Retention
21 (HS490)	0.16	Loss
17 (HS491)	0.17	Gain
20 (HS409)	0.26	Monosomy
24 (HS352)	0.27	Retention
12 (HS414)	0.29	Gain
9 (HS412)	0.30	Retention
23 (HS355)	0.32	Retention
8 (HS486)	0.39	Retention
22 (HS413)	0.57	Gain
14 (HS403)	0.70	Retention
11 (HS353)	1.08	Gain
3 (HS405)	2.79	Gain
7 (HS406)	3.70	Gain
13 (HS407)	21.27	Gain

a. Parenthesis indicates laboratory number.
b. Relative *DKFZp761PO423* transcript expression was normalized to *GAPDH*. The expression of *DKFZp761PO423* transcript expression in normal cerebella was set to 1. The data represent the relative expression compared to normal cerebella.

5.1.10 Expression analysis of 49 genes located on chromosome 8p

Microarray analysis revealed 49 downregulated genes that mapped to chromosome 8p. To evaluate whether any of 49 genes were potential TSG, a rapid screen for lack of expression of these genes in MB cell lines was performed. The underlying assumption of this approach was that TSG is likely to have absent expression in tumor cell lines. For instance, the TSG p16 is lost in a number of cell lines (Havrilesky et al. 2001). Conventional RT-PCR of 49 genes was performed in seven MB lines. The results showed that transcripts of 49 genes were detected in all cell lines examined, suggesting that these genes may not be involved in MB.

5.2 Identification of deregulated miRNAs on chromosome 8p

In year 2006, the concept of miRNA involvement in tumorigenesis began to emerge. A number of studies implicated that miRNAs might function as TSGs. Thus, I hypothesized that miRNAs located on chromosome 8p might be involved in MB oncogenesis. At that time, only three miRNAs were annotated on chromosome 8p. They were miR-124 on 8p23.1, miR-320 on 8p21.3 and miR-383 on 8p22. Both miR-124 and miR-383 were mapped to the homozygously deleted region. The potential involvement of these miRNAs in the development of MB was investigated.

Quantitative RT-PCR was performed to determine the expression levels of

miR-124, miR-320 and miR-383 in a series of 29 MBs and seven cell lines. As shown in Figure 7, 21 (72%) tumors showed significant down-regulation of miR-124 transcript by at least 2-fold, with 11 (38%) cases exhibiting reduced expression by >10-fold ($P< 0.01$), compared to mean expression level of 3 normal cerebella. With the exception of ONS-76, all MB cell lines displayed reduced miR-124 expression by >30-fold ($p<0.01$). No miR-124 transcript was detectable in ONS-76. Two anaplastic cases (case 1 and 2) showed the highest miR-124 expression among all samples examined, with case 1 displaying 1.6-fold higher level than normal cerebella and case 2 having normal level.

As depicted in Figure 7, 23 of 29 (79%) tumors showed significant downregulation of miR-383 by at least 2-fold ($p<0.01$), with 10 tumors displaying >10-fold reduced level compared to the mean expression level of three normal cerebella. Three tumors exhibited no detectable miR-383 transcripts and all were childhood cases. ONS-76 showed extremely low level of miR-383 (reduced by 43-fold compared to normal cerebella). The other MB lines did not express miR-383.

The expression pattern of miR-320 was heterogeneous compared to normal cerebella. Both overexpression and underexpression were observed in tumors. As shown in Figure 7, overexpression of miR-320 was detected in 6 of 29 (21%) MBs, ranging from 2- to 4-fold above normal level, and underexpression was observed in 8 of 29 (28%) tumors, ranging from 2- to 9-fold below normal level.

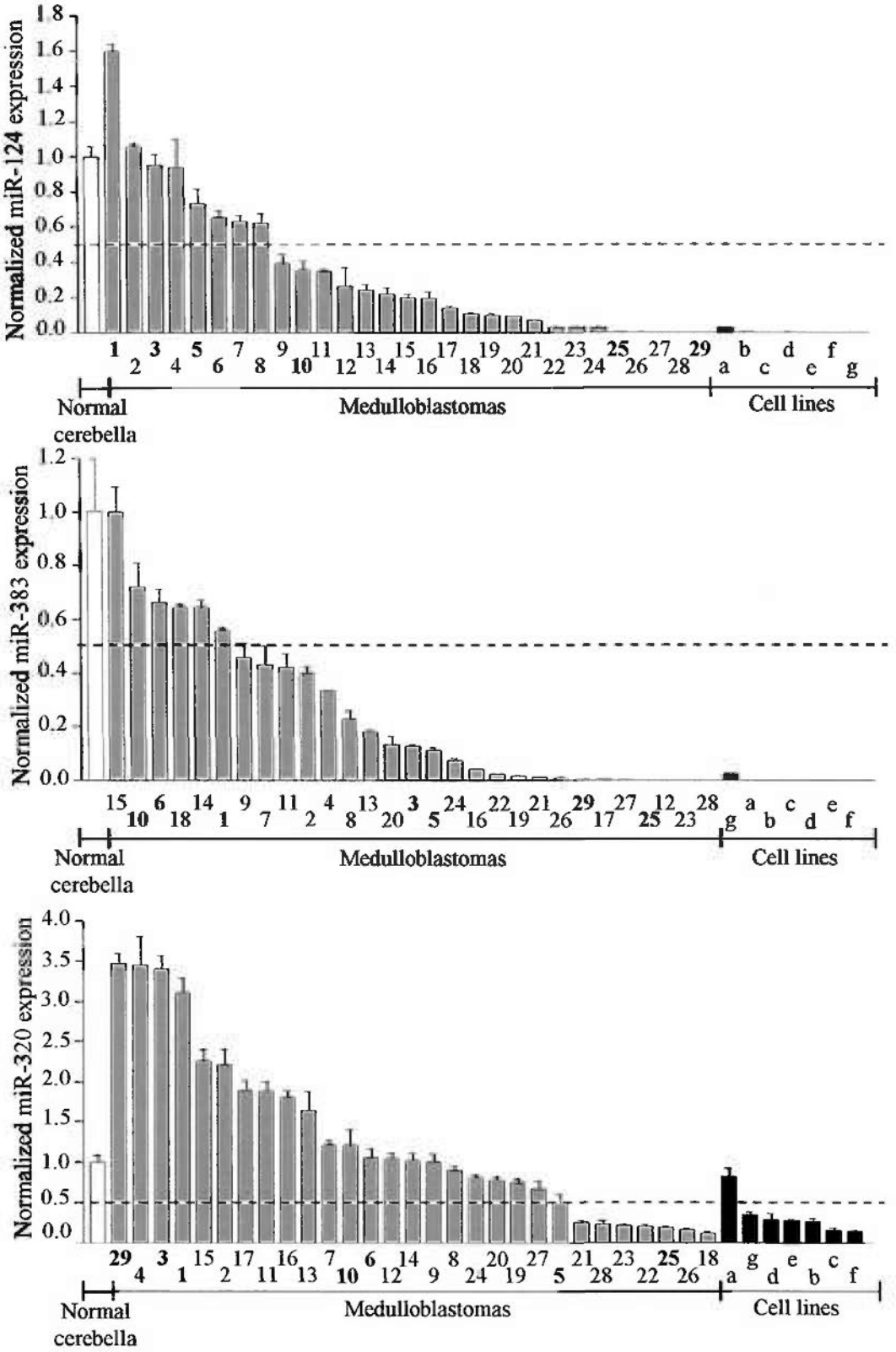

Figure 7. Expression profiles of miR-124, miR-383 and miR-320 in 29 MBs (grey bar), 3 normal cerebella (white bar) and 7 cell lines (black bar) as determined by microRNA assay. Reduced expressions of miR-124 and miR-383 are observed in 21 (72%) and 23 (79%) MBs, respectively. All 7 cell lines display decreased or absent expressions of miR-124 and miR-383. Expression of miR-320 is variable in MBs with 8 and 6 cases showing reduced and increased level, respectively. The number below the figure represents case number with bold indicates adult case. Small letter indicates cell line: a, D425; b, D458; c, D283; d, D384; e, D341; f, DAOY; g, ONS-76. Expression of miR-124, miR-383 and miR-320 was normalized to *GAPDH*. The data indicate the relative miRNA expression compared to average of normal cerebella. The dashed line represents the 2-fold cutoff relative to the mean expression of normal cerebella.

Statistical analysis showed no significant association between miR-124, miR-383 or miR-320 expression level and patient age (childhood versus adult) or gender. Taken together, the expression analysis indicated that miR-124 and miR-383 were significantly downregulated in a majority of tumors examined, suggesting that miR-124 and miR-383 might play a role in MB tumorigenesis. These deregulated miRNAs were thus investigated further. The diverse expression pattern of miR-320 suggested that this miRNA was unlikely to act as a TSG. No further work related to miR-320 was performed.

A review of literature revealed that miR-124 has been demonstrated as a brain-enriched miRNA (Lagos-Quintana et al. 2002) and was involved in regulation of neuronal differentiation (Krichevsky et al. 2006; Makeyev et al. 2007). This gives rise to the possibility that aberration in miR-124 may attribute to abnormal neuronal differentiation and thus MB tumorigenesis. Regarding miR-383, global miRNA expression analysis in 40 normal tissues demonstrated that it was a brain-enriched miRNA. The highest expression level of miR-383 expression was found in brain. Tissues included colon, thymus, testicle, ovary, prostate and peripheral blood mononuclear cell (PBMC) also expressed miR-383. Its expression was not detected in 32 normal tissues (Liang et al. 2007).

5.3 Correlation of miR-124 and allelic status on chromosome 8p23.1

Given that miR-124 is located on the homozygously deleted region, the correlation of miR-124 expression and allelic status of chromosome 8p was evaluated. Chromosome 8p allelic status was determined on paraffin sections of 29 MBs by two-color FISH analysis. The BAC clone RP11-403C10 served as the target clone to specifically mark chromosome 8p23.1 (miR-124 location), and the BAC clone RP11-67O16 detected chromosome 8q was designed as reference probe. In each case, a total of 200 interphase nuclei were analyzed. The result is summarized in Table 11.

Loss of 8p23.1 was demonstrated in 6 cases (21%). One case (case# 16) demonstrated homozygous deletion for chromosome 8p23.1 and 2 cases (case# 20 and 27) showed monosomy for chromosome 8. The remaining 3 cases (case# 5, 18, and 21) showed loss of 8p23.1 in >40% cell population. Gain of 8p23.1 was observed in 10 cases (case# 3, 7, 11, 12, 13, 15, 17, 19, 22, and 25) (34%). All of them displayed gain of 3-5 copies. The remaining cases (case# 1, 2, 4, 6, 8, 9, 10, 14, 23, 24, 26, 28, and 29) exhibited balanced 8p23.1. Interestingly, all cases exhibited chromosome 8p23.1 loss were children although the association did not reach statistical significance. Gain of 8p was observed in 2 adult and 8 childhood MBs. Two anaplastic cases (case 1 and 2) had chromosome 8p23.1 retention. Statistical analysis revealed no correlation between miR-124 expression and chromosome 8p status as illustrated in Table 12 (p=0.4926).

Table 11. Chromosome 8p status determined by FISH

Case No.	Chromosome 8p status
16	Homozygous deletion
21	Loss
18	Loss
5	Loss
20	Monosomy
27	Monosomy
15	Gain
3	Gain
12	Gain
13	Gain
7	Gain
11	Gain
17	Gain
22	Gain
19	Gain
25	Gain
6	Retention
28	Retention
9	Retention
24	Retention
23	Retention
8	Retention
4	Retention
26	Retention
2	Retention
29	Retention
10	Retention
1	Retention
14	Retention

Loss is defined as the presence of single target probe and reference probe signals (indicating monosomy) or fewer target probe signals than reference probe signals in >50% of the tumor cells.

Table 12. Correlation between miR-124 expression and chromosome 8p status in MB

Chromosome 8p status	Number of cases with reduced expression > 2-fold	Number of cases with reduced or increased expression < 2-fold
Homozygous deletion/ Loss/ Monosomy	5 (17%)	1 (3%)
Retention	8 (28%)	5 (17%)
Gain	8 (28%)	2 (7%)

However, 5 of 6 cases with 8p loss had reduced miR-124 with one case (case# 27) demonstrated a 288-fold downregulation of miR-124. The two anaplastic cases showed highest miR-124 expression were balanced at 8p23.1. Taken together, 8p23.1 loss may be one of the mechanisms responsible for reduced miR-124 expression in MB. Other regulatory mechanisms yet to be determined contributed to abnormality in miR-124 expression. Further analysis may need to be taken to determine the underlied mechanism for reduced miR-124 expression.

Statistical analysis showed that no association was found between chromosome 8p23.1 status and age, sex, and histological type.

5.4 Functional characterization of miR-124

5.4.1 Effects of ectopic expression of miR-124 on cell growth by MTT assay

To evaluate the effects of miR-124 overexpression on cell growth in MB, miR-124 mimic was transfected transiently into DAOY and ONS-76 cells followed by assessment of cell viability for four consecutive days by MTT assay. DAOY expressed barely detectable miR-124 transcript (4800-fold below normal cerebellar level) while ONS-76 showed no detectable miR-124 (Figure 7).

Optimization of transfection condition was performed using a fluorescent labeled miRNA negative control. DAOY and ONS-76 were transfected with varying

ratios of miRNA control and Lipofectamine 2000. Transfection efficiency was determined by examining the fraction of green fluorescent cells at 24 hours post-transfection. Transfection condition leading to 80%-90% of cells being fluorescently labeled was employed in subsequent experiment. The transfection condition is stated in Chapter 4.8.

As depicted in Figure 8, transfection of miRNA negative control into either cell lines showed no effect on cell growth over a period of 96 hours compared to mock. Notably, transfection of miR-124 mimic inhibited the growth of DAOY cells in a time-dependent manner ($p<0.05$). Cell growth was suppressed by 23% at 24 hours and by 72% at 96 hours post-transfection compared to mock. In ONS-76, restoration of miR-124 inhibited cell growth by 40% at 48 hours and by 70% at 96 hours post-transfection.

5.4.2 Effects of ectopic expression of miR-124 on cell growth by cell counting

To support the growth inhibitory effect of miR-124, viable cell counting was performed in DAOY and ONS-76 for 4 consecutive days after miR-124 transfection. As illustrated in Figure 9, restoration of miR-124 significantly reduced the viable cell number of DAOY at all time points examined ($p<0.05$). At 24 hours and 96 hours after transfection, cell number was reduced by 52% and 86% respectively compared to mock.

Table 13. Cell cycle profiling of MB cells after miR-124 transfection

	Proportion of cells (%)			
	sub-G1	G1	S	G2/M
DAOY				
Negative control	0.5 ± 0.4 **	59.6 ± 1.7 **	16.1 ± 1.8 **	24.3 ± 1.8 **
miR-124	4.5 ± 1.9	69.8 ± 4.8	9.3 ± 0.8	16.5 ± 2.7
ONS-76				
Negative control	0.3 ± 0.31	61.4 ± 1.8 **	17.4 ± 0.5 **	21.5 ± 2.4 **
miR-124	0.3 ± 0.05	91.7 ± 0.2	2.6 ± 0.6	5.3 ± 0.4

** $p<0.01$

DNA content was analysis by flow cytometry in DAOY and ONS-76 cells upon transfection of miR-124. The data represent the average percentage of cells in three individual experiments.

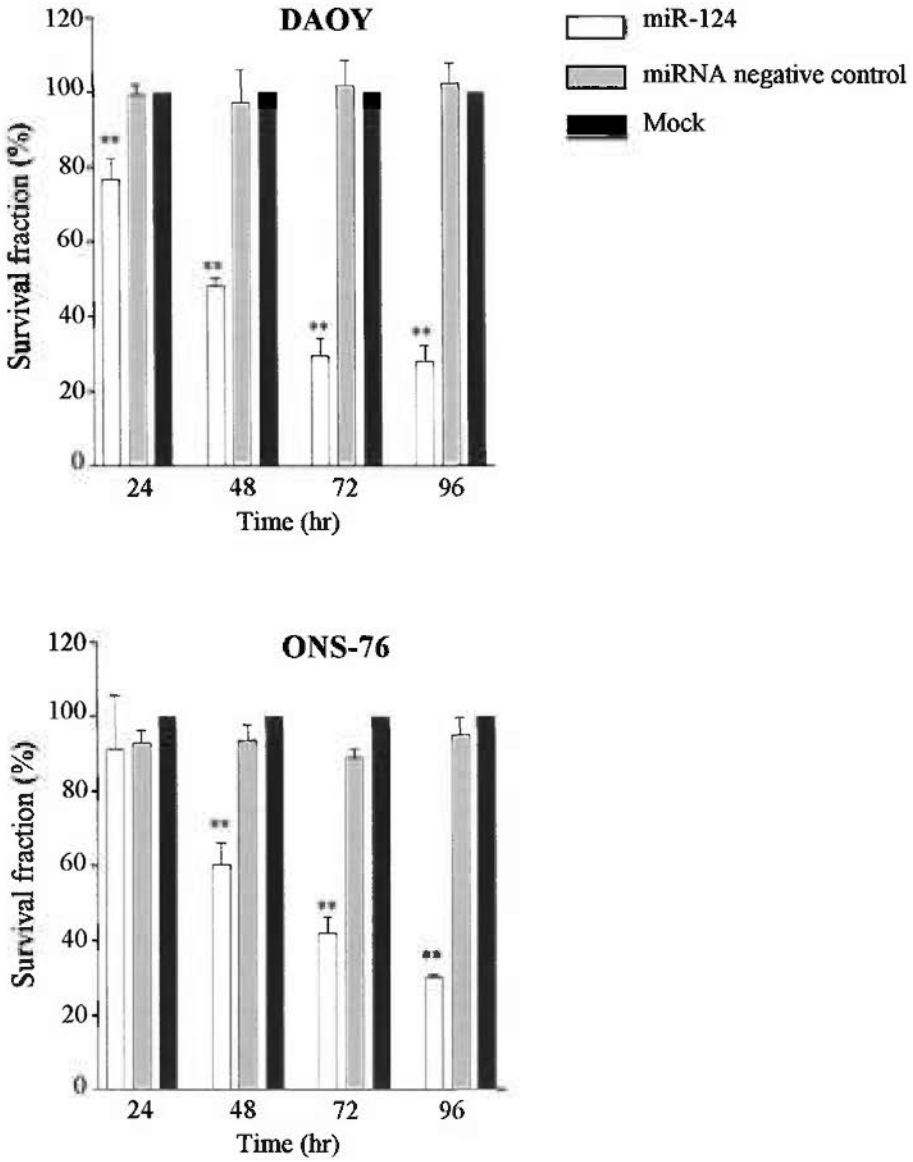

Figure 8. Effect of miR-124 overexpression on cell growth in MB by MTT assay. DAOY and ONS-76 cells (1.6-2.4 X 10^3 cells in 96-well plate) transfected with miRNAs were assayed for cell growth for 4 consecutive days. Ectopic expression of miR-124 in MB cells leads to a significant suppression of cell growth compared to mock. At 96 hr post-transfection, cell growth is suppressed by 72% and 70% in DAOY and ONS-76, respectively. The data are expressed as mean ± SD from 3 separate experiments. **, $p<0.01$.

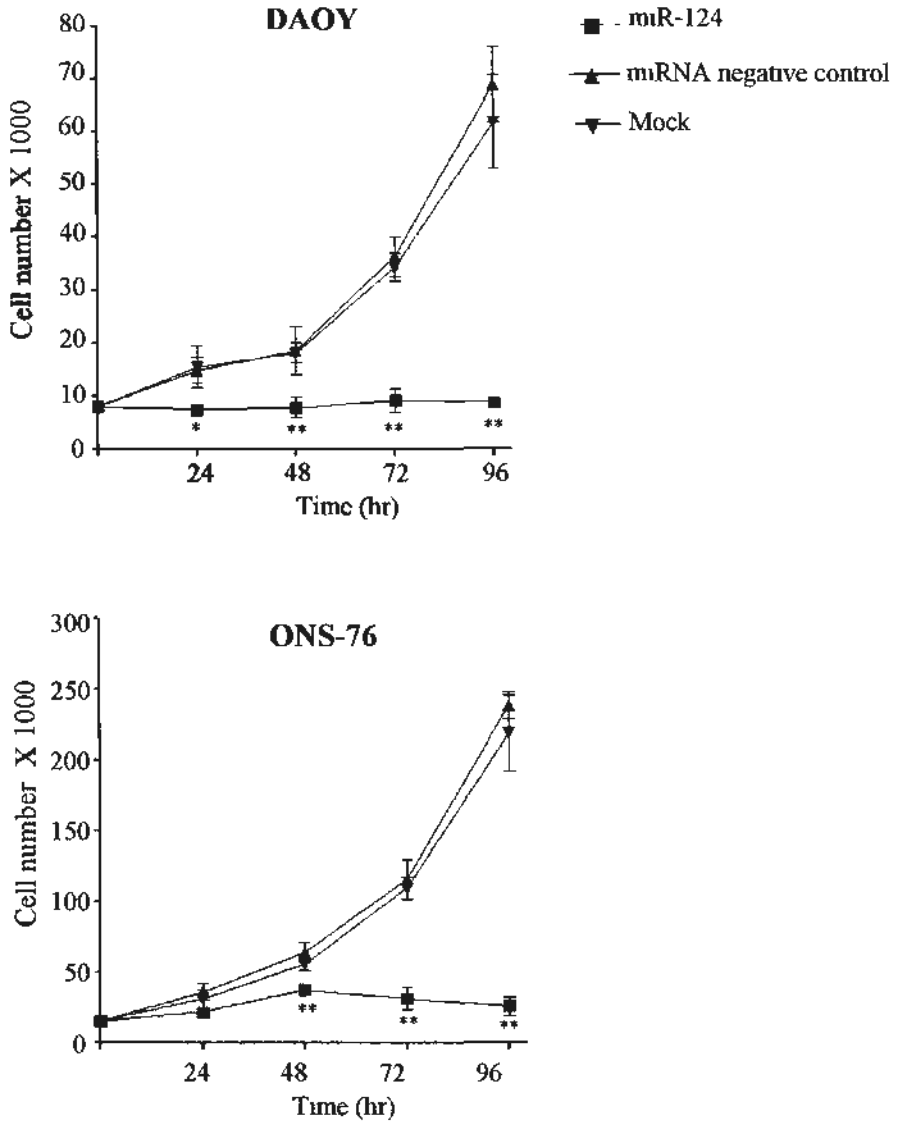

Figure 9. Effect of miR-124 overexpression on cell growth by viable cell counting DAOY and ONS-76 (0 8-1 2 X 10^4 cells in 24-well plate) transfected with miRNAs were subjected to cell counting using trypan blue exclusion assay for 4 successive days. Ectopic expression of miR-124 leads to a significant decrease in viable cell number compared to cells transfected with miRNA negative control or mock cells. At 96 hr post-transfection, viable cell number is reduced by 86% and 80% in DAOY and ONS-76 cells, respectively. The data are expressed as mean cell number ± SD from 3 separate experiments *, $p<0.05$, **, $p<0.01$.

No apparent difference in viable cell number was observed between cells transfected with miRNA negative control and mock. In ONS-76, significant growth inhibition was observed 48 hours after transfection and onwards. Viable cell number was decreased by 30% and 86% at 48 hours and 96 hours post-transfection compared to mock. Taken together, the MTT and cell count assays indicated that miR-124 had a growth suppressive effect in MB.

5.4.3 Effects of ectopic expression of miR-124 on cell cycle distribution

To determine the mechanism underlying growth inhibition by miR-124 in MB, cell cycle distribution was analyzed after miR-124 transfection. At 48 hours post-transfection, DAOY and ONS-76 were fixed, stained with propidium iodide and analyzed for DNA content by flow cytometry. The results are summarized in Table 13. In DAOY cells transfected with miR-124, a significant increase in G_1 fraction by 10% compared to control cells was observed. In addition, a 5-fold increase in the sub-G_1 fraction was observed, an indication of apoptosis. These changes were accompanied by a significant reduction in the S and G_2/M phases. Ectopic expression of miR-124 in ONS-76 resulted in a 30% increase in the percentage of cells in G_1 fraction. Concurrently, a decrease in the percentage of S-phase cells from 17% to 3% and of G_2/M-phase cells from 22% to 5% was detected in miR-124–transfected cells compared

Table 13. Cell cycle profiling of MB cells after miR-124 transfection

	Proportion of cells (%)			
	sub-G1	G1	S	G2/M
DAOY				
Negative control	0.5 ± 0.4 **	59.6 ± 1.7 **	16.1 ± 1.8 **	24.3 ± 1.8 **
miR-124	4.5 ± 1.9	69.8 ± 4.8	9.3 ± 0.8	16.5 ± 2.7
ONS-76				
Negative control	0.3 ± 0.31	61.4 ± 1.8 **	17.4 ± 0.5 **	21.5 ± 2.4 **
miR-124	0.3 ± 0.05	91.7 ± 0.2	2.6 ± 0.6	5.3 ± 0.4

** $p<0.01$

DNA content was analysis by flow cytometry in DAOY and ONS-76 cells upon transfection of miR-124. The data represent the average percentage of cells in three individual experiments.

to control cells. Taken together, the results suggested that miR-124 inhibited cell growth by blocking cell cycle progression at G_1.

5.4.4 Identification of miR-124 targets

The study by Lim et al. reported global miRNA expression pattern in HeLa cells after miR-124 transfection. They showed that the transcript levels of 174 genes were downregulated at 12 and 24 hours after miR-124 transfection and the 3'UTR of these downregulated transcripts had a significant propensity to pair to the seed region of miR-124, suggesting that these transcripts might be targets of miR-124. To identify potential miR-124 targets in MB, I employed a computational approach to predict miR-124 targets from the dataset generated by Lim et al. (Lim et al. 2005). The 174 downregulated genes from Lim et al's study were subjected to computational analysis using three miRNA target prediction algorthims, miRanda, PicTar, and TargetScan to determine if any of these genes was predicted as miR-124 targets. Such analysis returned a list of 35 potential targets predicted by at least two of the algorithms. Genes that were unknown and not implicated in tumorigenesis were filtered out. The candidate target list came down to 12 genes, including *CD164, CDK6, CTDSP2, IQGAP1, LAMC1, LASS2, MAPK14, PGRMC2, PTBP1, PTPN12, PTTG1IP, and SLC16A1.*

To evaluate whether miR-124 could modulate these genes in MB as in HeLa

cells, qRT-PCR was performed to determine the expression of these genes at 4 and 24 hours after miR-124 transfection in DAOY and ONS-76. As shown in Table 14, two genes, *SLC16A1* and *PTBP1*, showed markedly reduced expression at 4 to 24 hours post-transfection in both cell lines. *SLC16A1* expression was significantly decreased by 2.5-fold (p=0.0025) and 5.5-fold (p=0.0012) at 4 and 24 hours, respectively, after miR-124 transfection into DAOY, and decreased by 2.1-fold (p=0.01) and 5.9-fold (p=0.018) in ONS-76 over the same time points. *PTBP1* expression was reduced by 5.5-fold (p=0.002) and 4.3-fold in DAOY and ONS-76 (P=0.0069), respectively, at 24 hours after miR-124 transfection.

To test whether miR-124 expression would exert a negative regulation on SLC16A1 protein level, Western blot analysis was performed on five MB cell lines transfected with miR-124 mimic to determine SLC16A1 protein. The results showed that SLC16A1 protein level was reduced by 3.3-fold in DAOY and by more than 10-fold in ONS-76, D384, D458, D283, and D341 at 24 hours post miR-124 transfection (Figure 10) as compared to cells transfected with miRNA negative control. Taken together, these data suggested that miR-124 negatively regulated SLC16A1 at both transcript and protein levels in MBs.

5.4.5 Bioinformatic analysis of miR-124 binding site in 3'UTR of *SLC16A1*

Table 14. Candidate genes downregulated upon miR-124 transfection

	Quantitative RT-PCR								Microarray			
	DAOY				ONS-76				HeLa[1]			
	4 hr		24 hr		4 hr		24 hr		4 hr		12 hr	
Gene	Fold-change	P value	Fold-change	P value	Fold-change	P value	Fold-change	P value	Fold-change	P value	Fold-change	P value
CD164	-1.3	$2.5x10^{-1}$	-2.2	$7.0x10^{-2}$	-1.4	$2.7x10^{-1}$	-2.1	$5.0x10^{-2}$	-3.2	$1.0x10^{-17}$	-3.6	$6.1x10^{-18}$
CDK6	1	$7.4x10^{-1}$	-1.2	$7.0x10^{-2}$	1	$8.8x10^{-1}$	-1.4	$1.0x10^{-1}$	-1.8	$5.6x10^{-6}$	-3	$6.6x10^{-13}$
CTDSP2	1.3	$2.0x10^{-1}$	-1.3	$2.6x10^{-1}$	1.5	$6.0x10^{-2}$	1.15	$4.4x10^{-1}$	-3.4	$3.9x10^{-16}$	-3.8	$6.3x10^{-17}$
IQGAP1	1.1	$7.2x10^{-1}$	-1.2	$1.9x10^{-1}$	1.3	$2.7x10^{-1}$	1.1	$6.8x10^{-1}$	-2.2	$2.4x10^{-9}$	-3.5	$9.1x10^{-19}$
LAMC1	-1.4	$1.3x10^{-1}$	-1.1	$7.7x10^{-1}$	1.2	$4.1x10^{-1}$	1.1	$5.9x10^{-1}$	-2.4	$3.8x10^{-12}$	-3.9	$1.3x10^{-21}$
LASS2	1.1	$3.5x10^{-1}$	-6.8	$1.1x10^{-3}$	1.1	$8.4x10^{-1}$	-1.9	$8.0x10^{-2}$	-2.5	$6.6x10^{-14}$	-3	$1.8x10^{-15}$
MAPK14	-1.2	$2.6x10^{-1}$	1.1	$7.1x10^{-1}$	1.3	$2.1x10^{-1}$	2	$5.0x10^{-1}$	-1.7	$4.8x10^{-5}$	-2	$3.1x10^{-8}$
PGRMC2	1	$9.2x10^{-1}$	-1.4	$2.9x10^{-1}$	1.6	$1.7x10^{-1}$	1.8	$1.0x10^{-1}$	-2	$8.4x10^{-8}$	-2.2	$4.1x10^{-11}$
PTBP1	-1.2	$2.0x10^{-1}$	-5.5	$2.2x10^{-3}$	-1.4	$1.3x10^{-1}$	-4.3	$6.9x10^{-4}$	-2	$3.4x10^{-6}$	-3	$7.6x10^{-10}$
PTPN12	-1.1	$3.3x10^{-1}$	-1.3	$2.8x10^{-1}$	-1.5	$5.8x10^{-3}$	2	$9.0x10^{-4}$	-1.5	$6.9x10^{-4}$	-1.5	$4.1x10^{-4}$
PTTG1IP	1.2	$8.0x10^{-2}$	-1.2	$4.5x10^{-1}$	-1.4	$1.5x10^{-1}$	-1.4	$1.9x10^{-1}$	-1.8	$1.1x10^{-4}$	-2.2	$5.9x10^{-8}$
SLC16A1	-2.5	$2.5x10^{-3}$	-5.5	$1.2x10^{-4}$	-2.1	$1.0x10^{-2}$	-5.9	$1.8x10^{-4}$	-2.1	$2.7x10^{-7}$	-3	$1.4x10^{-14}$

[1] From Lim et al. 2005

A

```
SLC16A1
3'UTR          +1960 ├── miR-124 binding site ──┤+1982
Rat     5'ACAGTGTCATGAAGATTATAATATGTGCCTTAAGTTTTAGTTTT 3'
Mouse   5'ACAGTGTCATGAAGATTATAATATGTGCCTTAAGTTTTAGTTTT 3'
Human   5'ATAGTGTCATAAAGATTATAATATGTGCCTTAAGTTTTAGTCTT 3'
                          |||          |||||||
miR-124            3'ACCGUAA-GUGGCGCACGGAAUU5'
```

B

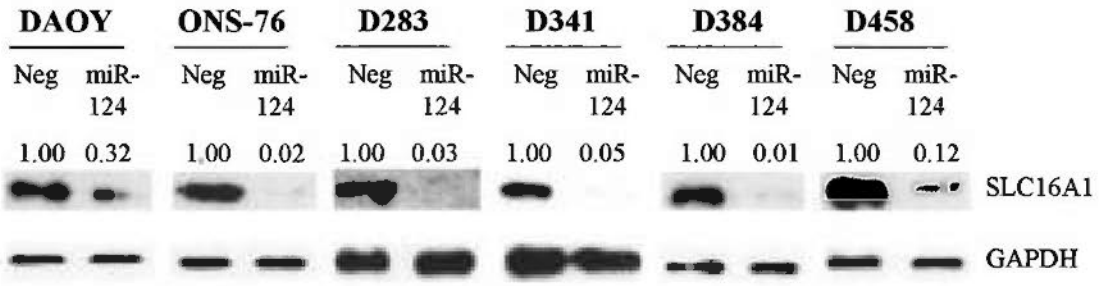

C

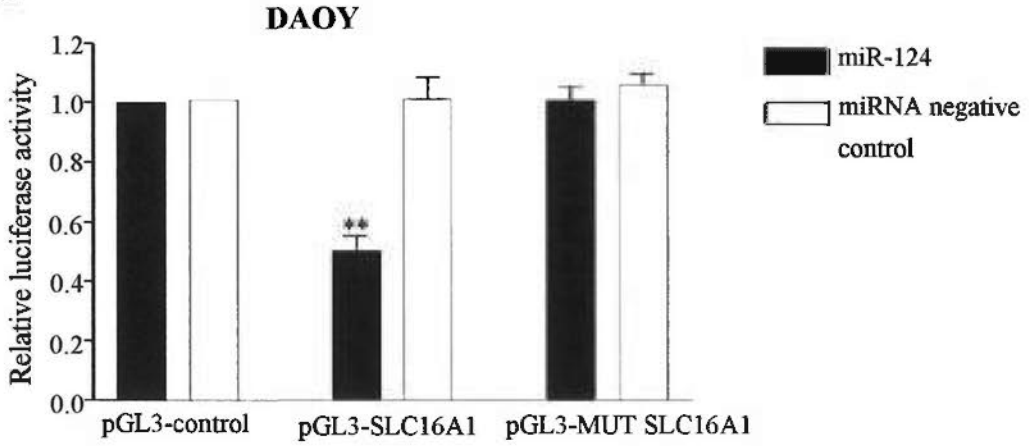

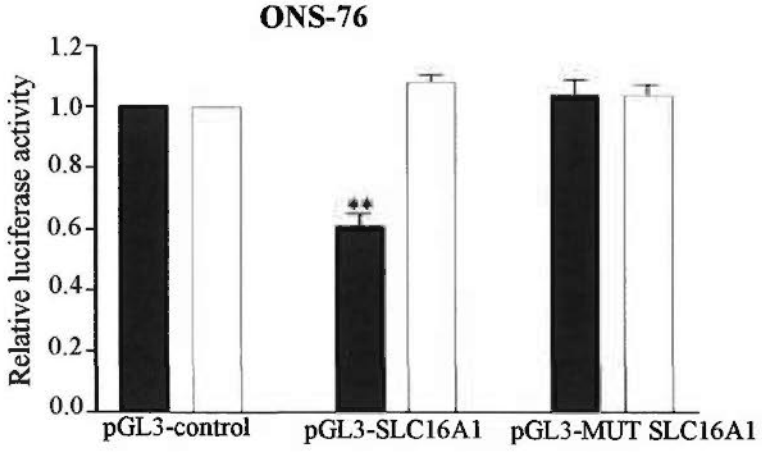

Figure 10. *SLC16A1* is a direct target of miR-124. (A) A schematic diagram of miR-124 MRE on 3'UTR of *SLC16A1*. The miR-124 MRE is conserved in human, rat and mouse. Perfect complementary base pairing is observed between the seed region of miR-124 (nucleotides 2-8) and miR-124 MRE. (B) Effects of miR-124 overexpression on SLC16A1 protein expression in MB. Cells transfected with miRNA were subjected to Western blot analysis at 48 hours post-transfection. Ectopic expression of miR-124 results in decreased levels of SLC16A1 by 3.2-fold in DAOY, 8.3-fold in D458, and >10-fold in ONS-76, D283, D341 and D384 compared to cells transfected with miRNA negative control (Neg). The number above the protein band represents relative intensity of SLC16A1 compared to control cells after normalization to GAPDH. The experiment was repeated three times. (C) Determination of interaction between miR-124 and MRE of *SLC16A1* by dual luciferase reporter assay. A 3'UTR fragment of *SLC16A1* containing MRE was cloned downstream of the firefly luciferase gene in pGL3-control vector (pGL3-SLC16A1). MB cells were co-transfected with the reporter construct, miR-124 or miRNA negative control and a renilla luciferase plasmid (pRL-TK for normalization of transfection efficiency). After 48 hr, transfected cells were evaluated for luciferase activity. The results show that luciferase activity is significantly suppressed by 50% and 40% respectively in DAOY and ONS-76 cotransfected with pGL3-SLC16A1 and miR-124 compared to cells cotransfected with pGL3-SLC16A1 and miRNA negative control. No decrease in luciferase activity is detected in cells cotransfected with mutant construct (pGL3-MUT-SLC16A1 in which a 9-bp substitution was created at the seed region of MRE) and miR-124. These results provide evidence that miR-124 interacts specifically with miR-124 MRE of SLC16A1. Three independent experiments were performed. **, $p<0.01$.

The nucleotide and protein sequences of *SLC16A1* are well conserved among human, mouse, and rat. The rodents share 85%-87% and 75% homology, respectively, in protein and coding sequences to human. Such high nucleotide sequence homology extends further to the first 600 bp of the 3'UTR, which contains a putative miR-124 miRNA response element (MRE). This binding site shows perfect complementarity at the seed region (positions 2-8) in miR-124 (Figure 10). The seed region is believed to be essential in target recognition (Doench et al. 2004; Lewis et al. 2003). The hybridization between *SLC16A1* and miR-124 is observed with a ΔG value of -13.4 kcal/mol, which is well within the range of a true miRNA target site (Zuker 2003). Moreover, of all candidate targets examined, *SLC16A1* is the only gene that was predicted as miR-124 target by all three algorithms employed.

5.4.6 Validation of *SLC16A1* as miR-124 target by luciferase reporter assay

To validate that *SLC16A1* is a miR-124 target, luciferase reporter assay was carried out to evaluate the interaction between MRE of *SLC16A1* and miR-124. The 2.0 kb-long 3' UTR of *SLC16A1* contains two XbaI sites. In order to clone the 3' UTR of *SLC16A1* downstream of a luciferase reporter vector, only the partial 3'UTR of *SLC16A1* contained the putative MRE and without the XbaI site was amplified and inserted downstream of a luciferase gene in the pGL3-control vector, and was

designated as pGL3-WT-SLC16A1. A mutant plasmid, named pGL3-MUT-SLC16A1, was also constructed by introducing a 9-bp substitution mutation in the 3'UTR. This mutation was designed to disrupt the putative base pairings between the seed region of miR-124 and the MRE of *SLC16A1*. These plasmids were then co-transfected into DAOY and ONS-76 with miR-124 mimic or miRNA negative control, together with a control plasmid encoding Renilla luciferase for correction of transfection efficiency. At 48 hours post-transfection, luciferase activity was determined. The results revealed a significant suppression of luciferase activity by 50% and 40%, respectively, in DAOY and ONS-76 cells co-transfected with construct bearing pGL3-WT-SLC16A1 and miR-124, when compared to cells cotransfected with pGL3-WT-SLC16A1 and miRNA control (Figure 10). More important, cells cotransfected with pGL3-MUT-SLC16A1 and miR-124 showed no inhibition of luciferase activity. These results indicated that miR-124 could specifically interact with the MRE of *SLC16A1* and thus negatively modulated the latter.

5.4.7 Determination of *SLC16A1* transcript level in primary MB

The *SLC16A1* transcript level in 29 MBs was assessed by qRT-PCR. Figure 11 illustrates that the *SLC16A1* transcript level was significantly enhanced in MB and cell lines ($p<0.01$). Enhanced *SLC16A1* expression was detected in 26 of 29 (90%) MBs,

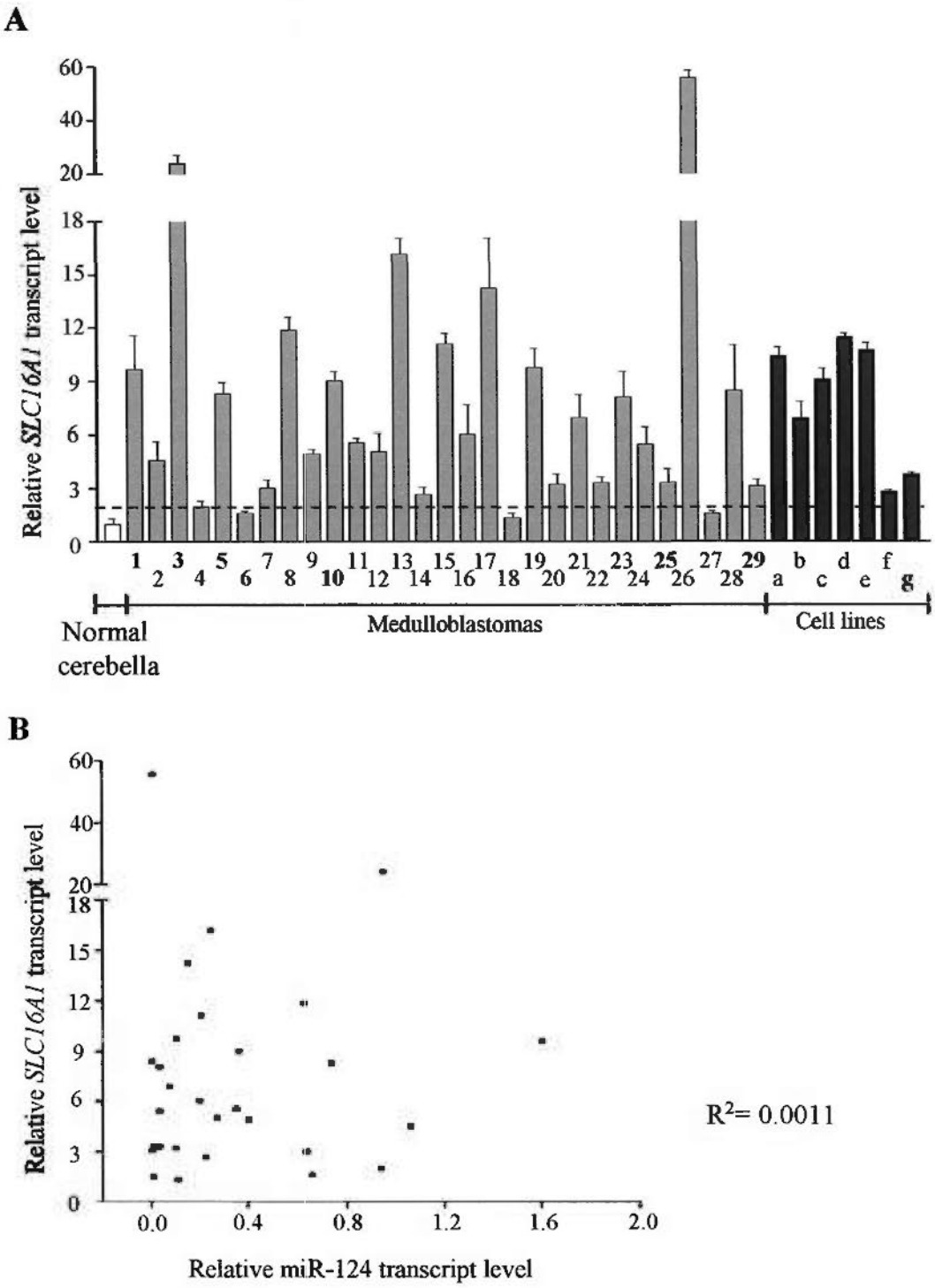

Figure 11. Expression profile of *SLC16A1* in MB by qRT-PCR. (A) The *SLC16A1* transcript level is significantly elevated in 26 of 29 MBs and all 7 cell lines examined compared to normal cerebella ($p<0.01$). The number below the figure represents case number with bold indicates adult case. Small letter indicates cell line: a, D425; b, D458; c, D283; d, D384; e, D341; f, DAOY; g, ONS-76. The dashed line represents 2-fold cutoff for overexpression relative to normal cerebella. The expression was normalized to *GAPDH*. The *SLC16A1* expression in normal cerebella was set to 1, and the expression of *SLC16A1* in MB represents the relative *SLC16A1* expression compared to normal cerebella. The data represent the average of three experiments ± SD. (B) A plot of *SLC16A1* expression versus miR-124 expression. No correlation is found between expressions of miR-124 and *SLC16A1*.

ranging from 2- to 56-fold above the mean expression level of three normal cerebella. Upregulation of *SLC16A1* mRNA was also observed in all 7 cell lines with a range between 3- and 12-fold above normal level. No correlation between miR-124 and *SLC16A1* levels was found in the series. Also, the *SLC16A1* level was not correlated with age or gender. The result suggests that *SLC16A1* transcript and miR-124 expression was not inversely correlated.

5.4.8 Depletion of *SLC16A1* suppressed cell growth

To delineate the biological significance of *SLC16A1*, expression of *SLC16A1* was depleted in DAOY and ONS-76 by two gene specific siRNAs independently. The siRNAs targeted exon 4 and exon 5 of *SLC16A1* were named siSLC16A1-1 and siSLC16A1-2, respectively. Cell viability was determined by MTT assay over a period of 96 hours. A negative siRNA with no sequence homology to any known human transcript was served as a control. The results revealed that cell viability was significantly impaired in siSLC16A1-transfected MB cells in a time-dependent manner. As showed in Figure 12, siSLC16A1-1 and siSLC16A1-2 decreased cell growth by 38% and 35% in DAOY, respectively, compared to the mock at 48 hours post transfection. Such suppression of cell growth was further enhanced to 50% at 96 hours. In ONS-76, knockdown of *SLC16A1* led to reduction in cell growth by 28-44%

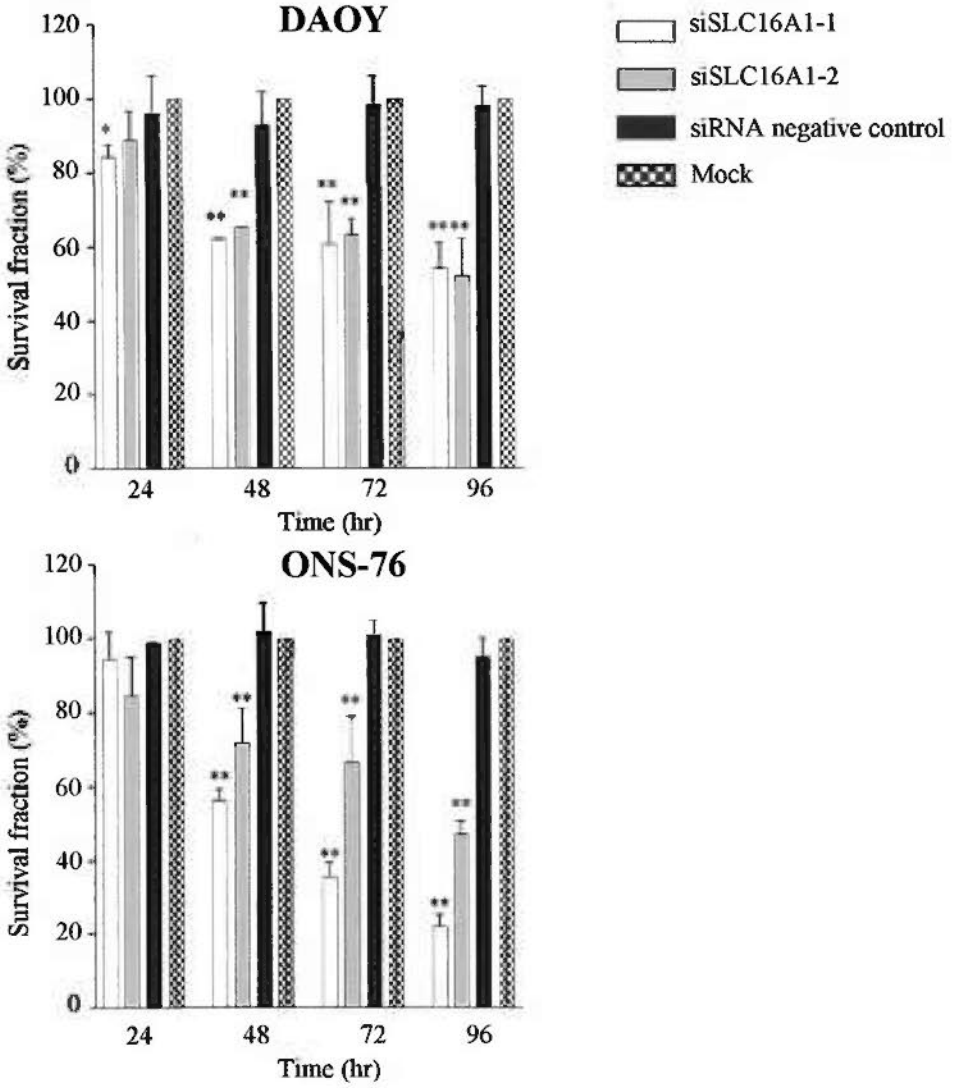

Figure 12. Effect of *SLC16A1* knockdown on cell growth in MB. Cells were transfected with 2 siRNAs against *SLC16A1* independently (siSLC16A1-1 and SLC16A1-2), a siRNA negative control or no siRNA (mock). Cell growth was monitored for 4 consecutive days post-transfection by MTT assay. Both *SLC16A1*-specific siRNAs significantly reduce cell growth in DAOY by 35-40% at 48 hr and by 50% at 96 hr, and in ONS-76 by 28% and 44% at 48 hr and 53% and 78% at 96 hr post-transfection compared to the mock. The data represent the average of survival fraction ± SD from 3 individual experiments. *, $p<0.05$; **, $p<0.01$.

compared to mock at 48 hours post-transfection. Cell viability was further reduced by 78% and 53% at 96 hours by siSLC16A1-1 and siSLC16A1-2, respectively. In both cell lines, no growth inhibition was observed in cells transfected with siRNA negative control. These data suggested that siRNAs against *SLC16A1* retarded cell growth in MB.

5.4.9 Depletion of *SLC16A1* induced cell death

To delineate the mechanism of cell growth inhibition in *SLC16A1*-depleted cells, an ELISA-based cell death assay was performed. This assay allows measurement of histone complexed DNA fragmentation (mono- and oligonucleosomes), a biochemical hallmark of apoptosis. After *SLC16A1* knockdown in DAOY and ONS-76 using siSLC16A1, the presence of mono- and oligonucleosomes was measured and then compared to cells transfected with siRNA negative control. The result revealed siRNAs against *SLC16A1* led to significant enhancement of cell death in DAOY and ONS-76 as illustrated in Figure 13. The increase in cell death, as indicated by enrichment factor, was observed as early as 24 hours post-transfection in both cell lines. In DAOY, siSLC16A1-1 led to an increase in enrichment factor from 3.0-fold at 24 hours to 4.1-fold at 96 hours. The other siRNA against *SLC16A1* (siSLC16A1-2) increased enrichment factor from 2.8-fold at 24 hours to 3.6-fold at 96 hours. Similarly,

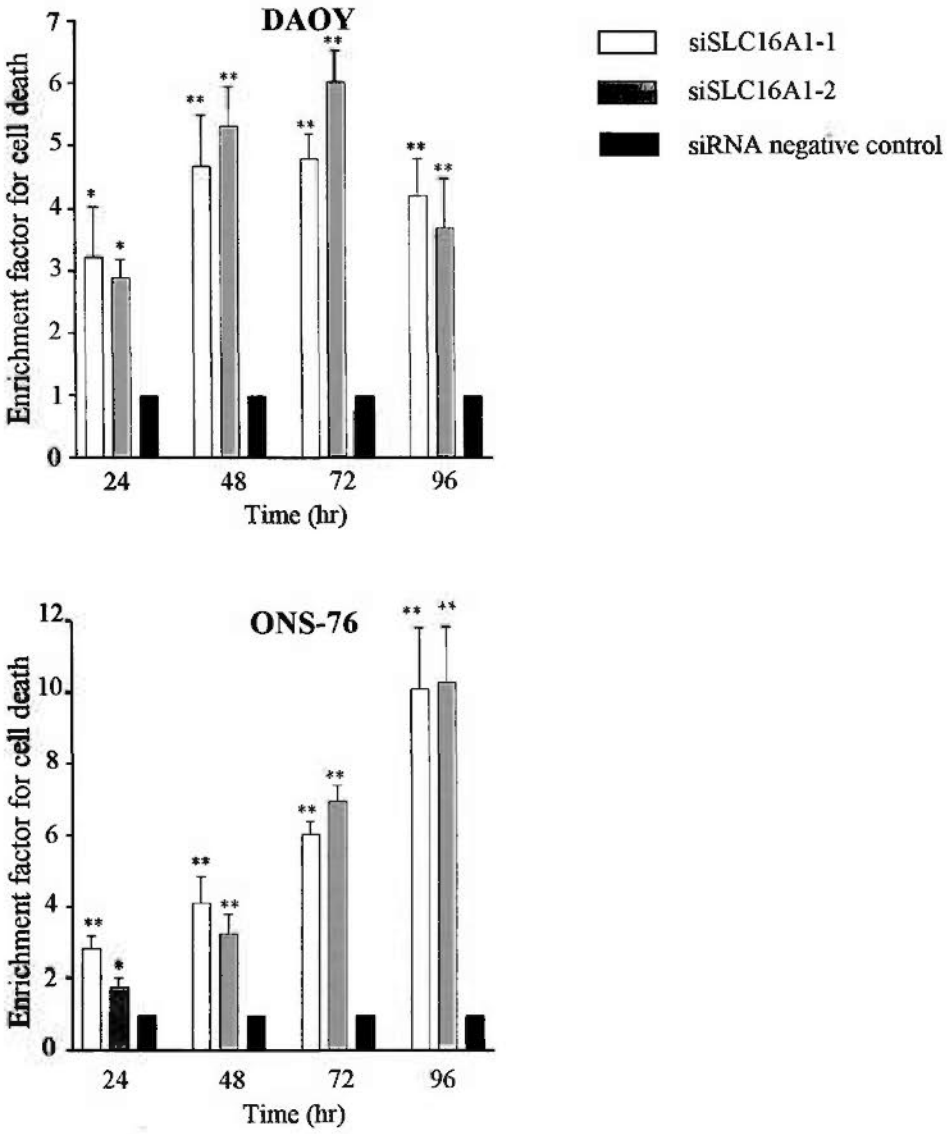

Figure 13. Effect of *SLC16A1* knockdown on cell death in MB. Cells were transfected with 2 siRNAs against *SLC16A1* independently (siSLC16A1-1 and SLC16A1-2) or a siRNA negative control. Cell lysates were harvested for 4 consecutive days post-transfection and quantified for the relative DNA fragmentation using a colorimetric assay. At 96 hr post transfection, the cell death enrichment factor increases by 3- to 6-fold and 2- to 10-fold in *SLC16A1* depleted DAOY and ONS-76, respectively, compared to negative control cells. The data represent the mean level of cell death ± SD from 3 individual experiments.

siSLC16A1-1 in ONS-76 showed an increased of enrichment factor from 2.8-fold at 24 hours to 9.8-fold at 96 hours. The siSLC16A1-2 enhanced the enrichment factor from 1.8-fold at 24 hours to 10.0-fold at 96 hours. Taken together, the data indicated that siRNAs against *SLC16A1* reduced cell growth by inducing cell death.

5.4.10 Overexpression of *PTBP1* expression

Previous study has shown that *PTBP1* is a target of miR-124 (Makeyev et al. 2007). Consistent with such finding, I have also demonstrated that *PTBP1* transcript level was reduced after miR-124 transfection in DAOY and ONS-76. It was of interested to investigate if a correlation existed between miR-124 and *PTBP1* expressions. To this end, qRT-PCR was performed to determine the *PTBP1* mRNA level in the same cohort of 29 MBs. The result revealed that *PTBP1* expression level was significantly overexpressed in MB (p=0.033) (Figure 14). Compared to normal cerebella, 18 (62%) MB showed 2- to 11-fold elevated level of *PTBP1* transcript. However, no correlation was found between the expression of miR-124 and that of *PTBP1* mRNA. The function of *PTBP1* did not investigated in this study. It has been demonstrated that miR-124 regulates *PTBP1* expression in the development of the nervous system (Makeyev et al. 2007). This suggested that multiple mechanisms including miR-124 might be involved in regulation of *PTBP1* transcript in MB.

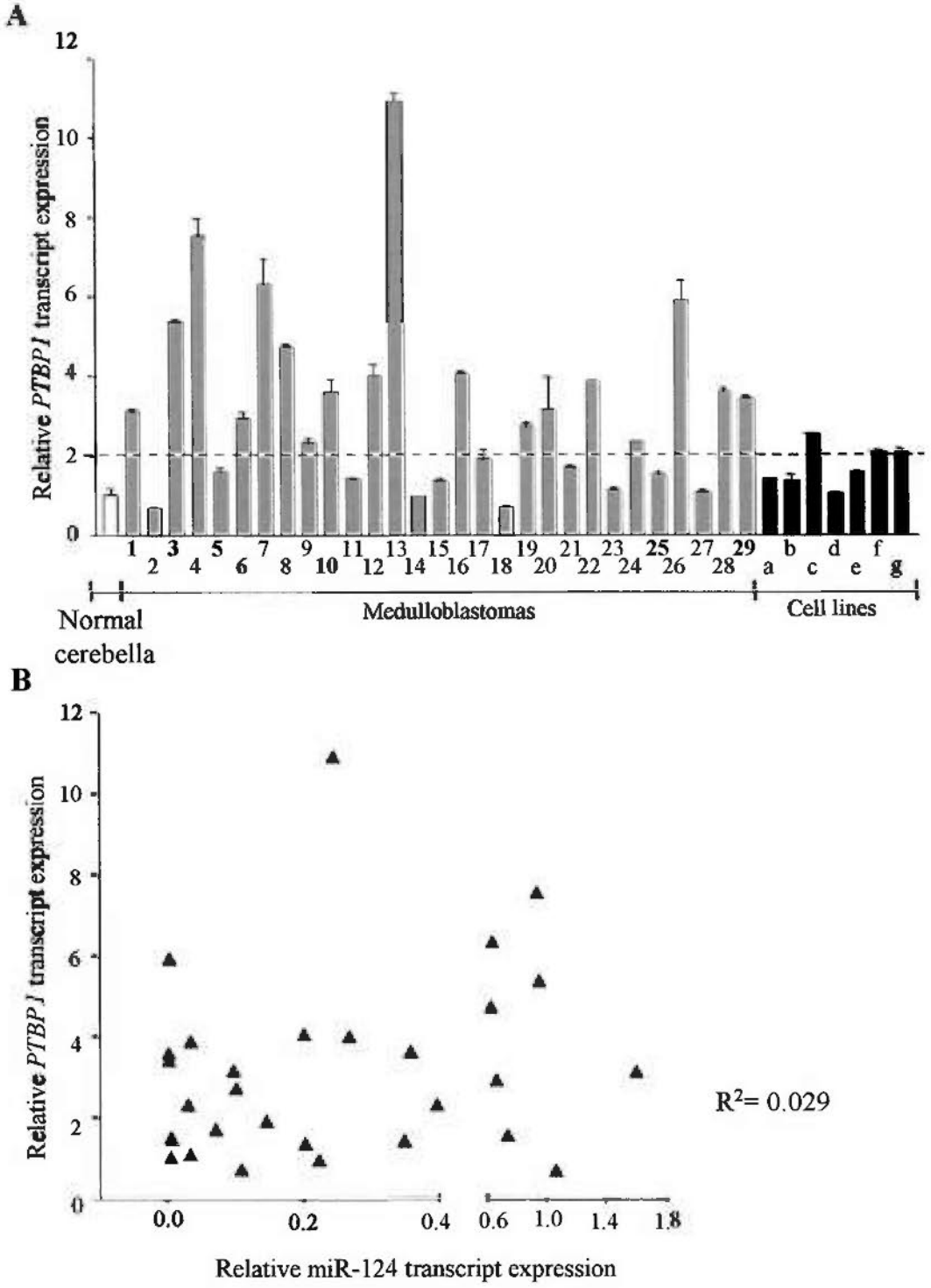

Figure 14. Expression profile of *PTBP1* in MB as determined by qRT-PCR. (A) The *PTBP1* transcript level is significantly elevated in 18 of 29 (62%) MBs and 3 of 7 cell lines examined compared to normal cerebella ($p<0.05$). The dashed line represents 2-fold cutoff for overexpression relative to normal cerebella. The number below the figure represents case number with bold indicates adult case. Small letter indicates cell line: a, D425; b, D458; c, D283; d, D384; e, D341; f, DAOY; g, ONS-76. The expression was normalized to *GAPDH*. The data represent the average of three experiments ± SD. (B) A plot of PTBP1 expression versus miR-124 expression. No correlation is found between expressions of miR-124 and *PTBP1*.

5.5 Functional characterization of miR-383

5.5.1 Optimization of transfection conditions for miR-383 mimic

To explore the biological functions of miR-383 in MB, Pre-miR™ miRNA Precursor miR-383 was transfected into four MB cell lines (DAOY, ONS-76, D283 and D458). The transfection efficiency was optimized using a FAM-labeled negative control. In negative control transfected cell, the appearance of green dot at the perinucleus was observed. The transfection condition in DAOY and ONS-76 was the same as in the transfection of miR-124 mimic. The condition for two suspension cell lines, D283 and D458 was determined by transfecting the negative control with Lipofectamine 2000 at various ratios. At 24 hours post-transfection, transfection efficiency was monitored by confocal microscopy, and green fluorescence labeled cells were considered positive for uptake of the molecules. The percentage of positive cells was determined by counting the green labeled cells at three different fields with 200 cells per field. Transfection at 16.7 nM revealed the highest transfection efficiency in both cell lines. D283 showed a 74% positive cells and D458 showed a 70% positive cells. Increasing the concentration to 33.3 nM did not significant alter the transfection efficiency. Moreover, compared to 16.7 nM, transfection efficiency was significant decreased in both cell lines when the concentration was reduced to 4.2 nM. The result suggested 16.7 nM would be the most optimized transfection condition and this condition would be applied in the subsequent

studies. The same concentration was applied in miR-124 transfection in DAOY and ONS-76 cells.

5.5.2 Effects of ectopic expression of miR-383 on cell growth by MTT assay

DAOY, ONS-76, D283 and D458 were transfected with miR-383 and the effect on cell growth was measured by MTT assay at 24, 48, 72, and 96 hours post-transfection. DAOY, D283 and D458 did not express detectable miR-383, and ONS-76 expressed minimum level of miR-383, at a level 43-fold less than normal cerebella (Figure 7). The result revealed that ectopic expression of miR-383 inhibited cell growth in a time-dependent manner in four MB cell lines examined (Figure 15). Moreover, the miRNA negative control exerted no significant growth effect in these cell lines. Compared to the mock, cell growth in DAOY was inhibited by 13%, 16%, 32% and 44% at 24, 48, 72 and 96 hours respectively. In ONS-76, miR-383 suppressed cell growth by 15%, 43%, 60% and 74% at 24, 48, 72 and 96 hours respectively. In both cell lines, statistical significance was observed in miR-383 transfected cells at all time points ($p<0.05$). Transfection of miR-383 in D283 showed reduced cell growth by 16% at 48 hours and 25% at 96h ($p<0.05$). In D458, cell growth was significantly decreased by 19% and 40% at 48 and 96 hours post-transfection ($p<0.05$).

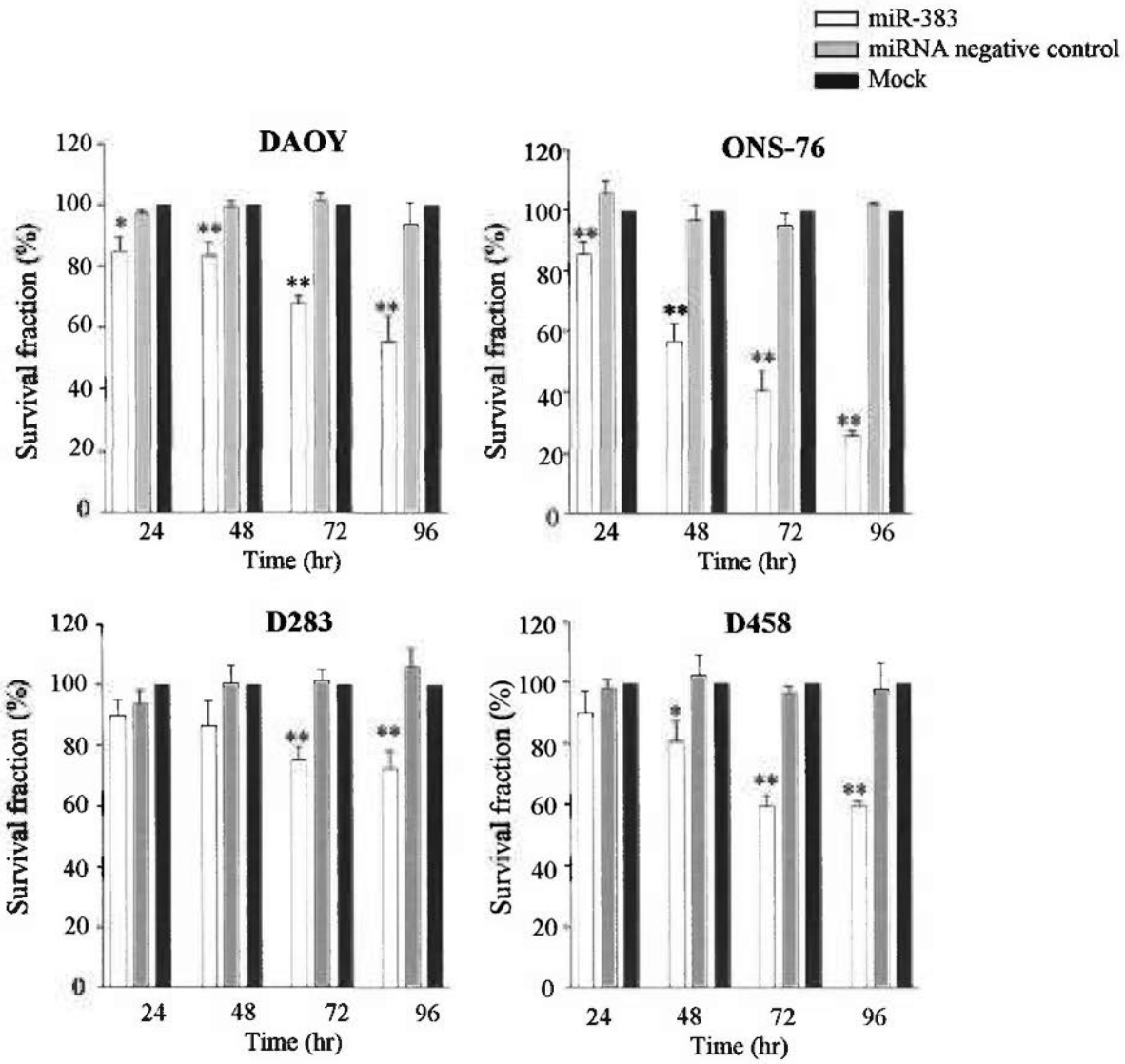

Figure 15. Effect of miR-383 overexpression on cell growth in MB. Cells transfected with miR-383 mimic, miRNA negative control or no miRNA (mock) were subjected to MTT assays for 4 consecutive days. Ectopic expression of miR-383 leads to suppression of cell growth as early as 24 hr post-transfection in DAOY and ONS-76. At 96 hr after transfection, cell growth is reduced by 44% in DAOY, 74% in ONS-76, 25% in D283 and 40% in D458 compared to mock. The experiment was performed in triplicate and repeated 3 times. *, $p<0.05$; **, $p<0.01$.

5.5.3 Effects of ectopic expression of miR-383 on cell growth by cell counting

To strengthen the growth suppressive role of miR-383 in MB, cell counting was carried out. The four MB lines were transfected with miR-383 or negative control, and cell number was determined at the same time interval as in MTT assay. Figure 16 illustrated transient transfection of miR-383 inhibited cell growth in DAOY. Compared to the negative control, cell number was reduced by 39%, 42%, and 66% at 48, 72, and 96 hours respectively ($p<0.05$). This growth suppression by miR-383 was also observed in ONS-76, D283, and D458 cells. In ONS-76, significant suppression of cell growth was observed at 48, 72, and 96 hours ($p<0.05$). At 48 hours, cell number was reduced by 53% compared to the negative control, and this reduction was increased to 76% at 96 hours. In the suspension lines, D283 and D458, significant growth retardation by miR-383 was found at 48, 72 and 96 hours ($p<0.05$). The cell number of D283 and D458 was decreased by 46% at 96h post-transfection. The cell number between the negative control and mock was not significant different among these four cell lines. Taken together, results from both MTT and cell count assays demonstrated that ectopic expression of miR-383 decreased cell viability by suppressing cell growth in MB.

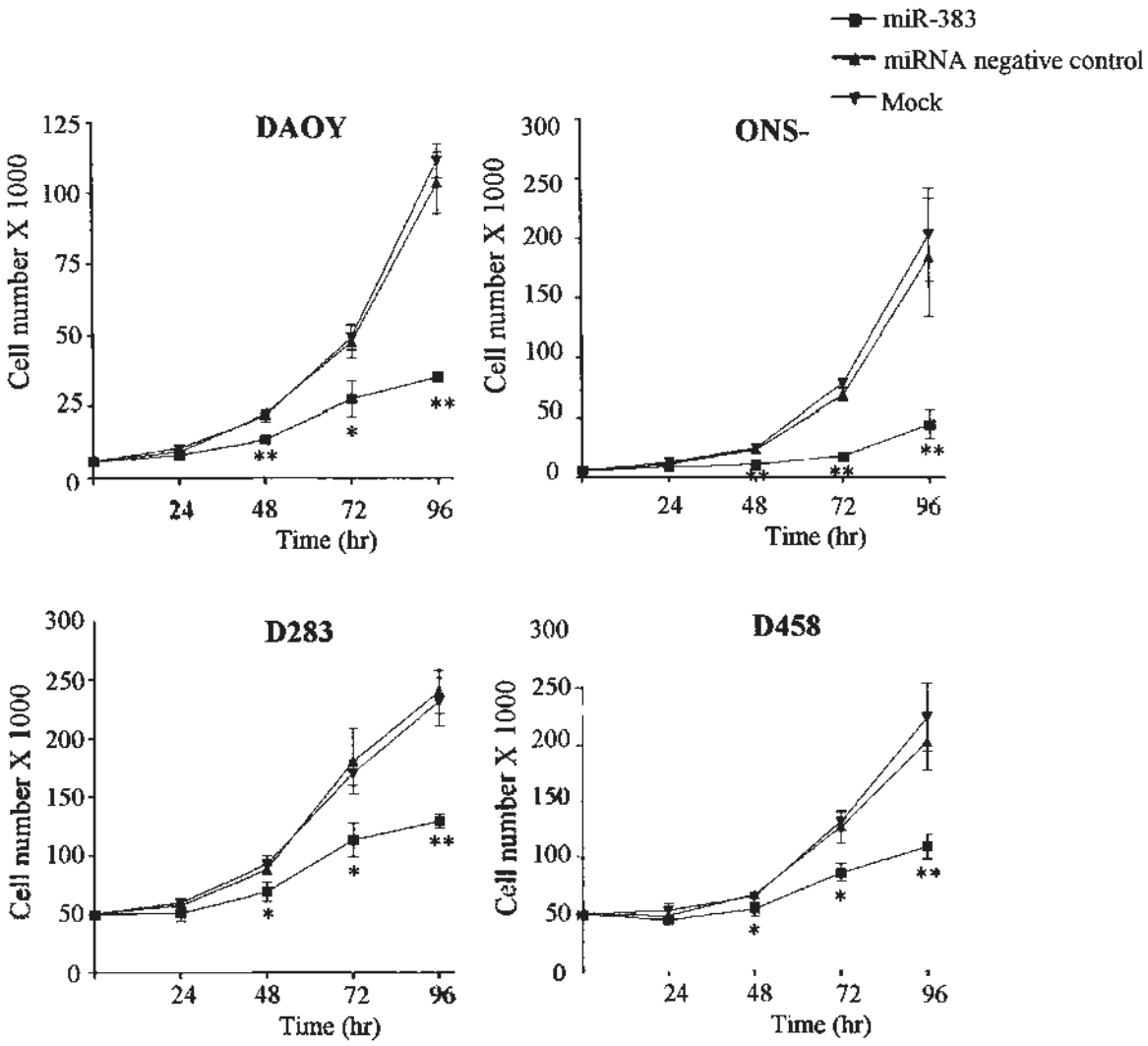

Figure 16. Effect of miR-383 overexpression on cell growth in MB by viable cell counting. Cells transfected with miR-383 mimic, miRNA negative control or no miRNA were subjected to viable cell counting using trypan blue exclusion assay for 4 consecutive days Ectopic expression of miR-383 results in a significant decrease in viable cell numbers from 48 hr to 96 hr in all 4 MB lines examined compared to mock transfection. The data are expressed as mean cell number ± SD from 3 separate experiments. *, $p<0.05$; **, $p<0.01$.

5.5.4 Effect of ectopic expression of miR-383 on cell cycle distribution

5.5.4.1 miR-383 induced G_1 arrest in ONS-76

To evaluate the effects of ectopic expression of miR-383 on cell cycle progression, flow cytometry analysis was performed in miR-383- and negative control-transfected cells.

ONS-76 transfected with miR-383 displayed significantly difference in the cell cycle distribution when compared to control cells. The proportion of miR-383 transfected ONS-76 cells in G1 phase was markedly increased, whereas the fraction of cells in the S and G2/M phases was significantly reduced as indicated in Table 15. This trend was evidenced as early as 24 hours post-transfection and persistently continued in the remaining study period. At 24 hours, 80.9% of miR-383-transfected cells was in the G1 phase compared to 57.6% in the control cells ($p<0.05$). MiR-383 enhanced the fraction of cells in G1 phase by 40%. This indicated that miR-383 overexpression induced G1 arrest. At the same time, the proportion of cells in S phase was reduced from 16.8% in the control cells to 4.8% in the miR-383-expressing cells, with a reduction of 71%. The fraction of G2/M was decreased from 25.4% in the control cells to 14.0% in the miR-383 expressed cells, with a decrease of 45%. At 72 hours, the proportion of G1 phase was enhanced from 56.0% in the control cells to 84.3% in the miR-383-transfected cells. Concurrently the fraction of S phase decreased

Table 15. Cell cycle profiling of ONS-76 cells after miR-383 transfection

sub-G1			
Time (h)	miR-383	Negative	p value
24	0.9%±0.8%	0.2%±0.1%	0.107622
48	0.8%±0.6%	0.1%±0.1%	0.051694
72	0.4%±0.7%	0.4%±0.0%	0.371666
96	0.3%±0.3%	0.4%±0.1%	0.642676
G1			
Time (h)	miR-383	Negative	p value
24	80.9%±1.4%	57.6%±1.4%	0.000036
48	86.0%±1.6%	60.4%±5.7%	0.011082
72	84.3%±0.6%	56.0%±0.5%	0.000001
96	83.4%±1.8%	64.1%±1.9%	0.000216
S			
Time (h)	miR-383	Negative	p value
24	4.8%±4.0%	16.8%±0.2%	0.000025
48	6.8%±4.6%	16.8%±2.7%	0.006132
72	4.7%±4.4%	16.0%±0.3%	0.006263
96	6.2%±5.4%	13.1%±1.7%	0.012936
G2/M			
Time (h)	miR-383	Negative	p value
24	14.0%±1.2%	25.4%±1.3%	0.000343
48	8.3%±0.3%	22.7%±3.1%	0.014933
72	9.7%±0.9%	27.6%±0.1%	0.000721
96	10.5%±1.6%	22.4%±0.4%	0.004383

The data represent the average of fraction of cells in cell cycle ± SD from three individual experiments.

from 16.0% to 4.7%, whereas the cells at G2/M phase diminished from 27.6% in the control cells to 9.7% in the miR-383-expressing cells.

5.5.4.2 miR-383 enhanced sub-G1 fraction and triggered apoptosis in D283

The cell cycle profiling analysis was only carried out at 48 and 96 hours post-transfection. It revealed that enforced miR-383 expression in D283 significantly elevated sub-G1 peak with a decrease in G2/M phase as shown in Table 16. At 48 hours, the proportion of sub-G1 phase was increased by 1.9-fold. A 14.3% of miR-383 expressed cells was in the sub-G1 phase as compared to a 7.5% in the control cells ($p<0.05$). The fraction of G2/M cells at this time was reduced by 25%, as 28.0% miR-383 expressed cells fell into G2/M phased compared to 37.4% control cells. The fraction of cells in sub-G1 and G2/M phases remained fairly constant at 96 hours. A 15.6% of miR-383 expressed cells was in sub-G1, and 22.8% of cells was in G2/M phase. This study highlighted that miR-383 transfected D283 cells were accumulated in the sub-G1 phase, and the appearance of sub-G1 population is a potential indication of apoptosis.

5.5.4.3 miR-383 enhanced subG1 and G1 fractions in D458

The present data suggested that alteration in cell cycle progression was slightly

Table 16. Cell cycle profiling of D283 cells after miR-383 transfection

sub-G1			
Time (h)	miR-383	Negative	p value
48	14.3%±1.9%	7.5%±0.3%	0.023705
96	15.6%±3.5%	5.9%±0.7%	0.035215
G1			
Time (h)	miR-383	Negative	p value
48	48.7%±2.1%	46.9%±0.7%	0.264807
96	50.1%±1.3%	55.5%±1.5%	0.009055
S			
Time (h)	miR-383	Negative	p value
48	8.9%±0.8%	8.3%±2.3%	0.667760
96	11.6%±0.9%	11.7%±0.7%	0.778027
G2/M			
Time (h)	miR-383	Negative	p value
48	28.0%±0.5%	37.4%±2.6%	0.021131
96	22.8%±1.8%	26.8%±1.4%	0.038534

The data represent the average of fraction of cells in cell cycle ± SD from three individual experiments.

different among cell lines. It was necessary to determine the cell cycle distribution D458 and DAOY upon miR-383 transfection. Table 17 illustrated significant alteration in cell cycle distribution as early as 24 hours post-transfection in D458 compared to the control. The fractions of cells in the sub-G1 and G1 phases were elevated, and at the same time, a reduction in cells in the S and G2/M phases was evidenced. At 24 hours, 3.8% of miR-383 transfected cells was in the sub-G1 phase as compared to 2.6% in the control cells, with a difference of 1.4-fold. At the same time, compared to the control, the fraction of cells in G1 phase was increased by 18% in the miR-383 transfected cells, whereas the fraction of cells in the S phase and G2/M phase was decreased by 10% and 30% respectively. The increase of sub-G1 phase was more apparent at 72 hours when the proportion of cell in the sub-G1 phase was further enhanced to 18.1%, a 4.8-fold increase compared to 24 hours. At the same time, significant blockage at the G1 phase was maintained. Additionally, the fraction of cells in S and G2/M phases was markedly reduced. Compared to 24 hours, the fraction of cells in the S and G2/M phase was reduced by 34% and 39% respectively. This result demonstrated miR-383 altered the cell cycle distribution by inducing G1 arrest and apoptosis.

5.5.4.4 miR-383 affected cell cycle disturbution in DAOY to a less extent

As illustrated in Table 18, DAOY did not exhibit a dramatic alteration in cell

Table 17. Cell cycle profiling of D458 cells after miR-383 transfection

sub-G1			
Time (h)	miR-383	Negative	p value
24	3.8%±0.1%	2.6%±0.3%	0.015233
48	12.2%±1.2%	3.5%±0.3%	0.003833
72	18.1%±2.0%	2.3%±0.1%	0.004986
96	13.9%±0.6%	4.0%±0.2%	0.000293
G1			
Time (h)	miR-383	Negative	p value
24	62.6%±0.4%	53.0%±0.9%	0.000762
48	62.9%±1.0%	53.2%±0.5%	0.000669
72	60.7%±1.8%	56.1%±0.4%	0.038957
96	63.9%±0.4%	57.3%±0.6%	0.000263
S			
Time (h)	miR-383	Negative	p value
24	12.5%±0.3%	13.8%±0.1%	0.014853
48	9.8%±0.5%	14.5%±0.2%	0.001156
72	8.3%±0.2%	13.6%±0.1%	0.000027
96	7.8%±0.2%	14.1%±0.3%	0.000035
G2/M			
Time (h)	miR-383	Negative	p value
24	21.2%±0.8%	30.6%±1.3%	0.001092
48	15.1%±0.4%	28.8%±0.7%	0.000037
72	12.9%±0.5%	28.0%±0.4%	0.000004
96	14.5%±0.8%	24.6%±1.0%	0.000281

The data represent the average of fraction of cells in cell cycle ± SD from three individual experiments.

Table 18. Cell cycle profiling of DAOY cells after miR-383 transfection

sub-G1			
Time (h)	miR-383	Negative	p value
24	0.2%±0.1%	0.3%±0.1%	0.6762764
48	0.1%±0.0%	0.1%±0.1%	0.4701011
72	0.4%±0.4%	0.2%±0.0%	0.3447141
96	0.8%±0.7%	0.1%±0.0%	0.243891
G1			
Time (h)	miR-383	Negative	p value
24	59.6%±1.3%	56.7%±1.9%	0.106261
48	62.3%±0.7%	56.8%±1.0%	0.0024626
72	66.1%±1.6%	62.1%±1.5%	0.0372318
96	64.0%±0.7%	60.3%±3.0%	0.1643685
S			
Time (h)	miR-383	Negative	p value
24	10.7%±0.6%	12.6%±0.3%	0.013189
48	11.8%±0.1%	15.7%±0.4%	0.002093
72	15.2%±0.7%	13.7%±0.9%	0.0917176
96	13.0%±1.3%	13.7%±0.9%	0.5207434
G2/M			
Time (h)	miR-383	Negative	p value
24	29.5%±0.8%	30.4%±2.1%	0.5391874
48	25.9%±0.6%	27.4%±1.2%	0.1552308
72	18.3%±1.8%	24.0%±0.8%	0.0187431
96	22.2%±1.9%	25.8%±2.2%	0.0994471

The data represent the average of fraction of cells in cell cycle ± SD from three individual experiments.

cycle profiling via overexpression of miR-383 as compared to ONS-76, D283 and D384. Nevertheless, compared to negative control, miR-383 led to a significant increase in G1 population at 48 and 72 hours, but this enhancement was not observed at 24 and 96 hours. At 48 hours, an increase in G1 phase was accomplished with a 4% decrease in S phase, whereas the G1 population accumulation was accomplished with a 6% decrease in G2/M phase at 72 hours. The result illustrated miR-383 blocked the cell cycle progression in DAOY cells.

5.5.5 Activation of PARP cleavage by miR-383

The fact that an accumulation of sub-G1 was evidenced in D283 and D458 upon restoration of miR-383 suggested that the growth inhibitory effect of miR-383 was possibly due to the induction of apoptosis. Thus, the level of poly(ADP-ribose) polymerase (PARP) cleavage was examined by immunoblotting. The cleavage of PARP protein by caspase-3 is known as an evidence for apoptosis (Simbulan-Rosenthal et al. 1998). The four MB cell lines were transfected with miR-383 or negative control. Cell lysates were harvested at different time points. As shown in Figures 17, induction of PARP cleavage was evidenced as early as 24 hours post-transfection in D283 and D458. After normalization with the loading control, PARP cleavage was increased by 3.2-fold at 24 hours compared to the negative control in D283. The PARP cleavage was further

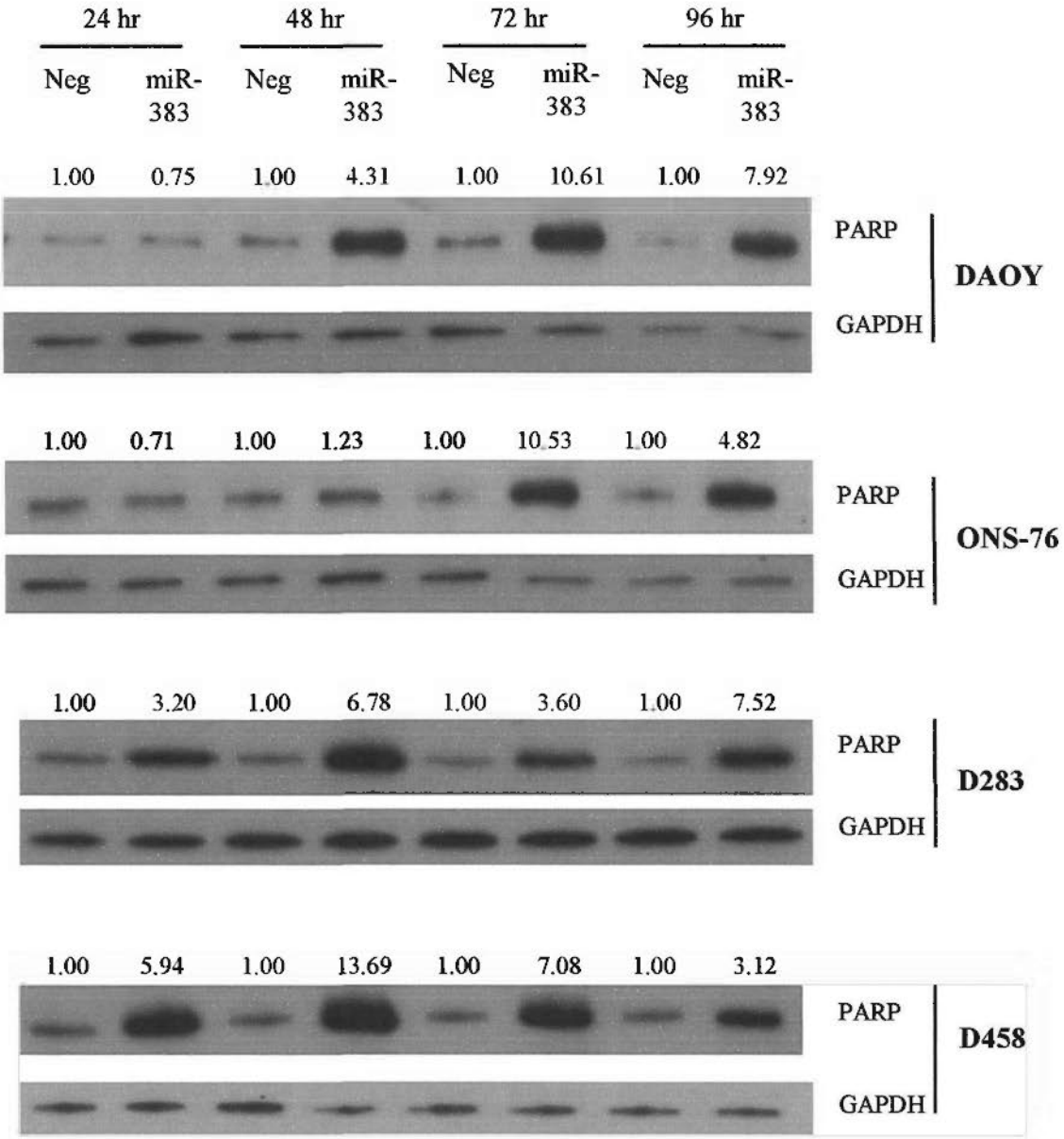

Figure 17. Effect of miR-383 overexpression on induced apoptosis in MB. Cells transfected with miR-383 mimic or miRNA negative control (Neg) were subjected to Western blot analysis using antibody specific for cleaved PARP, a marker of apopotsis. Ectopic expression of miR-383 leads to activation of PARP cleavage as early as 24 hr post-transfection. The cleaved PARP abundance attains maximal level at 72 hr after transfection in DAOY and ONS-76 and at 48 h post transfection in D283 and D458, and decreases thereafter. The decline in cleaved PARP level may be explained by the increased proportion of untransfected growing cells. The number above the protein band represents relative intensity of cleaved PARP compared to control cells after normalization to GAPDH. Each lane is loaded with 50 μg of cell lysates.

enhanced to 6.8-fold at 48 hours. In D458, PARP cleavage was upregulated from 5.9-fold at 24 hours to 13.7-fold at 48 hours. Although the cell cycle profiling did not reveal a significant change in sub-G1 phase, PARP cleavage was observed in DAOY and ONS-76. Compared to D283 and D458, activation of PARP cleavage in DAOY and ONS-76 occurred at a later time. In DAOY, activation of PARP cleavage was first detected at 48h and the induction maintained throughout the remaining study period. In ONS-76, accumulation of PARP cleavage was not found until 72 hours after transfection, and the level showed slightly decrease at 96h. Thus, the data demonstrated the growth inhibitory effect of miR-383 was partly due to the activation of PARP cleavage.

5.5.6 Induction of p21 protein expression in ONS-76

As shown previously by flow cytometry analysis, an accumulation of cell in the G1 phase was observed in ONS-76, indication for G1 arrest. To strengthen this finding, immunoblotting was employed to evaluate p21 protein expression. Increased p21 protein level would be indicative of G1 arrest (Waldman et al. 1995). All four MB cell lines were overexpressed with miR-383 and cell lysates were collected at different time points. As depicted in Figure 18, elevation of p21 protein was evidenced in ONS-76 upon restoration of miR-383 as early as 24 hours and further elevation in p21 protein

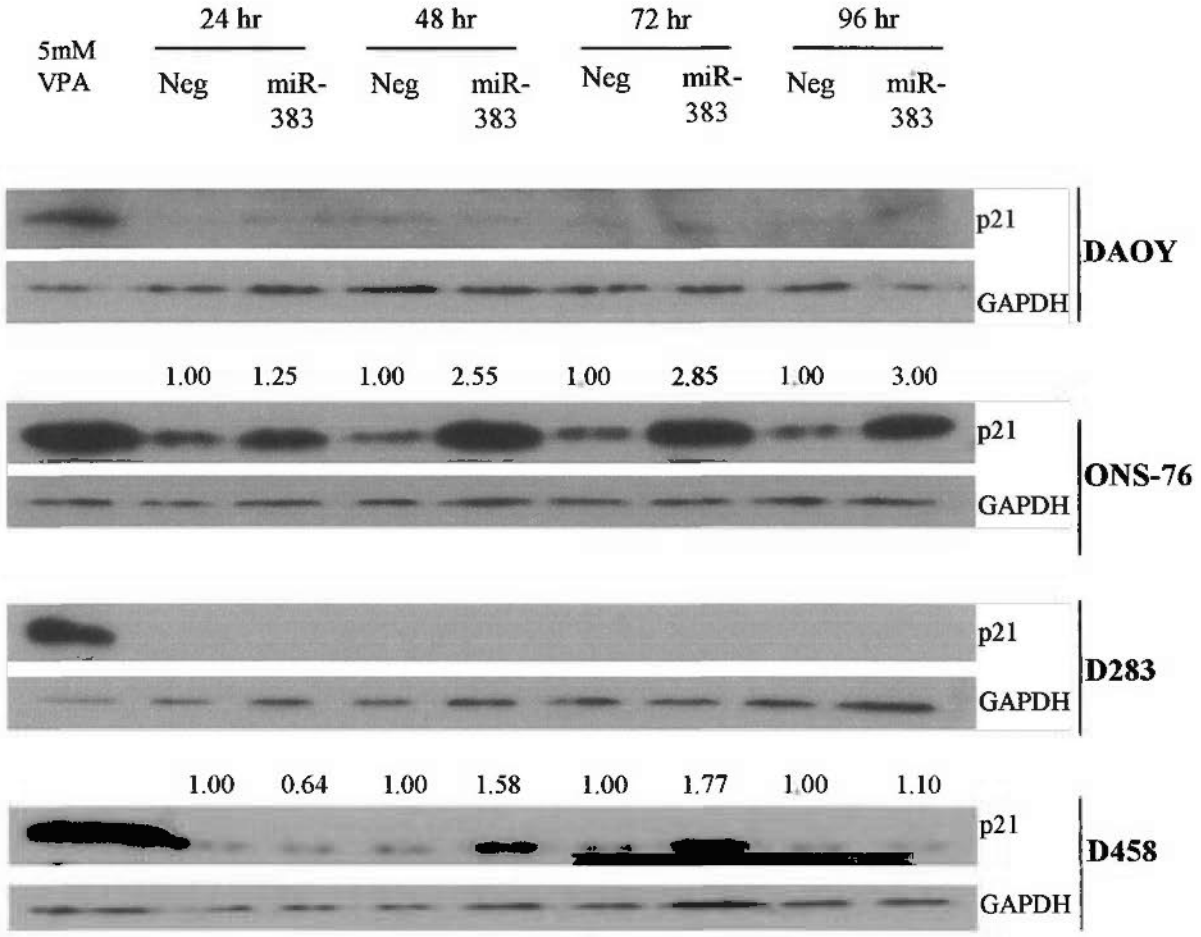

Figure 18. Effect of miR-383 overexpression on p21 activation in MB. Cells transfected with miR-383 mimic or miRNA negative control (Neg) were subjected to Western blot analysis using antibody specific for p21. Ectopic expression of miR-383 leads to enhanced p21 expression in ONS-76 and D458, but not in DAOY compared to control cells. D283 cells do not express p21. The number above the protein band represents relative intensity of p21 compared to control cells after normalization to GAPDH. Cells treated with 5 mM valproic acid (VPA) serve as positive control for p21 activation. Each lane is loaded with 50 μg of cell lysates. Three individual experiments were performed.

was observed at 48, 72, and 96 hours. Using GAPDH for normalization, compared to negative control, a 2.6-fold increase in p21 protein was observed in miR-383 expressed ONS-76 at 48 hours after post-transfection. At 96 hours, miR-383 expressed ONS-76 had a 3-fold elevation in p21 expression compared to negative control. This suggested that induction of p21 was one of the possible mechanisms for miR-383-induced cell growth inhibition and G1 arrest in ONS-76.

In D458, restoration of miR-383 slightly enhanced p21 protein level compared to negative control as illustrated in Figure 18. Increased p21 protein level was not observed until 48 hours post-transfection. At this time, p21 protein level was increased 1.6-fold in miR-383 expressed D458 cells compared to negative control. This p21 increased expression was also observed at 72 hours post-transfection when a 1.8-fold increase p21 expression was reported. However, further increase in p21 protein level as observed in ONS-76 was not detected in D458 at 96 hours post-transfection.

Although upregulation of p21 protein expression was reported in ONS-76 and D458 cells upon miR-383 restoration, this observation was not observed in DAOY and D283 cells as indicated in Figure 18. Throughout a period of 96 hours post-transfection, the protein level of p21 remained similar between miR-383 and negative control transfected Daoy cells. This result was not in agreement with the cell cycle analysis showing an increase in the percentage of G1 DAOY cells upon miR-383 restoration at

48 and 72 hours. Such discrepancy may be technical, as the western blotting may not be sensitive enough to detect a mild change. In D283, p21 protein was absence either in miR-383 or negative control transfected cells in all examined time points. These results indicated that the growth inhibition effect of miR-383 in D283 was not mainly a result of G1 arrest. And, this further illustrated multiple mechanisms were involved to suppress the cell growth in miR-383 expressed MB cells.

5.5.7 Finding miR-383 targets

5.5.7.1 Global gene expression profiling in miR-383 expressed ONS-76

To identify the potential target genes of miR-383, a systemic analysis based on combination of computational target prediction and comprehensive gene expression analysis was carried out. First, bioinformatics analysis was applied. The targets of miR-383 predicted by three miRNA prediction softwares, namely PicTar (http://pictar.bio.nyu.edu/), TargetScan (http://genes.mit.edu/tscan/targetscanS.html), and Human microRNA Targets (http://www.microrna.org/) were retrieved. Genes that were predicted by at least two of these softwares were extracted. A total of 210 genes were found as the candidate targets of miR-383. To narrow down the number of target genes, expression profiling was carried out to identify downregulated genes based on the assumption that transcript of miR-383 target genes would be suppressed upon

restoration of miR-383 expression. Thus, the gene expression between miR-383 transfected cells and negative cells at 4 and 12 hours post-transfection in ONS-76 was compared using Agilent 4 x 44k Whole Human Genome Oligo Microarrays. A total of 979 genes showed downregulation greater than 1.5-fold at 12 hour. However, only 23 of them were on the list of 210 refined putative targets of miR-383. These 23 genes were further assessed. To reduce the list of candidate targets, the unknown genes were not further studied, and 19 known genes were focused. Genes that are not implicated in tumorigenesis, anti-apoptosis and differentiation were excluded from further analysis. This was based on the assumption that a function of miR-383 target gene would relate to tumor development. Nevertheless, this approach was not to say other less well characterized genes or genes have not showed roles in tumorigenesis, anti-apoptosis and differentiation are not importance. Taking this approach hoped to enhance the probability of finding genes critical for MB development. A final list of 12 candidate genes obtained was subjected to validation by qRT-PCR.

5.5.7.2 Validation of microarray analysis

To confirm the microarray experiment, 12 potential miR-383 genes were analyzed for their expression by qRT-PCR. As shown in Table 19, all 12 genes showed significant downregulation at 12 and 24 hours post-transfection. This result is in

Table 19. Candidate genes downregulated upon miR-383 transfection

	Quantitative RT-PCR								Microarray	
	Daoy				ONS-76				ONS-76	
	12 hr		24 hr		12 hr		24 hr		4 hr	12 hr
Gene	Fold-change	P value	Fold-change	P value	Fold-change	P value	Fold-change	P value	Fold-change	Fold-change
RBMS1	-2.8	$2.1x10^{-5}$	-4.6	$4.7x10^{-6}$	-3.7	$1.5x10^{-3}$	-5.7	$1.6x10^{-3}$	-1.9	-3.3
MAPKAP1	-1.1	$8.9x10-^{3}$	-1.2	$4.8x10^{-2}$	-1.2	$4.5x10^{-2}$	-1.5	$7.1x10^{-5}$	1	-1.7
CTNNAL1	-1.7	$3.9x10^{-2}$	-3.7	$3.9x10^{-4}$	-2.5	$5.6x10^{-3}$	-9.8	$7.5\ x10^{-4}$	1	-2.2
PRDX3	-6.5	$6.5x10^{-6}$	-9.8	$1.6x10^{-3}$	-11.3	$7.4x10^{-5}$	-19.7	$3.0x10^{-4}$	-1.3	-6.6
SLC35A3	-1.7	$4.2x10^{-2}$	-3.6	$4.8x10^{-2}$	-1.9	$3.8x10^{-2}$	-3.9	$3.5x10^{-7}$	-1.1	-2.3
PREI3	-1.2	$3.9x10^{-1}$	-3.2	$2.4x10^{-4}$	1	$1.2x10^{-1}$	-1.3	$9.6x10^{-2}$	-1.4	-2.2
MAL2	-2.6	$1.3x10^{-4}$	-3.5	$1.0x10^{-5}$	-2.0	$7.3x10^{-4}$	-2.6	$7.2x10^{-4}$	-1.2	-2.5
SCD	-1.1	$9.2x10^{-2}$	-1.2	$6.7x10^{-2}$	-1.7	$8.6x10^{-2}$	-1.9	$4.9x10^{-2}$	-1.2	-1.9
CNIH	-2.5	$1.1x10^{-2}$	-3.5	$3.2x10^{-3}$	-2.6	$1.7x10^{-2}$	-2.6	$1.6x10^{-2}$	1	-1.8
NCKAP1	-1.1	$1.6x10^{-2}$	-2.6	$1.1x10^{-4}$	-1.7	$2.7x10^{-3}$	-2.5	$1.5x10^{-3}$	-1.1	-2.2
SOX5	-1.3	$1.5x10^{-3}$	-2.1	$1.0x10^{-2}$	-2.0	$1.7x10^{-2}$	-4.4	$5.1x10^{-4}$	-1.4	-1.7
STRN3	-1.8	$1.0x10^{-2}$	-2.5	$-4.6x10^{2}$	-1.6	$1.1x10^{-2}$	-1.6	$2.6x10^{-2}$	-1.3	-1.6

agreement with the microarray data. Out of these genes, *PRDX3* gene expression showed the most prominent reduction. In DAOY, *PRDX3* expression was decreased by 6.5-fold at 12 hour compared to the negative control. Its expression was further suppressed at 24 hours. Upon restoration of miR-383 in ONS-76, *PRDX3* transcript was repressed by 11.3-fold and 19.7-fold at 12 and 24 hours respectively. Besides, qRT-PCR also confirmed the repression of *RBMS1* transcript in DAOY and ONS-76. The introduction of miR-383 significant reduced *RBMS1* transcript by 4.6- and 5.7-fold in DAOY and ONS76, respectively. The facts that *PRDX3* and *RBMS1* were implicated in tumorigenesis and their transcript levels showed repression after ectopic expression of miR-383 prompted further experiments to confirm whether these two genes were the direct targets of miR-383.

5.5.8 Computational prediction for miR-383

Based on computational algorithms, *PRDX3* and *RBMS1* were potential targets of miR-383. The seed region of *PRDX3* forms perfect complementary base pairing to miR-383 and is highly conserved across human, mouse and rat. The schematic diagram in Figure 19 illustrates that a perfect complementarity exists between the 3'UTR of *PRDX3* and nucleotides 2-10 of the mature miR-383, which included the seed region (nt 2-8). Besides, the nucleotide and protein sequences of *PRDX3* are well conserved

A

```
PRDX3
3'UTR      +346 ├── miR-383 binding site ──┤ +368
Rat     5'CCAGCACTTAGTGAAAGCTTCTGATCAA-GGTCCT3'
Mouse   5'CCAGCACTTAATGGAAGCTTCTGATCAA-GGTCCT3'
Human   5'GCAACACACATTGAAAGCTTCTGATCAACGGTCCT3'
                      ||||   |  |||||||||
miR-383   3'UCGGUGUUA--GUGGAAGACUAGA5'
```

B

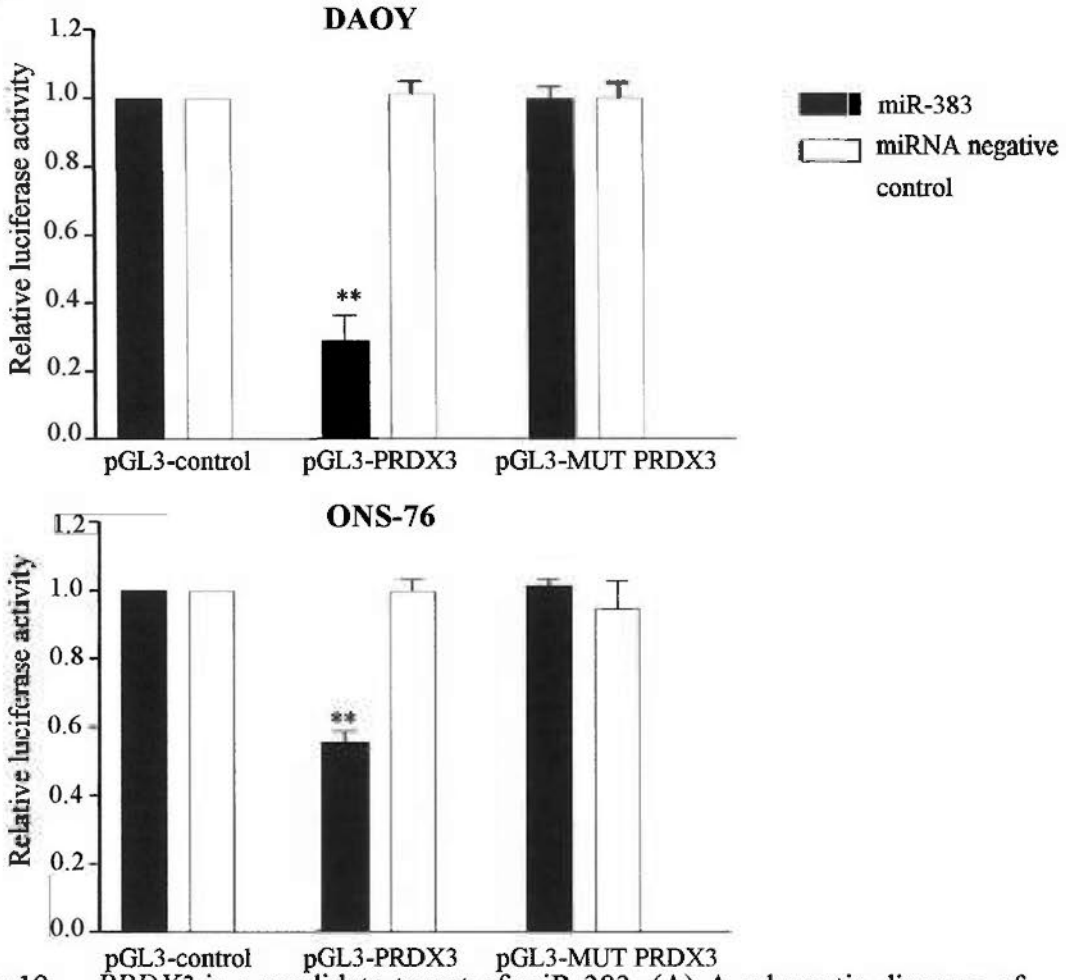

Figure 19. *PRDX3* is a candidate target of miR-383. (A) A schematic diagram of miR-383 MRE on 3'UTR of *PRDX3*. The miR-383 MRE is conserved in human, rat and mouse. Perfect complementary base pairing is observed between the seed region of miR-383 and MRE of *PRDX3*. (B) Evaluation of interaction between miR383 and MRE of *PRDX3* by dual luciferase reporter assay. MB cells were co-transfected with the reporter construct, miR-383 or miRNA negative control and a renilla luciferase plasmid (pRL-TK for normalization of transfection efficiency). After 48 hr, transfected cells were evaluated for luciferase activity. The results reveal that luciferase activity is significantly suppressed by 71% and 45% respectively in DAOY and ONS-76 cotransfected with pGL3-PRDX3 and miR-383 compared to cells cotransfected with pGL3-PRDX3 and miRNA negative control. No decrease in luciferase activity is detected in cells cotransfected with mutant construct. These results strongly indicate that miR-383 interacts specifically with miR-383 MRE of *PRDX3*. Three independent experiments were performed. **, $p<0.01$.

among human, mouse, and rat. The rodents share 74-76% and 85-86% homology, respectively, in nucleotide and protein sequences to human.

Figure 20 also illustrates that the complementary base pairing between 3'UTR of *RBMS1* and miR-383 at the seed region is perfect. The seed regions of *RBMS1* forms perfect complementary base pairing to miR-383 and is highly conserved across human, mouse and rat. The rodents share 90-91% and 96-97% homology, respectively, in nucleotide and protein sequences to human.

5.5.9 Regulation of *PRDX3* and *RBMS1* transcript by miR-383

To investigate the regulatory role of miR-383 in *PRDX3* and *RBMS1* gene expression, seven MB cell lines (DAOY, ONS-76, D283, D341, D384, D425 and D458), were transfected with either miR-383 or negative control, and at 48 hours post-transfection *PRDX3* and *RBMS1* transcript levels were studied by qRT-PCR. Figure 21 illustrates that *PRDX3* mRNA level was significantly decreased in all MB cell lines upon miR-383 restoration as compared to negative control ($p<0.05$). Upon miR-383 transfection, expression of *PRDX3* was suppressed by 7-fold in D458 by 5-fold in DAOY, ONS-76 and D425, and by 1.4- to 2.0-fold in D283, D341 and D384.

qRT-PCR showed that all MB lines, except D341, exhibited a significant downregulation of *RBMS1* transcript level at 48 hours after miR-383 transfection

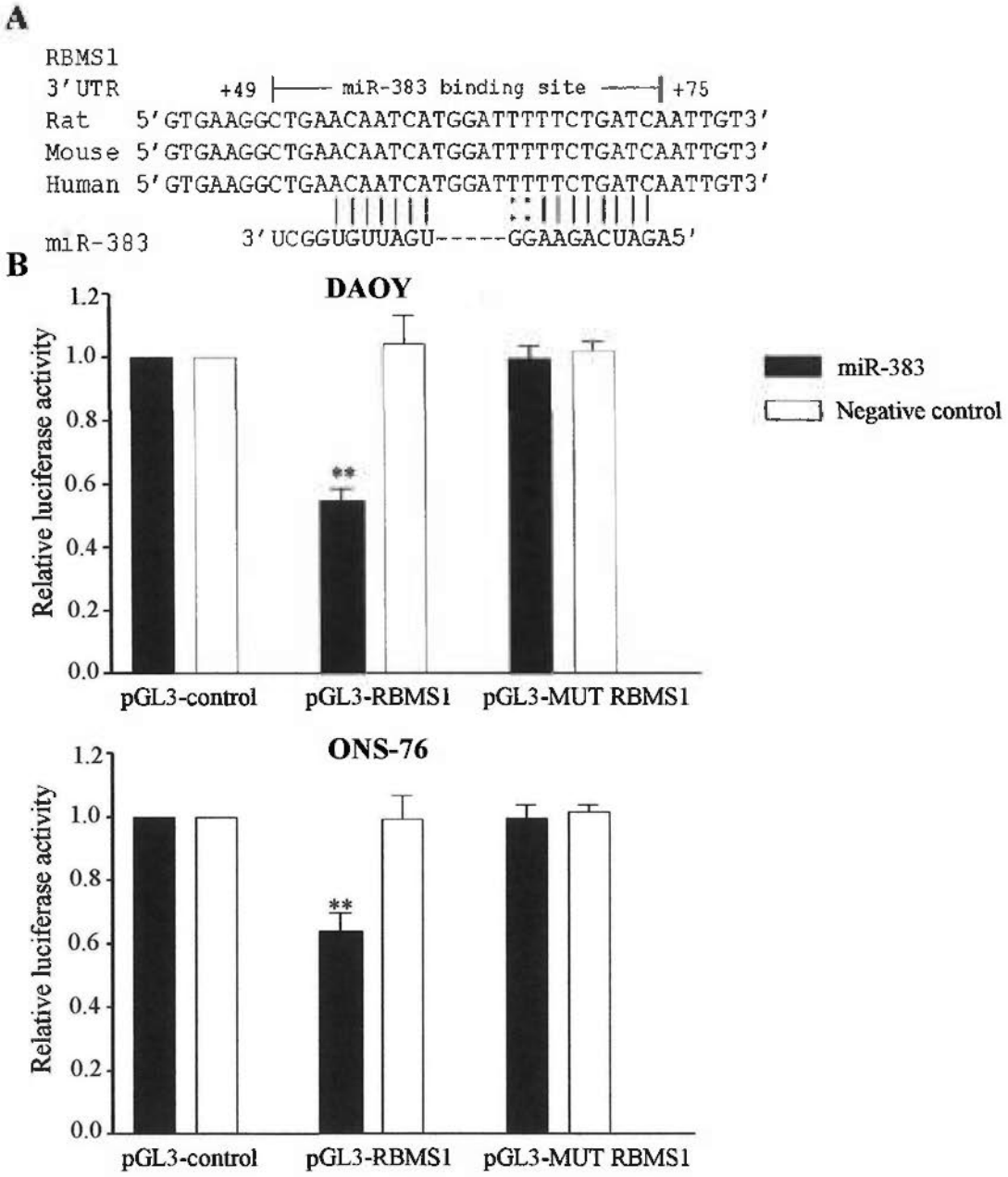

Figure 20. *RBMS1* is a candidate target of miR-383. (A) A schematic diagram of miR-383 MRE on 3'UTR of *RBMS1*. Perfect complementary base pairing is observed between MRE of *RBMS1* and 15 of 22 nucleotides (including the seed region) of mature miR-383. (B) Evaluation of interaction between miR-383 and MRE of *RBMS1* by dual luciferase reporter assay. Cells cotransfected with pGL3-RBMS1 and miR-383 shows significantly reduced luciferase activity compared to cells cotransfected with pGL3-RBMS1 and miRNA negative control. No decrease in luciferase activity is detected in cells cotransfected with mutant construct (pGL3-MUT RBMS1). These results strongly indicate that miR-383 interacts specifically with miR-383 MRE of *RBMS1*. Three independent experiments were conducted. **, $p<0.01$.

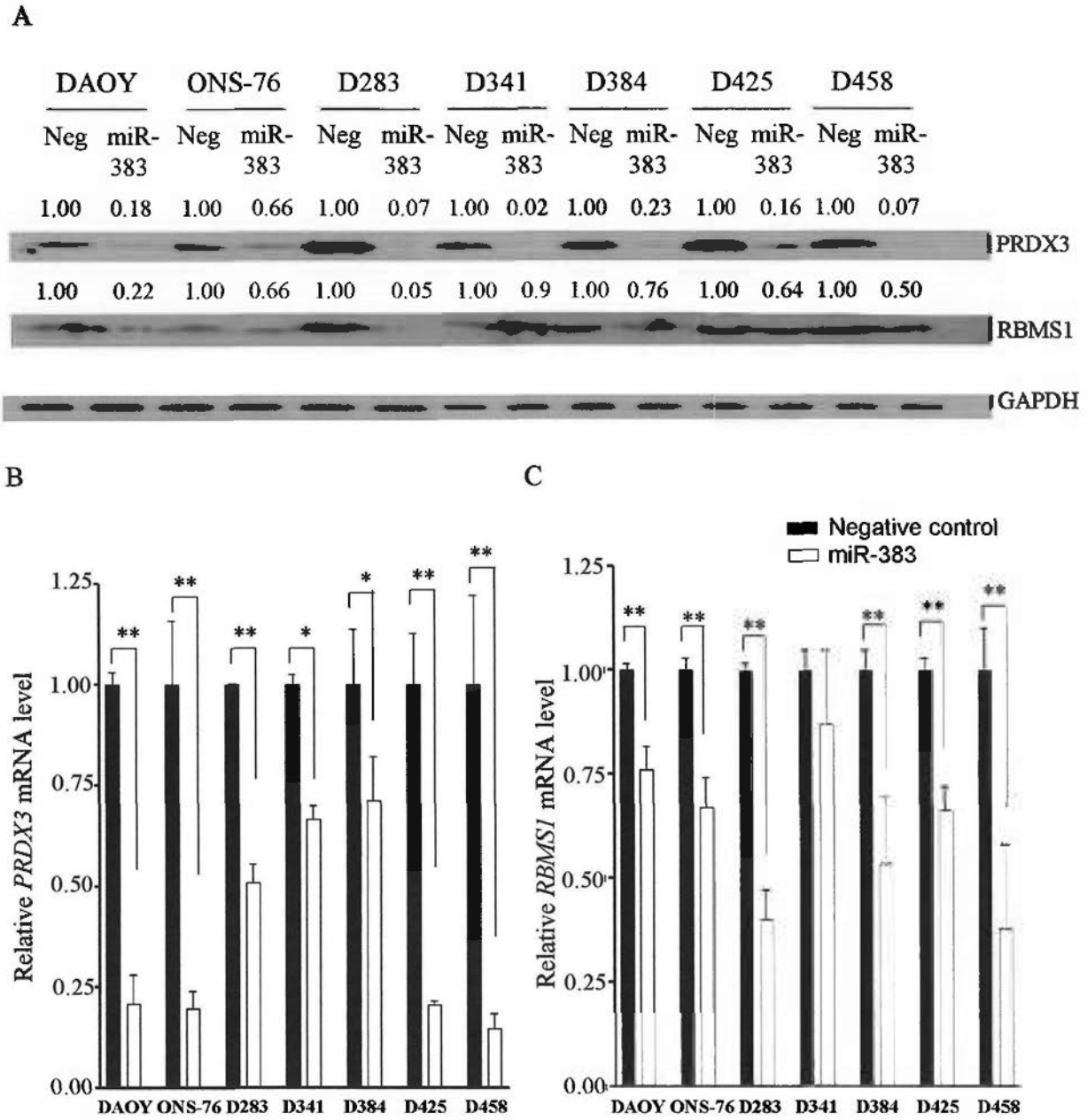

Figure 21. Effect of miR-383 overexpression on PRDX3 and RBMS1 expression by Western blot analysis (A) and qRT-PCR (B, C). Ectopic expression of miR-383 leads to decreased levels of PRDX3 protein (A) and transcript (B) in all 7 cell lines examined compared to cells transfected with miRNA negative control. Transfection of miR-383 results in reduced expression of RBMS1 protein (A) and mRNA (C) in 6 of 7 cell lines studied compared to control cells. Results of Western blotting and qRT-PCR are concordant. The value above protein band represents the relative protein level compared to the negative control after normalization to GAPDH. The relative transcript expression represents the relative mRNA level compared to the negative control transfected cells. Three independent experiments were performed. *, $p<0.05$; **, $p<0.01$.

($p<0.05$). Compared to negative control, introduction of miR-383 repressed *RBMS1* transcript level in D283 and D458 by 2.5-fold and 2.6-fold respectively. MiR-383 modulated *RBMS1* mRNA level in DAOY, ONS-76, D384, and D425 at reduced level between 1.2- to 1.9- fold. Taken together, ectopic expression of miR-383 decreased transcript levels of *PRDX3* and *RBMS1*, suggesting that these genes are miR-383 targets.

5.5.10 Regulation of PRDX3 and RBMS1 protein expression by miR-383

The PRDX3 and RBMS1 protein expressions were also examined in MB cell lines after miR-383 transfection. Cell lysates collected at 48 hours post-transfection were subjected to Western blot analysis for evaluation of PRDX3 and RBMS1 expression. As depicted in Figure 21, PRDX3 protein level was markedly reduced in all seven MB lines examined upon restoration of miR-383. The strongest protein inhibition was found in D283, D341 and D458. MiR-383 almost abolished PRDX3 expression in these cell lines. Moreover, strong protein suppression was demonstrated in DAOY, D384, and D425. By measuring the intensity of the protein bands, PRDX3 expression was reduced by 5.5-, 4.3- and 6.2-fold in DAOY, D384 and D425, respectively, compared to their respective negative controls. Such reduced expression was in line with the finding of decreased transcript level after miR-383 transfection, suggesting that

miR-383 can modulate PRDX3 at both translational and post-transcriptional levels.

Furthermore, western blotting revealed that expression of miR-383 almost completely abolished RBMS1 expression in D283, and suppressed RBMS1 protein expression in DAOY and D458 by 4.5-fold and 2-fold, respectively. MiR-383 modulated RBMS1 in DAOY, ONS-76, D384, and D425 at reduced levels between 1.1- to 1.6- fold. Such reduced expression was in line with the finding of decreased transcript level after miR-383 transfection. These data suggest that miR-383 regulated RBMS1 expression in MB cell lines.

5.5.11 Validation of *PRDX3* as miR-383 target by luciferase reporter assay

To evaluate whether miR-383 would interact with MRE in 3'UTR of *PRDX3*, a luciferase reporter plasmid containing the 3'UTR of *PRDX3* was prepared (pGL3-PRDX3). In addition, a mutant reporter plasmid, which was identical to pGL3-PRDX3 with the exception of the reverse order of seed region, was constructed (pGL3-MUT PRDX3). After normalization with renilla activity, luciferase activity was significantly downregulated in cells co-transfected with pGL3-PRDX3 and miR-383. In DAOY, a 71% reduction was observed, whereas 45% inhibition was seen in ONS-76 as illustrated in Figure 19. However, such reduction was not established in cells co-transfected with pGL3-PRDX3 and negative control or in cells co-transfected with

pGL3-MUT PRDX3 and miR-383. These results demonstrated a specific interaction between miR-383 and 3'UTR in *PRDX3* transcript to mediate gene repression.

5.5.12 Validation of *RBMS1* as miR-383 target by luciferase reporter assay

To show interaction between miR-383 and *RBMS1*, the 3'UTR of the *RBMS1* gene was cloned downstream of the luciferase reporter constructs (pGL3-RBMS1 and pGL3-MUT RBMS1). As depicted in Figure 20, co-transfection of the miR-383 and pGL3-RBMS1 markedly suppressed the normalized luciferase activity ($p<0.01$), whereas no such inhibitory effect was observed in the negative control. At 48 hours post-co-transfection, the luciferase activity was reduced in DAOY and ONS-76 by 45% and 36%, respectively. Furthermore, the luciferase activity reduction was abrogated when co-transfection of a mutated luciferase vector containing the seed region in a reverse orientation and miR-383. Thus, this finding suggested that miR-383 interacted specifically with the 3'UTR of *RBMS1* and inhibited RBMS1 expression.

5.5.13 Expression of *PRDX3* in gene specific siRNAs transfected cells

After confirming *PRDX3* as target gene of miR-383, the next question was whether these genes would mediate miR-383 effects on cellular processes. To this end, the knockdown effects of *PRDX3* on cell growth were evaluated in MB cells.

The knockdown effects of *PRDX3* on cell proliferation were examined. Two siRNAs specific for *PRDX3* (named siPRDX3-1 and siPRDX3-3) were employed to silence *PRDX3* gene expression in four cell lines and the subsequent biological effect was then assessed. Cells were transfected with two siRNAs against *PRDX3* or a negative control, and cell lysates were collected at 48 hours post-transfection. As shown in Figure 22, the two independent siRNAs almost completely abolished *PRDX3* transcript expression in DAOY, ONS-76, D283, and D458 compared to their respective negative controls. At 48 hours, compared to negative controls, siPRDX3-1 suppressed *PRDX3* mRNA level by 204-, 341-, 84-, and 117-fold in DAOY, ONS-76, D283, and D458, respectively. The siPRDX3-3 also downregulated *PRDX3* expression in these four cell lines by 60- to 171-fold and maximal downregulation by this siRNA was observed in D458. Moreover, the immunoblotting result, as represented in Figure 22, indicated that the two individual *PRDX3*-specific siRNAs depleted PRDX3 protein expression to a level almost undetectable in four MB cell lines. PRDX3 was expressed in negative control transfected cells. Taken together, delivery of two siRNAs against *PRDX3* could successfully silence gene expression in all four MB cell lines examined.

5.5.14 Effect of *PRDX3* depletion on cell growth by MTT assay

A

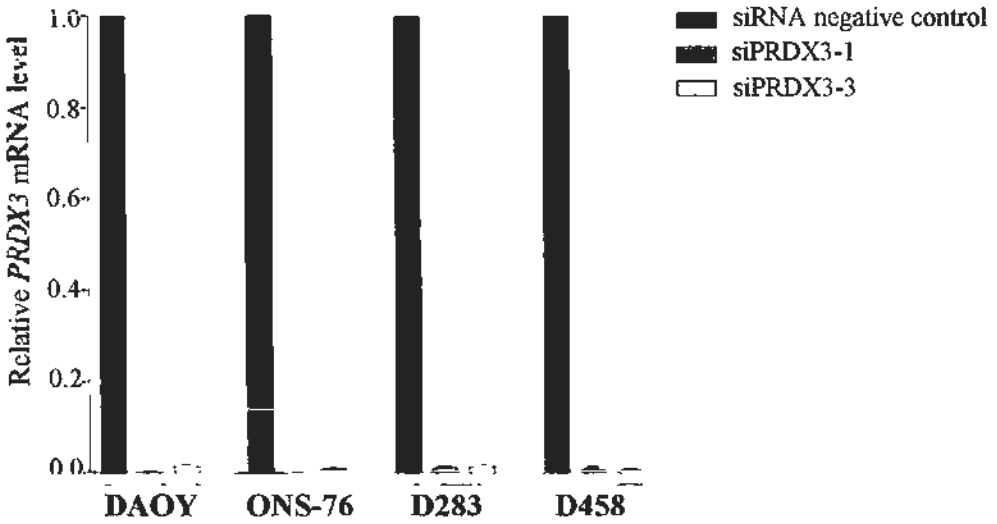

B

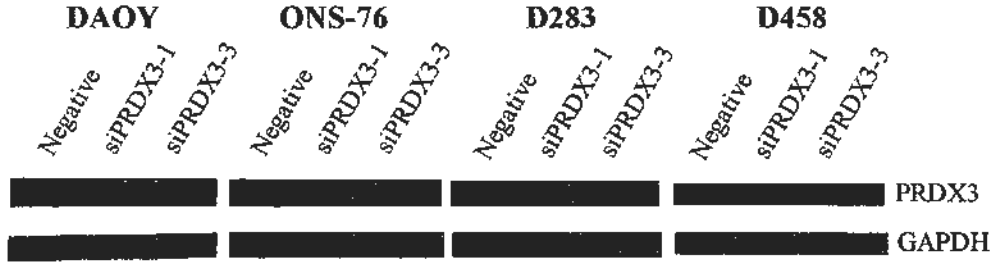

Figure 22. Suppression of *PRDX3* by siRNAs in MB. Cells were transfected with siRNAs targeting specifically to exons 4 and 5 of PRDX3 (siPRDX3-1 and siPRDX3-3), followed by determination of transcript and protein levels of PRDX3 by qRT-PCR (A) and Western blot analysis (B), respectively. MB cells transfected with PRDX3-specific siRNAs show reduced transcript and protein levels compared to cells transfected with siRNA negatve control. GAPDH serves as an internal control. The experiment was repeated three times.

To characterize the biological functions of *PRDX3*, the expression of *PRDX3* in four MB cell lines was silenced by two individual siRNAs and the effect on cell growth was measured by MTT assay on four successive days. The fluorescence labeled negative control was also included in the study to monitor the transfection efficiency and subsequent comparison. The result showed that two siRNAs mediated *PRDX3* suppression significantly inhibited four MB cell lines cell growth in a time-dependent manner as shown in Figure 23 ($p<0.05$). And, compared to mock (Lipofectamine 2000), the negative control had no effect on cell growth. In D283, induction of cell growth inhibition by suppression of *PRDX3* expression was evidenced as early as 24 hours post-transfection. Transfection of siPRDX3-1 (targets exon 4 of the gene) in D283 led to a significant reduced cell growth by 12% at 24 hours and 53% at 96 hours as compared to mock. The other siRNA (targets exon 5 of the gene) against *PRDX3* decreased cell growth by 6% at 24 hours and 12% at 96 hours. The cell growth inhibitory effect by siRNAs-mediated *PRDX3* silencing in ONS-76 and D458 was evidenced at 48 hours and afterwards as shown in Figures 23. In ONS-76, knockdown of *PRDX3* by siPRDX3-1 reduced cell growth by 13% and 24% at 48 and 96 hours, respectively. The siPRDX3-3 inhibited cell growth by 7% and 13% at 48 and 96 hours, respectively. In D458, a 21% and 50% reduction in cell growth as compared to mock was observed at 48 and 96 hours respectively, after the delivery of siPRDX3-1. The

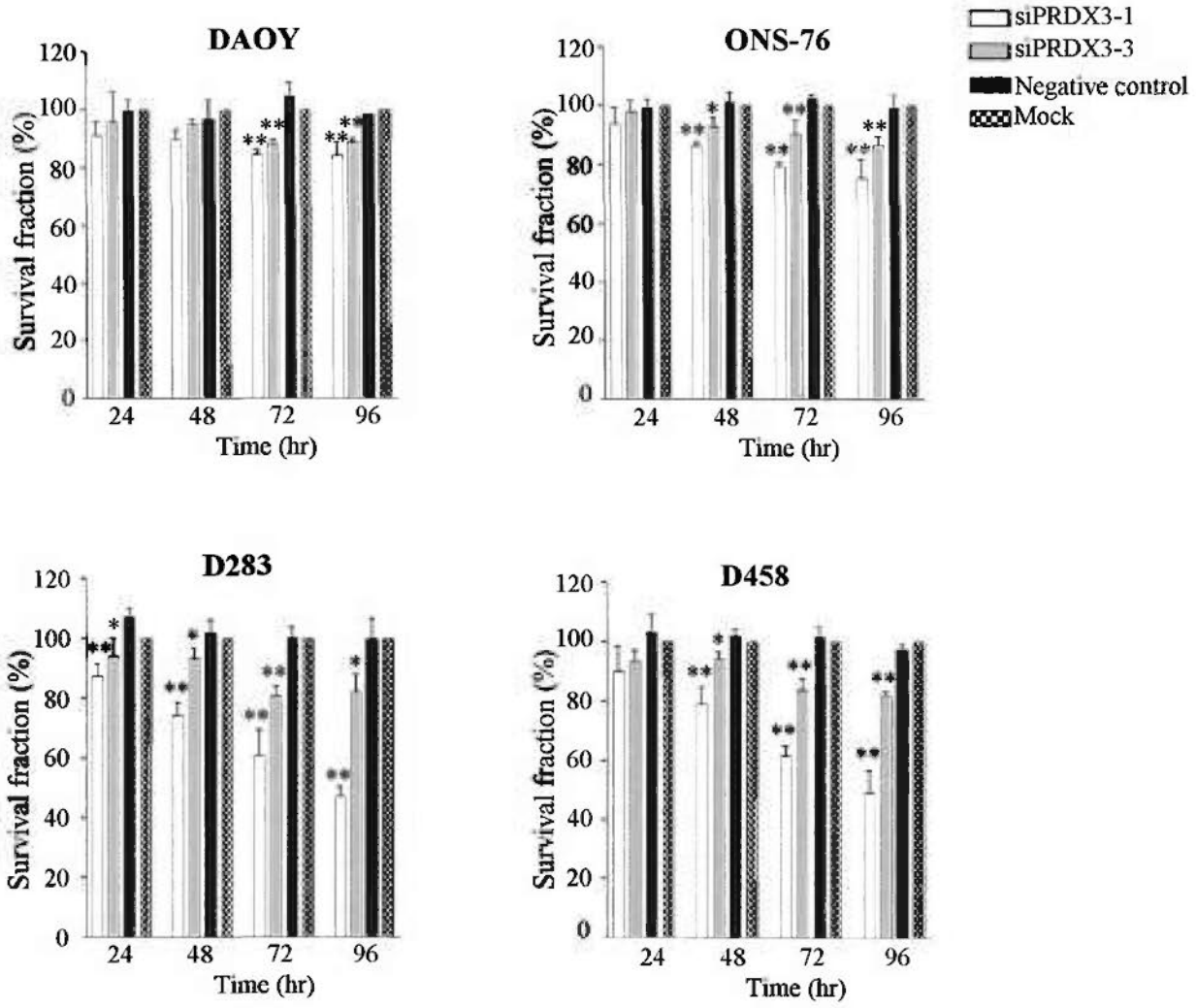

Figure 23. Effect of *PRDX3* knockdown on cell growth in MB. Cells were transfected with *PRDX3*-specific siRNAs and evaluated for cell growth by MTT assay. Knockdown of *PRDX3* leads to a significant reduction of cell growth in MB cells. Three independent experiments were conducted. *, $p<0.05$; **, $p<0.01$.

siPRDX3-3 decreased cell growth by 6-12% at a period of 48 to 96 hours after transfection. Significant inhibition in cell growth was observed in DAOY cells at 72 and 96 hours after siRNAs transfection. The two siRNAs against *PRDX3* led to a growth suppression by 12% and 15% at 96 hours post-transfection (Figure 23). Taken together, the results suggested that *PRDX3* plays a role in cell growth. It further supported miR-383 mediated cell growth inhibition by suppressing the expression of its target gene.

5.5.15 Effect of *PRDX3* depletion on cell growth by cell counting

To confirm the observation on cell growth inhibition mediated by *PRDX3* silencing, viable cell counting was employed. The four MB cell lines were transfected with two *PRDX3*-specific siRNAs, viable cell number was determined with trypan blue staining and hemocytometer counting in four successive days. As shown in Figure 24, compared to mock, significant cell growth inhibition was reported in all four cell lines upon siRNAs-mediated *PRDX3* silencing. And, in all four cell lines, no cell growth inhibitory effect was observed in negative control as compared to mock. In ONS-76, knockdown of *PRDX3* gene expression induced cell growth suppression as early as 48 hours after transfection. At 48 hours, cell number in siPRDX3-1 and siPRDX3-3 transfected ONS-76 cells was reduced by 52% and 29%, respectively compared to

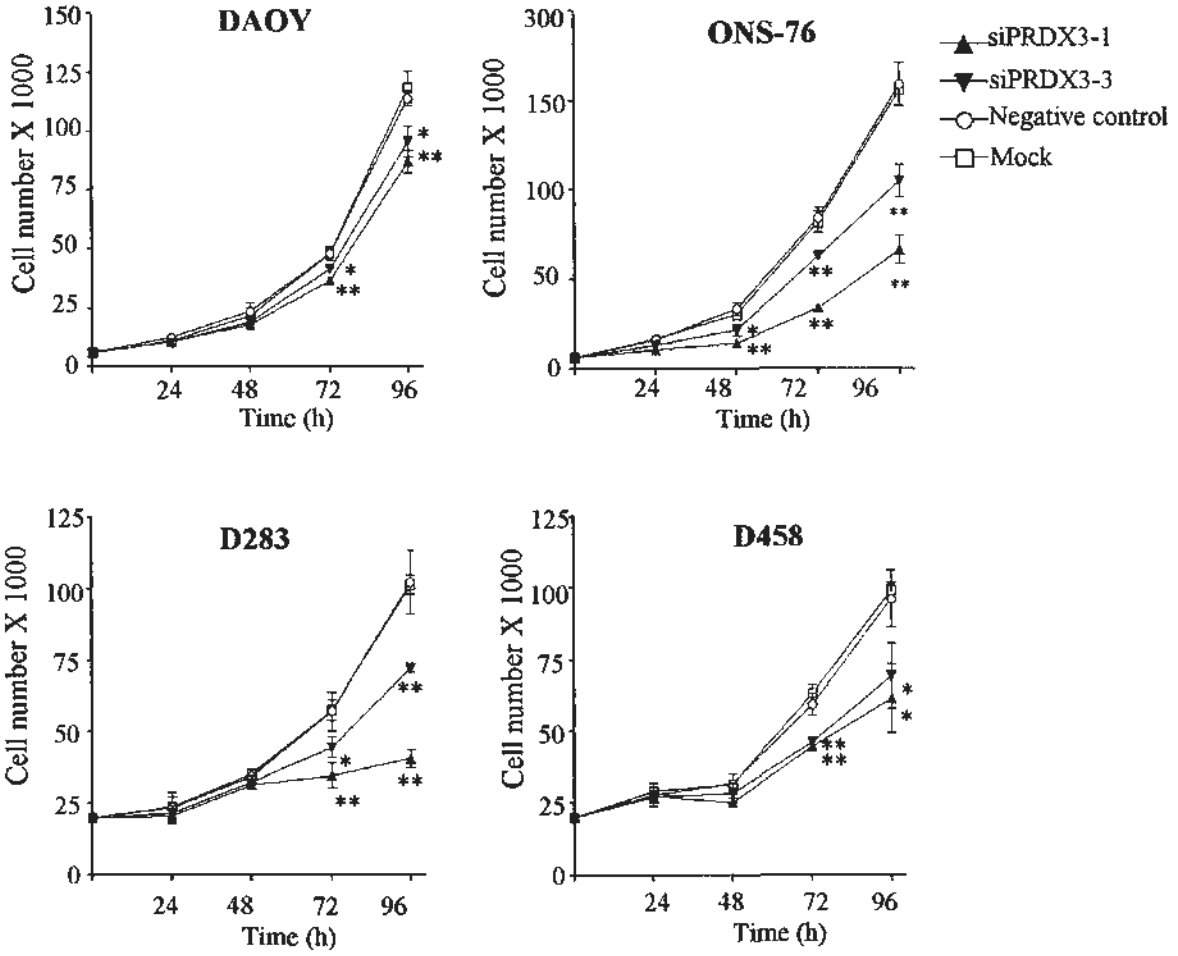

Figure 24. Effect of *PRDX3* knockdown on cell growth in MB by viable cell counting. Cells were transfected with PRDX3-specific siRNAs, followed by assessment of viable cell counting using the trypan blue exclusion assay for 4 consecutive days. Viable cell number is significantly reduced in PRDX3-depleted cells compared to mock. The data represent the mean ± SD of 3 individual experiments. *$p<0.05$;** $p<0.01$.

mock. Similar reduction in percentage of cell number was maintained afterward. At 96 hours, siPRDX3-1 and siPRDX3-3 suppressed cell number by 57% and 32%, respectively. In DAOY, D283, and D458, the growth inhibitory effect of *PRDX3* gene silencing was observed at and after 72 hours transfection. The siPRDX3-1 reduced cell growth of DAOY cells as compared to mock by 24% and 27% at 72 and 96 hours post-transfection, respectively. Also, siPRDX3-3 decreased cell number of DAOY cells by 14% at 72 hours and 19% at 96 hours. Although the growth inhibitory effect of delivery of siPRDX3-1 was more profound than that of siPRDX3-3, the difference did not reach statistical significance. In D458 cells, silencing *PRDX3* by siPRDX3-1 reduced cell number by 29% and 38% at 72 and 96 hours, respectively. The cell number in siPRDX3-3 transfected D458 cells as compared to mock was decreased by 26% at 72 hours and 30% at 96 hours. Same as DAOY cells, there was a trend showing that siPRDX3-1 induced greater cell growth inhibition than that of siPRDX3-3 in D458. Compared to mock, *PRDX3* depletion by siPRDX3-1 transfection suppressed cell number by 40% at 72 hours and 60% at 96 hours in D283 cells. The other siRNA, siPRDX3-3, decreased cell number of D283 cells 23%-29% at 72-96 hours post-transfection. A significant difference in cell number was observed between siPRDX3-1 and siPRDX3-3 transfected cells, indicating that siPRDX3-1 exerted a more prominent growth inhibitory effect than that of siPRDX3-3 in D283 cells. The results

further supported the cell growth inhibitory role of *PRDX3* in MB, and highlighted the mechanism which miR-383 mediated gene expression to regulate cell growth in MB.

5.5.16 PARP cleavage induction by suppression of *PRDX3* gene expression

To elucidate the mechanism of cell growth suppression induced by silencing *PRDX3* in MB cells, PARP protein cleavage level was assessed. The four MB cell lines were subjected to transfection with siRNAs against *PRDX3* or negative control. Cell lysates were collected in four successive days. PARP cleavage was then detected by immunoblotting and band intensity was measured and normalized with a loading control, GAPDH. The results revealed that silencing *PRDX3* by two individual siRNAs led to enhanced cleavage of PARP protein in all four cell lines compared to negative control. As shown in Figure 25, markedly increased in PARP cleavage was apparent in siRNA-mediated *PRDX3* silencing of D283 as early as 24 hours post-transfection, and was maintained during the course of study. Transfection of two independent siRNAs against *PRDX3* led to a 1.4 to 2-fold increased in PARP cleavage at 24 hours. Increased PARP cleavage was also detected in subsequent time period. In general, siPRDX3-1 transfected cells displayed a higher level of PARP cleavage than siPRDX3-3 transfected cells in D283. Depletion of *PRDX3* in D458 induced a slightly increase in PARP cleavage compared to negative control at 24 hours, and substantial upregulation of

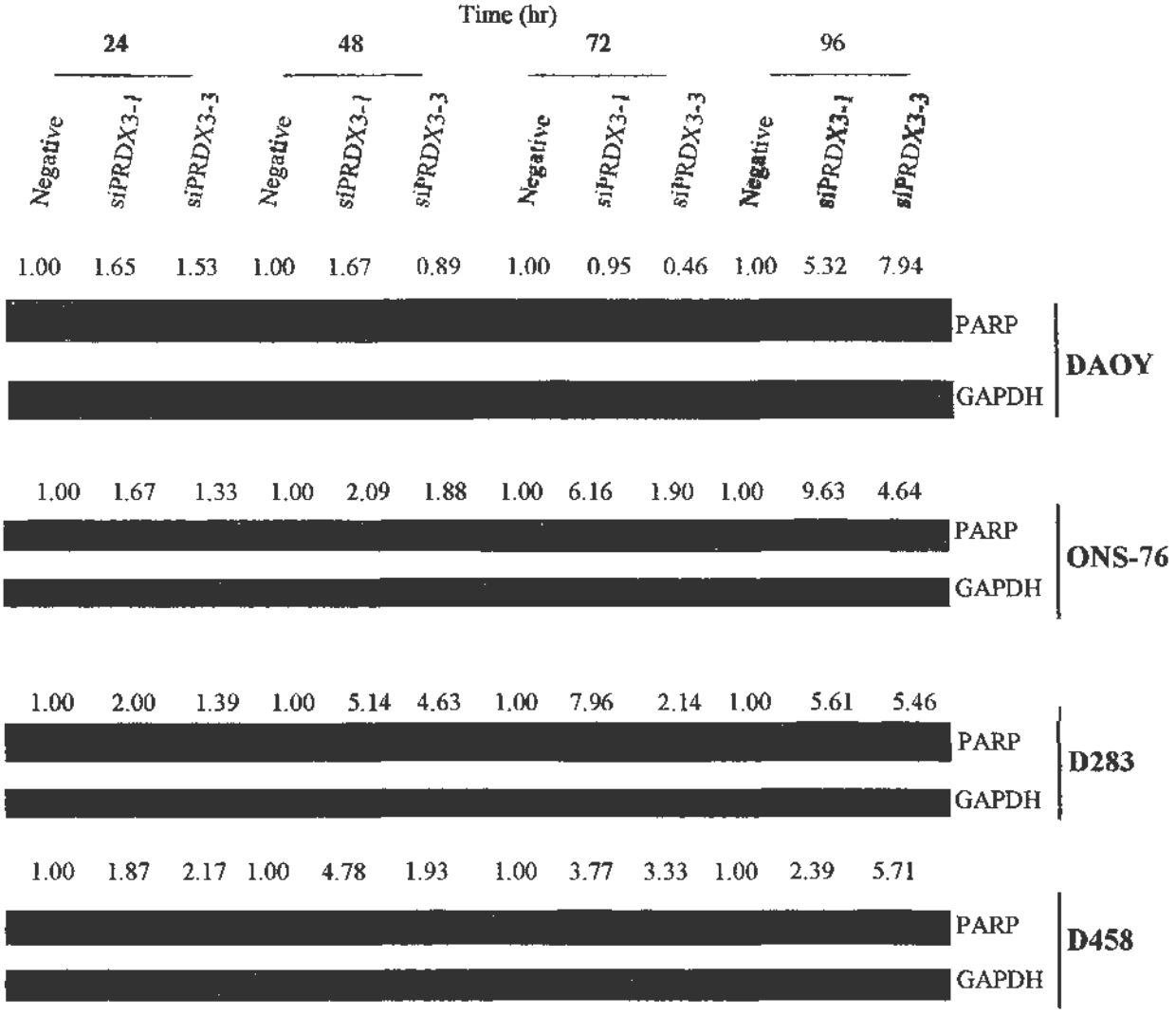

Figure 25. Effect of *PRDX3* knockdown on induced apoptosis in MB. Cells were transfected with siRNAs and probed for expression of cleaved PARP by Western blot analysis for 4 successive days. The results reveal that *PRDX3* knockdown leads to an upregulation of cleaved PARP in MB, indicating induction of apoptosis. The number above the protein band represents the relative cleaved PARP protein level compared to the negative control after normalization to GAPDH.

PARP cleavage was observed at 48 hours and afterward as illustrated in Figure 25. Moreover, *PRDX3*-silenced ONS-76 cells displayed a trend of rising PARP cleavage level from 24 hours to 96 hours after transfection (Figure 25). Lastly, in *PRDX3*-depleted DAOY cells, marked upregulation of PARP cleavage was observed at 96 hours post-transfection when siPRDX3-1 and siPRDX3-3 transfected cells showed a 5.3- and 7.9-fold increase in PARP cleavage level compared to negative control (Figure 25). Taken together, the results illustrated that depletion of *PRDX3* enhanced PARP cleavage expression in MB cell lines, suggesting that induction of apoptosis was one of the mechanisms for cell growth inhibition effect induced by knockdown of *PRDX3*.

5.5.17 Effects of *RBMS1* depletion on cell growth by MTT assay

DAOY and ONS-76 were transfected with *RBMS1*-specific siRNAs or negative control independently and cell growth was then measured by MTT assay at 24, 48, 72, and 96 hours. As depicted in Figure 26, depletion of RBMS1 with siRBMS1-1 led to inhibition of cell growth from 48 hours to 96 hours post-transfection. Cell growth was suppressed by 7% at 48 hours and 8% at 72 and 96 hours compared to mock in ONS-76. No alteration in cell growth was observed in cells transfected with siRNA negative control. However, transfection of the siRBMS1-2 in ONS-76 did not result in alteration in cell growth. In addition, significant change was not observed in *RBMS1* silenced

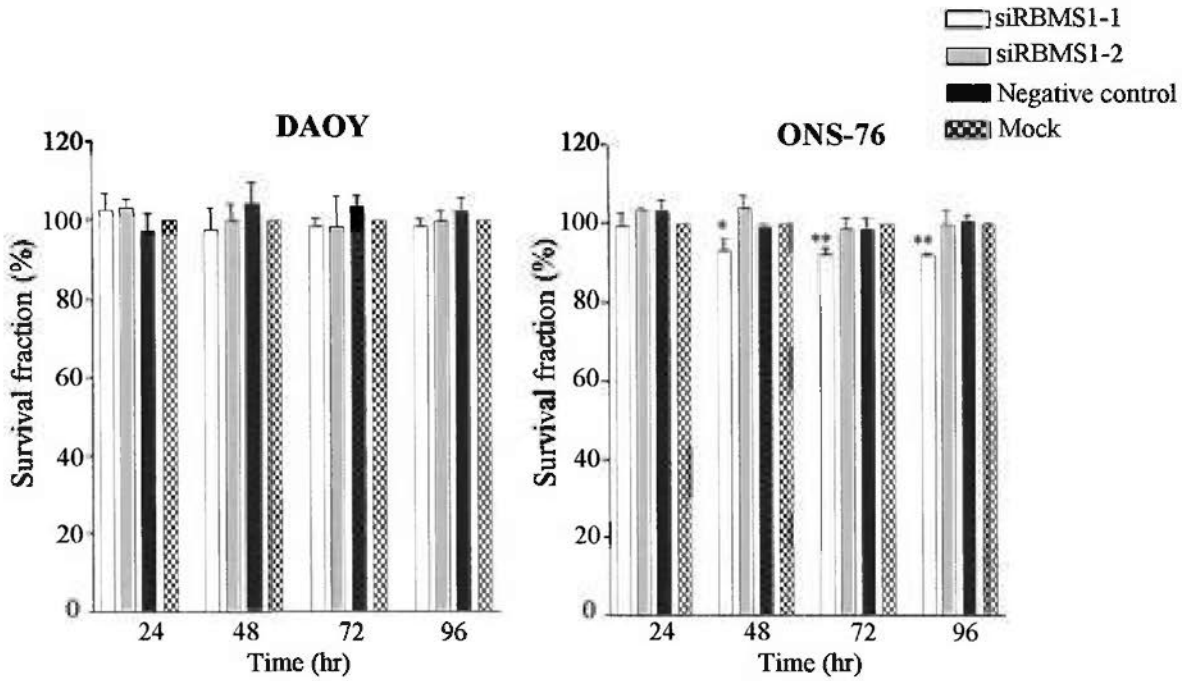

Figure 26. Effect of *RBMS1* knockdown on cell growth in MB. Cells were transfected with 2 siRNAs against *RBMS1* independently (siRBMS1-1 and siRBMS1-2), a siRNA negative control or no siRNA (mock). Cell growth was then monitored for 4 consecutive days by MTT assay. Knockdown of *RBMS1* does not significantly alter cell growth in DAOY. A modest suppression of cell growth is seen in ONS-76 at 48 hr to 96 hr after *RBMS1* knockdown. The data represent the mean ± SD of 3 independent experiments. *, $p<0.05$; **, $p<0.01$.

DAOY. Thus, the result indicated that knockdown *RBMS1* had a minimal effect on cell growth in MB. This finding could not rule out the possibility that *RBMS1* involved in tumorigensis through metastasis or angiogenesis mechanism. Further investigation is needed to clarify the role of *RBMS1* in MB tumorigenesis.

5.6 miR-124 and miR-383 in neuronal differentiation

5.6.1 Selection of P19 subclones for RA-induced neuronal differentiation

Mouse P19 is an embryonal carcinoma cell line that can be maintained in undifferentiated state but can be induced to differentiate into neurons by culturing them in the presence of RA (Jones-Villeneuve et al. 1982; Jones-Villeneuve et al. 1983). An early phase of commitment to neuronal fate occurs within two days after RA-treatment and a late phase of terminal differentiation happens from days five onwards (Brain et al. 1994). Thus, P19 could serve as a model for neuronal differentiation. A previous study demonstrated an upregulation of a set of brain-specific, brain-enriched, and brain-nonenriched miRNAs in P19 cells upon RA treatment (Sempere et al. 2004). These included brain-specific miR-9, -124a, -124b, -135, brain-enriched miR-9*, -125a, -125b, -128, and brain-nonenriched let-7a, let-7b, miR-30a, -30b, -30c, -30e, -98, -100, 103-1, -156, -218. Furthermore, miR-124 is known to modulate the neurite outgrowth in P19 cells (Yu et al. 2008). Increased miR-124 expression enhanced the neurite

outgrowth and extension while inhibition of miR-124 expression resulted in neurite outgrowth suppression. These results suggest a role of miRNAs in progression and determination of neuronal fate in mammals. To elucidate whether miR-383 was also involved in neuronal differentiation and maturation, P19 were induced to neuronal differentiation by RA treatment. The fact that P19 cells are heterogeneous with respect to their development potentials (Jones-Villeneuve et al. 1982), subclones of P19 cells were selected for this experimental study. Single P19 cells were first selected and expanded. A total of 11 subclones were screened for their differentiation potential towards neuronal cells in the presence of RA. Two criteria were used to select the appropriate subclones for further experiments. These were 1) expression of β-tubulin III (TUBB3) at day 10 after RA treatment, and 2) morphological change, that were the length of neurite outgrowth. Five subclones showed showed little or no neurite growth after RA treatment. These clones were discarded. The remaining six clones showed neurite growth with at least greater than three cell body size. These clones were then analyzed for TUBB3 expression by western blot analysis. Their expression was compared to parental cells that grew without any clone selection and yet were treated with RA. As shown in Figure 27, clone 12 and clone 22 had the strongest TUBB3 expression among the six subclones. Their expression was greater than that of parental cells. The expression level of two subclones, namely clone 4 and 10, showed similar

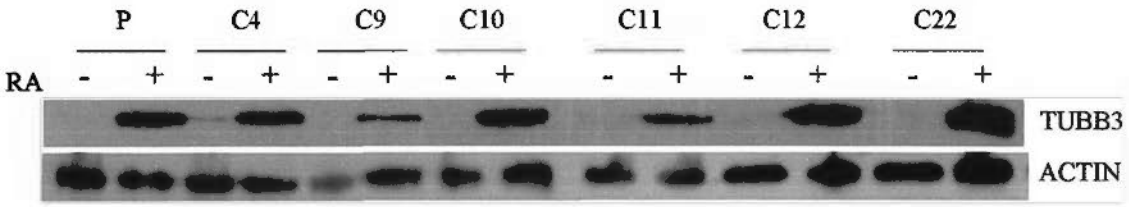

Figure 27. Expression of the neuronal marker β-tubulin III (TUBB3) in subclones of P19. Six single cells of P19 obtained by limiting dilution were expanded, treated with all-trans-retinoic acid (RA) to induce neuronal differentiation. Cell lysates were collected at day 10 and TUBB3 expression was examined by Western blot analysis. Two subclones (C12 and C22) show higher TUBB3 expression than parental cells (P) upon RA treatment. These clones are used in subsequent experiments. Actin is used a loading control. + and – indicate the presence and absence of RA treatment, respectively.

TUBB3 expression level to that of the parental cells. In contrast, clones 9 and 11 showed lower TUBB3 expression level compared to the parental cells. Thus, clones 12 (P19C12) and clone 22 (P19C22) were selected for further study.

5.6.2 Morphology change in RA-treated cells

Upon the RA treatment, morphological appearances were changed in both subclones of P19 cells. As shown in Figures 28 and 29, at 240 hours long possesses were extended out from the cell bodies in both subclones. These cells displayed as a monolayer layer of fibroblast-like cells extending out from cell bodies.

5.6.3 Expression of neuronal marker TUBB3 in RA-treated P19 subclones

To ensure the RA-induced neuronal differentiation carried out properly, neuronal specific marker TUBB3 was examined by western blot analysis. As shown in Figure 28 and 29, TUBB3 protein expression was not detected in both subclones in the absence of RA treatment. P19C12 cells, in the presence of RA treatment, expression of TUBB3 was induced at 96 hours, and the level showed an increasing trend during the study period with maximum level being detected at 240 hour. In RA-treated P19C22 cells, expression of TUBB3 was first detected at 72 hours when the protein level was scarcely observed. Enhancing TUBB3 protein level was found from then on until the end of

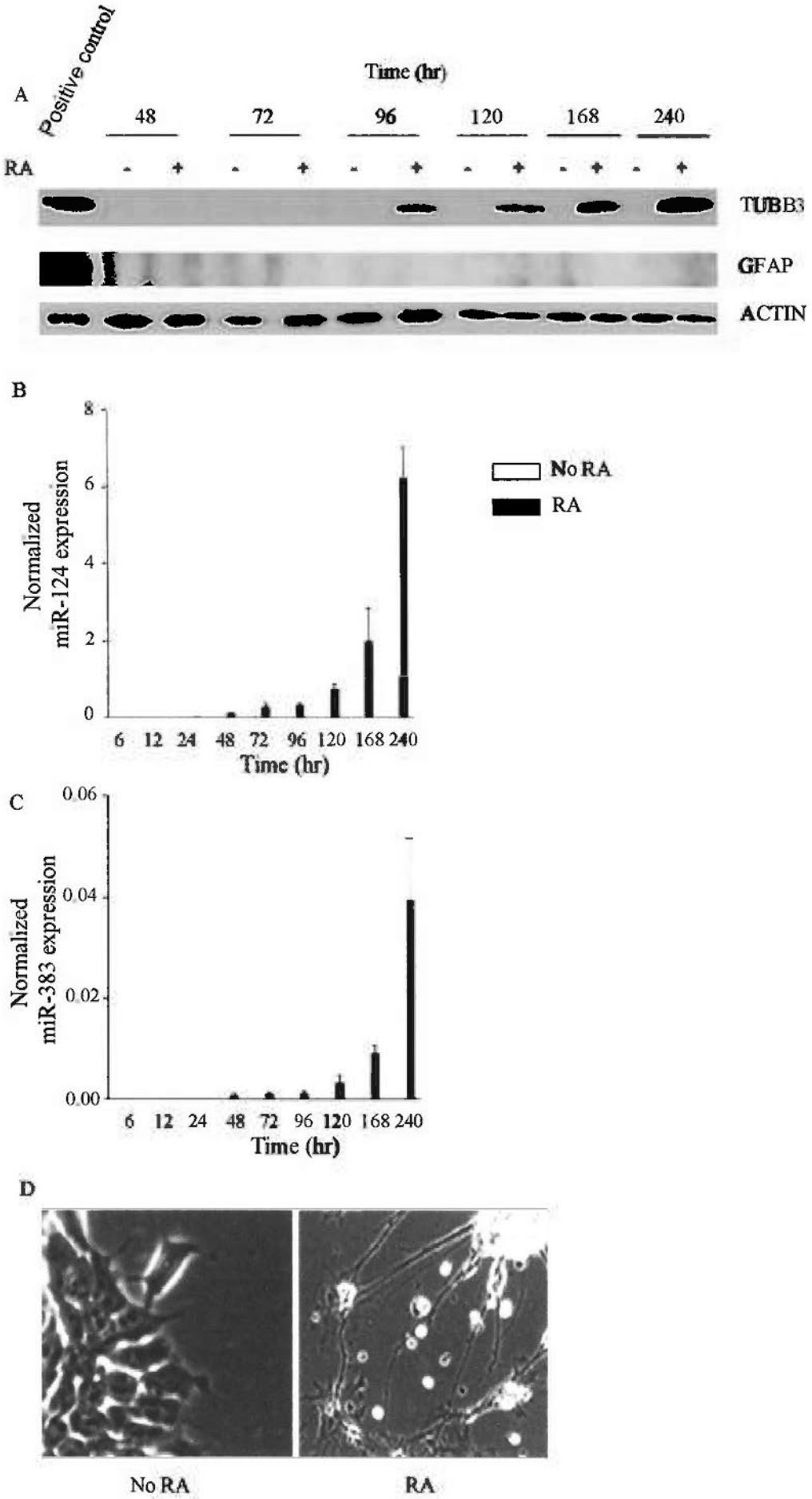
A
Positive control
Time (hr)
48
72
96
120
168
240
RA
- + - + - + - + - + - +
TUBB3
GFAP
ACTIN
B
Normalized miR-124 expression
8
6
4
2
0
6 12 24 48 72 96 120 168 240
Time (hr)
No RA
RA
C
Normalized miR-383 expression
0.06
0.04
0.02
0.00
6 12 24 48 72 96 120 168 240
Time (hr)
D
No RA
RA

Figure 28 Evaluation of miR-383 expression during RA induced neuronal differentiation of P19 subclone C12 (P19C12). (A) Western blot analysis reveals that upregulation of the neuronal marker β-tubulin III (TUBB3) is observed as early as 96 hr and reached a high level at 240 hr after treatment with all-trans-retinoic acid (RA), suggesting induction of neuronal differentiation. The astrocytic marker GFAP is not detectable during the 10-day studied period. Each lane is loaded with 50 μg of cell lysate. The first lane in the blot contains control cells U373, which express TUBB3 constitutively. Actin is used as a loading control. (B, C) qRT-PCR analysis shows that both miR-124 (B) and miR-383 (C) transcripts are detectable at 48 hr after RA treatment and the levels increase thereafter in a time-dependent manner. Of note is that the miR-383 level is about 100-fold lower than that of miR-124. (D) Representative micrograph showing neurite outgrowth from P19C12 cells at 10 days after RA treatment. An increase in the number and length of neurite-like structure is observed in RA-treated cells. Untreated cells exhibit polygonal morphology. The experiment was repeated three individual times.

A

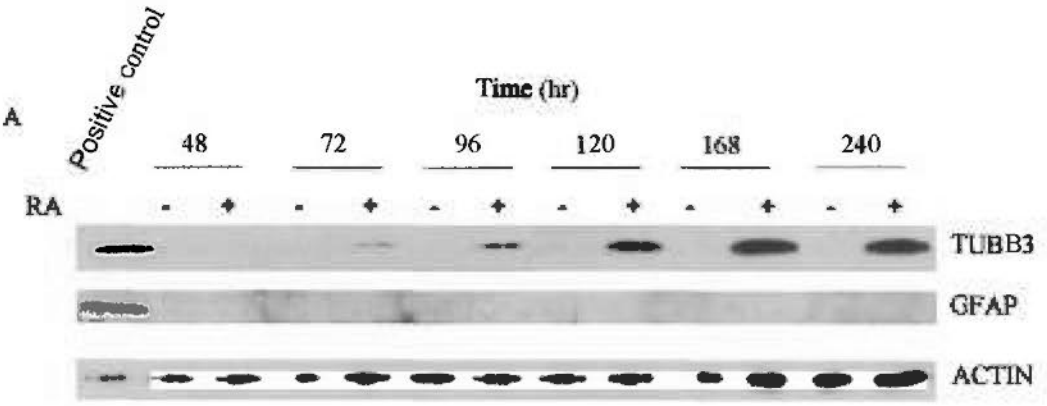
Positive control
Time (hr)
48
72
96
120
168
240
RA
- + - + - + - + - + - +
TUBB3
GFAP
ACTIN

B

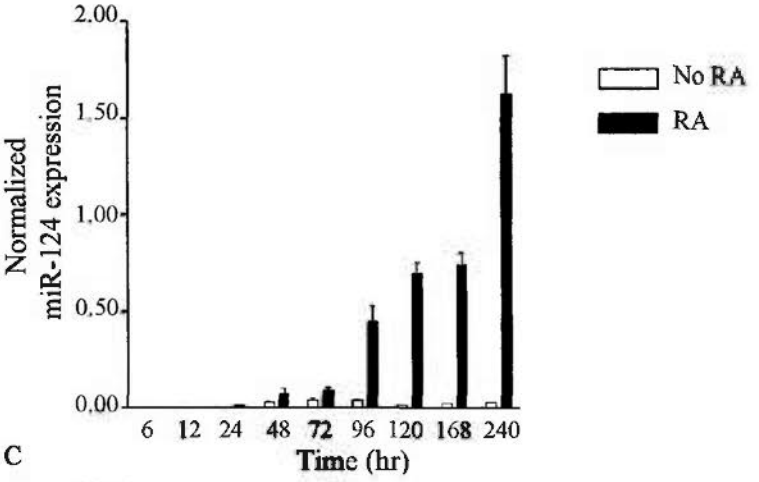
Normalized miR-124 expression
2.00
1.50
1.00
0.50
0.00
6 12 24 48 72 96 120 168 240
Time (hr)
No RA
RA

C

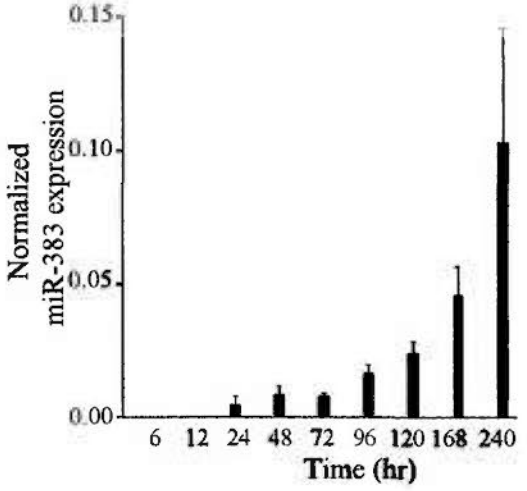
Normalized miR-383 expression
0.15
0.10
0.05
0.00
6 12 24 48 72 96 120 168 240
Time (hr)

D

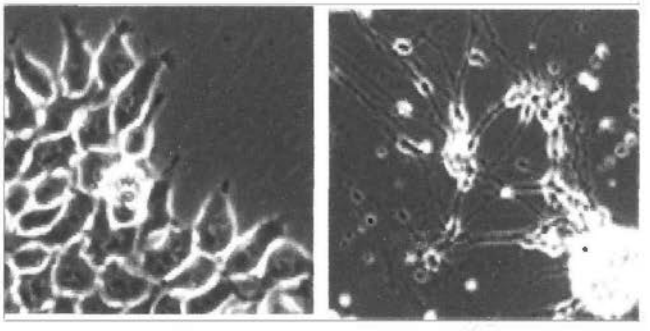

No RA RA

Figure 29. Evaluation of miR-383 expression during RA induced neuronal differentiation of P19 subclone C22 (P19C22). (A) Western blot analysis reveals that upregulation of the neuronal marker β-tubulin III (TUBB3) is observed at 72 hr and reached a high level at 240 hr after treatment with all trans retinoic acid (RA), suggesting induction of neuronal differentiation. The astrocytic marker GFAP is not detectable during the 10-day studied period. Each lane conatins 50 μg of cell lysate. The first lane in the blot contains control cells U373. Actin is used as a loading control. (B, C) qRT-PCR analysis shows that both miR-124 (B) and miR-383 (C) transcripts are detectable at 24 hr after RA treatment and the levels increase thereafter in a time-dependent manner. (D) Representative micrograph showing neurite outgrowth in P19C22 cells on day 10 after RA treatment. An increase in the number and length of neurite-like structure is observed in RA-treated cells. Untreated cells exhibit polygonal morphology. The experiment was repeated three individual times.

study. In both subclones, GFAP protein expression was not detected with or without RA treatment.

5.6.4 Induced neuronal differentiation in P19 subclones

To explore whether miR-383 expression was involved in neurogenesis, P19C12 and P19C22 were subjected to induced neuronal differentiation by RA treatment according to the procedures described by Jones-Villeneuve et al. (Jones-Villeneuve et al. 1983). Briefly, the cells were cultured as aggregates and exposed to RA in a bacterial petri dish. Subsequently, they were replated on poly-L-lysine coated culture dish. A previous study had demonstrated miR-124 is upregulated in RA treatment (Sempere et al. 2004); thus, miR-124 expression served as a control. Expression of miR-124 was examined from 6 to 240 hours post-RA treatment. For P19C12 and P19C22, there was a minimal miR-124 expression without RA treatment as shown in Figures 28 and 29. In P19C12, miR-124 was statistically upregulated starting from 24 hours after RA treatment ($p<0.05$). After normalized with GAPDH, a 10-fold increase in miR-124 expression was observed in P19C12 compared to the mock at 48 hours and miR-124 expression was increased onward. At 240 hour post-RA treatment, miR-124 expression was increased by 348-fold compared to the mock.

For P19C22, statistical significant in miR-124 expression was observed at 48

hours post-treatment (Figure 29). Compared to the mock, there was a 2-fold increase in miR-124 expression. Its expression was continuously upregulated during the period of experiment. At 240 hour, RA-treated P19C22 exhibited a 55-fold overexpression in miR-124 compared to the mock.

5.6.5 miR-383 expression in RA induced neuronal differentiated P19C12 and P19C22 cells

To investigate whether miR-383 is involved in neuronal differentiation, miR-383 was examined during the course of RA treatment. As shown in Figures 28 and 29, neither P19C12 nor P19C22 cells exhibited a detectable miR-383 expression without RA treatment. Upon RA induced differentiation, miR-383 expression was detectable as early as 48 hours post-RA treatment in P19C12 cells, and the expression increased 51-fold at 240 hour compared to its expression at 48 hours. Moreover, miR-383 expression was lower than miR-124 at all time points. For instance, its expression at 48 hours was 161-fold less than that of miR-124 at 48 hours.

In P19C22, detectable miR-383 expression was found at 24 hours after RA treatment. This was earlier than that in P19C12 cells. Continuously increased miR-383 expression was observed afterward. Compared to 24 hours, there was a 20-fold change in miR-383 expression at 240 hour. Similar to P19C12 cells, miR-383 expression was

lower than miR-124 expression from 24 to 240 hours.

5.6.6 *Sgcz* expression in RA induced neuronal differentiated P19C12 and P19C22

Sgcz is the host gene of miR-383 with miR-383 located in intron 1 of the *Sgcz* gene in both human and mouse. To investigate whether *Sgcz* and miR-383 were coexpressed during the course of induced neuronal differentiation, *Sgcz* transcript level was also examined and normalization was done using *Gapdh* transcript. As shown in Figure 30, *Sgcz* expression was not expressed in P19C12 and P19C22 in the absence of RA.

In P19C12, *Sgcz* expression appeared at 24 hours post-RA treatment when the mature miR-383 was still undetectable. Detectable miR-383 expression was found at 48 hours after RA treatment and occurred a day after the induction of *Sgcz* gene expression. *Sgcz* transcript level was increasing from 24 hours onward. At 72 hours, *Sgcz* expression was increased by 3.6-fold compared to that at 24 hours and its expression was increased by 126-fold by 240 hour. Most importantly, the expression of miR-383 and host gene *Sgcz* are significantly correlated as illustrated in Figure 30. The result indicates miR-383 was coordinately expressed with *Sgcz* and miR-383 was processed with the precursor *Sgcz* mRNA.

In P19C22, *Sgcz* expression first appeared at 24 hours and the expression was

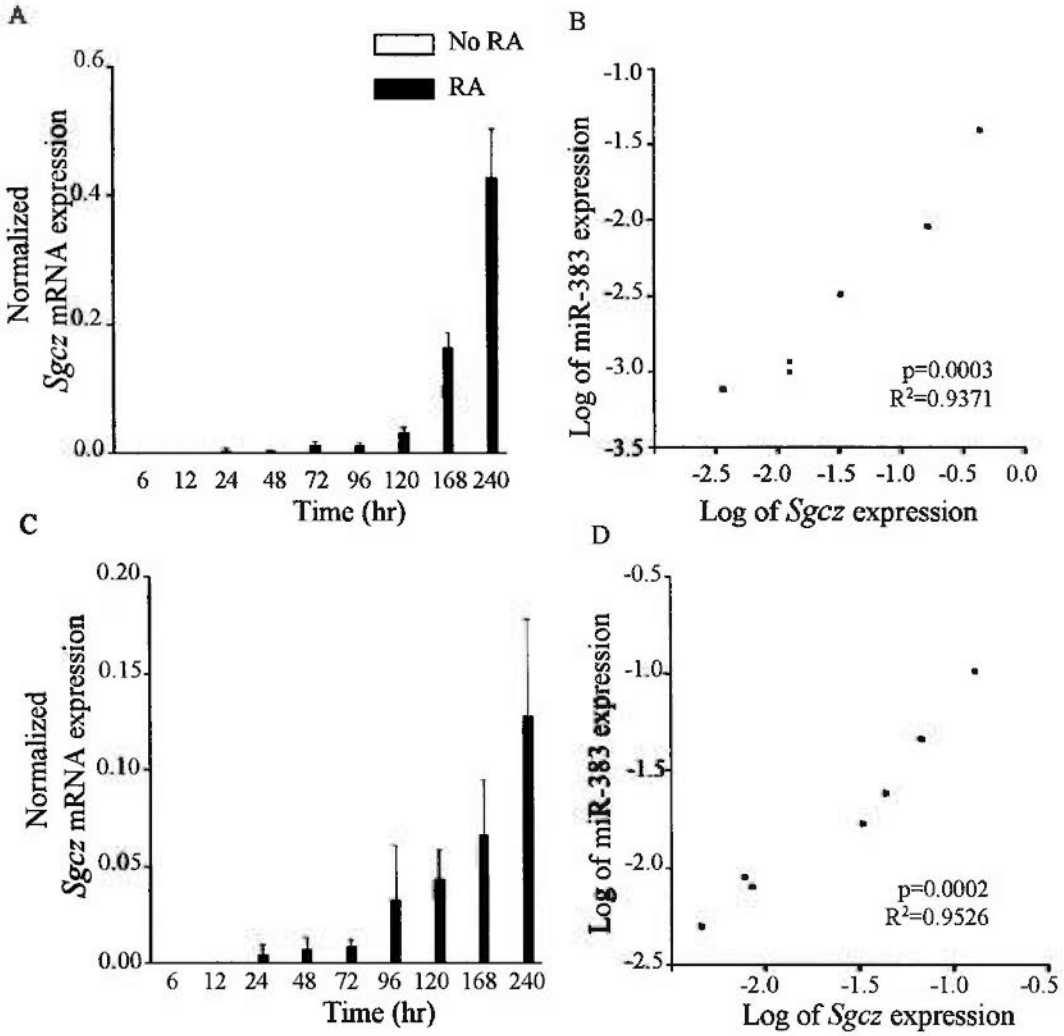

Figure 30. Expression analysis of *Sgcz*, the host gene of miR-383, during neuronal differentiation in P19C12 and P19C22 cells. Cells were treated with all-trans-retinoic acid and then evaluated for *Sgcz* expression by qRT-PCR. The result shows that miR-383 expression is detectable at 24 hr after RA treatment in P19C12 (A) and P19C22 (C). Sgcz expression is increasing onward. MiR-383 and *Sgcz* expression are significantly correlated in P19C12 (B) and P19C22 cells (D).

increasing afterward. This was the same time point when mature miR-383 transcript was first detected. Compared to 24 hours, *Sgcz* transcript was increased by 2, 2, 10, 10, 14 and 20-fold at 48, 72, 96, 120, 168 and 240 hours respectively. Similarly to P19C12, expression of miR-383 and host gene *Sgcz* are significantly correlated as illustrated in Figure 30, suggesting miR-383 and *Sgcz* were expressed in a parallel manner.

5.6.7 Expression features of miR-383 and its host gene *Sgcz*

In both subclones of P19, the expression of miR-383 and *Sgcz* were significantly correlated. As shown in Figure 30, the expression of miR-383 and *Sgcz* are significantly correlated in P19C12 ($p=0.0003$) and P19C22 cells ($p=0.0002$). One interesting finding was that *Sgcz* transcript abundance was greater than that of mature miR-383 at all time intervals by copy number based standard curve. For instance, when the first appearance of mature miR-383 (48 hours), *Sgcz* transcript level was 4 times higher than that of miR-383. And, *Sgcz* transcript level was 10 times higher than that of mature miR-383 at 240 hour. However, in P19C22, the *Sgcz* and miR-383 transcript were made in stoichiometric fashion. That was, a one to one transcript ratio was found between *Sgcz* and miR-383 between time interval 48 and 240 hours.

CHAPTER 6

DISCUSSION

6.1 Analysis of potential tumor-related genes on chromosome 8p

MB is the most common malignant CNS tumor in infants and children, with 85% of MBs being diagnosed in patients younger than 18 years of age (Korshunov et al. 2010). Over the last few decades, advances in surgical and adjuvant therapeutic treatments have improved the survival rate and clinical outcomes. At present, the cure rate for standard risk patients has increased to approximately 75%. However, the survival rate for the high risk patients is not encouraging, at around 25%. In addition, deleterious side effects, such as neurocognitive difficulties, endocrine, thyroid and growth hormone issues, and physical problems, are frequently observed in survivors as a result of therapy. A better understanding of MB biology would lead to development of novel therapeutic strategies that would reduce the side effects and enhance the survival rate.

Our group has previously identified loss of chromosome 8p as a frequent recurrent event in MB by CGH and microsatellite analysis. Finer mapping of the deletion region by microsatellite markers revealed a common homozygously deleted region at 8p22-23.1 and partial or interstitial deletions on chromosome 8p22-23.2. The results suggested that the presence of TSG(s) in these regions. The aims of my study

were to identify the candidate TSGs on chromosome 8p and to characterize their biological function in relation to tumorigenesis of MB. To this end, I had employed multiple approaches to identify the TSGs on chromosome 8p. First, I had gone through literature review to select potential tumor-related genes within the deletion regions. Two genes, *LZTS1* and *TUSC3*, were selected for analysis.

LZTS1 is located on 8p21.3. Downregulation of this gene was observed in multiple tumor types (Nonaka et al. 2005; Vecchione et al. 2001; Vecchione et al. 2002). Overexpression of *LZTS1* suppressed cell growth by inhibition of cell cycle progression (Ishii et al. 2001; Vecchione et al. 2001). These data suggested the involvement of *LZTS1* in tumorigenesis.

TUSC3 is located on chromosome 8p22. Loss of *TUSC3* expression was reported in ovarian cancer (Pils et al. 2005). Downregulation of *TUSC3* was correlated with metastasis, adverse staging, and adverse clinical outcome in carcinomas of larynx and pharynx (Guervós et al. 2007; Pils et al. 2005). These data supported a role of *TUSC3* in carcinogenesis.

Based on the hypothesis that TSG inactivation, in general, may result from absent or reduced expression due to allelic deletion, epigenetic modifications or other transcriptional silencing mechanisms, the transcript levels of *LZTS1* and *TUCS3* were evaluated by qRT-PCR. The results showed that downregulation of *LZTS1* occurred in a

minor fraction (5%) of MBs. This suggested *LZTS1* might play a minor role in MB formation. A limitation of this study on *LZTS1* analysis was the lack of data to conclude the mechanism for reduced *LZTS1* mechanism in this minor fraction of MBs. The qRT-PCR result also showed that 10% of MBs examined had reduced *TUSC3* expression compared to normal cerebella. This result was consistent with the findings that *TUSC3* expression was reduced or lost in ovarian, pancreatic and prostate tumors (Bashyam et al. 2005; MacGrogan et al. 1996; Pils et al. 2005).

My study also demonstrated that reduced *TUSC3* expression was observed in one case harboring a homozygously deleted interval covering 8p23.1 where *TUSC3* is located, suggesting that genomic loss might be one mechanism responsible for reduced *TUSC3* expression.

The other case (case 22) with *TUSC3* downregulation did not exhibit 8p loss, suggesting that other mechanisms might have regulated *TUSC3* expression. The presence of CpG island at the promoter and exon 1 of *TUSC3* prompted for investigation of DNA hypermethylation in case 22. The results showed that DNA hypermethylation was absent in case 22, suggesting that epigenetic silencing was unlikely the mechanism responsible for decreased expression in this tumor. However, because only 20 out of 67 CpG dinucleotides were examined, it was possible that DNA hypermethylation occurred at sites other than those studied in this study. Other

mechanism such as mutation may contribute to *TUSC3* downregulation.

Structural characterization of *TUSC3* has revealed the presence of consensus recognition sequences for Sp1 transcription factor (SP1), transcription factor AP-2 alpha (AP2) and TP53 in the promoter of *TUSC3* (El-Deiry et al. 1992; Imagawa et al. 1987; Kadonaga et al. 1987). Such predictions suggest that aberration in transcription factor binding or expression may cause a disruption in *TUSC3* expression. Thus, multiple mechanisms including chromosomal aberration, DNA methylation, or dysregulation of transcription factors might contribute to decreased *TUSC3* expression.

One limitation of this study on gene expression throughout this study was the limited number of the normal cerebella available for analysis. Three normal cerebella and two normal cerebella were used for qRT-PCR and global gene analysis, respectively. In order to show the gene expression in normal cerebella is similar and to strengthen the differential gene expression between normal cerebella and MBs, additional normal cerebella is needed.

Another limitation of this study is based on the assumption that potential TSG had reduced expression. Thus, expression based approach was taken. Other approaches would be taken to identify TSG. For instance, the next generation sequencing technology, a high throughput sequencing, that allows systematic analyses of the whole tumor genome would be taken. Gene mutation is identified prior to expression or

functional analysis.

Global gene expression profiling was my second approach towards the identification of TSG on chromosome 8p. This technique enables determination of expression of a large number of genes at one time. A comparison of gene expression between MBs and normal cerebella would allow the identification of differentially expressed genes that might be involved in MB oncogenesis. The expression profiling performed on seven MBs and two normal cerebella identified six differentially expressed genes, all of which were verified by qRT-PCR. The expression profiles of the six genes were concordant between the two techniques employed, indicating that the microarray results were reliable. Within the homozygously deleted region, *EFHA2* and *DKFZp761P0423*, showed most downregulation and they were further investigated.

Expression analysis revealed that 17 of 20 (85%) MBs examined exhibited significant downregulation of *EFHA2* transcript. Of cases with reduced *EFHA2* expression, four cases (cases 16, 20, 21 and 27) exhibited 8p allelic loss, five cases showed 8p gain, and eight cases had 8p retention. Chromosomal loss might be one mechanism for *EFHA2* downregulation in cases that demonstrated both allelic loss and *EFHA2* reduced expression. Statistical significance was not found between allelic status and *EFHA2* expression. However, it was interesting that the three cases without *EFHA2* downregulation had 8p gain.

Methylation analysis by MSP showed DNA methylation occurred exclusively at exon 1 of *EFHA2* in MB. A total of eight cases showed DNA methylation at exon 1 of *EFHA2* gene. Seven of them displayed reduced *EFHA2* expression. The results indicate that epigenetic silencing is another mechanism for *EFHA2* downregulation. Two cases (#20 and #27) displayed both allelic loss and DNA methylation at exon 1. Both of these cases demonstrated a 12-fold reduced expression compared to normal cerebellum. No tumors displayed DNA methylation on the promoter of *EFHA2*.

In summary, out of the 17 cases showed downregulation *EFHA2*, two cases displayed allelic loss; five cases exhibited DNA methylation, and two cases demonstrated both allelic loss and DNA methylation. The results illustrate that a fraction of MBs exhibited *EFHA2* dysregulation, and DNA methylation and/or allelic loss might be a regulatory mechanism for *EFHA2* downregulation. However, there were eight cases showing *EFHA2* downregulation without allelic loss of 8p or DNA methylation. Thus, other mechanisms such as DNA mutation and aberration in miRNA expression might contribute to *EFHA2* downregulation. Computational algorithm predicts miR-17 and miR-20a targeted *EFHA*. These two miRNAs were upregulated in MB (Uziel et al. 2009).

Protein domain search software, InterProScan, indicates EFHA2 protein contains a calcium binding EF hand domain. S100 proteins represent the largest gene

family that contains this domain (Heizmann et al. 2002). These proteins regulate biological processes included cell growth, motility, cell cycle progression, transcription and differentiation. A list of S100 proteins was known to be overexpressed in cancer (Emberley et al. 2004). The expression of S100 proteins had clinical implications for the diagnosis and prognosis (Emberley et al. 2004). It will remain to be elucidated whether EFHA2 exhibits growth suppressive function. This would be done by either overexpression or downregulation of *EFHA2* in MB cell lines.

The investigation of *DKFZp761P0423* gene expression by qRT-PCR analysis revealed that 70% of MBs had *DKFZp761P0423* reduced expression. Using a FISH probe targeted to chromosome 8p23.1 where this gene is located, loss or retained of chromosome 8p was found to be associated with reduced expression. These data suggest genomic loss of chromosome 8p was a mechanism for dysregulation of *DKFZp761P0423* gene. There were three cases displayed reduced expression and gain of chromosome 8, it was possible that DNA mutation contributed to *DKFZp761P0423* downregulation.

DKFZp761P0423, or *full name PRAGMIN,* has been recently identified as an effector of Rho family GTPase 2 (RND2) protein (Tanaka et al. 2006). RND2 is a member of the Rho family GTPases, which functions to switch between an inactive GDP-bound state and an active GTP-bound state. RND2 is expressed specifically in

neurons of brain and spinal cord (Nishi et al. 1999). Public database Aceview indicates the presence of *DKFZp761P0423* transcript in brain tissue. Overexpression of *DKFZp761P0423* and *RND2* inhibited neurite outgrowth and induced cell rounding (Tanaka et al. 2006). Silencing *DKFZp761P0423* led to neurite elongation (Tanaka et al. 2006). Taken together, the results suggest that *DKFZp761P0423* plays a role in neuronal morphology and neurite growth. The function of *DKFZp761P0423* in MB pathogenesis remains to be elucidated.

To investigate whether other genes on 8p would be important for MB tumorigenesis, I screened the expression pattern of 49 genes on 8p in seven MB cell lines. All of these genes showed reduced expression by microarray analysis. The underlying assumption was that inactivated TSG would likely have no expression in some MB cell lines. Conventional RT-PCR analysis revealed that all cell lines displayed expression for all of 49 genes examined, suggesting that these genes might not be involved in MB.

To summarize the work on chromosome 8p, two cancer-related genes, *LZTS1* and *TUSC3*, were examined. The result indicates a fraction of MB had reduced gene expression. Global gene expression analysis had revealed that 49 genes, including *EFHA2* and *DKFZp761P0423*, on chromosome 8p were dysregulated in MB. Expression analysis indicated that *EFHA2* and *DKFZp761P0423* were downregulated

in 85% and 70% of MBs, respectively. Chromosomal loss and/ or epigenetic modification were suggested for aberrant gene expression.

A limitation of this study was the lack of functional characterization of *EFHA2* and *DKFZp761P0423* in MB tumorigenesis. In my study, I focused on miRNA expression and functional analysis because miRNA was a new area to understand tumor development. Further experiments are needed to understand the roles of *EFHA2* and *DKFZp761P0423* in MB.

6.2 Identification and functional characterization of downregulated miRNAs in MB

While reviewing the literature, I noticed that the research on miRNAs was expanding rapidly. MiRNAs have been implicated in multiple biological processes including development, proliferation, and differentiation (Chen et al. 2004; Fang et al. 2010; Lou et al. 2010; Moss et al. 1997). They are important in regulation of gene expression through complementary base pairing to their targets genes. Recent studies have implicated the involvement of miRNAs in various cancers (Calin et al. 2002; He et al. 2005).

Thus, the question of the biological significance of miRNAs in MB development came to my mind. Specifically, could any miRNA located on chromosome 8p be involved in MB development? To address this question, I looked into the miRNAs database and found three miRNAs were mapped to chromosome 8p at that time. They

were miR-124, miR-320, and miR-383. MiR-124 is located on chromosome 8p23.1, which is approximately 0.1 Mb away from the homozygously deleted region. MiR-383 and miR-320 are located on 8p22 and 8p21.3, respectively. High frequency of LOH in these genomic locations was detected in MB. The role of these miRNAs in MB oncogenesis was undefined.

To this end, I performed qRT-PCR to determine the expression levels of miR-124, miR-383 and miR-320 in MBs. The results revealed downregulation of miR-124 in 72% of MBs examined, ranging from 2- to 2600-fold reduction compared to normal cerebella. Diminished expression of miR-383 was also observed in 79% of the same cohort of MBs, ranging from 2- to 588- fold reduction compared to normal cerebella. Additionally, all seven MB cell lines displayed reduced or lost expression of miR-124 and miR-383. Expression of miR-320 was variable in MBs, with 28% showing downregulation and 21% displaying upregulation compared to normal cerebella. Taken together, the results indicated miR-124 and miR-383 were underexpressed in MBs suggesting these RNA molecules might contribute to the MB oncogenesis.

In the latter half of the study, I focused on characterizing the functional roles of miR-124 and miR-383 and on identifying the target genes of these deregulated miRNAs in relation to MB development.

MiR-124 is highly conserved in both invertebrates and vertebrates. In

vertebrates, mature miR-124 is encoded by three conserved miR-124 genes, whereas in invertebrates *C. elegans* and *D. melanogaster* a single miR-124 gene is annotated. Nevertheless, the mature miR-124 sequence is the same in both invertebrates and vertebrates.

Expression of miR-124 is abundant in the brain of several species including human, rat, mouse, monkey, zebrafish and chicken (Cao et al. 2007; Lagos-Quintana et al. 2002, Liang et al. 2007; Miska et al. 2004; Wienholds et al. 2005). Out of 40 normal tissues examined, the highest miR-124 expression was detected in brain (Liang et al. 2007). Expression of miR-124 was detectable in three other types of tissue, including thymus and testicle. MiR-124 expression was 4- to 94-fold lower in these tissues compared to normal brain (Liang et al. 2007). Expression of miR-124 was absent in many tissues, including breast, colon, esophagus, heart, liver, lung, and pancreas, prostate and skeletal muscle (Liang et al. 2007).

High expression of miR-124 was detected in multiple regions of brain (Smirnova et al. 2005; Hohjoh and Fukushima 2007). In mature cerebellum, miR-124 constituted 26% of all miRNAs (Hohjoh and Fukushima 2007). MiR-124 also accounted for up to 46% miRNAs of all brain miRNAs (Lagos-Quintana et al. 2002). Interestingly, miR-124 was first detected in differentiating neurons and persisted in mature neurons (Krichevsky et al. 2003; Deo et al. 2006). Given that miR-124 is

encoded by three individual genes and the abundance of miR-124 in brain, it is not difficult to anticipate that miR-124 has multiple important functions in brain and these miR-124 genes may be actively transcribed to maintain high miR-124 expression for maintenance of functions.

Accumulated data have indicated that miR-124 plays a role in neurogenesis. Overexpression of miR-124 in non-neuronal HeLa cells led to downregulation of a large number of non-neuronal genes (Lim et al. 2005), whereas suppression of miR-124 in terminally differentiated cortical neurons resulted in an upregulation of non-neuronal transcripts (Conaco et al. 2006). These results suggest that a function of miR-124 is to maintain neuronal identity by suppression of non-neuronal gene transcript (Lim et al. 2005). Moreover, miR-124 was expressed at low level in neural progenitor cells and its expression was dramatically increased in differentiating and mature neurons (Krichevsky et al. 2003; Deo et al. 2006). Its temporal expression profile suggested that miR-124 might contribute to the development and maturation of neuronal cells. Indeed, it was found that miR-124 expression was remarkably upregulated in P19 mouse embryonal carcinoma cells upon RA treatment to induce neuronal differentiation (Sempere et al. 2004). And, overexpression of miR-124 triggered neuronal differentiation (Visvanathan et al. 2007) and promoted neurite outgrowth (Yu et al. 2008).

To delineate the mechanism of miR-124 mediated neuronal differentiation, chromatin immunoprecipitation (ChIP) experiment was performed to confirm that RE1 silencing transcription factor (REST) directly interacted with the RE-1 sites on three miR-124 genomic loci (Conaco et al. 2006). The disappearance of REST protein also coincided with the increase expression of miR-124 and the appearance of terminal differentiation in cortical neurons (Conaco et al. 2006). RE-1 is a conserved 23-bp repressor element site that is occupied by REST. In non-neuronal cells, REST functions to suppress neuronal gene expression through its recruitment of corepressor complex containing histone deacetylases and methyl CpG-binding protein MeCP2. During neuronal differentiation from progenitors to mature neurons, REST is downregulated. REST and its co-repressors are dissociated from the RE-1 sites, leading to activate the expression of neuronal gene transcripts (Ballas et al. 2005). Thus, it was proposed that miR-124 expression is suppressed by the occupation of REST in progenitor cells. During neuronal differentiation, miR-124 is released from the inhibition of REST. The upregulation of miR-124 expression enables suppression of non-neuronal genes.

Furthermore, miR-124 had a stimulatory effect on neuronal differentiation via modulating the expression of small C-terminal domain phosphatase 1 (SCP1) in the developing spinal cord and in P19 cells. SCP1 protein has an antineural function (Yeo et

al. 2005). Suppression of SCP1 protein induced neurogenesis, whereas constitutive SCP1 expression attenuates neurogenesis. Thus, miR-124 is likely to induce neurogenesis at least by downregulation of SCP1 (Visvanathan et al. 2007).

miR-124 has been implicated in the differentiation of mature neurons from progenitor cells through the regulation of PTBP1. PTBP1 is an RNA-binding protein which preferably binds to CU-rich sequences in pre-mRNAs and inhibits alternative splicing events (Black 2003; Licatalosi and Darnell 2006). It functions as a global repressor of neuron-specific alternative splicing in non-neural cells (Corrionero and Valcarcel 2009). Thus, in non-neural cells, expression of neuronal genes is suppressed by alternative splicing. PTBP1 protein was present in neural progenitor cells of the mouse embryo. Its expression was diminished in differentiating and mature neurons (Makeyev et al. 2007). Most important, it was demonstrated that overexpression of miR-124 induced not only neuronal differentiation but also a switch from general to global nervous system-specific alternative splicing in neuroblastoma cells CAD. And, these were in part through the reduced PTBP1 expression. Furthermore, downregulation of PTBP1 expression was required for miR-124-mediated neuronal differentiation and induced alternative splicing (Makeyev et al. 2007).

Aberrant miR-124 expression had been reported in multiple tumors including, CNS tumors (Pierson et al. 2008; Silber et al. 2008). In non-CNS tumors, reduced

miR-124 expression was reported in liver tumor cell lines and cervical tumors (Furuta et al. 2010; Wilting et al. 2010). In CNS tumors, Silber and his colleagues demonstrated miR-124 expression was underexpressed in anaplastic astrocytomas and glioblastomas (Siber et al. 2008). Overexpression of miR-124 promoted neuronal–like differentiation in stem cells and induced G1 arrest in glioma cells. The study conducted by Pierson et al. showed miR-124 expression was reduced in all four MB tumors compared to normal cerebellum and restoration of its expression inhibited cell growth (Pierson et al. 2008). A separate study conducted by Ferretti et al. also observed a reduced expression of miR-124 in MB tumors (Ferretti et al. 2009). My result on miR-124 expression is in concordance with both studies. Furthermore, the larger sample size in my study compared to Pierce et al. provides further solid evidence that miR-124 contributes to MB tumorigenesis.

The dual color FISH analysis employed gene-specific BAC clone revealed that reduced miR-124 expression was not directly related to chromosomal abnormality of 8p. In my study, miR-124 downregulation was observed in 72% and loss of 8p was found in 21% of tumors. The discrepancy between the miR-124 expression and 8p loss may be explained by abnormalities in chromosomal makeup. FISH quantifies the absolute DNA copy at specific loci in single nuclei (Eastmond and Pinkel 1990). However, it does not discriminate abnormal chromosomal segregation events, including duplication of

chimerism or somatic recombination (Jiang et al. 1995; Murthy et al. 2002). Thus, it was possible to observe cases with two copies of short arm of chromosome 8 and reduced miR-124 expression. For instance, imagine that one of the normal allele of miR-124 was loss, and the other allele was inactivated through DNA DNA methylation or mutation. Expression analysis for miR-124 would indicate a downregulation of miR-124. If this remaining allele was duplicated once or more, FISH result might indicate a normal copy number for case with single duplication and a copy gain for case with multiple duplication. Thus, the limitation of FISH in discrimination of chromosomal rearrangement events might explain the discordance between miR-124 expression and chromosomal abnormality.

The previous work conducted by my research group using CGH and microsatellite markers showed 8p loss is a frequency event (66%) in MB. In my study, only 6/29 (21%) MB displayed chromosome 8p loss. The discordance in the frequency of loss between these two sets of data could be explained by the differences in detection techniques. CGH provides an overview of copy number changes in DNA level. It permits the identification of regions of loss or gain relative to the DNA content of the entire genome. In CGH, the total genomic tumor DNA and the normal reference DNA were labeled and hybridized to a normal metaphase chromosome and fluorescence ratios provide a cytogenetic representation of DNA copy number variation. However,

this technology is limited by relative loose, fuzzy of the deletion borderlines. It has a resolution with about 10-20 Mb (Kallioniemi et al. 1994), and chromosomal change such as gain or loss with about 1-2 Mb can not be detected by CGH (Alimov et al. 2000). Moreover, CGH is not sensitive to detect structural changes such as chromosomal rearrangement. On the other hand, LOH identifies allelic imbalance based on comparison of genotypes between the tumor DNA samples and patient-matched control DNA samples using polymorphic microsatellite markers. These markers are short DNA repeated sequences. Given that the repeated sequence in maternal and paternal are differed in length in 60-80% of the cases, these markers are often informative. In case the repeats are differed in maternal and paternal, two bands are visualized. In contrast, in tumors one chromosome is lost, only one allele from the chromosome will be present. The limitation of LOH is that the results need to be cautiously interpreted. The apparent LOH may cause by other events such as uniparental disomy included heterodisomy and isodisomy. Examples are TP53 and RB1 (Murthy et al. 2002). Additionally, DNA gain may appear as allelic imbalance and incorrectly designated as LOH in the absence of CGH data. LOH cannot detect any amplification involved in tumor pathogenesis. Thus, the relative low frequency as detected by FISH in my cohort of tumors might represent a result of various chromosomal rearrangement and duplication followed by genomic loss. For instance,

the presence of two copies of chromosome 8p by FISH might represent a result of a loss followed by duplication of the remaining allele. Indeed, discrepancy between LOH and FISH result had been reported (Cheng et al. 2008; Kallioniemi et al. 1992). In one study of breast cancer revealed a discrepancy between RB1 copy number detected by FISH and LOH (Kallioniemi et al. 1992). The finding was explained by somatic recombination or duplication of chromosome 13 containing mutant RB1. Thus, the precise chromosomal structure in MB tumors needed to be defined by multiple techniques.

Mature miR-124 is transcribed from three precursor hairpin miRNAs located on three separate human genomic regions. miR-124-1 is located on chromosome 8p23.1, miR-124-2 on 8q12.3 and miR-124-3 on 20q13.33. In mouse, all three mature miR-124-1/-2/-3 are expressed in developing CNS (Deo et al. 2006). There is no information on the attribution of each precursor miR-124 toward the mature miR-124 in human. Optimal qRT-PCR primer design for discrimination of three precursor of miR-124 may be the first step toward determination of expression level of miR-124 precursors.

In addition, all three precursor miR-124s are located within the dense CpG islands. Epigenetic methylation has been proposed as a regulatory mechanism for miRNA expression (Saito et al. 2006). DNA hypermethylation of miR-124 has been

reported in multiple tumor types, including colon, breast, lung and liver cancers (Furuta et al. 2010; Lujambio et al. 2007). In hepatocellular carcinoma (HCC) cell lines, treatment with demethylation agent 5-aza-dC restored the expression of miR-124 (Furata et al. 2010); however, no miR-124 reactivation was observed in glioma cell lines upon 5-aza-dC treatment (Silber et al. 2008). These data suggested that the regulatory mechanism for miR-124 expression was tissue and tumor specific. Further investigation is needed to evaluate epigenetic mechanism for regulatory miR-124 expression in MB.

This study characterized the biological functions of miR-124. Restoration of miR-124 in miR-124-deficient MB cells significantly inhibited cell growth as revealed by MTT assay and viable cell counting. Furthermore, the cell growth inhibitory effect of miR-124 was mediated through blockage in cell cycle progression. These findings are consistent with the results in Pierson et al. study, that demonstrated miR-124 expression in MB cell lines induced cell proliferation inhibition (Pierson et al. 2008). In addition, my findings were in agreement with the study conducted by Silber et al., who demonstrated that ectopic expression of miR-124 inhibited proliferation of GBM cell lines via induction of G1 arrest (Silber et al. 2008). The cell growth inhibitory effect of miR-124 is not limited in CNS tumors as overexpression of miR-124 in HCC cell lines reduced cell proliferation by enhancing the fraction of cells in G0/G1 phase (Furuta et al.

2010). The observation of alteration in cell cycle profile in miR-124 transfected cells is in agreement with the finding demonstrated that a large number of genes in categories related to cell cycle and proliferation was altered in non-miR-124-expressed HepG2 cells upon miR-124 restoration (Wang and Wang 2006). Furthermore, a cell cycle regulator, CDK6, which regulates G1 progression of cell cycle, has been demonstrated as a target gene of miR-124 (Parry et al. 1999; Pierson et al. 2008). The result is in line with my finding illustrated that miR-124 altered cell cycle progression. In conclusion, miR-124 exhibits a growth suppressive function in MB.

To explore the biological functions of miR-124, one must identify its gene targets. I had identified *SLC16A1* as a direct target of miR-124 through systemic analysis. To begin, the dataset generated by Lim et al. was collected. Computational approach was then applied to identify candidate miR-124 targets. Expression of potential miR-124 targets was examined by qRT-PCR. At mRNA level, *SLC16A1* expression was significantly inhibited as early as four hours following miR-124 restoration, by 24 hours post-transfection the level was reduced by about 6-fold in DAOY and ONS-76 cells. At protein level, SLC16A1 expression was suppressed in all five MB cell lines examined at 48 hours after miR-124 re-expression. Luciferase reporter assay further confirmed that miR-124 specifically interacted with the 3'UTR of *SLC16A1* gene. These data suggest that miR-124 is a negative regulator of *SLC16A1* in

MB. Further analysis of *SLC16A1* expression level in primary MB tumors and cell lines revealed an elevation of *SLC16A1* transcripts in 90% of primary tumors and 100% of cell lines. Moreover, depletion of *SLC16A1* by two independent gene-specific siRNAs markedly inhibited cell growth compared to negative control. The growth suppressive effect of *SLC16A1* inhibition was accompanied by an enhancement in cell death. Taken together, *SLC16A1* expression depletion induced growth inhibitory effect in MB. And, knockdown of *SLC16A1* would elicit part or all of the biological effects induced by miR-124 overexpression in MB.

SLC16A1 gene is located on chromosome 1p12. It encodes for a proton-linked membrane carrier whose function is to transport monocarboxylates such as lactate, pyruvate and ketone bodies across cell membrane (Pierre and Pellerin 2005). In normal brain, SLC16A1 is found in the endothelial cells forming the blood vessel walls and astrocyte-like cells (Chiry et al. 2006).

It was observed that tumor cells rely on aerobic glycolysis to generate energy required for metabolic process, or known as "the Warburg effect" (Vander Heiden et al. 2009). This enables cancer cells to obtain fast energy source for rapid growth and proliferation. The major byproduct generated by this pathway is lactic acid. High lactic acid concentration has been detected in many solid tumors (Skoyum et al. 1997; Walenta et al. 1997), and its accumulation lowers intracellular pH. Activation of

monocarboxylate transporter can efflux excess lactic acid and maintain intracellular pH as tumors grow and proliferate. Indeed, elevated levels of SLA16A1 have been reported in a number of tumors (Fang et al. 2006; Mathupala et al. 2004). Thus, it is postulated that depletion of *SLC16A1* prevents export of lactic acid and causes a decrease of intracellular pH to a level that is lethal to cells.

Although *SLC16A1* is identified as a target of miR-124, no inverse correlation between miR-124 and *SLC16A1* transcript levels was observed in this study. One explanation is that multiple mechanisms regulate and fine tune *SLC16A1* expression. For example, *SLC16A1* would be regulated by multiple miRNAs. Indeed, computational analysis suggests that miR-9*, -29b, -29c, -183, -320 and -377 are potential regulators of *SLC16A1*. Moreover, expression of *SLC16A1* would be regulated by other genes. One potential regulator is MYC, whose up-regulation has been shown to elevate *SLC16A1* level (Schuhmacher et al. 2001). MYC is also a known oncogene in MB (Stearns et al. 2006). The final *SLC16A1* expression in MB could also determined by DNA methylation status as CpG islands are located in the promoter and exon 1 of the gene. In contrast to DNA hypermethylation, hypomethylation of the gene would possibly lead to overexpression. Lastly, genomic abnormalities, such as chromosomal gain/loss would have impact on *SLC16A1* expression. Gain of chromosome 1, where *SLC16A1* is located, had been described in MB (Inda et al. 2005; Shlomit et al. 2000).

In my search for candidate targets of miR-124 from Lim et al's gene list, eight genes did not show significant alteration in transcript levels after miR-124 transfection in MB cells compared with HeLa. This may be explained by the different techniques used in transcript quantification (real-time PCR vs microarray). Another possibility is that target genes may be regulated by multiple miRNAs. Such miRNAs expression profiling varies across different tissue samples. Indeed, miRNA expression was expressed in a tissue specific manner (Lagos-Quintana et al. 2002; Liang et al. 2007). Thus, it is possible that miRNAs are differentially expressed between MB cell lines and cervical carcinoma HeLa cells. Nevertheless, it cannot be excluded the possibility that some of these eight targets may be preferentially regulated at the translational level.

Previous study identified *PTBP1* as a target of miR-124. In my study, overexpression of *PTBP1* transcripts was detected in 62% MB tumors. Restoration of miR-124 in miR-124 deficient MB cells upregulated *PTBP1* transcript level by about 6-fold in DAOY and 4-fold in ONS-76. These data indicate *PTBP1* is a candidate target of miR-124 in MB. However, no association was found between miR-124 level and *PTBP1* expression in my cohort of samples. Possible explanation is that *PTBP1* transcript level is regulated by multiple mechanisms. Given that a dense CpG island is located at the promoter of *PTBP1*, epigenetic mechanism may play a role in *PTBP1* gene regulation. Furthermore, *PTBP1* may be regulated by multiple miRNAs.

Computational algorithms predict miR-9, -93, -137, -194, -330, and -381 targeted to *PTBP1*. Some of these miRNAs are known to express in brain. For instance, miR-9 and miR-137 are brain-enriched miRNAs (Sempere et al. 2005). Upregulation of miR-137 and downregulation of miR-9, -194, -330 and -381 were detected in MB (Ferretti et al. 2009). Functional analysis showed an anti-proliferation property of miR-9. Restoration of miR-9 in MB cells significantly decreased cell proliferation and colony formation, and a growth proliferation effect was observed when miR-9 was abolished (Ferretti et al. 2009). Thus, the detected level of *PTBP1* expression in this study may represent the consequent effects of multiple miRNAs.

In the present study, miR-383 is significantly reduced in 79% of MBs examined. The result strongly suggests aberrant miR-383 expression is a common event in MB. This finding was in line with Ferretti et al. showing miR-383 was downregulated in MB compared to normal cerebella by microarray analysis (Ferretti et al. 2007). Most important, this is the first study to characterize the functional roles of miR-383 in MB. Restoration of miR-383 in four MB cell lines suppressed cell growth as illustrated by MTT assay and cell counting. The growth suppressive effect of miR-383 was mediated by blockage of cell cycle progression, and induction of apoptosis as indicated by an alteration in cell cycle distribution and enhancement of PARP cleavage. Taken together, these results suggest miR-383 acts as a negative regulator of cell growth in MB.

My result is in line with the very recent study which demonstrated an induction of miR-383 in NT2 cells significantly inhibited cell proliferation, blocked cell cycle progression at G1 phase and enhanced apoptosis in NT2 cells (Lian et al. 2010). NT2 is a neuronally committed human teratocarcinoma cell line (Hsu and Everett 2001).

The flow cytometry analysis indicates that the mechanisms of miR-383-mediated cell growth inhibition among four MB cells were slightly different. In miR-383-expressed ONS-76, I speculate that blockage of cell cycle progression occurred preceded to apoptosis. This is supported by the occurrence order of G1 blockage and upregulation of cleaved PARP and p21 proteins. The appearance of G1 arrest occurred concurrently with a decrease in S and G2/M phases as early as 24 hours after transfection and sustained throughout a 96-hour study period. The blockage at G1 phase was concordance with the appearance of p21 upregulation. However, the expression level of the apoptosis-associated protein, cleaved PARP, was not enhanced until 72 hours and afterward. Thus, it was reasonable to speculate that cell death occurred after a prolong blockage in cell cycle.

In D458, restoration of miR-383 significantly increased both sub-G1 and G1 fractions. Induction of sub-G1 population was confirmed by the increase cleaved PARP level and blockage of G1 progression was confirmed by the upregulation of p21 protein. The increase of sub-G1 fraction indicates the inducation of apoptosis. Beside detection

of PARP protein, terminal deoxynucleotidyl transferase-mediated dUTP nick-end labeling (TUNEL) assay that detects DNA fragmentation and annexin V staining that detects phosphatidylserine residues at the outer plasma membrane leaflet can be performed to further illustrate the apoptosis phenotype in miR-383 expressed D458. Thus, induction of apoptosis and blockage of cell cycle progression were the mechanisms for miR-383 induced cell growth inhibition in D458.

Given that miR-383 transfected DAOY showed an increase in cleaved PARP protein, I believed apoptosis might account for miR-383 induced cell growth suppression of DAOY. Unlike other cell lines, G1 arrest was not noted in DAOY after transfection of miR-383. One explanation is that the cells bypassed G1 arrest and proceeded to apoptosis. And, this speculation is supported by the absence in upregulation of p21 protein in DAOY after miR-383 transfection. To understand the underlying mechanism for abrogation in G1 checkpoint by miR-383 in DAOY, further investigation is needed. However, it is possible that expression of miR-383 in DAOY induced a subset of cell-cycle related genes that were different from other cell lines. Other explanation is that DAOY was derived from a desmoplastic MB, and D283 and D458 were derived from classic MB. These two histological types of cells are known to be different in their genetic background (Pfister et al. 2010).

Up to now, very few studies have included miR-383 gene in expression analysis,

and the functions of miR-383 in normal brain are still waiting to be unveiled. However, two independent, comprehensive miRNA expression analysis identified miR-383 as a brain-enriched miRNA. The first study conducted by Liang et al. examined the 345 mature miRNAs in 40 normal tissues by qRT-PCR. The highest miR-383 expression was found in brain; other tissue types showed detectable miR-383 expression were thymus, testicle, ovary, prostate and peripheral blood mononuclear cell (PBMC), but at levels at least 4-fold lower than that of the brain (Liang et al. 2007). The remaining tissues were devoid of detectable miR-383 (Liang et al. 2007). The other study performed by Lee et al. analyzed a total of 224 miRNAs in 22 different human tissues. In agreement with Liang et al., miR-383 was observed as one of the 34 brain-enriched miRNAs (Lee et al. 2008). Moreover, Landgraf et al. showed that cerebellum expressed the highest miR-383 level among the different regions of brain including mid-brain, hippocampus, and frontal cortex in both human and mouse (Landgraf et al. 2007). Thus, the tissue-specific manner of miR-383 expression in brain and particular in cerebellum suggests that miR-383 has unique biological roles in brain and cerebellum.

Furthermore, similarly to miR-124, bioinformatics analysis showed miR-383 is a highly conserved miRNA. It is found in multiple species including the vertebrates, human, mouse, rat, chicken and Xenopus and the invertebrates *C. elegans* and *D.*

melanogaster. According to chicken embryo gene expression database (http://geisha.arizona.edu/geisha/index.jsp), miR-383 expression first appears at stage 3, which is marked by the induction of the anterior and posterior nervous system (Storey et al. 1992) and the presence of neural markers in chicken (Darnell et al. 1999). The expression of miR-383 is persistent throughout embryonic development from stages 7 to 21 during the development of chicken embryo. The expression pattern suggests an involvement of miR-383 in embryonic development of vertebrate system.

At present, two studies have implicated the role of miR-383 in oncogenesis of the brain tumors. Gaur et al. had examined 241 mature miRNAs in multiple tumors and identified a list of potential tumor cell type-specific-miRNAs (Gaur et al. 2007). Interestingly, miR-383 was identified as one of the potential CNS-specific tumor suppressor miRNAs. Its expression was not dysregulated in other tumor types. The qRT-PCR revealed that miR-383 expression was 83.6-fold reduced in tumors as compared to the normal brain tissues (Gaur et al. 2007). The study of global miRNA expression profiling in MB as conducted by Ferretti et al. also showed downregulation of miR-383 in MB compared to normal cerebellum (Ferretti et al. 2009). These results argue for a tumor-related property of miR-383.

This study also identified *PRDX3* is a target gene of miR-383. Luciferase reporter assay confirmed the inhibition of *PRDX3* expression was via the interaction of

miR-383 to the 3'UTR of *PRDX3*. In addition, knockdown of *PRDX3* of MB cells by two separate siRNAs induced cell growth inhibition as showed by MTT assay and cell counting, and induced cell death as illustrated by increase in PARP cleavage level. These results indicate that inhibition of *PRDX3* is functionally critical for growth suppressive function in MB. Most important, this study demonstrated that miR-383 targets *PRDX3*, and the tumor suppressive effect of miR-383, at least in part, is mediated through regulation of *PRDX3*.

It is worth to note that *PRDX3* is one of the predicted targets of miR-26a, -26b, -181b, -181c and -381. In Ferretti et al. study, decreased levels of all of these miRNAs was found in MB compared to normal cerebellum although the issue of putative targets of these reduced miRNAs did not address in the study (Ferretti et al. 2009).

PRDXs, peroxiredoxins, are thiol specific antioxidant enzymes that are found in all species except Borrelia burgdorferi (Hall et al. 2009). They are highly conserved in eukaryotes and prokaryotes. These enzymes possess antioxidant activity, and are part of the defense systems to combat the toxic reactive oxygen species (ROS). ROS including superoxide anion (O^{2-}), hydrogen peroxide (H_2O_2) and nitric oxide (NO^-) are constitutively generated from redox reactions during normal cellular metabolism. Mitochondria are major intracellular source of ROS, and O^{2-} and H_2O_2 are two major ROS species produced in mitochondria. Maintenance of precise physiological level of

ROS is essential for the cell proliferation, differentiation and activation of transcription factor (Finkel 2000; Karin and Shaulian 2001). At high level, ROS can damage DNA, proteins, carbohydrates and lipids (Klaunig et al. 1998). Mitochondrial DNA is more vulnerable to oxidative damage because mitochondria are the main site for ROS production, and mitochondria DNA, unlike chromosomal DNA, is not protected by histones. Thus, maintenance of proper antioxidative defense mechanism in mitochondria is essential for cellular function.

PRDXs are the major antioxidant enzyme in brain mitochondria responsible for H_2O_2 removal (Drechsel and Patel 2010). In mammals, a total of six peroxiredoxins (PRDX1 to PRDX6) have been identified in human, rat and mouse, and they are classified into three subfamilies based on the number and position of cysteine residues involved in catalytic reaction: atypical 2-Cys, typical 2-Cys and 1-Cys (Rhee et al. 2001; Seo et al. 2000; Wood et al. 2003). Each of these PRDXs has its subcellular localization. PRDX3 belongs to the 2-Cys subfamily. Other members in this subfamily are PDRX1, 2 and 4. The gene for *PRDX3* is located on chromosomal 10q26.11. *PRDX3* encodes a protein of 257-amino acid large, with 62 residues at the N-terminus as the mitochondrial-targeting sequence size (Yamamoto et al. 1989). The mitochondrial targeting sequence allows PRDX3 to transfer from the cytosol to mitochondria upon targeting sequence is cleaved during maturation (Araki et al. 1999; Chae et al. 1999;

Oberley et al. 2001; Watabe et al. 1994). Unlike the remaining five PRDXs which are localized in multiple compartments of cell, PRDX3 is only found in mitochondria but not in cytosol, nucleus, membrane, lysosome, and peroxisome (Kang et al. 1998; Wood et al. 2003). Expression of PRDX3 is abundant in mitochondria. Its expression is approximately 30 times higher than the other antioxidant enzyme, glutathione peroxidase, in mitochondria (Cadenas 2004; Chang et al. 2004). The only other PRDX that is localized in the mitochondria is the PRDX5. However, PRDX5 belongs to atypical 2-Cys subfamily and the abundance is nearly three times less than PRDX3 (De Simoni et al. 2008).

Accumulative evidence has showed that the functions of mitochondrial PRDXs are distinctively different from cytosol PRDXs. For examples, knockdown of cytosol *PRDX1* and *PRDX2* enhanced cytotoxicity of adriamycin in prostate cancer cells, whereas this differential chemosensitivity is not observed in depleted *PRDX3* cells (Shen and Nathan 2002).

As tumor cells is highly proliferation cells, tumor cells showed an increased ROS production compared to normal cells (Szatrowski and Nathan 1991; Burdon 1995). Generation of high level H_2O_2 was reported in tumor cells (Szatrowski and Nathan 1991). An imbalance between H_2O_2 generation and ability to neutralize the oxidant species could possibly lead to oxidative stress. Indeed, high level of H_2O_2 induced cell

death in brain tumors (Kitamura et al. 1999). I speculate that the level of antioxidant enzyme needs to be increased in tumor cells in order to combat the high ROS level that is toxic to cell. Indeed, immunohistochemistry has revealed that PRDX3 is overexpressed in 79.2-89% breast cancer (Karihtala et al. 2003; Noh et al. 2001). Upregulation of PRDX3 was reported in lung cancer and hepatocellular cancer (Choi et al. 2002; Park et al. 2006). These results suggest that upregulation of PRDX3 in cancer cells may be a mechanism to ensure toxic ROS removal during proliferation.

In this study, *RBMS1* was also identified as a target of miR-383. With the exception of D341, all cell lines transfected with miR-383 demonstrated a reduction of *RBMS1* at both mRNA and protein level, suggesting that miR-383 modulated *RBMS1* level through mRNA degradation and translational repression. In addition, the decrease in *RBMS1* by miR-383 was through a direct binding via miR-383 to *RBMS1* 3'UTR as illustrated by luciferase reporter assay. Depletion of *RBMS1* by two siRNAs slightly modulated cell growth of DAOY and ONS-76. The role of miR-383-mediated *RBMS1* in MB needs further investigation.

RBMS1 has been implicated in DNA replication. It was shown to interact with the replication origin of *MYC* gene (Negishi et al. 1994). RBMS1 was released from the DNA replication origin of *MYC* gene after it complexed with DNA polymerase to start replication by stimulating the polymerase activity (Niki et al. 2000a).

RBMS1 had also been suggested to play a role in promoting transformation activity. RBMS1 protein was shown to interact with MYC directly. In cooperation with *RAS*, *RBMS1* stimulated transformation activity of *MYC* (Niki et al. 2000b). *RBMS1* or *MYC* by itself had no transformation activity as examined by focus forming assay (Niki et al. 2000b).

Apoptosis is a programmed cell death. It is a coordinated event that leads to number of changes in biochemical and morphological features. The stereotypical morphological features in cells committed to apoptosis are cell shrinkage, mitochondrial leakage, membrane blebbing and the appearance of apoptotic bodies (Elmore 2007). Biochemically, two principle pathways govern apoptosis signaling: intrinsic and extrinsic pathways. The extrinsic pathway is triggered by the binding of ligands to death receptor and led to an activation of a number of caspases. The intrinsic pathway is initiated by ROS, leading to the release of cytochrome c from the mitochondria and an activation of caspase-3. Both pathways ultimately trigger PARP cleavage and execution of cell death (Nagarajah et al. 2004).

PARP encodes the enzyme poly(ADP-ribose) polymerase. The protein is involved in DNA damage repair by binding to DNA breaks and modifying nuclear proteins. In cells undergoing apoptosis, PARP is cleaved into two fragments with sizes of 89kDa and 24kDa from a full length 116kDa polypeptide. The inactive forms of

PARP prevents DNA damage to be repaired, and leads to apoptosis. Thus, the apparent of cleaved PARP is an induction for apoptosis.

In this study, overexpression of miR-383 induced the upregulation of cleaved PARP in MB cells. This observation was also in concordant with the upregulation of PARP in silenced *PRDX3*. Activation of PARP is an indication of apoptosis. To confirm the activation of apoptosis, annexin V staining would be done. Taken together, the anti-proliferative effect of miR-383 was partly, at least, mediated by an activation of apoptosis through a PRDX3-related pathway.

6.3 miRNAs expression in RA treated P19 cells

In the last part of my study, I explored the functional roles of miR-383 in neuronal differentiation. MiR-383 expression was examined in P19 cells upon RA-induced neuronal differentiation. These cells provided an attractive system for the study of neuronal differentiation. P19 cells are derived from a teratocarcinoma formed in C3H/He mice and are pluripotent. It can be induced to differentiation into three germline layers, namely endoderm, mesoderm and ectoderm, depending on the chemical inducers, culture techniques and culture conditions (Bain et al. 1994).

Two separate subclones of P19 were examined to ensure the observation was not an artifact. The result showed that miR-383 expression was absent in two RA untreated P19 subclones. Its expression in two subclones was detected at 24 hours and 48 hours

after RA treatment, and progressively accumulated to higher levels thereafter. The result suggested that RA induced upregulation of miR-383 in P19 cells.

Wei et al. reported an increase gene transcript between 16 to 48 hours after RA treatment in P19 cells (Wei et al. 2002). It was hypothesized that the increase reflected the need for commitment to neural differentiation (We et al. 2002).

Moreover, miR-383 expression was detected prior to the apparent of neuronal marker TUBB3. This result suggests that induction of miR-383 expression is an early event of RA induced neuronal differentiation in P19 cells.

Previously, Sempere et al. demonstrated a number of miRNAs were upregulated in RA treated P19 cells (Sempere et al. 2004). These miRNAs included brain-specific miRNAs (miR-9, -124a, -124b, -135), brain-enriched miRNAs (miR-9*, -125a, -125b, -128), and brain-nonenriched miRNAs (let-7a, let-7b, miR-30a, -30b, -30c, -30e, -98, -100, 103-1, -156, -218). The expression of these miRNAs was induced four days after RA treatment (Sempere et al. 2004). This time corresponds to a second wave of transcriptional activation of protein-encoding genes that are involved in terminal differentiation (Wei et al. 2002). Unlike these miRNAs, miR-383 showed increased expression no later than two days after RA treatment in my experiment. This time corresponds to an early phase of commitment to neuronal fate in P19 cells (Sempere et al. 2004). Thus, I postulate that miR-383 has a role at the early phrase of neuronal

differentiation. Further investigation needs to be done to clarify the temporal expression pattern of miR-383 during the course of neuronal differentiation.

Approximately 40% of all miRNAs are located within the introns of protein-coding genes (Rodriguez et al. 2004). Intronic miRNAs are typically coordinately expressed and processed with the host gene transcripts (Baskerville and Bartel 2005; Kim and Kim 2007; Wang et al. 2009). One example is the coexpression of mature forms of miR-33a and miR-33b and the *SREBP* host gene mRNA in human and mouse to control cholesterol homeostasis (Najafi-Shoushtari et al. 2010). Given that miR-383 is an intronic miRNA that resides in intron 1 of host gene *SGCZ* in both human and mouse, it is possible that miR-383 is transcribed in parallel with its host gene *SGCZ*. To understand the regulatory mechanism of miR-383, the expression of miR-383 host gene, *Sgcz*, was examined during RA induced neuronal differentiation of P19 cells. The result revealed that host gene *Sgcz* and miR-383 was significantly correlated during RA-induced neuronal differentiation in P19 cells, suggesting that transcription of miR-383 was processed in parallel with the precursor of *Sgcz* mRNA. Both miR-383 and *Sgcz* might have played a regulatory role in the execution of neuronal differentiation. Further investigation is needed to explore the biological functions of miR-383 and *Sgcz* in neuronal cell maturation.

SGCZ encodes a zeta-sarcoglycan protein with a size of 299 kDa. It is a

transmembrane protein with a large extracellular domain and a small intracellular domain. The protein is an integral component of the sarcoglycan complex, which makes up a part of the dystrophin-associated glycoprotein complex (DGC). An essential function of the DGC is to mediate interaction between extracellular matrix proteins, and disruption of DGC leads to membrane instability, membrane permeability defects and myofiber damage (Wheeler et al. 2002). SGCZ expression is reduced in muscular dystrophy (Wheeler et al. 2002). The biological roles of SGCZ in neuronal differentiation are still waiting to be unveiled; however, it can not be excluded that SGCZ is involved in neuronal differentiation through its interaction with extracellular matrix proteins. This speculation is supported by several observations. First, a number of genes with functions related to the extracellular matrix was upregulated in RA-induced neuronal differentiated P19 cell (Wei et al. 2002). Second, extracellular matrix related protein was able to accelerate neuronal maturation of P19 cells (Parnas and Linial 1997), whereas interference of extracellular protein related protein inhibited neuronal differentiation (Mani et al. 2000). Thus, establishment of proper connection between extracellular matrix proteins and DGC through SGCZ might regulate neuronal differentiation.

The question of how *SGCZ* and/or miR-383 are regulated is still unknown. Recent finding has revealed a regulatory mechanism of miR-124 expression by REST in

neurogenesis (Conaco et al. 2006). Such mechanism was unlikely to exist in the case of miR-383 and/or *SGCZ* as the RE-1 binding site database (www.bioinformatics.leeds.ac.uk/RE1db_mkII/) reveals that the closest putative RE-1 binding site is located about 5 Mb upstream of *SGCZ* gene in human and mouse (Bruce et al. 2004). However, using the transcription factor search program TFSEARCH (http://www.cbrc.jp/research/db/TFSEARCH.html), putative binding sites for transcription factors including OCT-1, OCT-7, and SOX5 are predicted located with 3 kb upstream of *SGCZ* gene. These transcription factors have been shown to play a role in neuronal differentiation (Fujii and Hamada 1993; Lai et al. 2008; Lakin et al. 1995). I speculate that transcription factors-mediated *Sgcz* and miR-383 expression might be one possible regulatory mechanisms of neuronal differentiation in my two P19 subclones. Furthermore, it is interesting to note that a dense CpG island is located in exon 1 of *Sgcz*, suggesting that epigenetic modification was a possible regulatory mechanism for both *Sgcz* and miR-383 expression. In fact, DNA methylation regulated neuronal maturation and tumorigenesis (Kurian et al. 2010; Nakahara et al. 2010; Sharma et al. 2010). Taken together, the expression of miR-383 and *Sgcz* in neuronal differentiation of P19 might be regulated by multiple mechanisms. Further examination is needed to delineate regulatory mechanisms of miR-383 and *Sgcz*.

CHAPTER 7

CONCLUSION AND PROPOSED FUTURE STUDIES

In this study, I have demonstrated that two miRNAs, miR-124 and miR-383, on chromosome 8p are aberrantly expressed in MB. I have further conducted a functional analysis of these two downregulated miRNAs in the pathogenesis of MB. Reduced miR-124 expression was observed in 72% in MB. Expression of miR-383 was downregulated in 79% of MB.

The functional study of miR-124 revealed that restoration of miR-124 inhibited cell proliferation, induced G1 arrest, and enhanced cell death of MB cells. These results highlight the potential importance of miR-124 in MB tumorigenesis. Moreover, I have identified *SLC16A1* as a target gene of miR-124. Ectopic expression of miR-124 reduced *SLC16A1* expression at transcription and translation levels, suggesting miR-124-mediated *SLC16A1* gene repression. Luciferase assay confirmed that miR-124 interacted with the 3'UTR of *SLC16A1*. The role of growth suppressive role of miR-124 in MB was at least partially mediated by targeting *SLC16A1* as suggested by the observation that depletion of *SLC16A1* inhibited cell growth and induced cell death.

Functional characterization of miR-383 showed miR-383 plays a growth suppressive role in MB. Introduction of miR-383 inhibited cell growth in MB cells. The growth suppressive effect was associated with blockage in cell cycle progression

and increased in apoptosis as indicated by the cell cycle profiling and enhancement of PARP cleavage. Further, combination of comprehensive expression analysis and computational prediction programs suggested *PRDX3* as a putative target gene of miR-383. Luciferase reporter assay confirmed a direct binding between 3'UTR of *PRDX3* and miR-383. Expression analysis demonstrated miR-383 suppressed *PRDX3* at mRNA and protein levels. Depletion of *PRDX3* impaired cell growth in MB cells. The growth suppression was associated with an increase in apoptosis as indicated by enhancement of cleaved PARP protein in *PRDX3* knockdown cells. Taken together, my study suggested that the cell growth inhibitory effect of miR-383 in MB was mediated at least partly by modulation of *PRDX3* expression.

Taken together, my study on molecular and functional characterization of miR-124 and miR-383 enhances the current understanding of the roles of miRNAs in MB pathogenesis. It is generally believed cancer is a result of accumulated abnormality. And, accumulated data have demonstrated that MB exhibits abnormality at chromosomal and protein-coding gene expression level. Now, the findings of my study add an additional message that miRNA, a new class of non-protein coding RNA, is also contributed to MB tumorigenesis.

This study has an implication on novel therapeutic treatment strategies of MB. Future treatments may involve the target of these aberrant miRNAs or pathway

associated with these aberrant miRNAs.

Lastly, this study demonstrated that both miR-124 and miR-383 are implicated in neuronal differentiation of P19 cells. Expression of miR-124 and miR-383 were significant upregulated in RA-induced P19 cells. Increased miRNAs expression was apparent prior to the induction of neuronal differentiation marker. This suggests enhanced miRNA expression may be an early event of neuronal differentiation of P19 cells. A significant correlation was found between expression of miR-383 and its host gene *Sgcz* in P19 cells. The result suggested that transcription of miR-383 and *Sgcz* were processed in parallel. Nevertheless, the exact interplay among miR-124, miR-383, and neuronal differentiation requires further extensive studies.

At present, several hypotheses have attempted to explain the formation of MB. One of the hypotheses argues that MB formation is a result of aberration in GCP development. In human, after birth, the GCP received a proliferation signal from Purkinje cells. This, in turn, initiates the massive expansion of GCP. Ultimately, the GCP exits cell cycle, moves into the inner zone of EGL where it begins to differentiate terminally. Abnormality in this developmental process such as absence of proliferation discontinuity or blockage of neuronal cell differentiation may be critical of MB formation. My results suggested that miR-124 and miR-383 implicated in neuronal differentiation and involved in cell growth are concordance with this hypothesis. I

propose that the normal process of GCP maturation and differentiation requires proper expression of miR-124 and miR-383. And, abnormality in miR-124 and miR-383 expression disrupts the normal developmental process leading to excessive proliferation and inability of terminally differentiation. This ultimately promotes the formation of MB. Further investigation is required to prove this postulation.

With the existing data, I propose the following studies to further understand MB pathologenesis.

The first study should evaluate the functional role of *EFHA2* and *DKFZp761P0423* in MB tumorigenesis. Allelic loss and DNA methylation did not explain all MBs exhibited reduced expression. Elucidate the mechanism of downregulation may shed a light on MB formation.

The second study should be performed to delineate the mechanism of *PRDX3*-mediated cell growth suppression in MB. As *PRDX3* is important in the protection against oxidative stress, examination of *PRDX3* in the regulation of ROS level may enhance the understanding of the regulatory mechanism of miR-383 in mediating cell growth suppression in MB.

Further, given that miRNAs are predicted to potentially target up to one third of protein-coding genes in human (Lewis et al. 2003), miR-383 may target multiple genes with diverse functions such as cell cycle regulation, cell proliferation, initiation and

progression of MB. Identification of these important regulators may provide further insights on MB pathogenesis and development of novel strategies against MB. Other putative miR-383 targets include *CDK2, CDK6, CCND1,* and *CCND2 and OTX2.* These genes play a role in cell cycle progression or developmental process, and are critical in MB pathogenesis. Future study may focus to explore whether miR-383 targets these genes.

Furthermore, the future study would aim to gain insights of miRNAs on patient stratification, in hope of improving current treatment strategy. Patient stratification is important in MB due to deleterious effect associated with aggressive treatment. At present, patient stratification is based on clinical parameters. In my opinion, to improve treatment protocol, the future stratification may base on an integration of clinical presentation and molecular parameters included gene expression signatures, chromosomal aberration, and miRNAs expression pattern. Thus, further investigation on miRNA profiling to identify patient stratification is needed.

Lastly, the future plan should attempt to identify miRNA markers that would distinguish non-WNT/SHH tumors. As shown in Northcott et al. study, the non-SHH/WNT subtypes were more related to each other and some of the genomic features in non-WNT/SHH tumors were overlapped (Northcott et al. 2011). Thus, I think detailed analysis of miRNAs expression pattern in MB may reveal additional

markers that enable to separate non-WNT/SHH subtypes.

REFERENCES

1 Adesina AM, Nalbantoglu J, Cavenee WK. p53 gene mutation and mdm2 gene amplification are uncommon in medulloblastoma. Cancer Res 1994; 54(21): 5649-51.

2. Aldosari N, Bigner SH, Burger PC, Becker L, Kepner JL, Friedman HS, McLendon RE. MYCC and MYCN oncogene amplification in medulloblastoma. A fluorescence in situ hybridization study on paraffin sections from the Children's Oncology Group. Arch Pathol Lab Med 2002; 126(5): 540-4.

3. Aldosari N, Rasheed BK, McLendon RE, Friedman HS, Bigner DD, Bigner SH. Characterization of chromosome 17 abnormalities in medulloblastomas. Acta Neuropathol 2000; 99: 345-351.

4. Alimov A, Kost-Alimova M, Liu J, Li C, Bergerheim U, Imreh S, Klein G, Zabarovsky ER. Combined LOH/CGH analysis proves the existence of interstitial 3p deletions in renal cell carcinoma. Oncogene 2000; 19(11): 1392-9.

5. Amati B, Alevizopoulos K, Vlach J. Myc and the cell cycle. Front Biosci 1998; 15(3): d250-68.

6. Ambros V, Bartel B, Bartel DP, Burge CB, Carrington JC, Chen X, Dreyfuss G, Eddy SR, Griffiths-Jones S, Marshall M, Matzke M, Ruvkun G, Tuschl T. A uniform system for microRNA annotation. RNA 2003; 9(3): 277-9.

7. Ambros V. The functions of animal microRNAs. Nature 2004; 431(7006): 350-5.

8. Andersen PK, Veng L, Juul-Madsen HR, Vingborg RK, Bendixen C, Thomsen B. Gene expression profiling, chromosome assignment and mutational analysis of the porcine Golgi-resident UDP-N-acetylglucosamine transporter SLC35A3. Mol Membr Biol 2007; 24(5-6): 519-30.

9. Araki M, Nanri H, Ejima K, Murasato Y, Fujiwara T, Nakashima Y, Ikeda M. Antioxidant function of the mitochondrial protein SP-22 in the cardiovascular system. J Biol Chem 1999; 274(4): 2271-8.

10. Argenti B, Gallo R, Di Marcotullio L, Ferretti E, Napolitano M, Canterini S, De Smaele E, Greco A, Fiorenza MT, Maroder M, Screpanti I, Alesse E, Gulino A. Hedgehog antagonist REN(KCTD11) regulates proliferation and apoptosis of

developing granule cell progenitors. J Neurosci 2005; 25(36): 8338-46.

11. Ashiya M, Grabowski PJ. A neuron-specific splicing switch mediated by an array of pre-mRNA repressor sites: evidence of a regulatory role for the polypyrimidine tract binding protein and a brain-specific PTB counterpart. RNA 1997; 3(9): 996-1015.

12. Avet-Loiseau H, Vénuat AM, Terrier-Lacombe MJ, Lellouch-Tubiana A, Zerah M, Vassal G. Comparative genomic hybridization detects many recurrent imbalances in central nervous system primitive neuroectodermal tumours in children. Br J Cancer 1999; 79(11-12), 1843-7.

13. Baek D, Villén J, Shin C, Camargo FD, Gygi SP, Bartel DP. The impact of microRNAs on protein output. Nature 2008; 455: 64–71.

14. Bagga S, Bracht J, Hunter S, Massirer K, Holtz J, Eachus R, Pasquinelli AE. Regulation by let-7 and lin-4 miRNAs results in target mRNA degradation. Cell 2005; 122(4): 553-63.

15. Bailey CC, Gnekow A, Wellek S, Jones M, Round C, Brown J, Phillips A, Neidhardt MK. Prospective randomised trial of chemotherapy given before radiotherapy in childhood medulloblastoma. International Society of Paediatric Oncology (SIOP) and the (German) Society of Paediatric Oncology (GPO): SIOP II. Med Pediatr Oncol 1995; 25(3): 166-78.

16. Bain G, Ray WJ, Yao M, Gottlieb DI. From embryonal carcinoma cells to neurons: the P19 pathway. Bioessays 1994; 16(5): 343-8.

17. Ballas N, Grunseich C, Lu DD, Speh JC, Mandel G. REST and its corepressors mediate plasticity of neuronal gene chromatin throughout neurogenesis. Cell 2005; 121(4): 645-57.

18. Bandres E, Agirre X, Bitarte N, Ramirez N, Zarate R, Roman-Gomez J, Prosper F, Garcia-Foncillas J. Epigenetic regulation of microRNA expression in colorectal cancer. Int J Cancer 2009; 125(11): 2737-43.

19. Bartel DP. MicroRNAs: genomics, biogenesis, mechanism, and function. Cell 2004; 116(2): 281-97.

20. Baskerville S, Bartel DP. Microarray profiling of microRNAs reveals frequent

coexpression with neighboring miRNAs and host genes. RNA 2005; 11(3): 241-7.

21. Batra SK, McLendon RE, Koo JS, Castelino-Prabhu S, Fuchs HE, Krischer JP, Friedman HS, Bigner DD, Bigner SH. Prognostic implications of chromosome 17p deletions in human medulloblastomas. J Neurooncol 1995; 24(1): 39-45.

22. Bayani J, Zielenska M, Marrano P, Kwan Ng Y, Taylor MD, Jay V, Rutka JT, Squire JA. Molecular cytogenetic analysis of medulloblastomas and supratentorial primitive neuroectodermal tumors by using conventional banding, comparative genomic hybridization, and spectral karyotyping. J Neurosurg 2000; 93(3): 437-48.

23. Behrens J, von Kries JP, Kühl M, Bruhn L, Wedlich D, Grosschedl R, Birchmeier W. Functional interaction of beta-catenin with the transcription factor LEF-1. Nature 1996; 382(6592): 638-42.

24. Beitzinger M, Peters L, Zhu JY, Kremmer E, Meister G. Identification of human microRNA targets from isolated Argonaute protein complexes. RNA Biol 2007; 4: 76–84.

25. Bentwich I, Avniel A, Karov Y, Aharonov R, Gilad S, Barad O, Barzilai A, Einat P, Einav U, Meiri E, Sharon E, Spector Y, Bentwich Z. Identification of hundreds of conserved and nonconserved human microRNAs. Nat Genet 2005; 37(7): 766-70.

26. Bernstein E, Caudy AA, Hammond SM, Hannon GJ. Role for a bidentate ribonuclease in the initiation step of RNA interference. Nature 2001; 409(6818): 363-6.

27. Bhattacharyya SN, Habermacher R, Martine U, Closs EI, Filipowicz W. Relief of microRNA-mediated translational repression in human cells subjected to stress. Cell 2006; 125, 1111–1124.

28. Bigner SH, Mark J, Friedman HS, Biegel JA, Bigner DD. Structural chromosomal abnormalities in human medulloblastoma. Cancer Genet Cytogenet 1988; 30(1): 91-101.

29. Blaeker H, Rasheed BK, McLendon RE, Friedman HS, Batra SK, Fuchs HE, Bigner SH. Microsatellite analysis of childhood brain tumors. Genes Chromosomes Cancer 1996; 15(1): 54-63.

30. Black DL. Mechanisms of alternative pre-messenger RNA splicing. Annu Rev

Biochem 2003 ; 72:291-336.

31. Bloomston M, Frankel WL, Petrocca F, Volinia S, Alder H, Hagan JP, Liu CG, Bhatt D, Taccioli C, Croce CM. MicroRNA expression patterns to differentiate pancreatic adenocarcinoma from normal pancreas and chronic pancreatitis. JAMA 2007; 297(17): 1901-8.

32. Bohnsack MT, Czaplinski K, Gorlich D. Exportin 5 is a RanGTP-dependent dsRNA-binding protein that mediates nuclear export of pre-miRNAs. RNA 2004; 10(2): 185-91.

33. Bonci D, Coppola V, Musumeci M, Addario A, Giuffrida R, Memeo L, D'Urso L, Pagliuca A, Biffoni M, Labbaye C, Bartucci M, Muto G, Peschle C, De Maria R. The miR-15a-miR-16-1 cluster controls prostate cancer by targeting multiple oncogenic activities. Nat Med 2008; 14(11): 1271-7.

34. Boras-Granic K, Wysolmerski JJ. Wnt signaling in breast organogenesis. Organogenesis 2008; 4(2): 116-22.

35. Borchert GM, Lanier W, Davidson BL. RNA polymerase III transcribes human microRNAs. Nat Struct Mol Biol 2006; 13(12): 1097-101.

36. Bottoni A, Piccin D, Tagliati F, Luchin A, Zatelli MC, degli Uberti EC. miR-15a and miR-16-1 down-regulation in pituitary adenomas. J Cell Physiol 2005; 204(1): 280-5.

37. Brennecke J, Hipfner DR, Stark A, Russell RB, Cohen SM. bantam encodes a developmentally regulated microRNA that controls cell proliferation and regulates the proapoptotic gene hid in Drosophila. Cell 2003; 113(1): 25-36.

38. Brennecke J, Stark A, Russell RB, Cohen SM. Principles of microRNA-target recognition. PLoS Biol 2005; 3(3): e85.

39. Brown HG, Kepner JL, Perlman EJ, Friedman HS, Strother DR, Duffner PK, Kun LE, Goldthwaite PT, Burger PC. "Large cell/anaplastic" medulloblastomas: a Pediatric Oncology Group Study. J Neuropathol Exp Neurol 2000; 59(10): 857-65.

40. Brown HG, Kepner JL, Perlman EJ, Friedman HS, Strother DR, Duffner PK, Kun LE, Goldthwaite PT, Burger PC. "Large cell/anaplastic" medulloblastomas: a Pediatric Oncology Group Study. J Neuropathol Exp Neurol 2000; 59(10): 857-65.

41. Bruce AW, Donaldson IJ, Wood IC, Yerbury SA, Sadowski MI, Chapman M, Göttgens B, Buckley NJ. Genome-wide analysis of repressor element 1 silencing transcription factor/neuron-restrictive silencing factor (REST/NRSF) target genes. Proc Natl Acad Sci U S A 2004; 101(28): 10458-63.

42. Bunt J, de Haas TG, Hasselt NE, Zwijnenburg DA, Koster J, Versteeg R, Kool M. Regulation of cell cycle genes and induction of senescence by overexpression of OTX2 in medulloblastoma cell lines. Mol Cancer Res 2010; 8(10): 1344-57.

43. Burdon RH. Superoxide and hydrogen-peroxide in relation to mammalian-cell proliferation. Free Radic. Biol. Med 1995; 18: 775–794.

44. Byrne JA, Maleki S, Hardy JR, Gloss BS, Murali R, Scurry JP, Fanayan S, Emmanuel C, Hacker NF, Sutherland RL, Defazio A, O'Brien PM. MAL2 and tumor protein D52 (TPD52) are frequently overexpressed in ovarian carcinoma, but differentially associated with histological subtype and patient outcome. BMC Cancer 2010; 10: 497.

45. Cadenas E. Mitochondrial free radical production and cell signaling. Mol Aspects Med 2004; 25(1-2): 17-26.

46. Cai X, Hagedorn CH, Cullen BR. Human microRNAs are processed from capped, polyadenylated transcripts that can also function as mRNAs. RNA 2004; 10(12): 1957-66.

47. Cai MY, Zhang B, He WP, Yang GF, Rao HL, Rao ZY, Wu QL, Guan XY, Kung HF, Zeng YX, Xie D. Decreased expression of PinX1 protein is correlated with tumor development and is a new independent poor prognostic factor in ovarian carcinoma. Cancer Sci 2010; 101(6): 1543-9.

48. Calabrese C, Poppleton H, Kocak M, Hogg TL, Fuller C, Hamner B, Oh EY, Gaber MW, Finklestein D, Allen M, Frank A, Bayazitov IT, Zakharenko SS, Gajjar A, Davidoff A, Gilbertson RJ. A perivascular niche for brain tumor stem cells. Cancer Cell 2007; 11(1): 69-82.

49. Calin GA, Dumitru CD, Shimizu M, Bichi R, Zupo S, Noch E, Aldler H, Rattan S, Keating M, Rai K, Rassenti L, Kipps T, Negrini M, Bullrich F, Croce CM. Frequent deletions and down-regulation of micro- RNA genes miR15 and miR16 at 13q14 in chronic lymphocytic leukemia. Proc Natl Acad Sci U S A 2002; 99(24): 15524-9.

50. Calin GA, Sevignani C, Dumitru CD, Hyslop T, Noch E, Yendamuri S, Shimizu M, Rattan S, Bullrich F, Negrini M, Croce CM. Human microRNA genes are frequently located at fragile sites and genomic regions involved in cancers. Proc Natl Acad Sci USA 2004; 101: 2999–3004.

51. Calin GA, Ferracin M, Cimmino A, Di Leva G, Shimizu M, Wojcik SE, Iorio MV, Visone R, Sever NI, Fabbri M, Iuliano R, Palumbo T, Pichiorri F, Roldo C, Garzon R, Sevignani C, Rassenti L, Alder H, Volinia S, Liu CG, Kipps TJ, Negrini M, Croce CM. A MicroRNA signature associated with prognosis and progression in chronic lymphocytic leukemia. N Engl J Med 2005; 353(17): 1793-801.

52. Canettieri G, Di Marcotullio L, Greco A, Coni S, Antonucci L, Infante P, Pietrosanti L, De Smaele E, Ferretti E, Miele E, Pelloni M, De Simone G, Pedone EM, Gallinari P, Giorgi A, Steinkühler C, Vitagliano L, Pedone C, Schinin ME, Screpanti I, Gulino A. Histone deacetylase and Cullin3-REN(KCTD11) ubiquitin ligase interplay regulates Hedgehog signalling through Gli acetylation. Nat Cell Biol 2010; 12(2): 132-42.

53. Cao X, Pfaff SL, Gage FH. A functional study of miR-124 in the developing neural tube. Genes Dev 2007; 21(5): 531-6.

54. Card DA, Hebbar PB, Li L, Trotter KW, Komatsu Y, Mishina Y, Archer TK.Oct4/Sox2-regulated miR-302 targets cyclin D1 in human embryonic stem cells. Mol Cell Biol 2008; 28(20): 6426-38.

55. Carpenter D, Stone DM, Brush J, Ryan A, Armanini M, Frantz G, Rosenthal A, de Sauvage FJ. Characterization of two patched receptors for the vertebrate hedgehog protein family. Proc Natl Acad Sci U S A 1998; 95(23): 13630-4.

56. Castellino RC, Barwick BG, Schniederjan M, Buss MC, Becher O, Hambardzumyan D, Macdonald TJ, Brat DJ, Durden DL. Heterozygosity for Pten promotes tumorigenesis in a mouse model of medulloblastoma. PLoS One 2010; 5(5): e10849.

57. Castro CP, Piscopo D, Nakagawa T, Derynck R. Cornichon regulates transport and secretion of TGFalpha-related proteins in metazoan cells. J Cell Sci 2007; 120(Pt 14): 2454-66.

58. Cattoretti G, Becker MH, Key G, Duchrow M, Schlüter C, Galle J, Gerdes J. Monoclonal antibodies against recombinant parts of the Ki-67 antigen (MIB 1 and MIB 3) detect proliferating cells in microwave-processed formalin-fixed paraffin sections. J

Pathol 1992; 168(4): 357-63.

59. Chae HZ, Kim HJ, Kang SW, Rhee SG. Characterization of three isoforms of mammalian peroxiredoxin that reduce peroxides in the presence of thioredoxin. Diabetes Res Clin Pract 1999; 45(2-3): 101-12.

60. Chan JA, Krichevsky AM, Kosik KS. MicroRNA-21 is an antiapoptotic factor in human glioblastoma cells. Cancer Res 2005; 65(14): 6029-33.

61. Chang Q, Pang JC, Li J, Hu L, Kong X, Ng HK. Molecular analysis of PinX1 in medulloblastomas. Int J Cancer 2004; 109(2): 309-14.

62. Chang TS, Cho CS, Park S, Yu S, Kang SW, Rhee SG. Peroxiredoxin III, a mitochondrion-specific peroxidase, regulates apoptotic signaling by mitochondria. J Biol Chem 2004; 279(40): 41975-84.

63. Chang Q, Pang JC, Li KK, Poon WS, Zhou L, Ng HK. Promoter hypermethylation profile of RASSF1A, FHIT, and sFRP1 in intracranial primitive neuroectodermal tumors. Hum Pathol 2005; 36: 1265-72.

64. Chang TC, Yu D, Lee YS, Wentzel EA, Arking DE, West KM, Dang CV, Thomas-Tikhonenko A, Mendell JT. Widespread microRNA repression by Myc contributes to tumorigenesis. Nat Genet 2008; 40(1): 43-50.

65. Chen CZ, Li L, Lodish HF, Bartel DP. MicroRNAs modulate hematopoietic lineage differentiation. Science 2004; 303(5654): 83-6.

66. Chen JF, Mandel EM, Thomson JM, Wu Q, Callis TE, Hammond SM, Conlon FL, Wang DZ. The role of microRNA-1 and microRNA-133 in skeletal muscle proliferation and differentiation. Nat. Genet. 2006; 38: 228–233.

67. Chen HC, Chen GH, Chen YH, Liao WL, Liu CY, Chang KP, Chang YS, Chen SJ. MicroRNA deregulation and pathway alterations in nasopharyngeal carcinoma. Br J Cancer 2009; 100(6): 1002-11.

68. Chen Y, Liu W, Chao T, Zhang Y, Yan X, Gong Y, Qiang B, Yuan J, Sun M, Peng X. MicroRNA-21 down-regulates the expression of tumor suppressor PDCD4 in human glioblastoma cell T98G. Cancer Lett 2008; 272(2): 197-205.

69. Chen ZL, Zhao XH, Wang JW, Li BZ, Wang Z, Sun J, Tan FW, Ding DP, Xu XH, Zhou F, Tan XG, Hang J, Shi SS, Feng XL, He J. microRNA-92a promotes lymph node metastasis of human esophageal squamous cell carcinoma via E-cadherin. J Biol Chem 2010 (online).

70. Chendrimada TP, Gregory RI, Kumaraswamy E, Norman J, Cooch N, Nishikura K, Shiekhattar R. TRBP recruits the Dicer complex to Ago2 for microRNA processing and gene silencing. Nature 2005; 436(7051): 740-4.

71. Chendrimada TP, Finn KJ, Ji X, Baillat D, Gregory RI, Liebhaber SA, Pasquinelli AE, Shiekhattar R. MicroRNA silencing through RISC recruitment of eIF6. Nature 2007; 447(7146): 823-8.

72. Chenevix-Trench G, Wicking C, Berkman J, Sharpe H, Hockey A, Haan E, Oley C, Ravine D, Turner A, Goldgar D, Searle J, and Wainwright B. Further localization of the gene for nevoid basal cell carcinoma syndrome (NBCCS) in 15 Australasian families: linkage and loss of heterozygosity. Am J Hum Genet 1993; 53(3): 760-7.

73. Cheng LC, Pastrana E, Tavazoie M, Doetsch F. miR-124 regulates adult neurogenesis in the subventricular zone stem cell niche. Nat Neurosci 2009; 12(4): 399-408.

74. Cheng L, MacLennan GT, Zhang S, Wang M, Zhou M, Tan PH, Foster S, Lopez-Beltran A, Montironi R. Evidence for polyclonal origin of multifocal clear cell renal cell carcinoma. Clin Cancer Res 2008; 14(24): 8087-93.

75. Childs G, Fazzari M, Kung G, Kawachi N, Brandwein-Gensler M, McLemore M, Chen Q, Burk RD, Smith RV, Prystowsky MB, Belbin TJ, Schlecht NF. Low-level expression of microRNAs let-7d and miR-205 are prognostic markers of head and neck squamous cell carcinoma. Am J Pathol 2009; 174(3): 736-45.

76. Chiry O, Pellerin L, Monnet-Tschudi F, Fishbein WN, Merezhinskaya N, Magistretti PJ, Clarke S. Expression of the monocarboxylate transporter MCT1 in the adult human brain cortex. Brain Res 2006; 1070: 65-70.

77. Cho YJ, Tsherniak A, Tamayo P, Santagata S, Ligon A, Greulich H, Berhoukim R, Amani V, Goumnerova L, Eberhart CG, Lau CC, Olson JM, Gilbertson RJ, Gajjar A, Delattre O, Kool M, Ligon K, Meyerson M, Mesirov JP, Pomeroy SL. Integrative Genomic Analysis of Medulloblastoma Identifies a Molecular Subgroup That Drives

Poor Clinical Outcome. J Clin Oncol 2011; 29(11): 1424-30.

78. Choi JH, Kim TN, Kim S, Baek SH, Kim JH, Lee SR, Kim JR. Overexpression of mitochondrial thioredoxin reductase and peroxiredoxin III in hepatocellular carcinomas. Anticancer Res 2002; 22(6A): 3331-5.

79. Chomczynski P, Sacchi N. Single-step method of RNA isolation by acid guanidinium thiocyanate-phenol-chloroform extraction. Anal Biochem 1987; 162(1): 156-9.

80. Chua PJ, Lee EH, Yu Y, Yip GW, Tan PH, Bay BH. Silencing the Peroxiredoxin III gene inhibits cell proliferation in breast cancer. Int J Oncol 2010; 36(2): 359-64.

81. Ciafrè SA, Galardi S, Mangiola A, Ferracin M, Liu CG, Sabatino G, Negrini M, Maira G, Croce CM, Farace MG. Extensive modulation of a set of microRNAs in primary glioblastoma. Biochem Biophys Res Commun 2005; 334(4): 1351-8.

82. Clarke MF, Dick JE, Dirks PB, Eaves CJ, Jamieson CH, Jones DL, Visvader J, Weissman IL, Wahl GM. Cancer stem cells--perspectives on current status and future directions: AACR Workshop on cancer stem cells. Cancer Res 2006; 66(19): 9339-44.

83. Clifford SC, Lusher ME, Lindsey JC, Langdon JA, Gilbertson RJ, Straughton D, Ellison DW. Wnt/Wingless pathway activation and chromosome 6 loss characterize a distinct molecular sub-group of medulloblastomas associated with a favorable prognosis. Cell Cycle 2006; 5(22): 2666-70.

84. Clifford SC, O'Toole K, Ellison DW. Chromosome 1q gain is not associated with a poor outcome in childhood medulloblastoma: requirements for the validation of potential prognostic biomarkers. Cell Cycle 2009; 8(5): 787.

85. Coco S, Valdora F, Bonassi S, Scaruffi P, Stigliani S, Oberthuer A, Berthold F, Andolfo I, Servidei T, Riccardi R, Basso E, Iolascon A, Tonini GP. Chromosome 9q and 16q loss identified by genome-wide pooled-analysis are associated with tumor aggressiveness in patients with classic medulloblastoma. OMICS 2011; 15(5), 273-80.

86. Conaco C, Otto S, Han JJ, Mandel G. Reciprocal actions of REST and a microRNA promote neuronal identity. Proc Natl Acad Sci U S A 2006; 103(7): 2422-7.

87. Corcoran DL, Pandit KV, Gordon B, Bhattacharjee A, Kaminski N, Benos PV.

Features of mammalian microRNA promoters emerge from polymerase II chromatin immunoprecipitation data. PLoS One 2009; 4(4): e5279.

88. Corney DC, Hwang CI, Matoso A, Vogt M, Flesken-Nikitin A, Godwin AK, Kamat AA, Sood AK, Ellenson LH, Hermeking H, Nikitin AY. Frequent downregulation of miR-34 family in human ovarian cancers. Clin Cancer Res 2010; 16(4): 1119-28.

89. Correa TC, Brohem CA, Winnischofer SM, da Silva Cardeal LB, Sasahara RM, Taboga SR, Sogayar MC, Maria-Engler SS. Downregulation of the RECK-tumor and metastasis suppressor gene in glioma invasiveness. J Cell Biochem 2006; 99(1): 156-67.

90. Corrionero A, Valcárcel J. RNA processing: Redrawing the map of charted territory. Mol Cell 2005; 36(6): 918-9.

91. Cowan R, Hoban P, Kelsey A, Birch JM, Gattamaneni R, Evans DG. The gene for the naevoid basal cell carcinoma syndrome acts as a tumour-suppressor gene in medulloblastoma. Br J Cancer 1997; 76(2): 141-5.

92. Crawford JR, MacDonald TJ, Packer RJ. Medulloblastoma in childhood: new biological advances. Lancet Neurol 2007; 6: 1073–1085.

93. Cullen BR. Transcription and processing of human microRNA precursors. Mol Cell. 2004; 16(6): 861-5.

94. Curran EK, Sainani KL, Le GM, Propp JM, Fisher PG. Gender affects survival for medulloblastoma only in older children and adults: a study from the Surveillance Epidemiology and End Results Registry. Pediatr Blood Cancer 2009; 52(1): 60-4.

95. Darnell DK, Stark MR, Schoenwolf GC. Timing and cell interactions underlying neural induction in the chick embryo. Development 1999; 126(11): 2505-14.

96. Das P, Puri T, Suri V, Sharma MC, Sharma BS, Sarkar C. Medulloblastomas: a correlative study of MIB-1 proliferation index along with expression of c-Myc, ERBB2, and anti-apoptotic proteins along with histological typing and clinical outcome. Childs Nerv Syst 2009; 25(7): 825-35.

97. De Bont JM, Packer RJ, Michiels EM, den Boer ML, Pieters R. Biological background of pediatric medulloblastoma and ependymoma: a review from a translational research perspective. Neuro Oncol 2008; 10(6): 1040-60.

98. De Bortoli M, Castellino RC, Lu XY, Deyo J, Sturla LM, Adesina AM, Perlaky L, Pomeroy SL, Lau CC, Man TK, Rao PH, Kim JY. Medulloblastoma outcome is adversely associated with overexpression of EEF1D, RPL30, and RPS20 on the long arm of chromosome 8. BMC Cancer 2006; 6: 223.

99. De Haas T, Hasselt N, Troost D, Caron H, Popovic M, Zadravec-Zaletel L, Grajkowska W, Gottardo NG, Gajjar A. Current therapy for medulloblastoma. Curr Treat Options Neurol 2006; 8: 319–334.

100. De Simoni S, Goemaere J, Knoops B. Silencing of peroxiredoxin 3 and peroxiredoxin 5 reveals the role of mitochondrial peroxiredoxins in the protection of human neuroblastoma SH-SY5Y cells toward MPP+. Neurosci Lett 2008; 433(3): 219-24.

101. DeChiara C, Borghese A, Fiorillo A, Genesio R, Conti A, D'Amore R, Pettinato G, Varone A, Maggi G. Cytogenetic evaluation of isochromosome 17q in posterior fossa tumors of children and correlation with clinical outcome in medulloblastoma. Detection of a novel chromosomal abnormality. Childs Nerv Syst 2002; 18(8): 380-4.

102. Decker CJ, Parker R. Mechanisms of mRNA degradation in eukaryotes. Trends Biochem Sci 1994; 19(8): 336-40.

103. Denli AM, Tops BB, Plasterk RH, Ketting RF, Hannon GJ. Processing of primary microRNAs by the Microprocessor complex. Nature 2004; 432(7014): 231-5.

104. Deo M, Yu JY, Chung KH, Tippens M, Turner DL. Detection of mammalian microRNA expression by in situ hybridization with RNA oligonucleotides. Dev Dyn 2006; 235(9): 2538-48.

105. Di C, Liao S, Adamson DC, Parrett TJ, Broderick DK, Shi Q, Lengauer C, Cummins JM, Velculescu VE, Fults DW, McLendon RE, Bigner DD, Yan H. Identification of OTX2 as a medulloblastoma oncogene whose product can be targeted by all-trans retinoic acid. Cancer Res 2005; 65(3): 919-24.

106. Di Marcotullio L, Ferretti E, De Smaele E, Argenti B, Mincione C, Zazzeroni F, Gallo R, Masuelli L, Napolitano M, Maroder M, Modesti A, Giangaspero F, Screpanti I, Alesse E, Gulino A. REN(KCTD11) is a suppressor of Hedgehog signaling and is deleted in human medulloblastoma. Proc Natl Acad Sci U S A 2004; 101(29): 10833-8.

107. Diederichs S, Haber DA. Dual role for argonautes in microRNA processing and posttranscriptional regulation of microRNA expression. Cell 2007; 131(6): 1097-108.

108. Doench JG, Sharp PA. Specificity of microRNA target selection in translational repression. Genes Dev 2004; 18(5): 504-11.

109. Dong Z, Pang JS, Ng MH, Poon WS, Zhou L, Ng HK. Identification of two contiguous minimally deleted regions on chromosome 1p36.31-p36.32 in oligodendroglial tumours. Br J Cancer 2004; 91(6): 1105-11.

110. Drechsel DA, Patel M. Respiration-dependent H2O2 removal in brain mitochondria via the thioredoxin/peroxiredoxin system. J Biol Chem 2010; 285(36): 27850-8.

111. Easow, G., Teleman, A.A. and Cohen, S.M. Isolation of microRNA targets by miRNP immunopurification. RNA 2007; 13: 1198–1204.

112. Eastmond DA, Pinkel D. Detection of aneuploidy and aneuploidy-inducing agents in human lymphocytes using fluorescence in situ hybridization with chromosome-specific DNA probes. Mutat Res 1990; 234(5): 303-18.

113. Eberhart CG, Tihan T, Burger PC. Nuclear localization and mutation of beta-catenin in medulloblastomas. J Neuropathol Exp Neurol 2000; 59(4): 333-7.

114. Eberhart CG, Kratz JE, Schuster A, Goldthwaite P, Cohen KJ, Perlman EJ, Burger PC. Comparative genomic hybridization detects an increased number of chromosomal alterations in large cell/anaplastic medulloblastomas. Brain Pathol 2002; 12(1): 36-44.

115. Eberhart CG, Burger PC. Anaplasia and grading in medulloblastomas. Brain Pathol 2003; 13(3): 376-85.

116. Eberhart CG, Kratz J, Wang Y, Summers K, Stearns D, Cohen K, Dang CV, Burger PC. Histopathological and molecular prognostic markers in medulloblastoma: c-myc, N-myc, TrkC, and anaplasia. J Neuropathol Exp Neurol 2004; 63(5): 441-9.

117. Eberhart CG. Molecular diagnostics in embryonal brain tumors. Brain Pathol 2011; 21(1): 96-104.

118. Edwards D. Non-linear normalization and background correction in one-channel

cDNA microarray studies. Bioinformatics 2003; 19(7): 825-33.

119. Ehebauer M, Hayward P, Martinez-Arias A. Notch signaling pathway. Sci STKE 2006; 2006(364): cm7.

120. Eilers M, Eisenman RN. Myc's broad reach. Genes Dev 2008; 22(20): 2755-66.

121. Ellison D. Classifying the medulloblastoma: insights from morphology and molecular genetics. Neuropathol Appl Neurobiol 2002; 28(4): 257-82.

122. Ellison D, Clifford SC, Gajjar A, Gilbertson RJ. What's new in neuro-oncology? Recent advances in medulloblastoma. Eur J Paediatr Neurol 2003; 7(2): 53-66.

123. Ellison DW, Onilude OE, Lindsey JC, Lusher ME, Weston CL, Taylor RE, Pearson AD, Clifford SC; United Kingdom Children's Cancer Study Group Brain Tumour Committee. beta-Catenin status predicts a favorable outcome in childhood medulloblastoma: the United Kingdom Children's Cancer Study Group Brain Tumour Committee. J Clin Oncol 2005; 23(31): 7951-7.

124. Ellison DW, Kocak M, Dalton J, Megahed H, Lusher ME, Ryan SL, Zhao W, Nicholson SL, Taylor RE, Bailey S, Clifford SC. Definition of Disease-Risk Stratification Groups in Childhood Medulloblastoma Using Combined Clinical, Pathologic, and Molecular Variables. J Clin Oncol 2010 (online).

125. Elmore S. Apoptosis: a review of programmed cell death. Toxicol Pathol 2007; 35(4): 495-516.

126. Emberley ED, Murphy LC, Watson PH. S100 proteins and their influence on pro-survival pathways in cancer. Biochem Cell Biol 2004; 82(4): 508-15.

127. Enright AJ, John B, Gaul U, Tuschl T, Sander C, Marks DS. MicroRNA targets in Drosophila.Genome Biol 2003; 5(1): R1.

128. Epstein DJ, Marti E, Scott MP, McMahon AP. Antagonizing cAMP-dependent protein kinase A in the dorsal CNS activates a conserved Sonic hedgehog signaling pathway. Development 1996; 122(9): 2885-94.

129. Ernst A, Campos B, Meier J, Devens F, Liesenberg F, Wolter M, Reifenberger G, Herold-Mende C, Lichter P, Radlwimmer B. De-repression of CTGF via the miR-17-92

cluster upon differentiation of human glioblastoma spheroid cultures. Oncogene 2010; 29(23): 3411-22.

130. Ertan Y, Sezak M, Demirağ B, Kantar M, Cetingül N, Turhan T, Erşahin Y, Mutluer S, Anacak Y, Akalin T. Medulloblastoma: clinicopathologic evaluation of 42 pediatric cases. Childs Nerv Syst 2009; 25(3): 353-6.

131. Evans AE, Jenkin RD, Sposto R, Ortega JA, Wilson CB, Wara W, Ertel IJ, Kramer S, Chang CH, Leikin SL, Hammond GD. The treatment of medulloblastoma. Results of a prospective randomized trial of radiation therapy with and without CCNU, vincristine, and prednisone. J Neurosurg. 1990; 72(4): 572-82.

132. Evans DG, Farndon PA, Burnell LD, Gattamaneni HR, Birch JM. The incidence of Gorlin syndrome in 173 consecutive cases of medulloblastoma. Br J Cancer 1991; 64(5): 959-61.

133. Fan X, Paetau A, Aalto Y, Valimaki M, Sane T, Poranen A, Castresana JS, Knuutila S. Gain of chromosome 3 and loss of 13q are frequent alterations in pituitary adenomas. Cancer Genet Cytogenet 2001; 128: 97-103.

134. Fan X, Mikolaenko I, Elhassan I, Ni X, Wang Y, Ball D, Brat DJ, Perry A, Eberhart CG. Notch1 and notch2 have opposite effects on embryonal brain tumor growth. Cancer Res 2004; 64(21): 7787-93.

135. Fan X, Matsui W, Khaki L, Stearns D, Chun J, Li YM, Eberhart CG. Notch pathway inhibition depletes stem-like cells and blocks engraftment in embryonal brain tumors. Cancer Res 2006; 66(15): 7445-52.

136. Fang J, Quinones QJ, Holman TL, Morowitz MJ, Wang Q, Zhao H, Sivo F, Maris JM, Wahl ML. The H+-linked moncarboxylate transporter (MCT1/SLC16A1): a potential therapeutic target for high-risk neuroblastoma. Mol Pharmol 2006; 70: 2108-15.

137. Fang L, Deng Z, Shatseva T, Yang J, Peng C, Du WW, Yee AJ, Ang LC, He C, Shan SW, Yang BB. MicroRNA miR-93 promotes tumor growth and angiogenesis by targeting integrin-β8. Oncogene 2010; 30(7): 806-21.

138. Farndon PA, Del Mastro RG, Evans DG, Kilpatrick MW. Location of gene for Gorlin syndrome. Lancet 1992; 339(8793): 581-2.

139. Farwell JR, Flannery JT. Adult occurrence of medulloblastoma. Acta Neurochir (Wien) 1987; 86(1-2): 1-5.

140. Fattet S, Haberler C, Legoix P, Varlet P, Lellouch-Tubiana A, Lair S, Manie E, Raquin MA, Bours D, Carpentier S, Barillot E, Grill J, Doz F, Puget S, Janoueix-Lerosey I, Delattre O. Beta-catenin status in paediatric medulloblastomas: correlation of immunohistochemical expression with mutational status, genetic profiles, and clinical characteristics. J Pathol 2009; 218(1): 86-94.

141. Ferretti E, De Smaele E, Miele E, Laneve P, Po A, Pelloni M, Paganelli A, Di Marcotullio L, Caffarelli E, Screpanti I, Bozzoni I, Gulino A. Concerted microRNA control of hedgehog signalling in cerebellar neuronal progenitor and tumour cells. EMBO J 2008; 27: 2616–2627.

142. Finkel T. Redox-dependent signal transduction. FEBS Lett 2000; 476(1-2): 52-4.

143. Foley KP, Eisenman RN. Two MAD tails: what the recent knockouts of Mad1 and Mxi1 tell us about the MYC/MAX/MAD network. Biochim Biophys Acta 1999; 1423(3): M37-47.

144. Fujii H, Hamada H. A CNS-specific POU transcription factor, Brn-2, is required for establishing mammalian neural cell lineages. Neuron 1993; 11(6): 1197-206.

145. Fujisawa H, Misaki K, Takabatake Y, Hasegawa M, Yamashita J. Cyclin D1 is overexpressed in atypical teratoid/rhabdoid tumor with hSNF5/INI1 gene inactivation. J Neurooncol 2005; 73(2): 117-24.

146. Furuta M, Kozaki KI, Tanaka S, Arii S, Imoto I, Inazawa J. miR-124 and miR-203 are epigenetically silenced tumor-suppressive microRNAs in hepatocellular carcinoma. Carcinogenesis 2010; 31(5): 766-76.

147. Gailani MR, Bale SJ, Leffell DJ, DiGiovanna JJ, Peck GL, Poliak S, Drum MA, Pastakia B, McBride OW, Kase R, Greene M, Mulvihill JJ, Balea AE. Developmental defects in Gorlin syndrome related to a putative tumor suppressor gene on chromosome 9. Cell 1992; 69(1): 111-7.

148. Gajjar A, Chintagumpala M, Ashley D, Kellie S, Kun LE, Merchant TE, Woo S, Wheeler G, Ahern V, Krasin MJ, Fouladi M, Broniscer A, Krance R, Hale GA, Stewart CF, Dauser R, Giangaspero F, Rigobello L, Badiali M, Loda M, Andreini L, Basso G,

149. Zorzi F, Montaldi A.Large-cell medulloblastomas. A distinct variant with highly aggressive behavior. Am J Surg Pathol 1992; 16(7): 687-93.

150. Gajjar A, Hernan R, Kocak M, Fuller C, Lee Y, McKinnon PJ, Wallace D, Lau C, Chintagumpala M, Ashley DM, Kellie SJ, Kun L, Gilbertson RJ. Clinical, histopathologic, and molecular markers of prognosis: toward a new disease risk stratification system for medulloblastoma. J Clin Oncol 2004; 22(6): 984-93.

151. Gajjar A, Chintagumpala M, Ashley D, Kellie S, Kun LE, Merchant TE, Woo S, Wheeler G, Ahern V, Krasin MJ, Fouladi M, Broniscer A, Krance R, Hale GA, Stewart CF, Dauser R, Sanford RA, Fuller C, Lau C, Boyett JM, Wallace D, Gilbertson RJ. Risk-adapted craniospinal radiotherapy followed by high-dose chemotherapy and stem-cell rescue in children with newly diagnosed medulloblastoma (St Jude Medulloblastoma-96): long-term results from a prospective, multicentre trial. Lancet Oncol 2006; 7(10): 813-20.

152. Gajjar A, Pizer B. Role of high-dose chemotherapy for recurrent medulloblastoma and other CNS primitive neuroectodermal tumors. Pediatr Blood Cancer 2010; 54(4): 649-51.

153. Gal H, Pandi G, Kanner AA, Ram Z, Lithwick-Yanai G, Amariglio N, Rechavi G, Givol D. MIR-451 and Imatinib mesylate inhibit tumor growth of Glioblastoma stem cells. Biochem Biophys Res Commun. 2008; 376(1): 86-90.

154. Galli R, Binda E, Orfanelli U, Cipelletti B, Gritti A, De Vitis S, Fiocco R, Foroni C, Dimeco F, Vescovi A. Isolation and characterization of tumorigenic, stem-like neural precursors from human glioblastoma. Cancer Res 2004; 64(19): 7011-21.

155. Gaur A, Jewell DA, Liang Y, Ridzon D, Moore JH, Chen C, Ambros VR, Israel MA. Characterization of microRNA expression levels and their biological correlates in human cancer cell lines. Cancer Res 2007; 67(6): 2456-68.

156. Geling A, Steiner H, Willem M, Bally-Cuif L, Haass C A gamma-secretase inhibitor blocks Notch signaling in vivo and causes a severe neurogenic phenotype in zebrafish. EMBO Rep 2002; 3: 688-94.

157. Geyer JR, Sposto R, Jennings M, Boyett JM, Axtell RA, Breiger D, Broxson E, Donahue B, Finlay JL, Goldwein JW, Heier LA, Johnson D, Mazewski C, Miller DC, Packer R, Puccetti D, Radcliffe J, Tao ML, Shiminski-Maher T; Children's Cancer

Group. Multiagent chemotherapy and deferred radiotherapy in infants with malignant brain tumors: A report from the Children's Cancer Group. J Clin Oncol 2005; 23:7621–7631.

158. Ghebranious N, Burmester JK, Glurich I, McPherson E, Ivacic L, Kislow J, Rasmussen K, Kumar V, Raggio CL, Blank RD, Jacobsen FS, Faciszewski T, Womack J, Giampietro PF. Evaluation of SLC35A3 as a candidate gene for human vertebral malformations. Am J Med Genet A 2006; 140(12): 1346-8.

159. Ghosh D, Srivastava GP, Xu D, Schulz LC, Roberts RM. A link between SIN1 (MAPKAP1) and poly(rC) binding protein 2 (PCBP2) in counteracting environmental stress. Proc Natl Acad Sci U S A 2008; 105(33): 11673-8.

160. Giangaspero F, Rigobello L, Badiali M, Loda M, Andreini L, Basso G, Zorzi F, Montaldi A. Large-cell medulloblastomas. A distinct variant with highly aggressive behavior. Am J Surg Pathol 1992; 16(7): 687-93.

161. Giangaspero F, Eberhart CG, Ellison DW, et al. Medulloblastoma . In: Louis DN, Ohgaki H, Wiestler OD, editors. WHO Classification of Tumours of the Nervous System. Lyon: IARC; 2007.

162. Gilbertson RJ, Ellison DW. The origins of medulloblastoma subtypes. Annu Rev Pathol 2008; 3: 341-65.

163. Gilbertson R, Wickramasinghe C, Hernan R, Balaji V, Hunt D, Jones-Wallace D, Crolla J, Perry R, Lunec J, Pearson A, Ellison D. Clinical and molecular stratification of disease risk in medulloblastoma. Br J Cancer 2001; 85(5): 705-12.

164. Gilhuis HJ, Anderl KL, Boerman RH, Jeuken JM, James CD, Raffel C, Scheithauer BW, Jenkins RB. Comparative genomic hybridization of medulloblastomas and clinical relevance: eleven new cases and a review of the literature. Clin Neurol Neurosurg 2000; 102(4): 203-209.

165. Giordana MT, Migheli A, Pavanelli E. Isochromosome 17q is a constant finding in medulloblastoma. An interphase cytogenetic study on tissue sections. Neuropathol Appl Neurobiol 1998; 24(3): 233-8.

166. Giraldez AJ, Cinalli RM, Glasner ME, Enright AJ, Thomson JM, Baskerville S, Hammond SM, Bartel DP, Schier AF. MicroRNAs regulate brain morphogenesis in

zebrafish. Science 2005; 308(5723): 833-8.

167. Godlewski J, Nowicki MO, Bronisz A, Williams S, Otsuki A, Nuovo G, Raychaudhury A, Newton HB, Chiocca EA, Lawler S. Targeting of the Bmi-1 oncogene/stem cell renewal factor by microRNA-128 inhibits glioma proliferation and self-renewal. Cancer Res 2008; 68(22): 9125-30.

168. Goldstein AM, Stewart C, Bale AE, Bale SJ, Dean M. Localization of the gene for the nevoid basal cell carcinoma syndrome. Am J Hum Genet 1994; 54(5): 765-73.

169. Gordon MD, Nusse R. Wnt signaling: multiple pathways, multiple receptors, and multiple transcription factors. J Biol Chem 2006; 281(32): 22429-33.

170. Gorlin RJ. Nevoid basal-cell carcinoma syndrome. Medicine (Baltimore) 1987; 66(2): 98-113.

171. Goswami S, Tarapore RS, Teslaa JJ, Grinblat Y, Setaluri V, Spiegelman VS. MicroRNA-340-mediated degradation of microphthalmia-associated transcription factor mRNA is inhibited by the coding region determinant-binding protein. J Biol Chem 2010; 285(27): 20532-40.

172. Gregory RI, Yan KP, Amuthan G, Chendrimada T, Doratotaj B, Cooch N, Shiekhattar R. The Microprocessor complex mediates the genesis of microRNAs. Nature 2004; 432(7014): 235-40.

173. Gregory RI, Chendrimada TP, Cooch N, Shiekhattar R. Human RISC couples microRNA biogenesis and posttranscriptional gene silencing. Cell 2005; 123(4): 631-40.

174. Griffiths-Jones S. The microRNA Registry. Nucleic Acids Res 2004; 32: D109-11.

175. Grimson A, Srivastava M, Fahey B, Woodcroft BJ, Chiang HR, King N, Degnan BM, Rokhsar DS, Bartel DP. Early origins and evolution of microRNAs and Piwi-interacting RNAs in animals. Nature 2008; 455(7217): 1193-7.

176. Grishok A, Pasquinelli AE, Conte D, Li N, Parrish S, Ha I, Baillie DL, Fire A, Ruvkun G, Mello CC. Genes and mechanisms related to RNA interference regulate expression of the small temporal RNAs that control C. elegans developmental timing.

Cell 2001; 106(1): 23-34.

177. Grotzer MA, Hogarty MD, Janss AJ, Liu X, Zhao H, Eggert A, Sutton LN, Rorke LB, Brodeur GM, Phillips PC. MYC messenger RNA expression predicts survival outcome in childhood primitive neuroectodermal tumor/medulloblastoma. Clin Cancer Res 2001; 7(8): 2425-33.

178. Grotzer MA, Janss AJ, Fung K, Biegel JA, Sutton LN, Rorke LB, Zhao H, Cnaan A, Phillips PC, Lee VM, Trojanowski JQ. TrkC expression predicts good clinical outcome in primitive neuroectodermal brain tumors. J Clin Oncol 2000; 18(5): 1027-35.

179. Guervós MA, Marcos CA, Hermsen M, Nuño AS, Suárez C, Llorente JL. Deletions of N33, STK11 and TP53 are involved in the development of lymph node metastasis in larynx and pharynx carcinomas. Cell Oncol 2007; 29(4): 327-34.

180. Guessous F, Li Y, Abounader R. Signaling pathways in medulloblastoma. J Cell Physiol 2008; 217(3): 577-83.

181. Gulino A, Arcella A, Giangaspero F. Pathological and molecular heterogeneity of medulloblastoma. Curr Opin Oncol 2008; 20(6): 668-75.

182. Gurney JG, Kadan-Lottick N. Brain and other central nervous system tumors: rates, trends, and epidemiology. Curr Opin Oncol 2001; 13(3): 160-6.

183. Haase AD, Jaskiewicz L, Zhang H, Lainé S, Sack R, Gatignol A, Filipowicz W. TRBP, a regulator of cellular PKR and HIV-1 virus expression, interacts with Dicer and functions in RNA silencing. EMBO Rep 2005; 6(10): 961-7.

184. Haberler C, Slavc I, Czech T, Gelpi E, Heinzl H, Budka H, Urban C, Scarpatetti M, Ebetsberger-Dachs G, Schindler C, Jones N, Klein-Franke A, Maier H, Jauk B, Kiefer A, Hainfellner JA. Histopathological prognostic factors in medulloblastoma: high expression of survivin is related to unfavourable outcome. Eur J Cancer 2006; 42(17): 2996-3003.

185. Hadjipanayis CG, Van Meir EG. Brain cancer propagating cells: biology, genetics and targeted therapies. Trends Mol Med 2009; 15(11): 519-30.

186. Hahn H, Christiansen J, Wicking C, Zaphiropoulos PG, Chidambaram A, Gerrard B, Vorechovsky I, Bale AE, Toftgard R, Dean M, Wainwright B. A mammalian patched

homolog is expressed in target tissues of sonic hedgehog and maps to a region associated with developmental abnormalities. J Biol Chem 1996; 271(21): 12125-8.

187. Hahn H, Wicking C, Zaphiropoulous PG, Gailani MR, Shanley S, Chidambaram A, Vorechovsky I, Holmberg E, Unden AB, Gillies S, Negus K, Smyth I, Pressman C, Leffell DJ, Gerrard B, Goldstein AM, Dean M, Toftgard R, Chenevix-Trench G, Wainwright B, Bale AE. Mutations of the human homolog of Drosophila patched in the nevoid basal cell carcinoma syndrome. Cell 1996; 85(6): 841-51.

188. Hall A, Karplus PA, Poole LB. Typical 2-Cys peroxiredoxins--structures, mechanisms and functions. FEBS J 2009; 276(9): 2469-77.

189. Hallahan AR, Pritchard JI, Hansen S, Benson M, Stoeck J, Hatton BA, Russell TL, Ellenbogen RG, Bernstein ID, Beachy PA, Olson JM. The SmoA1 mouse model reveals that notch signaling is critical for the growth and survival of sonic hedgehog-induced medulloblastomas. Cancer Res 2004; 64(21): 7794-800.

190. Hamilton SR, Liu B, Parsons RE, Papadopoulos N, Jen J, Powell SM, Krush AJ, Berk T, Cohen Z, Tetu B, Burger PC, Wood PA, Taqi F, Booker SV, Petersen GM, Offerhaus JA, Tersmette AC, Giardiello FM, Vogelstein B, Kinzler KW. The molecular basis of Turcot's syndrome. N Engl J Med 1995; 332(13): 839-47.

191. Han J, Lee Y, Yeom KH, Kim YK, Jin H, Kim VN. The Drosha-DGCR8 complex in primary microRNA processing. Genes Dev 2004; 18(24): 3016-27.

192. Hartmann W, Digon-Söntgerath B, Koch A, Waha A, Endl E, Dani I, Denkhaus D, Goodyer CG, Sörensen N, Wiestler OD, Pietsch T. Phosphatidylinositol 3'-kinase/AKT signaling is activated in medulloblastoma cell proliferation and is associated with reduced expression of PTEN. Clin Cancer Res 2006; 12(10): 3019-27.

193. Hashimoto Y, Akiyama Y, Otsubo T, Shimada S, Yuasa Y. Involvement of epigenetically silenced microRNA-181c in gastric carcinogenesis. Carcinogenesis 2010; 31(5): 777-84.

194. Havrilesky LJ, Alvarez AA, Whitaker RS, Marks JR, Berchuck A. Loss of expression of the p16 tumor suppressor gene is more frequent in advanced ovarian cancers lacking p53 mutations. Gynecol Oncol 2001; 83(3): 491-500.

195. He TC, Sparks AB, Rago C, Hermeking H, Zawel L, da Costa LT, Morin PJ,

Vogelstein B, Kinzler KW. Identification of c-MYC as a target of the APC pathway. Science 1998; 281(5382): 1509-12.

196. He L, Hannon GJ. MicroRNAs: small RNAs with a big role in gene regulation. Nat Rev Genet 2004; 5(7): 522-31.

197. He L, Thomson JM, Hemann MT, Hernando-Monge E, Mu D, Goodson S, Powers S, Cordon-Cardo C, Lowe SW, Hannon GJ, Hammond SM. A microRNA polycistron as a potential human oncogene. Nature 2005; 435(7043): 828-33.

198. Heinzelmann-Schwarz VA, Gardiner-Garden M, Henshall SM, Scurry J, Scolyer RA, Davies MJ, Heinzelmann M, Kalish LH, Bali A, Kench JG, Edwards LS, Bergh PM Vanden, Hacker NF, Sutherland RL, O'Brien PM. A distinct molecular profile associated with mucinous epithelial ovarian cancer. Clin Cancer Res 2004; 10: 4427–36.

199. Heizmann CW, Fritz G, Schäfer BW. S100 proteins: structure, functions and pathology. Front Biosci 2002; 7: d1356-68.

200. Helseth E, Due-Tonnessen B, Wesenberg F, Lote K, Lundar T. Posterior fossa medulloblastoma in children and young adults (0–19 years): survival and performance. Childs Nerv Syst 1999; 15: 451-5.

201. Hemmati HD, Nakano I, Lazareff JA, Masterman-Smith M, Geschwind DH, Bronner-Fraser M, Kornblum HI. Cancerous stem cells can arise from pediatric brain tumors. Proc Natl Acad Sci U S A 2003; 100(25):15178-83.

202. Henriksson M, Lüscher B. Proteins of the Myc network: essential regulators of cell growth and differentiation. Adv Cancer Res 1996; 68: 109-82.

203. Herms J, Neidt I, Lüscher B, Sommer A, Schürmann P, Schröder T, Bergmann M, Wilken B, Probst-Cousin S, Hernáiz-Driever P, Behnke J, Hanefeld F, Pietsch T, Kretzschmar HA. C-MYC expression in medulloblastoma and its prognostic value. Int J Cancer 2000; 89(5): 395-402.

204. Hess D, Chisholm JW, Igal RA. Inhibition of stearoylCoA desaturase activity blocks cell cycle progression and induces programmed cell death in lung cancer cells. PLoS One. 2010; 5(6): e11394.

205. Hipfner DR, Weigmann K, Cohen SM. The bantam gene regulates Drosophila

growth. Genetics 2002; 161(4): 1527-37.

206. Hirabayashi S, Nakagawa K, Sumita K, Hidaka S, Kawai T, Ikeda M, Kawata A, Ohno K, Hata Y. Threonine 74 of MOB1 is a putative key phosphorylation site by MST2 to form the scaffold to activate nuclear Dbf2-related kinase 1. Oncogene 2008; 27(31): 4281-92.

207. Hohjoh H, Fukushima T. Expression profile analysis of microRNA (miRNA) in mouse central nervous system using a new miRNA detection system that examines hybridization signals at every step of washing. Gene 2007; 391(1-2): 39-44.

208. Hooper JE, Scott MP. The Drosophila patched gene encodes a putative membrane protein required for segmental patterning. Cell 1989; 59(4): 751-65.

209. Hsu WL, Everett RD. Human neuron-committed teratocarcinoma NT2 cell line has abnormal ND10 structures and is poorly infected by herpes simplex virus type 1. J Virol 2001; 75(8): 3819-31.

210. Huang RP, Wu JX, Fan Y, Adamson ED. UV activates growth factor receptors via reactive oxygen intermediates. J Cell Biol 1996; 133(1): 211-20.

211. Huang H, Mahler-Araujo BM, Sankila A, Chimelli L, Yonekawa Y, Kleihues P, Ohgaki H. APC mutations in sporadic medulloblastomas. Am J Pathol 2000; 156(2): 433-7.

212. Humphreys, D.T., Westman, B.J., Martin, D.I. and Preiss, T. MicroRNAs control translation initiation by inhibiting eukaryotic initiation factor 4E/cap and poly(A) tail function. Proc. Natl. Acad. Sci. U S A 2005; 102: 16961–16966.

213. Hutvágner G, McLachlan J, Pasquinelli AE, Bálint E, Tuschl T, Zamore PD. A cellular function for the RNA-interference enzyme Dicer in the maturation of the let-7 small temporal RNA. Science 2001; 293(5531): 834-8.

214. Iacobuzio-Donahue CA, Maitra A, Olsen M, Lowe AW, van Heek NT, Rosty C, Walter K, Sato N, Parker A, Ashfaq R, Jaffee E, Ryu B, Jones J, Eshleman JR, Yeo CJ, Cameron JL, Kern SE, Hruban RH, Brown PO, Goggins M. Exploration of global gene expression patterns in pancreatic adenocarcinoma using cDNA microarrays. Am J Pathol 2003; 162: 1151–1162.

215. Ibáñez-Ventoso C, Vora M, Driscoll M. Sequence relationships among C. elegans, D. melanogaster and human microRNAs highlight the extensive conservation of microRNAs in biology. PLoS One 2008; 3(7): e2818.

216. Ignatova TN, Kukekov VG, Laywell ED, Suslov ON, Vrionis FD, Steindler DA. Human cortical glial tumors contain neural stem-like cells expressing astroglial and neuronal markers in vitro. Glia 2002; 39(3): 193-206.

217. Inda MM, Mercapide J, Muñoz J, Coullin P, Danglot G, Tuñon T, Martínez-Peñuela JM, Rivera JM, Burgos JJ, Bernheim A, Castresana JS. PTEN and DMBT1 homozygous deletion and expression in medulloblastomas and supratentorial primitive neuroectodermal tumors. Oncol Rep 2004; 12(6): 1341-7.

218. Inda MM, Perot C, Guillaud-Bataille M, Danglot G, Rey JA, Bello MJ, Fan X, Eberhart C, Zazpe I, Portillo E, Tuñón T, Martínez-Peñuela JM, Bernheim A, Castresana JS. Genetic heterogeneity in supratentorial and infratentorial primitive neuroectodermal tumours of the central nervous system. Histopathology 2005; 47(6): 631-7.

219. Ishii H, Vecchione A, Murakumo Y, Baldassarre G, Numata S, Trapasso F, Alder H, Baffa R, Croce CM. FEZ1/LZTS1 gene at 8p22 suppresses cancer cell growth and regulates mitosis. Proc Natl Acad Sci U S A 2001; 98(18): 10374-9.

220. Itoh K, Krupnik VE, Sokol SY. Axis determination in Xenopus involves biochemical interactions of axin, glycogen synthase kinase 3 and beta-catenin. Curr Biol 1998; 10: 591-4.

221. Jakymiw A, Lian S, Eystathioy T, Li S, Satoh M, Hamel JC, Fritzler MJ, Chan EK. Disruption of GW bodies impairs mammalian RNA interference. Nat Cell Biol 2005; 7(12): 1267-74.

222. Jaros E, Perry RH, Adam L, Kelly PJ, Crawford PJ, Kalbag RM, Mendelow AD, Sengupta RP, Pearson AD. Prognostic implications of p53 protein, epidermal growth factor receptor, and Ki-67 labelling in brain tumours. Br J Cancer 1992; 66(2): 373-85.

223. Jazdzewski K, Murray EL, Franssila K, Jarzab B, Schoenberg DR, de la Chapelle A. Common SNP in pre-miR-146a decreases mature miR expression and predisposes to papillary thyroid carcinoma. Proc Natl Acad Sci U S A 2008; 105(20): 7269-74.

224. Jenkin D, Shabanah MA, Shail EA, Gray A, Hassounah M, Khafaga Y, Kofide A, Mustafa M, Schultz H. Prognostic factors for medulloblastoma. Int J Radiat Oncol Biol Phys 2000; 47(3): 573-84.

225. Jiang J, Gill BS, Wang GL, Ronald PC, Ward DC. Metaphase and interphase fluorescence in situ hybridization mapping of the rice genome with bacterial artificial chromosomes. Proc Natl Acad Sci U S A 1995; 92(10): 4487-91.

226. Jiang J, Lee EJ, Gusev Y, Schmittgen TD. Real-time expression profiling of microRNA precursors in human cancer cell lines. Nucleic Acids Res 2005; 33(17): 5394-403.

227. John B, Enright AJ, Aravin A, Tuschl T, Sander C, Marks DS. Human MicroRNA targets. PLoS Biol 2004; 2(11): e363.

228. Johnson RL, Rothman AL, Xie J, Goodrich LV, Bare JW, Bonifas JM, Quinn AG, Myers RM, Cox DR, Epstein EH Jr, Scott MP. Human homolog of patched, a candidate gene for the basal cell nevus syndrome. Science 1996; 272(5268): 1668-71.

229. Johnston RJ, Hobert O. A microRNA controlling left/right neuronal asymmetry in Caenorhabditis elegans. Nature 2003; 426(6968): 845-9.

230. Johnson SM, Grosshans H, Shingara J, Byrom M, Jarvis R, Cheng A, Labourier E, Reinert KL, Brown D, Slack FJ. RAS is regulated by the let-7 microRNA family. Cell 2005; 120: 635–647.

231. Jones DP. Disruption of mitochondrial redox circuitry in oxidative stress. Chem Biol Interact 2006; 163(1-2): 38-53.

232. Jones-Villeneuve EM, McBurney MW, Rogers KA, Kalnins VI. Retinoic acid induces embryonal carcinoma cells to differentiate into neurons and glial cells. J Cell Biol 1982; 94(2): 253-62.

233. Jones-Villeneuve EM, Rudnicki MA, Harris JF, McBurney MW. Retinoic acid-induced neural differentiation of embryonal carcinoma cells. Mol Cell Biol. 1983; 3(12): 2271-9.

234. Jordan CT, Guzman ML, Noble M. Cancer stem cells. N Engl J Med 2006; 355(12): 1253-61.

235. Jozwiak J, Grajkowska W, Wlodarski P. Pathogenesis of medulloblastoma and current treatment outlook. Med Res Rev 2007; 27(6): 869-90.

236. Kallioniemi A, Kallioniemi OP, Waldman FM, Chen LC, Yu LC, Fung YK, Smith HS, Pinkel D, Gray JW. Detection of retinoblastoma gene copy number in metaphase chromosomes and interphase nuclei by fluorescence in situ hybridization. Cytogenet Cell Genet 1992; 60(3-4): 190-3.

237. Kang SW, Chae HZ, Seo MS, Kim K, Baines IC, Rhee SG. Mammalian peroxiredoxin isoforms can reduce hydrogen peroxide generated in response to growth factors and tumor necrosis factor-alpha. J Biol Chem 1998; 273(11): 6297-302.

238. Karihtala P, Mäntyniemi A, Kang SW, Kinnula VL, Soini Y. Peroxiredoxins in breast carcinoma. Clin Cancer Res 2003; 9(9): 3418-24.

239. Karin M, Shaulian E. AP-1: linking hydrogen peroxide and oxidative stress to the control of cell proliferation and death. IUBMB Life 2001; 52(1-2): 17-24.

240. Kenney AM, Rowitch DH. Sonic hedgehog promotes G(1) cyclin expression and sustained cell cycle progression in mammalian neuronal precursors. Mol Cell Biol 2000; 20(23): 9055-67.

241. Kenney AM, Cole MD, Rowitch DH. Nmyc upregulation by sonic hedgehog signaling promotes proliferation in developing cerebellar granule neuron precursors. Development 2003; 130(1): 15-28.

242. Kent OA, Chivukula RR, Mullendore M, Wentzel EA, Feldmann G, Lee KH, Liu S, Leach SD, Maitra A, Mendell JT. Repression of the miR-143/145 cluster by oncogenic Ras initiates a tumor-promoting feed-forward pathway. Genes Dev 2010; 24(24): 2754-9.

243. Kershman J. The medulloblast and medulloblastoma: A study of human embryos. Arch Neurol Psychiatry 1938; 40(5): 937-967.

244. Ketting RF, Fischer SE, Bernstein E, Sijen T, Hannon GJ, Plasterk RH. Dicer functions in RNA interference and in synthesis of small RNA involved in developmental timing in C. elegans. Genes Dev 2001; 15(20): 2654-9.

245. Khalil EM.Treatment results of adults and children with medulloblastoma NCI,

Cairo University experience. J Egypt Natl Canc Inst 2008; 20(2): 175-86.

246. Khvorova A, Reynolds A, Jayasena SD. Functional siRNAs and miRNAs exhibit strand bias. Cell 2003; 115(2): 209-16.

247. Kieffer-Renaux V, Bulteau C, Grill J, Kalifa C, Viguier D, Jambaque I. Patterns of neuropsychological deficits in children with medulloblastoma according to craniospatial irradiation doses. Dev Med Child Neurol 2000; 42(11): 741-5.

248. Kieft JS, Grech A, Adams P, Doudna JA. Mechanisms of internal ribosome entry in translation initiation. Cold Spring Harb Symp Quant Biol 2001; 66: 277-83.

249. Kim YK, Kim VN. Processing of intronic microRNAs. EMBO J 2007; 26(3): 775-83.

250. Kim K, Yu M, Han S, Oh I, Choi YJ, Kim S, Yoon K, Jung M, Choe W. Expression of human peroxiredoxin isoforms in response to cervical carcinogenesis. Oncol Rep 2009; 21(6): 1391-6.

251. Kim VN, Han J, Siomi MC. Biogenesis of small RNAs in animals. Nat Rev Mol Cell Biol 2009; 10(2): 126-39.

252. Kiriakidou M, Tan GS, Lamprinaki S, De Planell-Saguer M, Nelson PT, Mourelatos Z. An mRNA m7G cap binding-like motif within human Ago2 represses translation. Cell 2007; 129(6): 1141-51.

253. Kitamura Y, Ota T, Matsuoka Y, Tooyama I, Kimura H, Shimohama S, Nomura Y, Gebicke-Haerter PJ, Taniguchi T. Hydrogen peroxide-induced apoptosis mediated by p53 protein in glial cells. Glia 1999; 25(2): 154-64.

254. Klaunig JE, Xu Y, Isenberg JS, Bachowski S, Kolaja KL, Jiang J, Stevenson DE, Walborg EF Jr. The role of oxidative stress in chemical carcinogenesis. Environ Health Perspect 1998; 106 Suppl 1: 289-95.

255. Knudson AG Jr. Mutation and cancer: statistical study of retinoblastoma. Proc Natl Acad Sci U S A 1971; 68(4): 820-3.

256. Koch A, Waha A, Tonn JC, Sörensen N, Berthold F, Wolter M, Reifenberger J, Hartmann W, Friedl W, Reifenberger G, Wiestler OD, Pietsch T. Somatic mutations of

WNT/wingless signaling pathway components in primitive neuroectodermal tumors. Int J Cancer 2001; 93(3): 445-9.

257. Kok KH, Ng MH, Ching YP, Jin DY. Human TRBP and PACT directly interact with each other and associate with dicer to facilitate the production of small interfering RNA. J Biol Chem 2007; 282(24): 17649-57.

258. Kondo T, Oue N, Mitani Y, Kuniyasu H, Noguchi T, Kuraoka K, Nakayama H, Yasui W. Loss of heterozygosity and histone hypoacetylation of the PINX1 gene are associated with reduced expression in gastric carcinoma. Oncogene 2005; 24(1): 157-64.

259. Kool M, Koster J, Bunt J, Hasselt NE, Lakeman A, van Sluis P, Troost D, Meeteren NS, Caron HN, Cloos J, Mrsić A, Ylstra B, Grajkowska W, Hartmann W, Pietsch T, Ellison D, Clifford SC, Versteeg R. Integrated genomics identifies five medulloblastoma subtypes with distinct genetic profiles, pathway signatures and clinicopathological features. PLoS One 2008; 3(8): e3088.

260. Korshunov A, Remke M, Werft W, Benner A, Ryzhova M, Witt H, Sturm D, Wittmann A, Schöttler A, Felsberg J, Reifenberger G, Rutkowski S, Scheurlen W, Kulozik AE, von Deimling A, Lichter P, Pfister SM. Adult and pediatric medulloblastomas are genetically distinct and require different algorithms for molecular risk stratification. J Clin Oncol 2010; 28(18): 3054-60.

261. Kozaki K, Imoto I, Mogi S, Omura K, Inazawa J. Exploration of tumor-suppressive microRNAs silenced by DNA hypermethylation in oral cancer. Cancer Res 2008; 68(7): 2094-105.

262. Krek A, Grün D, Poy MN, Wolf R, Rosenberg L, Epstein EJ, MacMenamin P, da Piedade I, Gunsalus KC, Stoffel M, Rajewsky N. Combinatorial microRNA target predictions. Nat Genet 2005; 37(5): 495-500.

263. Krichevsky AM, Sonntag KC, Isacson O, Kosik KS. Specific microRNAs modulate embryonic stem cell-derived neurogenesis. Stem Cells 2006; 24: 857–864.

264. Kunschner LJ, Kuttesch J, Hess K, Yung WK. Survival and recurrence factors in adult medulloblastoma: the M.D. Anderson Cancer Center experience from 1978 to 1998. Neurooncology 2001; 3: 167-73.

265. Kurian JR, Keen KL, Terasawa E. Epigenetic changes coincide with in vitro primate GnRH neuronal maturation. Endocrinology 2010; 151(11): 5359-68.

266. Kwak PB, Iwasaki S, Tomari Y. The microRNA pathway and cancer.Cancer Sci 2010; 101(11): 2309-15.

267. Kwan KY, Lam MM, Krsnik Z, Kawasawa YI, Lefebvre V, Sestan N. SOX5 postmitotically regulates migration, postmigratory differentiation, and projections of subplate and deep-layer neocortical neurons. Proc Natl Acad Sci U S A 2008; 105(41): 16021-6.

268. Lagos-Quintana M, Rauhut R, Lendeckel W, Tuschl T. Identification of novel genes coding for small expressed RNAs. Science 2001; 294(5543): 853-8.

269. Lagos-Quintana M, Rauhut R, Yalcin A, Meyer J, Lendeckel W, Tuschl T. Identification of tissue-specific microRNAs from mouse. Curr Biol 2002; 12(9): 735-9.

270. Lai T, Jabaudon D, Molyneaux BJ, Azim E, Arlotta P, Menezes JR, Macklis JD. SOX5 controls the sequential generation of distinct corticofugal neuron subtypes. Neuron 2008; 57(2): 232-47.

271. Lakin ND, Palmer R, Lillycrop KA, Howard MK, Burke LC, Thomas NS, Latchman DS. Down regulation of the octamer binding protein Oct-1 during growth arrest and differentiation of a neuronal cell line. Brain Res Mol Brain Res 1995; 28(1): 47-54.

272. Lambertz I, Nittner D, Mestdagh P, Denecker G, Vandesompele J, Dyer MA, Marine JC. Monoallelic but not biallelic loss of Dicer1 promotes tumorigenesis in vivo. Cell Death Differ 2010; 17(4): 633-41.

273. Landgraf P, Rusu M, Sheridan R, Sewer A, Iovino N, Aravin A, Pfeffer S, Rice A, Kamphorst AO, Landthaler M, Lin C, Socci ND, Hermida L, Fulci V, Chiaretti S, Foà R, Schliwka J, Fuchs U, Novosel A, Müller RU, Schermer B, Bissels U, Inman J, Phan Q, Chien M, Weir DB, Choksi R, De Vita G, Frezzetti D, Trompeter HI, Hornung V, Teng G, Hartmann G, Palkovits M, Di Lauro R, Wernet P, Macino G, Rogler CE, Nagle JW, Ju J, Papavasiliou FN, Benzing T, Lichter P, Tam W, Brownstein MJ, Bosio A, Borkhardt A, Russo JJ, Sander C, Zavolan M, Tuschl T. A mammalian microRNA expression atlas based on small RNA library sequencing. Cell 2007; 129(7): 1401-14.

274. Lapidot T, Sirard C, Vormoor J, Murdoch B, Hoang T, Caceres-Cortes J, Minden M, Paterson B, Caligiuri MA, Dick JE. A cell initiating human acute myeloid leukaemia after transplantation into SCID mice. Nature 1994; 367(6464): 645-8.

275. Lee EJ, Baek M, Gusev Y, Brackett DJ, Nuovo GJ, Schmittgen TD. Systematic evaluation of microRNA processing patterns in tissues, cell lines, and tumors. RNA 2008; 14(1): 35-42.

276. Lee RC, Feinbaum RL, Ambros V. The C. elegans heterochronic gene lin-4 encodes small RNAs with antisense complementarity to lin-14. Cell 1993; 75(5): 843-54.

277. Lee YJ, Swencki B, Shoichet S, Shivdasani RA. A possible role for the high mobility group box transcription factor Tcf-4 in vertebrate gut epithelial cell differentiation. J Biol Chem 1999; 274(3): 1566-72.

278. Lee Y, Jeon K, Lee JT, Kim S, Kim VN. MicroRNA maturation: stepwise processing and subcellular localization. EMBO J 2002; 21(17): 4663-70.

279. Lee Y, Ahn C, Han J, Choi H, Kim J, Yim J, Lee J, Provost P, Rådmark O, Kim S, Kim VN. The nuclear RNase III Drosha initiates microRNA processing. Nature 2003; 425(6956): 415-9.

280. Lee Y, Kim M, Han J, Yeom KH, Lee S, Baek SH, Kim VN. MicroRNA genes are transcribed by RNA polymerase II. EMBO J 2004; 23(20): 4051-60.

281. Lee Y, Hur I, Park SY, Kim YK, Suh MR, Kim VN. The role of PACT in the RNA silencing pathway. EMBO J 2006; 25(3): 522-32.

282. Lee Y, Kawagoe R, Sasai K, Li Y, Russell HR, Curran T, McKinnon PJ. Loss of suppressor-of-fused function promotes tumorigenesis. Oncogene 2007; 26(44): 6442-7.

283. Lee EY, Ji H, Ouyang Z, Zhou B, Ma W, Vokes SA, McMahon AP, Wong WH, Scott MP. Hedgehog pathway-regulated gene networks in cerebellum development and tumorigenesis. Proc Natl Acad Sci U S A 2010; 107(21): 9736-41.

284. Leonard JR, Cai DX, Rivet DJ, Kaufman BA, Park TS, Levy BK, Perry A. Large cell/anaplastic medulloblastomas and medullomyoblastomas: clinicopathological and genetic features. J Neurosurg 2001; 95(1): 82-8.

285. Lewis BP, Shih IH, Jones-Rhoades MW, Bartel DP, Burge CB. Prediction of mammalian microRNA targets. Cell 2003; 115(7): 787-98.

286. Lewis BP, Burge CB, Bartel DP. Conserved seed pairing, often flanked by adenosines, indicates that thousands of human genes are microRNA targets. Cell 2005; 120(1): 15-20.

287. Li W, Duan R, Kooy F, Sherman SL, Zhou W, Jin P. Germline mutation of microRNA-125a is associated with breast cancer. J Med Genet 2009; 46(5): 358-60.

288. Lian J, Tian H, Liu L, Zhang XS, Li WQ, Deng YM, Yao GD, Yin MM and Sun F. Downregulation of microRNA-383 is associated with male infertility and promotes testicular embryonal carcinoma cell proliferation by targeting IRF1. Cell Death and Disease 2010 (online).

289. Licatalosi DD, Darnell RB. Splicing regulation in neurologic disease. Neuron 2006; 52(1): 93-101.

290. Lim LP, Lau NC, Garrett-Engele P, Grimson A, Schelter JM, Castle J, Bartel DP, Linsley PS, Johnson JM. Microarray analysis shows that some microRNAs downregulate large numbers of target mRNAs. Nature 2005; 433(7027): 769-73.

291. Lindsey JC, Hill RM, Megahed H, Lusher ME, Schwalbe EC, Cole M, Hogg TL, Gilbertson RJ, Ellison DW, Bailey S, Clifford SC. TP53 Mutations in Favorable-Risk Wnt/Wingless-Subtype Medulloblastomas. J Clin Oncol 2011; 29(12):e344-6.

292. Lingel A, Simon B, Izaurralde E, Sattler M. Structure and nucleic-acid binding of the Drosophila Argonaute 2 PAZ domain. Nature 2003; 426(6965): 465-9.

293. Liu J, Carmell MA, Rivas FV, Marsden CG, Thomson JM, Song JJ, Hammond SM, Joshua-Tor L, Hannon GJ. Argonaute2 is the catalytic engine of mammalian RNAi. Science. 2004 Sep 3;305(5689):1437-41.

294. Liu X, Kim CN, Yang J, Jemmerson R, Wang X. Induction of apoptotic program in cell-free extracts: requirement for dATP and cytochrome c. Cell 1996; 86(1): 147-57.

295. Liu N, Williams AH, Kim Y, McAnally J, Bezprozvannaya S, Sutherland LB, Richardson JA, Bassel-Duby R, Olson EN. An intragenic MEF2-dependent enhancer directs muscle-specific expression of microRNAs 1 and 133. Proc Natl Acad Sci U S A

2007; 104(52): 20844-9.

296. Lo KC, Ma C, Bundy BN, Pomeroy SL, Eberhart CG, Cowell JK. Gain of 1q is a potential univariate negative prognostic marker for survival in medulloblastoma. Clin Cancer Res 2007a; 13(23): 7022-8.

297. Lo KC, Rossi MR, Eberhart CG, Cowell JK. Genome wide copy number abnormalities in pediatric medulloblastomas as assessed by array comparative genome hybridization. Brain Pathol 2007b; 17(3), 282-96.

298. Lou Y, Yang X, Wang F, Cui Z, Huang Y. MicroRNA-21 promotes the cell proliferation, invasion and migration abilities in ovarian epithelial carcinomas through inhibiting the expression of PTEN protein. Int J Mol Med 2010; 26(6): 819-27.

299. Lu J, Getz G, Miska EA, Alvarez-Saavedra E, Lamb J, Peck D, Sweet-Cordero A, Ebert BL, Mak RH, Ferrando AA, Downing JR, Jacks T, Horvitz HR, Golub TR. MicroRNA expression profiles classify human cancers. Nature 2005; 435(7043): 834-8.

300. Lu Z, Liu M, Stribinskis V, Klinge CM, Ramos KS, Colburn NH, Li Y. MicroRNA-21 promotes cell transformation by targeting the programmed cell death 4 gene. Oncogene 2008; 27(31): 4373-9.

301. Lujambio A, Ropero S, Ballestar E, Fraga MF, Cerrato C, Setién F, Casado S, Suarez-Gauthier A, Sanchez-Cespedes M, Git A, Spiteri I, Das PP, Caldas C, Miska E, Esteller M. Genetic unmasking of an epigenetically silenced microRNA in human cancer cells. Cancer Res 2007; 67(4): 1424-9.

302. Lujambio A, Calin GA, Villanueva A, Ropero S, Sánchez-Céspedes M, Blanco D, Montuenga LM, Rossi S, Nicoloso MS, Faller WJ, Gallagher WM, Eccles SA, Croce CM, Esteller M. A microRNA DNA methylation signature for human cancer metastasis. Proc Natl Acad Sci U S A 2008; 105(36); 13556-61.

303. Lo KC, Rossi MR, Eberhart CG, Cowell JK. Genome wide copy number abnormalities in pediatric medulloblastomas as assessed by array comparative genome hybridization. Brain Pathol. 2007; 17(3): 282-96.

304. Ma JB, Ye K, Patel DJ. Structural basis for overhang-specific small interfering RNA recognition by the PAZ domain. Nature 2004; 429(6989): 318-22.

305. Ma L, Young J, Prabhala H, Pan E, Mestdagh P, Muth D, Teruya-Feldstein J, Reinhardt F, Onder TT, Valastyan S, Westermann F, Speleman F, Vandesompele J, Weinberg RA. miR-9, a MYC/MYCN-activated microRNA, regulates E-cadherin and cancer metastasis. Nat Cell Biol 2010; 12(3): 247-56.

306. McManamy CS, Pears J, Weston CL, Hanzely Z, Ironside JW, Taylor RE, Grundy RG, Clifford SC, Ellison DW; Clinical Brain Tumour Group. Nodule formation and desmoplasia in medulloblastomas - defining the nodular/desmoplastic variant and its biological behaviour. Brain Pathol 2007;17: 151–64.

307. Makeyev EV, Zhang J, Carrasco MA, Maniatis T. The microRNA miR-124 promotes neuronal differentiation by triggering brain-specific alternative pre-mRNA splicing. Mol Cell 2007; 27: 435–448.

308. Malzkorn B, Wolter M, Liesenberg F, Grzendowski M, Stühler K, Meyer HE, Reifenberger G. Identification and functional characterization of microRNAs involved in the malignant progression of gliomas. Brain Pathol 2010; 20(3): 539-50.

309. Mani S, Schaefer J, Meiri KF. Targeted disruption of GAP-43 in P19 embryonal carcinoma cells inhibits neuronal differentiation. As well as acquisition of the morphological phenotype. Brain Res 2000; 853(2): 384-95.

310. Marino S. Medulloblastoma: developmental mechanisms out of control. Trends Mol Med. 2005; 11(1): 17-22.

311. Martin MM, Lee EJ, Buckenberger JA, Schmittgen TD, Elton TS. MicroRNA-155 regulates human angiotensin II type 1 receptor expression in fibroblasts. J Biol Chem 2006; 281(27): 18277-84.

312. Maru DM, Singh RR, Hannah C, Albarracin CT, Li YX, Abraham R, Romans AM, Yao H, Luthra MG, Anandasabapathy S, Swisher SG, Hofstetter WL, Rashid A, Luthra R. MicroRNA-196a is a potential marker of progression during Barrett's metaplasia-dysplasia-invasive adenocarcinoma sequence in esophagus. Am J Pathol 2009; 174(5): 1940-8.

313. Masri J, Bernath A, Martin J, Jo OD, Vartanian R, Funk A, Gera J. mTORC2 activity is elevated in gliomas and promotes growth and cell motility via overexpression of rictor. Cancer Res 2007; 67(24): 11712-20.

314. Mathews DH, Sabina J, Zuker M, Turner DH. Expanded sequence dependence of thermodynamic parameters improves prediction of RNA secondary structure. J Mol Biol 1999; 288(5): 911-40.

315. Mathonnet G, Fabian MR, Svitkin YV, Parsyan A, Huck L, Murata T, Biffo S, Merrick WC, Darzynkiewicz E, Pillai RS, Filipowicz W, Duchaine TF, Sonenberg N. MicroRNA inhibition of translation initiation in vitro by targeting the cap-binding complex eIF4F. Science 2007; 317(5845): 1764-7.

316. Mathupala SP, Parajuli P, Sloan AE. Silencing of monocarboxylate transporters via small interfering ribonucleic acid inhibits glycolysis and induces cell death in malignant glioma: an in vitro study. Neurosurgery 2004; 55: 1410-9.

317. Mavier P, Guigui B, Preaux AM, Rosenbaum J, Lescs MC, Zafrani ES, Dhumeaux D. In vitro toxicity of hydrogen peroxide against normal vs. tumor rat hepatocytes: role of catalase and of the glutathione redox cycle. Hepatology 1988; 8(6): 1673-8.

318. McCabe MG, Ichimura K, Liu L, Plant K, Backlund LM, Pearson DM, Collins VP. High-resolution array-based comparative genomic hybridization of medulloblastomas and supratentorial primitive neuroectodermal tumors. J Neuropathol Exp Neurol 2006; 65: 549-561.

319. McCabe MG, Ichimura K, Pearson DM, Liu L, Clifford SC, Ellison DW, Collins VP. Novel mechanisms of gene disruption at the medulloblastoma isodicentric 17p11 breakpoint. Genes Chromosomes Cancer 2009; 48(2): 121-31.

320. McCabe MG, Ichimura K, Liu L, Plant K, Bäcklund LM, Pearson DM, Collins VP. High-resolution array-based comparative genomic hybridization of medulloblastomas and supratentorial primitive neuroectodermal tumors. J Neuropathol Exp Neurol 2006; 65(6): 549-61.

321. McMahon AP, Bradley A. The Wnt-1 (int-1) proto-oncogene is required for development of a large region of the mouse brain. Cell 1990; 62(6): 1073-85.

322. McManamy CS, Lamont JM, Taylor RE, Cole M, Pearson AD, Clifford SC, Ellison DW; United Kingdom Children's Cancer Study Group. Morphophenotypic variation predicts clinical behavior in childhood non-desmoplastic medulloblastomas. J Neuropathol Exp Neurol 2003; 62(6): 627-32.

323. Mendrzyk F, Radlwimmer B, Joos S, Kokocinski F, Benner A, Stange DE, Neben K, Fiegler H, Carter NP, Reifenberger G, Korshunov A, Lichter P. Genomic and protein expression profiling identifies CDK6 as novel independent prognostic marker in medulloblastoma. J Clin Oncol 2005; 23(34): 8853-62.

324. Mendrzyk F, Korshunov A, Toedt G, Schwarz F, Korn B, Joos S, Hochhaus A, Schoch C, Lichter P, Radlwimmer B. Isochromosome breakpoints on 17p in medulloblastoma are flanked by different classes of DNA sequence repeats. Genes Chromosomes Cancer 2006; 45: 401-410.

325. Meister G, Landthaler M, Patkaniowska A, Dorsett Y, Teng G, Tuschl T. Human Argonaute2 mediates RNA cleavage targeted by miRNAs and siRNAs. Mol Cell 2004; 15(2): 185-97.

326. Merchant TE, Pollack IF, Loeffler JS. Brain tumors across the age spectrum: biology, therapy, and late effects. Semin Radiat Oncol 2010; 20(1): 58-66.

327. Michiels EM, Weiss MM, Hoovers JM, Baak JP, Voûte PA, Baas F, Hermsen MA. Genetic alterations in childhood medulloblastoma analyzed by comparative genomic hybridization. J Pediatr Hematol Oncol 2002; 24(3): 205-10.

328. Miller JR, Hocking AM, Brown JD, Moon RT. Mechanism and function of signal transduction by the Wnt/beta-catenin and Wnt/Ca2+ pathways. Oncogene 1999; 18(55): 7860-72.

329. Min HS, Lee YJ, Park K, Cho BK, Park SH. Medulloblastoma: histopathologic and molecular markers of anaplasia and biologic behavior. Acta Neuropathol 2006; 112(1): 13-20.

330. Miralbell R, Tolnay M, Bieri S, Probst A, Sappino AP, Berchtold W, Pepper MS, Pizzolato G. Pediatric medulloblastoma: prognostic value of p53, bcl-2, Mib-1, and microvessel density. J Neurooncol 1999; 45(2): 103-10.

331. Miska EA, Alvarez-Saavedra E, Townsend M, Yoshii A, Sestan N, Rakic P, Constantine-Paton M, Horvitz HR. Microarray analysis of microRNA expression in the developing mammalian brain. Genome Biol 2004; 5(9): R68.

332. Miyazaki T, Liu ZJ, Kawahara A, Minami Y, Yamada K, Tsujimoto Y, Barsoumian EL, Permutter RM, Taniguchi T. Three distinct IL-2 signaling pathways mediated by

bcl-2, c-myc, and lck cooperate in hematopoietic cell proliferation. Cell 1995; 81(2): 223-31.

333. Molenaar M, van de Wetering M, Oosterwegel M, Peterson-Maduro J, Godsave S, Korinek V, Roose J, Destrée O, Clevers H. XTcf-3 transcription factor mediates beta-catenin-induced axis formation in Xenopus embryos. Cell 1996; 86(3): 391-9.

334. Moss EG, Lee RC, Ambros V. The cold shock domain protein LIN-28 controls developmental timing in C. elegans and is regulated by the lin-4 RNA. Cell 1997; 88(5): 637-46.

335. Mulhern RK, Palmer SL, Merchant TE, Wallace D, Kocak M, Brouwers P, Krull K, Chintagumpala M, Stargatt R, Ashley DM, Tyc VL, Kun L, Boyett J, Gajjar A. Neurocognitive consequences of risk-adapted therapy for childhood medulloblastoma. J Clin Oncol 2005; 23(24): 5511-9.

336. Murthy SK, DiFrancesco LM, Ogilvie RT, Demetrick DJ. Loss of heterozygosity associated with uniparental disomy in breast carcinoma. Mod Pathol 2002; 15(12): 1241-50.

337. Nagarajah NS, Vigneswaran N, Zacharias W. Hypoxia-mediated apoptosis in oral carcinoma cells occurs via two independent pathways. Mol Cancer 2004; 3(1): 38.

338. Najafi-Shoushtari SH, Kristo F, Li Y, Shioda T, Cohen DE, Gerszten RE, Näär AM.MicroRNA-33 and the SREBP host genes cooperate to control cholesterol homeostasis. Science 2010; 328(5985): 1566-9.

339. Nakahara Y, Northcott PA, Li M, Kongkham PN, Smith C, Yan H, Croul S, Ra YS, Eberhart C, Huang A, Bigner D, Grajkowska W, Van Meter T, Rutka JT, Taylor MD. Genetic and epigenetic inactivation of Kruppel-like factor 4 in medulloblastoma. Neoplasia. 2010; 12(1): 20-7.

340. Nakano Y, Guerrero I, Hidalgo A, Taylor A, Whittle JR, Ingham PW. A protein with several possible membrane-spanning domains encoded by the Drosophila segment polarity gene patched. Nature 1989; 341(6242): 508-13.

341. Nam DH, Wang KC, Kim YM, Chi JG, Kim SK, Cho BK. The effect of isochromosome 17q presence, proliferative and apoptotic indices, expression of c-erbB-2, bcl-2 and p53 proteins on the prognosis of medulloblastoma. J Korean Med

Sci 2000; 15(4): 452-6.

342. Negishi Y, Nishita Y, Saëgusa Y, Kakizaki I, Galli I, Kihara F, Tamai K, Miyajima N, Iguchi-Ariga SM, Ariga H. Identification and cDNA cloning of single-stranded DNA binding proteins that interact with the region upstream of the human c-myc gene. Oncogene. 1994; 9(4): 1133-43.

343. Ng IO, Liang ZD, Cao L, Lee TK. DLC-1 is deleted in primary hepatocellular carcinoma and exerts inhibitory effects on the proliferation of hepatoma cell lines with deleted DLC-1. Cancer Res 2000; 60(23): 6581-4.

344. Nicholson JC, Ross FM, Kohler JA, Ellison DW. Comparative genomic hybridization and histological variation in primitive neuroectodermal tumours. Br J Cancer 1999; 80(9): 1322-31.

345. Nicolas FE, Pais H, Schwach F, Lindow M, Kauppinen S, Moulton V, Dalmay T. Experimental identification of microRNA-140 targets by silencing and overexpressing miR-140. RNA 2008; 14: 2513–2520.

346. Niki T, Galli I, Ariga H, Iguchi-Ariga SM. MSSP, a protein binding to an origin of replication in the c-myc gene, interacts with a catalytic subunit of DNA polymerase alpha and stimulates its polymerase activity. FEBS Lett 2000a; 475(3): 209-12.

347. Niki T, Izumi S, Saëgusa Y, Taira T, Takai T, Iguchi-Ariga SM, Ariga H. MSSP promotes ras/myc cooperative cell transforming activity by binding to c-Myc. Genes Cells 2000b; 5(2): 127-41.

348. Nishi M, Takeshima H, Houtani T, Nakagawara K, Noda T, Sugimoto T. RhoN, a novel small GTP-binding protein expressed predominantly in neurons and hepatic stellate cells. Brain Res Mol Brain Res 1999; 67(1): 74-81.

349. Nishizaki T, Harada K, Kubota H, Ozaki S, Ito H, Sasaki K. Genetic alterations in pediatric medulloblastomas detected by comparative genomic hybridization. Pediatr Neurosurg 1999; 31(1): 27-32.

350. Niu Z, Iyer D, Conway SJ, Martin JF, Ivey K, Srivastava D, Nordheim A, Schwartz RJ. Serum response factor orchestrates nascent sarcomerogenesis and silences the biomineralization gene program in the heart. Proc Natl Acad Sci U S A 2008; 105(46): 17824-9.

351. Noh DY, Ahn SJ, Lee RA, Kim SW, Park IA, Chae HZ. Overexpression of peroxiredoxin in human breast cancer. Anticancer Res 2001; 21(3B): 2085-90.

352. Nonaka D, Fabbri A, Roz L, Mariani L, Vecchione A, Moore GW, Tavecchio L, Croce CM, Sozzi G. Reduced FEZ1/LZTS1 expression and outcome prediction in lung cancer. Cancer Res 2005; 65(4): 1207-12.

353. Northcott PA, Fernandez-L A, Hagan JP, Ellison DW, Grajkowska W, Gillespie Y, Grundy R, Van Meter T, Rutka JT, Croce CM, Kenney AM, Taylor MD. The miR-17/92 polycistron is up-regulated in sonic hedgehog-driven medulloblastomas and induced by N-myc in sonic hedgehog-treated cerebellar neural precursors. Cancer Res 2009; 69(8): 3249-55.

354. Northcott PA, Nakahara Y, Wu X, Feuk L, Ellison DW, Croul S. Multiple recurrent genetic events converge on control of histone lysine methylation in medulloblastoma. Nat Genet 2009; 41: 465–472.

355. Northcott PA, Korshunov A, Witt H, Hielscher T, Eberhart CG, Mack S, Bouffet E, Clifford SC, Hawkins CE, French P, Rutka JT, Pfister S, Taylor MD. Medulloblastoma Comprises Four Distinct Molecular Variants. J Clin Oncol 2010 (online).

356. Nottrott S, Simard MJ, Richter JD. Human let-7a miRNA blocks protein production on actively translating polyribosomes. Nat Struct Mol Biol 2006; 13(12): 1108-14.

357. Nottrott S, Simard MJ, Richter JD. Petersen CP, Bordeleau ME, Pelletier J, Sharp PA. Short RNAs repress translation after initiation in mammalian cells. Mol Cell 2006; 21(4): 533-42.

358. O'Donnell KA, Wentzel EA, Zeller KI, Dang CV, Mendell JT. c-Myc-regulated microRNAs modulate E2F1 expression. Nature 2005; 435(7043): 839-43.

359. Oberley TD, Verwiebe E, Zhong W, Kang SW, Rhee SG. Localization of the thioredoxin system in normal rat kidney. Free Radic Biol Med 2001; 30(4): 412-24.

360. Oh J, Takahashi R, Kondo S, Mizoguchi A, Adachi E, Sasahara RM, Nishimura S, Imamura Y, Kitayama H, Alexander DB, Ide C, Horan TP, Arakawa T, Yoshida H, Nishikawa S, Itoh Y, Seiki M, Itohara S, Takahashi C, Noda M. The membrane-anchored MMP inhibitor RECK is a key regulator of extracellular matrix

integrity and angiogenesis. Cell 2001; 107(6): 789-800.

361. Olsen PH, Ambros V. The lin-4 regulatory RNA controls developmental timing in Caenorhabditis elegans by blocking LIN-14 protein synthesis after the initiation of translation. Dev Biol 1999; 216: 671–680.

362. Onda K, Davis RL, Edwards MS. Comparison of bromodeoxyuridine uptake and MIB 1 immunoreactivity in medulloblastomas determined with single and double immunohistochemical staining methods. J Neurooncol 1996; 29(2): 129-36.

363. Orellana C, Hernandez-Martí M, Martínez F, Castel V, Millán JM, Alvarez-Garijo JA, Prieto F, Badía L. Pediatric brain tumors: loss of heterozygosity at 17p and TP53 gene mutations. Cancer Genet Cytogenet 1998; 102(2): 93-9.

364. Orford K, Crockett C, Jensen JP, Weissman AM, Byers SW. Serine phosphorylation-regulated ubiquitination and degradation of beta-catenin. J Biol Chem 1997; 272(40): 24735-8.

365. Packer RJ, Gajjar A, Vezina G, Rorke-Adams L, Burger PC, Robertson PL, Bayer L, LaFond D, Donahue BR, Marymont MH, Muraszko K, Langston J, Sposto R. Phase III study of craniospinal radiation therapy followed by adjuvant chemotherapy for newly diagnosed average-risk medulloblastoma. J Clin Oncol 2006; 24(25): 4202-8.

366. Packham G, Cleveland JL. c-Myc and apoptosis. Biochim Biophys Acta. 1995; 1242(1): 11-28.

367. Pais H, Nicolas FE, Soond SM, Swingler TE, Clark IM, Chantry A, Moulton V, Dalmay T. Analyzing mRNA expression identifies Smad3 as a microRNA-140 target regulated only at protein level. RNA 2010; 16(3): 489-94.

368. Pampalakis G, Diamandis EP, Katsaros D, Sotiropoulou G. Down-regulation of dicer expression in ovarian cancer tissues. Clin Biochem 2010; 43(3): 324-7.

369. Pan E, Pellarin M, Holmes E, Smirnov I, Misra A, Eberhart CG, Burger PC, Biegel JA, Feuerstein BG. Isochromosome 17q is a negative prognostic factor in poor-risk childhood medulloblastoma patients. Clin Cancer Res 2005; 11(13): 4733-40.

370. Pang JC, Dong Z, Zhang R, Liu Y, Zhou LF, Chan BW, Poon WS, Ng HK. Mutation analysis of DMBT1 in glioblastoma, medulloblastoma and oligodendroglial

tumors. Int J Cancer 2003; 105(1): 76-81.

371. Pang JC, Kwok WK, Chen Z, Ng HK. Oncogenic role of microRNAs in brain tumors. Acta Neuropathol 2009; 117(6): 599-611.

372. Pannuti A, Foreman K, Rizzo P, Osipo C, Golde T, Osborne B, Miele L. Targeting Notch to target cancer stem cells. Clin Cancer Res 2010; 16(12): 3141-52.

373. Papagiannakopoulos T, Shapiro A, Kosik KS. MicroRNA-21 targets a network of key tumor-suppressive pathways in glioblastoma cells. Cancer Res 2008; 68(19): 8164-72.

374. Park JH, Kim YS, Lee HL, Shim JY, Lee KS, Oh YJ, Shin SS, Choi YH, Park KJ, Park RW, Hwang SC. Expression of peroxiredoxin and thioredoxin in human lung cancer and paired normal lung. Respirology 2006; 11(3): 269-75.

375. Parker R, Song H. The enzymes and control of eukaryotic mRNA turnover. Nat Struct Mol Biol 2004; 11(2): 121-7.

376. Parnas D, Linial M. Acceleration of neuronal maturation of P19 cells by increasing culture density. Brain Res Dev Brain Res 1997; 101(1-2): 115-24.

377. Parry D, Mahony D, Wills K, Lees E. Cyclin D-CDK subunit arrangement is dependent on the availability of competing INK4 and p21 class inhibitors. Mol Cell Biol 1999; 19(3): 1775-83.

378. Pasquinelli AE, Reinhart BJ, Slack F, Martindale MQ, Kuroda MI, Maller B, Hayward DC, Ball EE, Degnan B, Müller P, Spring J, Srinivasan A, Fishman M, Finnerty J, Corbo J, Levine M, Leahy P, Davidson E, Ruvkun G. Conservation of the sequence and temporal expression of let-7 heterochronic regulatory RNA. Nature 2000; 408(6808): 86-9.

379. Perek M, Osterheld MC, Ellison D, Baas F, Versteeg R, Kool M. Molecular risk stratification of medulloblastoma patients based on immunohistochemical analysis of MYC, LDHB, and CCNB1 expression. Clin Cancer Res 2008; 14(13): 4154-60.

380. Pestova TV, Shatsky IN, Fletcher SP, Jackson RJ, Hellen CU. A prokaryotic-like mode of cytoplasmic eukaryotic ribosome binding to the initiation codon during internal translation initiation of hepatitis C and classical swine fever virus RNAs. Genes Dev

1998; 12(1): 67-83.

381. Petersen CP, Bordeleau ME, Pelletier J, Sharp PA. Short RNAs repress translation after initiation in mammalian cells. Mol Cell 2006; 21: 533–542.

382. Pfeffer S, Sewer A, Lagos-Quintana M, Sheridan R, Sander C, Grässer FA, van Dyk LF, Ho CK, Shuman S, Chien M, Russo JJ, Ju J, Randall G, Lindenbach BD, Rice CM, Simon V, Ho DD, Zavolan M, Tuschl T. Identification of microRNAs of the herpesvirus family. Nat Methods 2005; 2(4): 269-76.

383. Pfister S, Remke M, Benner A, Mendrzyk F, Toedt G, Felsberg J, Wittmann A, Devens F, Gerber NU, Joos S, Kulozik A, Reifenberger G, Rutkowski S, Wiestler OD, Radlwimmer B, Scheurlen W, Lichter P, Korshunov A. Outcome prediction in pediatric medulloblastoma based on DNA copy-number aberrations of chromosomes 6q and 17q and the MYC and MYCN loci. J Clin Oncol 2009; 27(10): 1627-36.

384. Pfister SM, Korshunov A, Kool M, Hasselblatt M, Eberhart C, Taylor MD. Molecular diagnostics of CNS embryonal tumors. Acta Neuropathol 2010; 120(5): 553-66.

385. Pierre K, Pellerin L. Monocarboxylate transporters in the central nervous system: distribution, regulation and function. J Neurochem 2005; 94: 1-14.

386. Pierson J, Hostager B, Fan R, Vibhakar R. Regulation of cyclin dependent kinase 6 by microRNA 124 in medulloblastoma. J Neurooncol 2008; 90(1): 1-7.

387. Pietsch T, Waha A, Koch A, Kraus J, Albrecht S, Tonn J, Sörensen N, Berthold F, Henk B, Schmandt N, Wolf HK, von Deimling A, Wainwright B, Chenevix-Trench G, Wiestler OD, Wicking C. Medulloblastomas of the desmoplastic variant carry mutations of the human homologue of Drosophila patched. Cancer Res 1997; 57(11): 2085-8.

388. Pillai RS, Bhattacharyya SN, Artus CG, Zoller T, Cougot N, Basyuk E, Bertrand E, Filipowicz W. Inhibition of translational initiation by Let-7 MicroRNA in human cells. Science 2005; 309(5740): 1573-6.

389. Pils D, Horak P, Gleiss A, Sax C, Fabjani G, Moebus VJ, Zielinski C, Reinthaller A, Zeillinger R, Krainer M. Five genes from chromosomal band 8p22 are significantly down-regulated in ovarian carcinoma: N33 and EFA6R have a potential impact on overall survival. Cancer 2005; 104(11): 2417-29.

390. Plaumann M, Seitz S, Frege R, Estevez-Schwarz L, Scherneck S. Analysis of DLC-1 expression in human breast cancer. J Cancer Res Clin Oncol. 2003; 129(6): 349-54.

391. Pleasure SJ, Lee VM. NTera 2 cells: a human cell line which displays characteristics expected of a human committed neuronal progenitor cell. J Neurosci Res 1993; 35(6): 585-602.

392. Pramanik P, Sharma MC, Mukhopadhyay P, Singh VP, Sarkar C. A comparative study of classical vs. desmoplastic medulloblastomas. Neurol India 2003; 51(1): 27-34.

393. Quackenbush J. Microarray data normalization and transformation. Nat Genet 2002; 32 Suppl: 496-501.

394. Raffel C, Thomas GA, Tishler DM, Lassoff S, Allen JC. Absence of p53 mutations in childhood central nervous system primitive neuroectodermal tumors. Neurosurgery 1993; 33(2): 301-5.

395. Raffel C. Medulloblastoma: molecular genetics and animal models. Neoplasia 2004; 4: 310-22.

396. Rasheed BK, Stenzel TT, McLendon RE, Parsons R, Friedman AH, Friedman HS, Bigner DD, Bigner SH. PTEN gene mutations are seen in high-grade but not in low-grade gliomas. Cancer Res 1997; 57(19): 4187-90.

397. Reardon DA, Michalkiewicz E, Boyett JM, Sublett JE, Entrekin RE, Ragsdale ST, Valentine MB, Behm FG, Li H, Heideman RL, Kun LE, Shapiro DN, Look AT. Extensive genomic abnormalities in childhood medulloblastoma by comparative genomic hybridization. Cancer Res 1997; 57(18): 4042-7.

398. Reifenberger J, Wolter M, Weber RG, Megahed M, Ruzicka T, Lichter P, Reifenberger G. Missense mutations in SMOH in sporadic basal cell carcinomas of the skin and primitive neuroectodermal tumors of the central nervous system. Cancer Res 1998; 58(9): 1798-803.

399. Reinhart BJ, Slack FJ, Basson M, Pasquinelli AE, Bettinger JC, Rougvie AE, Horvitz HR, Ruvkun G. The 21-nucleotide let-7 RNA regulates developmental timing in Caenorhabditis elegans. Nature 2000; 403: 901-906.

400. Rhee SG, Kang SW, Chang TS, Jeong W, Kim K. Peroxiredoxin, a novel family of peroxidases. IUBMB Life 2001; 52(1-2): 35-41.

401. Ribi K, Relly C, Landolt MA, Alber FD, Boltshauser E, Grotzer MA. Outcome of medulloblastoma in children: long-term complications and quality of life. Neuropediatrics 2005; 36(6): 357-65.

402. Rickert CH, Paulus W. Epidemiology of central nervous system tumors in childhood and adolescence based on the new WHO classification. Childs Nerv Syst 2001; 17(9): 503-11.

403. Rickert CH, Paulus W. Comparative genomic hybridization in central and peripheral nervous system tumors of childhood and adolescence. J Neuropathol Exp Neurol 2004; 63: 399–417.

404. Robarge KD, Brunton SA, Castanedo GM, Cui Y, Dina MS, Goldsmith R, Gould SE, Guichert O, Gunzner JL, Halladay J, Jia W, Khojasteh C, Koehler MF, Kotkow K, La H, Lalonde RL, Lau K, Lee L, Marshall D, Marsters JC Jr, Murray LJ, Qian C, Rubin LL, Salphati L, Stanley MS, Stibbard JH, Sutherlin DP, Ubhayaker S, Wang S, Wong S, Xie M. GDC-0449-a potent inhibitor of the hedgehog pathway. Bioorg Med Chem Lett 2009; 19(19): 5576-81.

405. Roberts RO, Lynch CF, Jones MP, Hart MN. Medulloblastoma: a population-based study of 532 cases. J Neuropathol Exp Neurol 1991; 50(2): 134-44.

406. Rodriguez A, Griffiths-Jones S, Ashurst JL, Bradley A. Identification of mammalian microRNA host genes and transcription units. Genome Res 2004; 14(10A): 1902-10.

407. Rossi MR, Conroy J, McQuaid D, Nowak NJ, Rutka JT, Cowell JK. Array CGH analysis of pediatric medulloblastomas. Genes Chromosomes Cancer 2006; 45(3), 290-303.

408. Rood BR, Zhang H, Weitman DM, Cogen PH. Hypermethylation of HIC-1 and 17p allelic loss in medulloblastoma. Cancer Res. 2002 Jul 1;62(13):3794-7.

409. Rossi MR, Conroy J, McQuaid D, Nowak NJ, Rutka JT, Cowell JK. Array CGH analysis of pediatric medulloblastomas. Genes Chromosomes Cancer. 2006; 45(3): 290-303.

410. Rudin CM, Hann CL, Laterra J, Yauch RL, Callahan CA, Fu L, Holcomb T, Stinson J, Gould SE, Coleman B, LoRusso PM, Von Hoff DD, de Sauvage FJ, Low JA. Treatment of medulloblastoma with hedgehog pathway inhibitor GDC-0449. N Engl J Med 2009; 361(12):1173-8.

411. Russo C, Pellarin M, Tingby O, Bollen AW, Lamborn KR, Mohapatra G, Collins VP, Feuerstein BG. Comparative genomic hybridization in patients with supratentorial and infratentorial primitive neuroectodermal tumors. Cancer 1999; 86(2): 331-9.

412. Rutkowski S, Bode U, Deinlein F, Ottensmeier H, Warmuth-Metz M, Soerensen N, Graf N, Emser A, Pietsch T, Wolff JE, Kortmann RD, Kuehl J. Treatment of early childhood medulloblastoma by postoperative chemotherapy alone. N Engl J Med 2005; 352(10): 978-86.

413. Rutkowski S, Bode U, Deinlein F, Ottensmeier H, Warmuth-Metz M, Soerensen N, Graf N, Emser A, Pietsch T, Wolff JE, Kortmann RD, Kuehl J. Treatment of early childhood medulloblastoma by postoperative chemotherapy alone. N Engl J Med 2005; 352: 978–986.

414. Rutkowski S, von Bueren A, von Hoff K, Hartmann W, Shalaby T, Deinlein F, Warmuth-Metz M, Soerensen N, Emser A, Bode U, Mittler U, Urban C, Benesch M, Kortmann RD, Schlegel PG, Kuehl J, Pietsch T, Grotzer M. Prognostic relevance of clinical and biological risk factors in childhood medulloblastoma: results of patients treated in the prospective multicenter trial HIT'91. Clin Cancer Res 2007; 13(9): 2651-7.

415. Rutkowski S, Gerber NU, von Hoff K, Gnekow A, Bode U, Graf N, Berthold F, Henze G, Wolff JE, Warmuth-Metz M, Soerensen N, Emser A, Ottensmeier H, Deinlein F, Schlegel PG, Kortmann RD, Pietsch T, Kuehl J; German Pediatric Brain Tumor Study Group. Treatment of early childhood medulloblastoma by postoperative chemotherapy and deferred radiotherapy. Neuro Oncol 2009; 11(2): 201-10.

416. Rutkowski S, von Hoff K, Emser A, Zwiener I, Pietsch T, Figarella-Branger D, Giangaspero F, Ellison DW, Garre ML, Biassoni V, Grundy RG, Finlay JL, Dhall G, Raquin MA, Grill J. Survival and prognostic factors of early childhood medulloblastoma: an international meta-analysis. J Clin Oncol 2010; 28(33): 4961-8.

417. Saito Y, Jones PA. Epigenetic activation of tumor suppressor microRNAs in human cancer cells. Cell Cycle 2006; 5(19): 2220-2.

418. Salinas PC, Nusse R. Regional expression of the Wnt-3 gene in the developing mouse forebrain in relationship to diencephalic neuromeres. Mech Dev 1992; 39(3): 151-60.

419. Salinas PC, Fletcher C, Copeland NG, Jenkins NA, Nusse R. Maintenance of Wnt-3 expression in Purkinje cells of the mouse cerebellum depends on interactions with granule cells. Development 1994; 120(5): 1277-86.

420. Salzman DW, Shubert-Coleman J, Furneaux H. P68 RNA helicase unwinds the human let-7 microRNA precursor duplex and is required for let-7-directed silencing of gene expression. J Biol Chem 2007; 282(45): 32773-9.

421. Sand M, Gambichler T, Skrygan M, Sand D, Scola N, Altmeyer P, Bechara FG. Expression Levels of the microRNA Processing Enzymes Drosha and Dicer in Epithelial Skin Cancer. Cancer Invest 2010; 28(6): 649-53.

422. Sanford RA, Fuller C, Lau C, Boyett JM, Wallace D, Gilbertson RJ. Risk-adapted craniospinal radiotherapy followed by high-dose chemotherapy and stem-cell rescue in children with newly diagnosed medulloblastoma (St Jude Medulloblastoma-96): long-term results from a prospective, multicentre trial. Lancet Oncol 2006; 7(10): 813-20.

423. Sanghamitra M, Talukder I, Singarapu N, Sindhu KV, Kateriya S, Goswami SK. WD-40 repeat protein SG2NA has multiple splice variants with tissue restricted and growth responsive properties. Gene 2008; 420(1): 48-56.

424. Sarin S, O'Meara MM, Flowers EB, Antonio C, Poole RJ, Didiano D, Johnston RJ Jr, Chang S, Narula S, Hobert O. Genetic screens for Caenorhabditis elegans mutants defective in left/right asymmetric neuronal fate specification. Genetics 2007; 176(4): 2109-30.

425. Sarver AL, Li L, Subramanian S. MicroRNA miR-183 functions as an oncogene by targeting the transcription factor EGR1 and promoting tumor cell migration. Cancer Res. 2010; 70(23): 9570-80.

426. Saury JM, Emanuelson I. Cognitive consequences of the treatment of medulloblastoma among children. Pediatr Neurol 2011; 44(1): 21-30.

427. Saydam O, Shen Y, Würdinger T, Senol O, Boke E, James MF, Tannous BA,

Stemmer-Rachamimov AO, Yi M, Stephens RM, Fraefel C, Gusella JF, Krichevsky AM, Breakefield XO. Downregulated microRNA-200a in meningiomas promotes tumor growth by reducing E-cadherin and activating the Wnt/beta-catenin signaling pathway. Mol Cell Biol 2009; 29(21): 5923-40.

428. Saydam O, Senol O, Wurdinger T, Mizrak A, Ozdener GB, Stemmer-Rachamimov AO, Yi M, Stephens R, Krichevsky AM, Saydam N, Brenner GJ, Breakefield XO. miRNA-7 attenuation in schwannoma tumors stimulates growth by upregulating three oncogenic signaling pathways. Cancer Res 2010 (online).

429. Scaglia N, Igal RA. Inhibition of Stearoyl-CoA Desaturase 1 expression in human lung adenocarcinoma cells impairs tumorigenesis. Int J Oncol 2008; 33(4): 839-50.

430. Schetter AJ, Leung SY, Sohn JJ, Zanetti KA, Bowman ED, Yanaihara N, Yuen ST, Chan TL, Kwong DL, Au GK, Liu CG, Calin GA, Croce CM, Harris CC. MicroRNA expression profiles associated with prognosis and therapeutic outcome in colon adenocarcinoma. JAMA 2008; 299: 425–436.

431. Scheurlen WG, Schwabe GC, Joos S, Mollenhauer J, Sörensen N, Kühl J. Molecular analysis of childhood primitive neuroectodermal tumors defines markers associated with poor outcome. J Clin Oncol 1998; 16(7): 2478-85.

432. Schiffer D, Bortolotto S, Bosone I, Cancelli I, Cavalla P, Schiffer P, Piva R. Cell-cycle inhibitor p27/Kip-1 expression in non-astrocytic and non-oligodendrocytic human nervous system tumors. Neurosci Lett 1999; 264(1-3): 29-32.

433. Schofield D, West DC, Anthony DC, Marshal R, Sklar J. Correlation of loss of heterozygosity at chromosome 9q with histological subtype in medulloblastomas. Am J Pathol 1995; 146(2): 472-80.

434. Schuhmacher M, Kohlhuber F, Michael Hölzel M, Kaiser C, Burtscher H, Jarsch M, Bornkamm GW, Laux G, Polack A, Weidle UH, Eick D. The transcriptional program of a human B cell line in response to Myc. Nucleic Acids Res 2001; 29: 397-406.

435. Schütz BR, Scheurlen W, Krauss J, du Manoir S, Joos S, Bentz M, Lichter P. Mapping of chromosomal gains and losses in primitive neuroectodermal tumors by comparative genomic hybridization. Genes Chromosomes Cancer 1996; 16(3): 196-203.

436. Schwarz DS, Hutvágner G, Du T, Xu Z, Aronin N, Zamore PD. Asymmetry in the

assembly of the RNAi enzyme complex. Cell 2003; 115(2): 199-208.

437. Schickel R, Park SM, Murmann AE, Peter ME. miR-200c regulates induction of apoptosis through CD95 by targeting FAP-1. Mol Cell 2010; 38(6): 908-15.

438. Scott DK, Straughton D, Cole M, Bailey S, Ellison DW, Clifford SC. Identification and analysis of tumor suppressor loci at chromosome 10q23.3-10q25.3 in medulloblastoma. Cell Cycle 2006; 5(20): 2381-9.

439. Segal RA, Goumnerova LC, Kwon YK, Stiles CD, Pomeroy SL. Expression of the neurotrophin receptor TrkC is linked to a favorable outcome in medulloblastoma. Proc Natl Acad Sci U S A 1994; 91(26): 12867-71.

440. Sehm T, Sachse C, Frenzel C, Echeverri K. miR-196 is an essential early-stage regulator of tail regeneration, upstream of key spinal cord patterning events. Dev Biol 2009; 334(2): 468-80.

441. Selbach M, Schwanhäusser B, Thierfelder N, Fang Z, Khanin R, Rajewsky N. Widespread changes in protein synthesis induced by microRNAs. Nature 2008; 455: 58–63.

442. Sempere LF, Freemantle S, Pitha-Rowe I, Moss E, Dmitrovsky E, Ambros V. Expression profiling of mammalian microRNAs uncovers a subset of brain-expressed microRNAs with possible roles in murine and human neuronal differentiation. Genome Biol 2004; 5(3): R13.

443. Seo MS, Kang SW, Kim K, Baines IC, Lee TH, Rhee SG. Identification of a new type of mammalian peroxiredoxin that forms an intramolecular disulfide as a reaction intermediate. J Biol Chem 2000; 275(27): 20346-54.

444. Sertel S, Eichhorn T, Sieber S, Sauer A, Weiss J, Plinkert PK, Efferth T. Factors determining sensitivity or resistance of tumor cell lines towards artesunate. Chem Biol Interact 2010; 185(1): 42-52.

445. Sevignani C, Calin GA, Siracusa LD, Croce CM. Mammalian microRNAs: a small world for fine-tuning gene expression. Mamm Genome 2006; 17: 189–202.

446. Sharma RP, Gavin DP, Grayson DR. CpG methylation in neurons: message, memory, or mask? Neuropsychopharmacology 2010; 35(10): 2009-20.

447. Shlomit R, Ayala AG, Michal D, Ninett A, Frida S, Boleslaw G, Gad B, Gideon R, Shlomi C. Gains and losses of DNA sequences in childhood brain tumors analyzed by comparative genomic hybridization. Cancer Genet Cytogenet 2000; 121(1): 67-72.

448. Shridhar V, Lee J, Pandita A, Itturia S, Avula R, Staub J, Morrissey M, Calhoun E, Sen A, Kalli K, Keeney G, Roche P, Cliby W, Lu K, Schmandt R, Mills GB, Bast RC, Jr, James CD, Couch FJ, Hartmann LC, Lillie J, Smith DI. Genetic analysis of early versus late-stage ovarian tumors. Cancer Res 2001; 61: 5895–5904.

449. Silber J, Lim DA, Petritsch C, Persson AI, Maunakea AK, Yu M, Vandenberg SR, Ginzinger DG, James CD, Costello JF, Bergers G, Weiss WA, Alvarez-Buylla A, Hodgson JG. miR-124 and miR-137 inhibit proliferation of glioblastoma multiforme cells and induce differentiation of brain tumor stem cells. BMC Med 2008; 6: 14.

450. Simeone A, Puelles E, Acampora D. The Otx family. Curr Opin Genet Dev 2002; 12: 409–15.

451. Simon HU, Haj-Yehia A, Levi-Schaffer F. Role of reactive oxygen species (ROS) in apoptosis induction. Apoptosis 2000; 5(5): 415-8.

452. Singh SK, Clarke ID, Terasaki M, Bonn VE, Hawkins C, Squire J, Dirks PB. Identification of a cancer stem cell in human brain tumors. Cancer Res 2003; 63(18): 5821-8.

453. Singh SK, Hawkins C, Clarke ID, Squire JA, Bayani J, Hide T, Henkelman RM, Cusimano MD, Dirks PB. Identification of human brain tumour initiating cells. Nature 2004; 432(7015): 396-401.

454. Skoyum R, Eide K, Berg K, Rofstad EK. Energy metabolism in human melanoma cells under hypoxic and acidic conditions in vitro. Br J Cancer 1997; 76: 421-8.

455. Slaby O, Lakomy R, Fadrus P, Hrstka R, Kren L, Lzicarova E, Smrcka M, Svoboda M, Dolezalova H, Novakova J, Valik D, Vyzula R, Michalek J. MicroRNA-181 family predicts response to concomitant chemoradiotherapy with temozolomide in glioblastoma patients. Neoplasma 2010; 57(3): 264-9.

456. Slebos RJ, Lee MH, Plunkett BS, Kessis TD, Williams BO, Jacks T, Hedrick L, Kastan MB, Cho KR. p53-dependent G1 arrest involves pRB-related proteins and is disrupted by the human papillomavirus 16 E7 oncoprotein. Proc Natl Acad Sci U S A

1994; 91(12): 5320-4.

457. Smalley MJ, Dale TC. Wnt signalling in mammalian development and cancer. Cancer Metastasis Rev 1999; 18(2): 215-30.

458. Smith AG, Popov N, Imreh M, Axelson H, Henriksson M. Expression and DNA-binding activity of MYCN/Max and Mnt/Max during induced differentiation of human neuroblastoma cells. J Cell Biochem 2004; 92(6): 1282-95.

459. Song JJ, Liu J, Tolia NH, Schneiderman J, Smith SK, Martienssen RA, Hannon GJ, Joshua-Tor L. The crystal structure of the Argonaute2 PAZ domain reveals an RNA binding motif in RNAi effector complexes. Nat Struct Biol 2003; 10(12): 1026-32.

460. Song JJ, Smith SK, Hannon GJ, Joshua-Tor L. Crystal structure of Argonaute and its implications for RISC slicer activity. Science 2004; 305(5689): 1434-7.

461. Spahn M, Kneitz S, Scholz CJ, Stenger N, Rüdiger T, Ströbel P, Riedmiller H, Kneitz B. Expression of microRNA-221 is progressively reduced in aggressive prostate cancer and metastasis and predicts clinical recurrence. Int J Cancer 2010; 127(2): 394-403.

462. Sredni ST, Bonaldo MD, Costa FF, Huang CC, Hamm CA, Rajaram V, Tomita T, Goldman S, Bischof JM, Soares MB. Upregulation of mir-221 and mir-222 in atypical teratoid/rhabdoid tumors: potential therapeutic targets. Childs Nerv Syst 2010; 26(3): 279-83.

463. Stark A, Brennecke J, Russell RB, Cohen SM. Identification of Drosophila MicroRNA targets. PLoS Biol. 2003; 1(3): E60.

464. Stearns D, Chaudhry A, Abel TW, Burger PC, Dang CV, Eberhart CG. c-myc overexpression causes anaplasia in medulloblastoma. Cancer Res 2006; 66: 673-81.

465. Stecca B, Ruiz i Altaba A. The therapeutic potential of modulators of the Hedgehog-Gli signaling pathway. J Biol 2002; 1(2): 9.

466. Storey KG, Crossley JM, De Robertis EM, Norris WE, Stern CD. Neural induction and regionalisation in the chick embryo. Development 1992; 114(3): 729-41.

467. Sun R, Fu X, Li Y, Xie Y, Mao Y. Global gene expression analysis reveals reduced

abundance of putative microRNA targets in human prostate tumours. BMC Genomics 2009; 10: 93.

468. Svoboda M, Izakovicova Holla L, Sefr R, Vrtkova I, Kocakova I, Tichy B, Dvorak J. Micro-RNAs miR125b and miR137 are frequently upregulated in response to capecitabine chemoradiotherapy of rectal cancer. Int J Oncol 2008; 33(3): 541-7.

469. Swartling FJ, Grimmer MR, Hackett CS, Northcott PA, Fan QW, Goldenberg DD, Lau J, Masic S, Nguyen K, Yakovenko S, Zhe XN, Gilmer HC, Collins R, Nagaoka M, Phillips JJ, Jenkins RB, Tihan T, Vandenberg SR, James CD, Tanaka K, Taylor MD, Weiss WA, Chesler L. Pleiotropic role for MYCN in medulloblastoma. Genes Dev 2010; 24(10): 1059-72.

470. Szatrowski TP, Nathan CF. Production of large amounts of hydrogen peroxide by human tumor cells. Cancer Res 1991; 51(3): 794-8.

471. Tabori U, Baskin B, Shago M, Alon N, Taylor MD, Ray PN, Bouffet E, Malkin D, Hawkins C. Universal poor survival in children with medulloblastoma harboring somatic TP53 mutations. J Clin Oncol 2010; 28(8): 1345-50.

472. Taby R, Issa JP. Cancer epigenetics. CA Cancer J Clin 2010; 60(6), 376-92.

473. Tagawa H, Seto M. A microRNA cluster as a target of genomic amplification in malignant lymphoma. Leukemia 2005; 19(11): 2013-6.

474. Taipale J, Beachy PA. The Hedgehog and Wnt signalling pathways in cancer. Nature 2001; 411(6835): 349-54.

475. Takei H, Nguyen Y, Mehta V, Chintagumpala M, Dauser RC, Adesina AM. Low-level copy gain versus amplification of myc oncogenes in medulloblastoma: utility in predicting prognosis and survival. Laboratory investigation. J Neurosurg Pediatr 2009; 3(1): 61-5.

476. Tam W. Identification and characterization of human BIC, a gene on chromosome 21 that encodes a noncoding RNA. Gene 2001; 274(1-2): 157-67.

477. Tanaka H, Katoh H, Negishi M. Pragmin, a novel effector of Rnd2 GTPase, stimulates RhoA activity J Biol Chem 2006; 281(15): 10355-64.

478. Taylor MD, Liu L, Raffel C, Hui CC, Mainprize TG, Zhang X, Agatep R, Chiappa S, Gao L, Lowrance A, Hao A, Goldstein AM, Stavrou T, Scherer SW, Dura WT, Wainwright B, Squire JA, Rutka JT, Hogg D. Mutations in SUFU predispose to medulloblastoma. Nat Genet 2002; 31(3): 306-10.

479. Taylor MD, Poppleton H, Fuller C, Su X, Liu Y, Jensen P, Magdaleno S, Dalton J, Calabrese C, Board J, Macdonald T, Rutka J, Guha A, Gajjar A, Curran T, Gilbertson RJ. Radial glia cells are candidate stem cells of ependymoma. Cancer Cell 2005; 8(4): 323-35.

480. Tetsu O, McCormick F. Beta-catenin regulates expression of cyclin D1 in colon carcinoma cells. Nature 1999; 398(6726): 422-6.

481. Thomas KR, Capecchi MR. Targeted disruption of the murine int-1 proto-oncogene resulting in severe abnormalities in midbrain and cerebellar development. Nature 1990; 346(6287): 847-50.

482. Thompson MC, Fuller C, Hogg TL, Dalton J, Finkelstein D, Lau CC, Chintagumpala M, Adesina A, Ashley DM, Kellie SJ, Taylor MD, Curran T, Gajjar A, Gilbertson RJ. Genomics identifies medulloblastoma subgroups that are enriched for specific genetic alterations. J Clin Oncol 2006; 24(12): 1924-31.

483. Tiscornia G, Izpisúa Belmonte JC. MicroRNAs in embryonic stem cell function and fate. Genes Dev 2010; 24(24): 2732-41.

484. Tong CY, Hui AB, Yin XL, Pang JC, Zhu XL, Poon WS, Ng HK. Detection of oncogene amplifications in medulloblastomas by comparative genomic hybridization and array-based comparative genomic hybridization. J Neurosurg 2004; 100(2 Suppl Pediatrics): 187-93.

485. Toyota M, Suzuki H, Sasaki Y, Maruyama R, Imai K, Shinomura Y, Tokino T. Epigenetic silencing of microRNA-34b/c and B-cell translocation gene 4 is associated with CpG island methylation in colorectal cancer. Cancer Res 2008; 68(11): 4123-32.

486. Traiffort E, Angot E, Ruat M. Sonic Hedgehog signaling in the mammalian brain. J Neurochem 2010; 113(3): 576-90.

487. Tsuda M, Kamimura K, Nakato H, Archer M, Staatz W, Fox B, Humphrey M, Olson S, Futch T, Kaluza V, Siegfried E, Stam L, Selleck SB. The cell-surface

proteoglycan Dally regulates Wingless signalling in Drosophila. Nature 1999; 400(6741): 276-80.

488. Ueda R, Yoshida K, Kawase T, Kawakami Y, Toda M. Preferential expression and frequent IgG responses of a tumor antigen, SOX5, in glioma patients. Int J Cancer 2007; 120(8): 1704-11.

489. Valastyan S, Reinhardt F, Benaich N, Calogrias D, Szász AM, Wang ZC, Brock JE, Richardson AL, Weinberg RA. A pleiotropically acting microRNA, miR-31, inhibits breast cancer metastasis. Cell 2009; 137(6): 1032-46.

490. Visone R, Russo L, Pallante P, De Martino I, Ferraro A, Leone V, Borbone E, Petrocca F, Alder H, Croce CM, Fusco A. MicroRNAs (miR)-221 and miR-222, both overexpressed in human thyroid papillary carcinomas, regulate p27Kip1 protein levels and cell cycle. Endocr Relat Cancer 2007; 14(3): 791-8.

491. van Dijk E, Cougot N, Meyer S, Babajko S, Wahle E, Séraphin B. Human Dcp2: a catalytically active mRNA decapping enzyme located in specific cytoplasmic structures. EMBO J 2002; 21(24): 6915-24.

492. Vander Heiden MG, Cantley LC, Thompson CB. Understanding the Warburg effect: the metabolic requirements of cell proliferation. Science 2009; 324(5930): 1029-33.

493. Vázquez I, Maicas M, Marcotegui N, Conchillo A, Guruceaga E, Roman-Gomez J, Calasanz MJ, Agirre X, Prosper F, Odero MD. Silencing of hsa-miR-124 by EVI1 in cell lines and patients with acute myeloid leukemia. Proc Natl Acad Sci U S A 2010; 107(44): E167-8;

494. Vecchione A, Ishii H, Baldassarre G, Bassi P, Trapasso F, Alder H, Pagano F, Gomella LG, Croce CM, Baffa R. FEZ1/LZTS1 is down-regulated in high-grade bladder cancer, and its restoration suppresses tumorigenicity in transitional cell carcinoma cells. Am J Pathol 2002; 160(4): 1345-52.

495. Venkataraman S, Alimova I, Fan R, Harris P, Foreman N, Vibhakar R. MicroRNA 128a increases intracellular ROS level by targeting Bmi-1 and inhibits medulloblastoma cancer cell growth by promoting senescence. PLoS One 2010; 5(6): e10748.

496. Visvanathan J, Lee S, Lee B, Lee JW, Lee SK. The microRNA miR-124 antagonizes the anti-neural REST/SCP1 pathway during embryonic CNS development.

Genes Dev 2007; 21(7): 744-9.

497. von Hoff K, Hartmann W, von Bueren AO, Gerber NU, Grotzer MA, Pietsch T, Rutkowski S. Large cell/anaplastic medulloblastoma: outcome according to myc status, histopathological, and clinical risk factors. Pediatr Blood Cancer 2010; 54(3): 369-76.

498. Voorhoeve PM, le Sage C, Schrier M, Gillis AJ, Stoop H, Nagel R, Liu YP, van Duijse J, Drost J, Griekspoor A, Zlotorynski E, Yabuta N, De Vita G, Nojima H, Looijenga LH, Agami R. A genetic screen implicates miRNA-372 and miRNA-373 as oncogenes in testicular germ cell tumors. Cell 2006; 124(6): 1169-81.

499. Vorechovský I, Tingby O, Hartman M, Strömberg B, Nister M, Collins VP, Toftgård R. Somatic mutations in the human homologue of Drosophila patched in primitive neuroectodermal tumours. Oncogene 1997; 15(3): 361-6.

500. Waha A, Waha A, Koch A, Meyer-Puttlitz B, Weggen S, Sörensen N, Tonn JC, Albrecht S, Goodyer CG, Berthold F, Wiestler OD, Pietsch T. Epigenetic silencing of the HIC-1 gene in human medulloblastomas. J Neuropathol Exp Neurol 2003; 62(11): 1192-201.

501. Wakiyama M, Takimoto K, Ohara O, Yokoyama S. let-7 microRNA-mediated mRNA deadenylation and translational repression in a mammalian cell-free system. Genes Dev 2007; 21: 1857–1862.

502. Walenta S, Salameh A, Lyng H, Evensen JF, Mitze M, Rofstad EK, Mueller-Klieser W. Correlation of high lactate levels in head and neck tumors with incidence of metastasis. Am J Pathol 1997; 150: 409-15.

503. Waldman T, Kinzler KW, Vogelstein B. p21 is necessary for the p53-mediated G1 arrest in human cancer cells. Cancer Res 1995; 55(22), 5187-90.

504. Walter AW, Mulhern RK, Gajjar A, Heideman RL, Reardon D, Sanford RA, Xiong X, Kun LE. Survival and neurodevelopmental outcome of young children with medulloblastoma at St Jude Children's Research Hospital. J Clin Oncol 1999; 17(12): 3720-8.

505. Wang Y, Huso D, Cahill H, Ryugo D, Nathans J. Progressive cerebellar, auditory, and esophageal dysfunction caused by targeted disruption of the frizzled-4 gene. J Neurosci 2001; 21(13): 4761-71.

506. Wang B, Love TM, Call ME, Doench JG, Novina CD. Recapitulation of short RNA-directed translational gene silencing in vitro. Mol Cell 2006; 22(4): 553-60.

507. Wang X, Wang X. Systematic identification of microRNA functions by combining target prediction and expression profiling. Nucleic Acids Res 2006; 34(5): 1646-52.

508. Wang D, Lu M, Miao J, Li T, Wang E, Cui Q. Cepred: predicting the co-expression patterns of the human intronic microRNAs with their host genes. PLoS One 2009; 4(2): e4421.

509. Watabe S, Kohno H, Kouyama H, Hiroi T, Yago N, Nakazawa T. Purification and characterization of a substrate protein for mitochondrial ATP-dependent protease in bovine adrenal cortex. J Biochem 1994; 115(4): 648-54.

510. Wechsler-Reya R, Scott MP. The developmental biology of brain tumors. Annu Rev Neurosci 2001; 24: 385-428.

511. Wei Y, Harris T, Childs G. Global gene expression patterns during neural differentiation of P19 embryonic carcinoma cells. Differentiation 2002; 70(4-5): 204-19.

512. Wetmore C, Eberhart DE, Curran T. Loss of p53 but not ARF accelerates medulloblastoma in mice heterozygous for patched. Cancer Res 2001; 61(2): 513-6.

513. Wheeler MT, Zarnegar S, McNally EM. Zeta-sarcoglycan, a novel component of the sarcoglycan complex, is reduced in muscular dystrophy. Hum Mol Genet 2002; 11(18): 2147-54.

514. Widelitz RB. Wnt signaling in skin organogenesis. Organogenesis 2008; 4(2): 123-33.

515. Wienholds E, Kloosterman WP, Miska E, Alvarez-Saavedra E, Berezikov E, de Bruijn E, Horvitz HR, Kauppinen S, Plasterk RH. MicroRNA expression in zebrafish embryonic development. Science 2005; 309(5732): 310-1.

516. Wiesner C, Winsauer G, Resch U, Hoeth M, Schmid JA, van Hengel J, van Roy F, Binder BR, de Martin R. Alpha-catulin, a Rho signalling component, can regulate NF-kappaB through binding to IKK-beta, and confers resistance to apoptosis. Oncogene

2008; 27(15): 2159-69.

517. Wightman B, Ha I, Ruvkun G. Posttranscriptional regulation of the heterochronic gene lin-14 by lin-4 mediates temporal pattern formation in C. elegans. Cell 1993; 75: 855-862.

518. Wilson JE, Pestova TV, Hellen CU, Sarnow P. Initiation of protein synthesis from the A site of the ribosome. Cell 2000; 102(4): 511-20.

519. Wong CM, Lee JM, Ching YP, Jin DY, Ng IO. Genetic and epigenetic alterations of DLC-1 gene in hepatocellular carcinoma. Cancer Res 2003; 63(22): 7646-51.

520. Wong QW, Ching AK, Chan AW, Choy KW, To KF, Lai PB, Wong N. MiR-222 Overexpression Confers Cell Migratory Advantages in Hepatocellular Carcinoma through Enhancing AKT Signaling. Clin Cancer Res 2010; 16(3): 867-75.

521. Wood ZA, Schröder E, Robin Harris J, Poole LB. Structure, mechanism and regulation of peroxiredoxins. Trends Biochem Sci 2003; 28(1): 32-40.

522. Wu L, Belasco JG. Micro-RNA regulation of the mammalian lin-28 gene during neuronal differentiation of embryonal carcinoma cells. Mol Cell Biol 2005; 25(21): 9198-208.

523. Wu J, Qian J, Li C, Kwok L, Cheng F, Liu P, Perdomo C, Kotton D, Vaziri C, Anderlind C, Spira A, Cardoso WV, Lü J. miR-129 regulates cell proliferation by downregulating Cdk6 expression. Cell Cycle 2010; 9(9): 1809-18.

524. Wuchty S, Fontana W, Hofacker IL, Schuster P. Complete suboptimal folding of RNA and the stability of secondary structures. Biopolymers 1999; 49(2): 145-65.

525. Xie J, Johnson RL, Zhang X, Bare JW, Waldman FM, Cogen PH, Menon AG, Warren RS, Chen LC, Scott MP, Epstein EH Jr. Mutations of the PATCHED gene in several types of sporadic extracutaneous tumors. Cancer Res 1997; 57(12): 2369-72.

526. Xu P, Vernooy SY, Guo M, Hay BA. The Drosophila microRNA Mir-14 suppresses cell death and is required for normal fat metabolism. Curr Biol 2003; 13(9): 790-5.

527. Yamamoto T, Matsui Y, Natori S, Obinata M. Cloning of a housekeeping-type gene (MER5) preferentially expressed in murine erythroleukemia cells. Gene 1989; 80(2):

337-43.

528. Yan KS, Yan S, Farooq A, Han A, Zeng L, Zhou MM. Structure and conserved RNA binding of the PAZ domain. Nature 2003; 426(6965): 468-74.

529. Yanaihara N, Caplen N, Bowman E, Seike M, Kumamoto K, Yi M, Stephens RM, Okamoto A, Yokota J, Tanaka T, Calin GA, Liu CG, Croce CM, Harris CC. Unique microRNA molecular profiles in lung cancer diagnosis and prognosis. Cancer Cell 2006; 9(3): 189-98.

530. Yang HY, Jeong DK, Kim SH, Chung KJ, Cho EJ, Yang U, Lee SR, Lee TH. The role of peroxiredoxin III on late stage of proerythrocyte differentiation. Biochem Biophys Res Commun 2007; 359(4): 1030-6.

531. Yekta S, Shih IH, Bartel DP. MicroRNA-directed cleavage of HOXB8 mRNA. Science 2004; 304(5670): 594-6.

532. Yeom KH, Lee Y, Han J, Suh MR, Kim VN. Characterization of DGCR8/Pasha, the essential cofactor for Drosha in primary miRNA processing. Nucleic Acids Res 2006; 34(16): 4622-9.

533. Yi R, Qin Y, Macara IG, Cullen BR. Exportin-5 mediates the nuclear export of pre-microRNAs and short hairpin RNAs. Genes Dev 2003; 17(24): 3011-6.

534. Yin XL, Pang JC, Liu YH, Chong EY, Cheng Y, Poon WS, Ng HK. Analysis of loss of heterozygosity on chromosomes 10q, 11, and 16 in medulloblastomas. J Neurosurg 2001; 94(5): 799-805.

535. Yin XL, Pang JC, Ng HK. Identification of a region of homozygous deletion on 8p22-23.1 in medulloblastoma. Oncogene 2002; 21(9): 1461-8.

536. Yokota N, Nishizawa S, Ohta S, Date H, Sugimura H, Namba H, Maekawa M. Role of Wnt pathway in medulloblastoma oncogenesis. Int J Cancer 2002; 101(2): 198-201.

537. Yokota N, Mainprize TG, Taylor MD, Kohata T, Loreto M, Ueda S, Dura W, Grajkowska W, Kuo JS, Rutka JT. Identification of differentially expressed and developmentally regulated genes in medulloblastoma using suppression subtraction hybridization. Oncogene 2004; 23(19): 3444-53.

538. Yong WH, Raffel C, von Deimling A, Louis DN. The APC gene in Turcot's syndrome. N Engl J Med 1995; 333(8): 524.

539. Yu JY, Chung KH, Deo M, Thompson RC, Turner DL. MicroRNA miR-124 regulates neurite outgrowth during neuronal differentiation. Exp Cell Res 2008; 314(14): 2618-33.

540. Yuan BZ, Jefferson AM, Baldwin KT, Thorgeirsson SS, Popescu NC, Reynolds SH. DLC-1 operates as a tumor suppressor gene in human non-small cell lung carcinomas. Oncogene 2004; 23(7): 1405-11.

541. Zawlik I, Zakrzewska M, Witusik M, Golanska E, Kulczycka-Wojdala D, Szybka M, Piaskowski S, Wozniak K, Zakrzewski K, Papierz W, Liberski PP, Rieske P. KCTD11 expression in medulloblastoma is lower than in adult cerebellum and higher than in neural stem cells. Cancer Genet Cytogenet 2006; 170(1): 24-8.

542. Zeltzer PM, Boyett JM, Finlay JL, Albright AL, Rorke LB, Milstein JM, Allen JC, Stevens KR, Stanley P, Li H, Wisoff JH, Geyer JR, McGuire-Cullen P, Stehbens JA, Shurin SB, Packer RJ. Metastasis stage, adjuvant treatment, and residual tumor are prognostic factors for medulloblastoma in children: conclusions from the Children's Cancer Group 921 randomized phase III study. J Clin Oncol 1999; 17(3): 832-45.

543. Zeng Y, Yi R, Cullen BR. MicroRNAs and small interfering RNAs can inhibit mRNA expression by similar mechanisms. Proc Natl Acad Sci U S A 2003; 100(17): 9779-84.

544. Zeng Y. Principles of micro-RNA production and maturation. Oncogene 2006; 25(46): 6156-62.

545. Zeltzer PM, Boyett JM, Finlay JL, Albright AL, Rorke LB, Milstein JM, Allen JC, Stevens KR, Stanley P, Li H, Wisoff JH, Geyer JR, McGuire-Cullen P, Stehbens JA, Shurin SB, Packer RJ. Metastasis stage, adjuvant treatment, and residual tumor are prognostic factors for medulloblastoma in children: conclusions from the Children's Cancer Group 921 randomized phase III study. J Clin Oncol 1999; 17: 832-45.

546. Zenz T, Mohr J, Eldering E, Kater AP, Bühler A, Kienle D, Winkler D, Dürig J, van Oers MH, Mertens D, Döhner H, Stilgenbauer S. miR-34a as part of the resistance network in chronic lymphocytic leukemia. Blood 2009; 113(16): 3801-8.

547. Zhang Y, Chao T, Li R, Liu W, Chen Y, Yan X, Gong Y, Yin B, Liu W, Qiang B, Zhao J, Yuan J, Peng X. MicroRNA-128 inhibits glioma cells proliferation by targeting transcription factor E2F3a. J Mol Med 2009; 87(1): 43-51.

548. Zhao Y, Samal E, Srivastava D. Serum response factor regulates a muscle-specific microRNA that targets Hand2 during cardiogenesis. Nature 2005; 436(7048): 214-20.

549. Zhou XZ, Lu KP. The Pin2/TRF1-interacting protein PinX1 is a potent telomerase inhibitor. Cell 2001; 107(3): 347-59.

550. Zhu W, Chan EK, Li J, Hemmerich P, Tan EM. Transcription activating property of autoantigen SG2NA and modulating effect of WD-40 repeats. Exp Cell Res 2001; 269(2): 312-21.

551. Zhou H, Clapham DE. Mammalian MagT1 and TUSC3 are required for cellular magnesium uptake and vertebrate embryonic development. Proc Natl Acad Sci U S A 2009; 106(37): 15750-5.

552. Ziegelbauer, J.M., Sullivan, C.S. and Ganem, D. Tandem array-based expression screens identify host mRNA targets of virus-encoded microRNAs. Nat Genet 2009; 41: 130–134.

553. Zitterbart K, Filkova H, Tomasikova L, Necesalova E, Zambo I, Kantorova D, Slamova I, Vranova V, Zezulkova D, Pesakova M, Pavelka Z, Veselska R, Kuglik P, Sterba J. Low-level copy number changes of MYC genes have a prognostic impact in medulloblastoma. J Neurooncol 2010; 102(1): 25-33.

554. Zuker M. Mfold web server for nucleic acid folding and hybridization prediction. Nucleic Acids Res 2003; 31(13): 3406-15.

555. Zoratti M, Szabò I. The mitochondrial permeability transition. Biochim Biophys Acta 1995; 1241(2): 139-76.

556. Zurawel RH, Chiappa SA, Allen C, Raffel C. Sporadic medulloblastomas contain oncogenic beta-catenin mutations. Cancer Res 1998; 58(5): 896-9.

557. Zurawel RH, Allen C, Chiappa S, Cato W, Biegel J, Cogen P, de Sauvage F, Raffel C. Analysis of PTCH/SMO/SHH pathway genes in medulloblastoma. Genes Chromosomes Cancer 2000; 27(1): 44-51.

Zurawel RH, Allen C, Wechsler-Reya R, Scott MP, Raffel C. Evidence that haploinsufficiency of Ptch leads to medulloblastoma in mice.Genes Chromosomes Cancer 2000; 28(1): 77-81.